Effects of Installation Sequence of Concrete Rigid Inclusions by Ground-Displacement Piling Method on Previously Installed Columns

Huu Hung Nguyen

A thesis in fulfilment of the requirements for the award of the degree

DOCTOR OF PHILOSOPHY

School of Civil and Environmental Engineering

Faculty of Engineering and Information Technology

October 2018

Certificate of Original Authorship

I, **Huu Hung Nguyen**, declare that this thesis, submitted in fulfilment of the requirements for the award of Doctor of Philosophy, in the School of Civil and Environmental Engineering, Faculty of Engineering and Information Technology at the University of Technology Sydney.

This thesis is wholly my own work unless otherwise referenced or acknowledged. In addition, I certify that all information sources and literature used are indicated in the thesis. This document has not been submitted for qualifications at any other academic institution. This research is supported by an Australian Government Research Training Program Scholarship.

Signature: Production Note:
Signature removed prior to publication.

Date: 23 October 2018

Acknowledgment

I wish to express sincere gratitude to my principal supervisor A/Prof Hadi Khabbaz and my co-supervisor A/Prof Behzad Fatahi for their invaluable guidance and support over the course of this research.

The Australian Postgraduate Award from Australian Government and the funding from Roads and Maritime Services of NSW, Fulton Hogan, SMEC and Menard Oceania are gratefully acknowledged. I would also like to thank UTS Graduate Research School and Faculty of Engineering and Information Technology for high-quality support and several generous travel grants.

Much of the laboratory equipment was constructed at the University workshop led by Mr Laurence Stonard. Special thanks to Dr Lam Nguyen, Mr Peter Brown, Mr Richard Turnell, Mr Antonio Reyno, Dr Thang Pham, and Dr Hamed Mahdavi for their assistance and support with the complexities of the model test set-up, data logging system, signal conditioning, and 3D scanning. My appreciation is extended to Dr Richard Kelly, Mr Philippe Vincent, Dr Jeff Hsi, Professor Mark Randolph, Dr David Oliveira, Dr Thanh Vo, Dr Thevaragavan Muttuvel, Mr Michal Krzeminski, and Dr Ali Parsa for many valuable technical discussions, to Professor John Carter for the use of CAMFE code, and to Mr Ross Barker for providing access to the laboratory equipment. My special thanks go to my colleagues at the UTS Geotechnical Research Group for fostering an enjoyable working environment.

Finally, I greatly thank my lovely wife, Tam, and my parents for their unconditional love and support.

List of Research Papers

The following technical papers were written during this research project:

- Nguyen, H.H., Khabbaz, H. & Fatahi, B. 2018, 'A Numerical Comparison of Installation Sequences of Plain Concrete Rigid Inclusions', **Computers & Geotechnics**, submitted 2 January 2018; accepted 2 September 2018, published online 21 September 2018, https://doi.org/10.1016/j.compgeo.2018.09.001.
- Nguyen, H.H., Khabbaz, H., Fatahi, B. & Kelly, R. 2016, 'Bridge Pile Response to Lateral Soil Movement Induced by Installation of Controlled Modulus Columns', **Procedia Engineering**, vol. 143, pp. 475-482, https://doi.org/10.1016/j.proeng.2016.06.060.
- Nguyen, H.H., Khabbaz, H., Fatahi, B. & Hsi, J. 2017, 'Effects of installing controlled modulus columns on previously installed columns', the **19th International Conference on Soil Mechanics and Geotechnical Engineering** - Seoul, South Korea, , pp. 2611-2614, https://www.issmge.org/publications/online-library.
- Nguyen, H.H., Khabbaz, H., Fatahi, B., Santos, R., Marix-Evans, M. & Vincent, P. 2016, 'Installation Effect of Controlled Modulus Columns on Nearby Existing Structures', **Geochina International Conference** 2016, vol. GSP 264, pp. 125-133, https://ascelibrary.org/doi/10.1061/9780784480076.015.
- Nguyen, H.H., Fatahi, B. & Khabbaz, H. 2014, 'Challenges in assessing the installation effects of controlled modulus columns on behaviour of surrounding soils', **The Fourth International Conference on Géotechnique, Construction Materials and Environment**, Brisbane, Australia, pp. 44-49.
- Nguyen, H.H., Khabbaz, H., Fatahi, B., Vincent, P. & Marix-Evans, M. 2014, 'Sustainability considerations for ground improvement technique using controlled

modulus columns', **Australian Geomechanics Society,** "Resilient Geotechnics", Sydney Australia, pp. 170 - 184.

- Nguyen, H.H., Khabbaz, H. & Fatahi, B. 2018, 'Model Test on the Responses of Early Age Concrete Inclusions in Soft Ground Subject to Nearby Installations', Canadian Geotechnical Journal (in preparation).
- Nguyen, H.H., Khabbaz, H. & Fatahi, B. 2018, 'Effects of Pile Penetration in Comparison with Combined Cylindrical and Spherical Cavity Expansions: Experimental and Numerical Studies', International Journal of Geomechanics (in preparation).

Huu Hung Nguyen, Behzad Fatahi and Hadi Khabbaz received the award of the best paper for their paper titled: *'Challenges in assessing the installation effects of controlled modulus columns on behaviour of surrounding soils'*, presented in The Fourth International Conference on Géotechnique, Construction Materials and Environment, Brisbane, Australia in November 2014.

Abstract

Ground improvement techniques using concrete injected column (CIC) or controlled modulus column (CMC) have been widely used since 1980s. However, impacts of ground displacement induced by the techniques have not been studied adequately. This project advances both experimental and numerical bases for assessing effects of installing CICs or CMCs on the surrounding soils and previously installed columns, with interests given to installation sequence and behaviour of concrete inclusion at early age.

Three-dimensional numerical modelling was conducted to investigate how groups of columns installed in different sequences could affect previously installed columns. The assessment included coupled consolidation analyses in large strain mode, considering soil-column interaction. CMC installation was modelled numerically with the combined use of cylindrical and spherical cavity expansion theories. Where possible, the results were compared with analytical solutions and published field cases. The study revealed that the use of different installation sequences resulted in noticeable differences in the soil responses near existing CMCs as well as the difference in the bending moments generated in the previously installed columns.

A soil-displacement piling rig and a fully instrumented soil tank were also designed and built in the laboratory to simulate column installations and to study the soil behaviour and the responses of previously built columns to nearby installations. A group of concrete columns were cast in-situ in soft soil using low strength concrete. The installation effects in terms of soil behaviours and structural responses of the columns were well captured by 3D laser scanning, soil miniature instrumentation, and a customised strain gauge system installed in CMCs. Test results revealed complex interactions between the soil and the columns, which are otherwise often difficult to observe in the field.

Contents

List of Figures

List of Tables

List of Symbols

The following symbols were used in this thesis:

Δu	excess pore water pressure
Δu_{sp}	excess pore water pressure due to spherical cavity expansion
$\Delta_{z,min}$	smallest width of *FLAC*^{3D} zone
δ	column lateral deflection
κ	swell-recompression index
λ	virgin compression index
ν'	soil's effective Poisson's ratio
ν'_c	Poisson's ratio of concrete
ρ_c	concrete density
ρ_d	dry density of soil
ρ_{sat}	soil saturated unit weight
σ'_1	major principal stress in CMC
σ'_3	minor principal stress in CMC
σ_c	unconfined compressive strength of grout specimen or intact concrete
σ_{st}	indirect tensile strength of grout specimen
σ_t	tensile strength of concrete
$\sigma'_{v,o}$	in-situ vertical effective stress
$\sigma'_{h,o}$	in-situ horizontal effective stress
υ	specific volume
υ_{ref}	reference specific volume
ϕ'_{cs}	soil's effective friction angle
ϕ'	effective friction angle
ϕ'_i	interface friction angle
ψ_c	dilation angle of concrete
---	---
C_c	soil compression index
C_k	permeability change index
C_r	soil recompression index
c'	effective cohesion of soil
c'_i	interface effective adhesion
c_v	vertical coefficient of consolidation

D	CMC or column diameter
d_{pile}	pile diameter
E' or E_s	drained Young's modulus of soil
E_{c}	Young's modulus of concrete
e_o	initial (or current) void ratio
f_{ck}	characteristic cylinder strength of concrete at 28 days
f'_{ck}	characteristic cylindrical strength of grout at 28 days
$f_{\mathrm{ck}}(\mathrm{t})$	characteristic cylinder strength of concrete or grout at age of t days
$f_{\mathrm{ctd,pl}}$	mean tensile strength of plain concrete (e.g. CMC)
f_{ctm}	mean tensile strength of concrete
$f_{\mathrm{ctm\ (t)}}$	mean tensile strength of concrete at t days.
G	shear modulus of soil
G_{s}	specific gravity of soil
I	area moment of inertia
K	bulk modulus of soil
K_0	coefficient of earth pressure at rest
K_{f}	fluid bulk modulus
k *or* k_{h}	hydraulic conductivity of soil
k_{n}	interface normal stiffness
k_{o}	initial permeability
k_{s}	interface shear stiffness
L	column length
M	slope of the critical state line
M *or* $M(z)$	column bending moment
m	Hoek Brown material constant
N	constant in K_0 equation
n	porosity
OCR	over consolidation ratio of soil
p'	mean effective stress of soil
p'_c	pre-consolidation pressure of soil
p'_o	initial mean effective stress in the soil
p'_{ref}	reference pre-consolidation pressure (i.e. 1 kPa)
q	deviatoric stress
R	radial distance from column axis

R_p	radial position of elastic-plastic boundary (cylindrical cavity)
R_{sp}	radial position of elastic-plastic boundary (spherical cavity)
r_{CMC}	CMC radius
r_{c}	column radius
r_f	radius of expanded cavity
r_i	initial radius of cavity
r_{pile}	radius of pile
S	Hoek-Brown material constant
s	column spacing
s_{c}	coefficient taking into account the cement type
s_{u}	undrained shear strength of soil
$u_{\max}$	maximum excess pore water pressure
$\mathrm{u_o}$	in-situ pore water pressure
V	shear force in CMC
V *or* $\mathrm{v_{norm}}$	non-dimensional pile penetration velocity
$\mathrm{v_p}$	vertical pile penetration velocity
$\mathrm{w_p}$	plastic limit
R_p	radial position of elastic-plastic boundary (cylindrical cavity)
R_{sp}	radial position of elastic-plastic boundary (spherical cavity)

CHAPTER 1 Introduction

1.1 Background and Problem Statement

Building contractors and engineers face numerous challenges when designing and building structures over soft soils (Han & Gabr 2002; Liu, Ng & Fei 2007). In most cases, ground improvement works are required to minimise excessive soil settlement and stability issues associated with soft soils. Since the 1970s, piled supported embankments have been a subject of intensive studies (Ghosh, Fatahi & Khabbaz 2016; Hewlett & Randolph 1988; Holmberg 1979; Van Eekelen, Bezuijen & van Tol 2013). In the last 25 years, this geotechnical solution combined with drilled displacement columns (DDC) or controlled modulus columns (CMC) has been one of the most effective ways for reducing short-term and long-term deformations of weak soil under road embankments, warehouses and seaports (Fok et al. 2012; Plomteux, Porbaha & Spaulding 2004; Suleiman et al. 2016).

Unlike stone columns (Ambily & Gandhi 2007; Castro & Karstunen 2010) and deep soil mixing (Huang & Han 2009; Porbaha 1998), CMCs are built in the ground with a piling rig equipped with a hollow displacement auger that displaces the surrounding soils laterally with minimal spoil return to the ground surface (Plomteux, Porbaha & Spaulding 2004). The time for target results using CMC can be compared with other ground improvement methods, referring to Figure 1.1 (Higgins 2014; Larisch, Kelly & Muttuvel 2015).

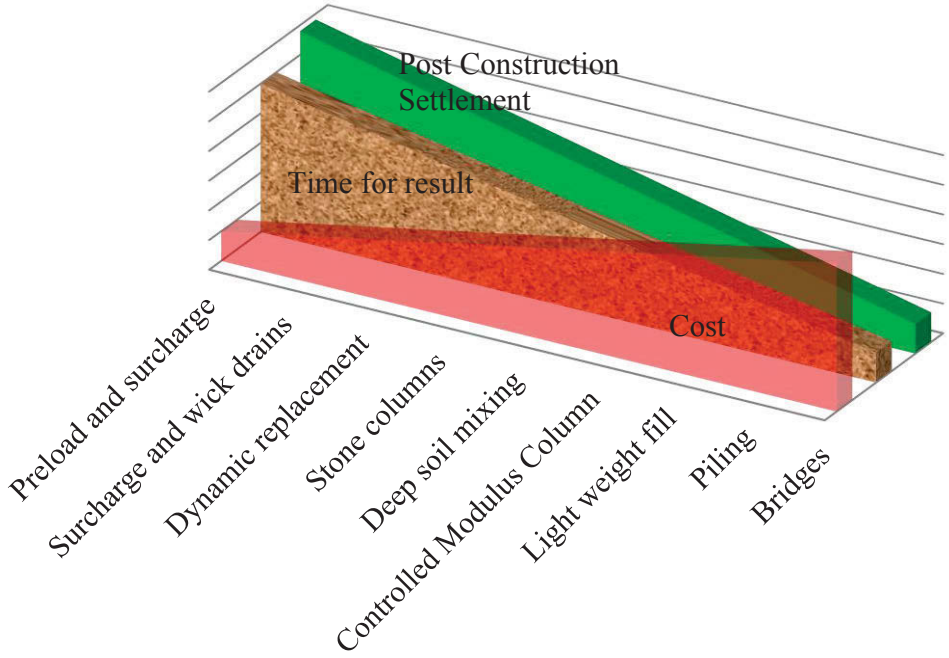

Figure 1.1 Cost, time for the result, and performance considerations of different ground improvement methods (modified after Higgins 2014)

The installation method of CMC can be categorised as full displacement piling similar to driven or jacked piles. These result in substantial reduction in spoil disposal or treatment, and reduce the risk of bored-hole collapsing. The large deformation of soil induced by CMC installation increases the stresses in the ground such that, in theory, they could enhance the load bearing capacity of the rigid inclusions. Figure 1.2 illustrates good quality CMCs with well-formed shafts and regular diameters. The presence of small and localised cracks is generally acceptable similar to the most type of unreinforced concrete structures.

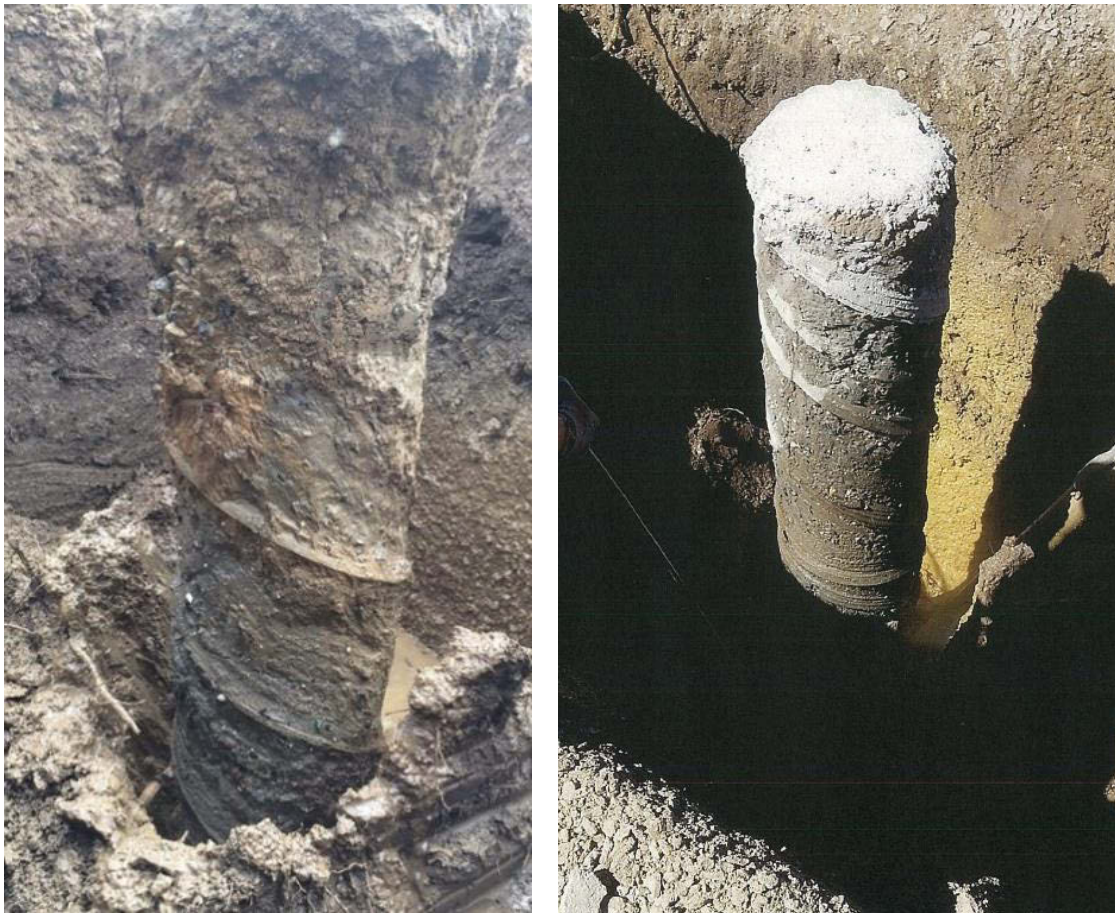

Figure 1.2 Typical shape of excavated columns presenting sound characteristics (Nguyen et al. 2014)

The application of a full displacement piling technique in the column installation process makes CMC ground improvement one of the most cost effective and sustainable methods (Masse et al. 2011; Nguyen et al. 2014). However, loadings associated with the movement of soil due to installation can have an adverse effect on nearby columns installed beforehand (Larisch, Kelly & Muttuvel 2015; Plomteux, Porbaha & Spaulding 2004; Turatsinze & Garros 2008), particularly when the columns are closely spaced.

The risk of damaging the freshly grouted surrounding columns due to nearby installations has been reported in the past (Brown 2005; Hewitt, Summerell & Huang 2009; Plomteux, Porbaha & Spaulding 2004). Newly installed CMCs are susceptible to an imposed load,

due to the slow strength gain of fly ash concrete at early ages (Mehta 2004), low strength intended for ground improvement purposes (McCarthy & Dhir 2005; Plomteux, Porbaha & Spaulding 2004; Turatsinze & Garros 2008), and pre-existing micro-cracks that naturally develop in most concrete. Unless a proper installation sequence is considered, defects and cross-sectional shear failure may develop in the columns, which often lead to damage, loss of verticality, and reduced flexural stiffness (King et al. 2017; Larisch, Kelly & Muttuvel 2015).

Unlike bored piles, the CMC installation process is a closed system and rather difficult for visual observations. According to geotechnical practitioners in New South Wales Australia, cracks most probably developed within some upper 3 m of existing CMCs during nearby CMC installations. This directly affects the construction quality and the long term performance of CMCs. Hence, the above concerns are of practical significance in the process of project planning and feasibility study (Larisch, Kelly & Muttuvel 2015).

Good contracting practice has called for early trials and excavation of "calibration" columns to confirm that the combination of selected design parameters (e.g. grid spacing and the column diameter for a given type of soil) and retained methodology do not present a risk to the structural integrity of the columns installed (Nguyen et al. 2014). While field trials are highly recommended prior to construction commencement (Larisch, Kelly & Muttuvel 2015), ongoing research is required to seek a precise solution to minimise any potential damages on the concrete columns installed by ground-displacement methods.

1.2 Scope and Objectives

This research aims to advance the knowledge of the installation effects of soil-displacement concrete columns for ground improvement works on surrounding soils and previously installed columns, with special interests on the installation sequences and the behaviour of concrete inclusion at the early stage of hardening. In this research, numerical and experimental approaches were carried out with the following specific research scopes and objectives:

1. To provide an insightful review of the current knowledge on the installation effects of soil-displacement concrete columns for ground improvement purposes.
2. To present the results of a 3D large strain numerical approach to compare the effects of using different installation sequences of soil-displacement columns on the surrounding soils and the already-installed columns. The numerical model was based on the theory of cylindrical and spherical cavity expansions and was compared with the existing analytical solutions. The study aims to investigate how the curing periods affected the behaviour of existing CMCs subjected to nearby installations.
3. To present the design, construction and operation of a state-of-the-art instrumented soil tank and a penetration system for the laboratory model test. Cast in-situ reduced scale concrete inclusions were constructed and the installation effects of soil-displacement concrete piles on the surrounding soils and previously installed columns were investigated, with particular interests on the early curing age of the already-placed concrete columns.
4. To validate a numerical model for assessing the installation effects due to soil-displacement installation methods. The proposed numerical model was a large strain numerical approach based on the idea of the combined use of the cylindrical and

spherical cavity expansions. The validation was carried out using the results of the laboratory model test, which explores the evolution of the excess pore water pressure and the consolidation settlement induced by the jacked pile penetration and the subsequent soil consolidation.

5. To explore the practical construction aspects of CMC, and to present a number of sustainability considerations and potential areas in CMC identified for further technological development.

1.3 Thesis Outline

The layout of the thesis is described below:

- Chapter 1 presents the research background, introduces the controlled modulus column (CMC) ground improvement technique or soil-displacement concrete columns, and describes the installation-effect related issues that need to be addressed, along with the aims and scope of the present research.

- Chapter 2 delivers a comprehensive review of the literature relevant to methods of installing CMCs, installation effects of CMC and other full-displacement piling techniques, and effects of using different installation sequences. Existing analytical and numerical approaches to assess installation effects, properties of CMC grout at the early age, and important aspects of physical modelling are reviewed. The findings of this Chapter are summarized and important knowledge gaps are highlighted.

- Chapter 3 describes a numerical approach to investigate how groups of CMC installed in different sequences could affect columns installed previously. Two different installation sequences adopted to assess the effects of installing new columns beside

existing ones are described. Coupled consolidation analyses in large strain mode and incorporating soil-CMC interaction were carried out using the three-dimensional finite difference software package *FLAC*^{3D}. Appropriate plasticity models were used to model soil and CMCs. The validation using various existing analytical methods was presented.

- Chapter 4 presents the results of a large-scale laboratory simulation to investigate the behaviour of concrete columns at various curing ages subjected to loadings from adjacent column installations. The results of the model test were presented in terms of soil heave by 3D soil surface scans, excess pore water pressures, and stress changes and the bending moment induced in the affected column.

- Chapter 5 presents the results of the laboratory model test in which the penetration of a full displacement pile into soft soils was conducted to provide a validation exercise for a proposed numerical model. The large strain numerical approach with a combined use of the cylindrical and spherical cavity expansions are explained. The predicted and measured excess pore water pressure and consolidation settlement are compared and discussed.

- Chapter 6 presents some practical and construction aspects of CMC installation effects. Firstly, the results of a numerical investigation on the CMC installation effect on an existing bridge pile using the three-dimensional finite difference software package *FLAC*^{3D} are presented. Secondly, the key sustainability aspects of using CMC and potential aspects of CMC for further development are discussed.

- Chapter 7 summarises the thesis, together with the key findings and recommendations for future research.

CHAPTER 2 Literature Review

This chapter consists of seven main sections, which survey the existing works on the installation effects of CMCs or drilled displacement columns for ground improvement. Section 2.1 presents the effects of using soil-displacement piling method for CMC ground improvement solution. Section 2.2 discusses several field case studies and reduced-scale model tests on the installation effects of CMC or general drilled displacement columns, with a special interest on the effects of the installation sequences. Section 2.3 presents properties of CMC grout, modelling techniques, and material models.

Section 2.4 presents the analytical methods for assessing installation effects, while Section 2.5 presents the challenges of numerical modelling incorporating the construction sequence. Section 2.6 presents several considerations for laboratory model tests undertaken to investigate the responses of columns due to displacement piling and subsequent grouting. The last section summarises the gap and limitations in the existing literature.

2.1 CMC – Displacement Piling for Ground Improvement

2.1.1 History of CMCs

Since the 1970s, piled supported embankment has been a subject of intensive study (Ghosh, Fatahi & Khabbaz 2016; Hewlett & Randolph 1988; Holmberg 1979; Van Eekelen, Bezuijen & van Tol 2013). The advancement in the ground improvement technology lead to the replacement of expensive traditional piling methods by cost-

effective techniques such as stone columns (Ambily & Gandhi 2007; Castro & Karstunen 2010; Priebe 1995), cement soil mixing (Huang & Han 2009; Nguyen, Fatahi & Khabbaz 2014; Shen, Han & Du 2008), jet grouted columns (Shen et al. 2013; Wang et al. 2013) and drilled displacement piles (Brown 2005).

Since most piled embankment projects have stringent project completion deadlines, concrete rigid inclusions installed by the drilled displacement piling method for ground improvement works have gained increasing popularity. The displacement auger piling methods have a long history since the 1960s (Larisch 2014; Slatter 2000; Van Impe 1988). Various design shapes for the screw displacement augers namely the Atlas pile (Van Impe 1988), Spire pile (Bustamante & Gianeselli 1998), De Waal pile, and Omega pile (Kurian & Shah 2009; Van Impe 1988) were proposed in the past.

Developed in France by Menard Soltraitement in 1994 and patented in the USA (Cognon 2004; Masse et al. 2017), CMC may be regarded as the second generation of screw displacement piling techniques for ground improvement. Despite using a similar auger concept as the previous auger design, the design innovation in CMC has been advanced further in terms of efficiency. Today, variations of this technique in terms of auger shapes or construction process include Controlled Stiffness Columns (CSC), Drilled Displacement Columns (DDC) (Larisch, Kelly & Muttuvel 2015) and Concrete Injected Columns (CIC) (Hewitt, Summerell & Huang 2009; Hsi 2008).

In the last 25 years, CMC has been widely used as an effective ground improvement technique to strengthen soft soil in road construction areas and has been described well in the texts by Plomteux, Porbaha & Spaulding (2004) and Pearlman & Porbaha (2006), amongst others. The technique has been used considerably in Europe with increasing

popularity in the USA, Australia, and Asia. A selected number of successful CMC projects in the world are summarised in Table 2.1.

Table 2.1 CMC ground improvement projects

Project	**Location**	**Reference**
Kempsey Bypass Alliance – North Approach of McCleay River Bridge	New South Wales, Australia	Wong & Muttuvel (2012a)
The Breakwater Road Realignment - construction of a 640 m long multi-span bridge over the Barwon River	Victoria, Australia	Fok et al. (2012)
Freeway construction as part of the European route E372	Lublin, Poland	Michalowski et al. (2018)
Nouvelle Autoroute 30 Project in Beauharnois, Quebec - Beauharnois Canal Bridge	Quebec City, Canada	Chatte & Lauzon (2011)
Garden State Parkway Bridge over Mullica River	New Jersey, United States	Wilson-Fahmy, Ro & Leiendecker (2011)

2.1.2 CMC Displacement Auger

As illustrated in Figure 2.1, the displacement auger consists of three segments: (*i*) the lowest segment has two pitches of screw flange, (*ii*) the middle segment also has screw flanges but welded with vertical blades and (*iii*) the uppermost portion has a larger core diameter with thin screw flange and a reverse helix (Cognon 2004; Masse et al. 2017). As the auger penetrates the ground, the cuttings at the auger tip are carried upwards between auger flights of segment *i*. At segments *ii* and *iii*, the presence of the vertical blades and the discontinuity of the auger flight of the upper large displacement body prevent soils from moving upward in the spiral flight, and force soils to move outwards. As result, the installation process does not generate spoils to the ground surface.

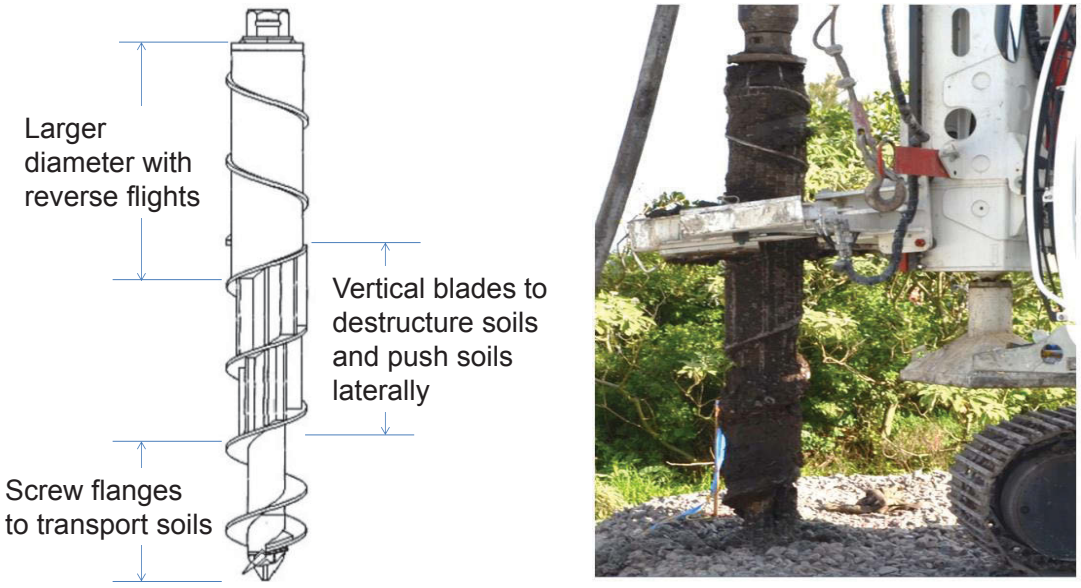

(a) *(b)*

Figure 2.1 CMC auger: (a) Patented hollow displacement auger (modified after Cognon 2004) (b) Displacement auger at the Gerringong Project site in NSW, Australia

2.1.3 CMC Installation Process

Prior to CMC installation, a granular working platform is constructed for the safe operation of CMC rig. The CMC rig has powerful thrust and is equipped with a displacement auger attached to the Kelly bar (Figure 2.2). The column installation process involves penetration of a displacement auger into the ground under the torque and downward thrust provided by the drilling rig (Figure 2.2); followed by grout injection through the hollow stem of the drilling tool while the drilling tool is withdrawn. During concrete injection, a medium pressure was used to pump the concrete Figure 2.3. Larisch, Kelly & Muttuvel (2015) indicated that the average concrete overconsumption of approximately 28% during drilled displacement installation, mostly occurring in soft soil.

Columns are often installed through the weak soil layer and embedded at least 0.5m into the stiffer ground. In practice, auger penetration continues 0.5 m to 1 m after substantially increased resistance to drilling is encountered (Michalowski et al. 2018). Menard was able to install up to 40 m long Controlled Modulus Columns during construction of oil tanks in Raceland, Louisiana, US.

Figure 2.2 A CMC piling rig used in Gerringong, NSW, Australia

Figure 2.3 A piling rig for CMC construction with a mast length of 25.2 m (photo courtesy of Menard GMBH)

In most cases, a CMC is a non-reinforced concrete inclusion installed in the ground to reduce the loads on the foundation soils, especially weak or unsuitable grounds. Besides CMC rigid inclusions, a load transfer platform (LTP) over the soil-column matrix helps reducing differential settlement and transferring loads to columns towards the stiff stratum (Figure 2.4). The diameter of CMC (d_{CMC}) varies from 0.3 m to 0.45 m and the column spacing varies from 1.35 m (or 3× d_{CMC}) to 2.25 m (or 5× d_{CMC}). CMCs are often arranged in square or triangle patterns (Fok et al. 2012) and the spacing may be variable to provide transition zones (Hsi 2008).

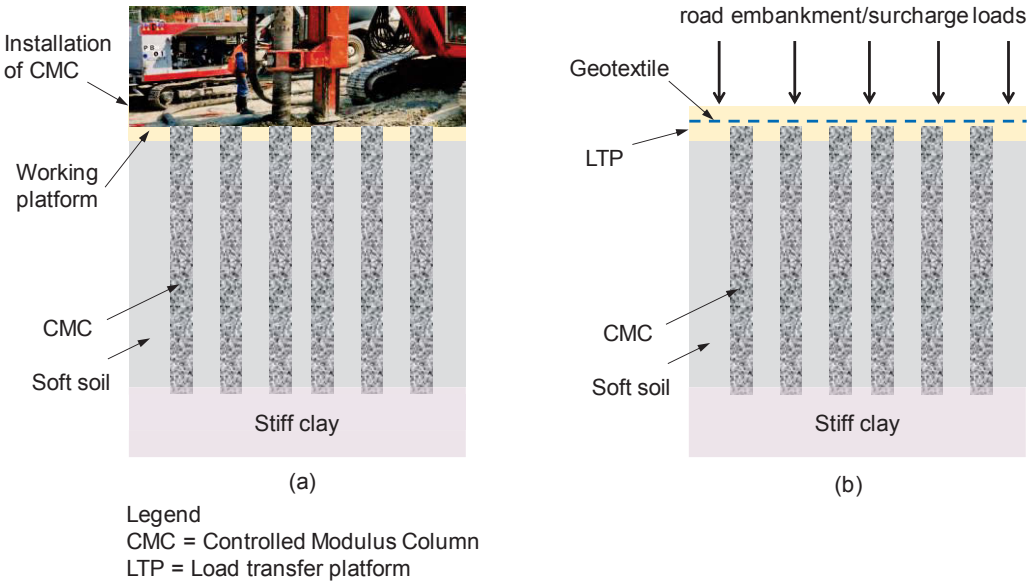

Figure 2.4 CMC ground improvement method: (a) installation of CMC, and (b) construction of LTP after columns installation

The typical applications of CMC involve bridge approach embankments (Figure 2.5), port development and warehouse foundation with the aim to reduce both total and differential settlements and to accelerate construction (Fok et al. 2012; Wong & Muttuvel 2012b).

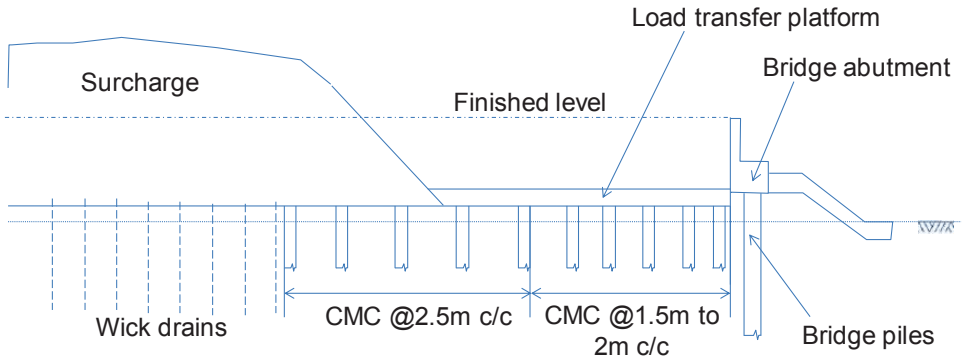

Figure 2.5 Typical ground improvement design along the bridge approach embankment

Since auger continuously supports the soils during installation, the risk of borehole cave-in and necking is reduced as compared to the bored pile method (Pearlman 2012). Experience shows that many bored piling projects suffered extended delay due to the unforeseen ground conditions. In addition, as auger displaces the soil aside, the generation

of minimal soil cuttings contributes towards sustainability (Masse et al. 2011; Michalowski et al. 2018; Suleiman et al. 2016). This feature is particularly essential for construction projects involving contaminated or landfill sites, acid sulphate soils or soils with significant organic contents, where reduction of cost for spoil disposal and handling can be achieved, as compared to the contiguous flight auger (CFA) piling or bored piles (Masse et al. 2011; Walker, Masse & Swift 2011).

2.2 Installation Effects and Installation Sequence

2.2.1 Construction Site at an Elementary School in the USA

Field investigation to study the installation effects of CMC on the surrounding soils has been reported by Suleiman et al. (2016). The field study consisted of installing one 320 mm-diameter CMC and four surrounding reinforced CMCs with a diameter of 395 mm. The diameter of these CMCs is generally smaller than the CMC size used in Australia. The ground consisted of 1.2 m thick sand, over very soft sandy organic soils extending to a depth of approximately 7.6 m, which overlay bedrock. The groundwater table was found at 1.6 m below ground surface. The standard penetration test (SPT) results indicate the presence of soft clay with recorded SPT N values was zero. The results of several triaxial and consolidation tests were provided. The CMCs were installed in very soft sandy organic soils until auger refusal.

Suleiman et al. (2016) installed four push-in pressure sensors at 2 m depth and four shape acceleration arrays (SAA) to capture stress, pore water pressure and the lateral displacement in soft silty soil throughout column installation and static load test. Four SAAs were installed together with a polyvinyl chloride (PVC) casing into a predrilled hole. One SAA was customised and did not fit well with the casing, and hence did not give good results. The study revealed the followings:

- The zone affected by the CMC installation extended to 4R to 6R (R is the CMC radius) from the outer surface of the CMC shaft.
- Pressure sensors and shape acceleration arrays indicated that the surrounding soils experienced an increase in horizontal stresses and lateral movement throughout the CMC installation.
- At the end of CMC installation, the readings from the pressure sensors indicated an increase in the horizontal soil stress by 2 kPa recorded within 1D (i.e. one diameter) distance from the CMC, by 8 kPa within 2D distance, and then with decreasing trend with increasing distance from the CMC. This result may not necessarily incorrect or unreasonable, but it indicates that the results may be influenced by the accuracy and reliability of the equipment.
- Some stress relaxation by approximately 2 kPa to 3 kPa was recorded at the end of the installation. After installation, the stress recorded around the central CMC increased and was greater than stresses recorded at the end of the installation.
- The maximum soil displacements recorded at radial distances of 450 mm, 750 mm and 1050 mm from the centre of the CMC were approximately 13 mm, 8 mm and 3 mm, respectively.
- The recorded soil displacement showed a clear decreasing trend with increasing distance from the CMC. The excess pore water pressure also fell quickly.

While there have been many research papers published on CMCs, the field study by Suleiman et al. (2016) is one of the first major in-depth research works on installation effects. However, this study only investigated the short-term effects of CMC installation and construction sequences were not considered. Since the soil contained a large amount of silt and sand, the excess pore water pressure dissipated quickly after installation. Although the speed of installation was fast, it is believed that the excess pore water

pressure generated during installation had partially dissipated by the time the installation was completed.

2.2.2 Channel Tunnel Rail Link (CTRL)

At the Tank Hill Road South Embankment project in the UK, CMCs were used to improve the very soft ground under the access embankment of a road crossing over the Channel Tunnel Rail Link (CTRL). The columns were arranged in a square pattern and the column spacing varied from 1 m to 1.7 m. The column lengths varied from 7.5 m to 12.5 m.

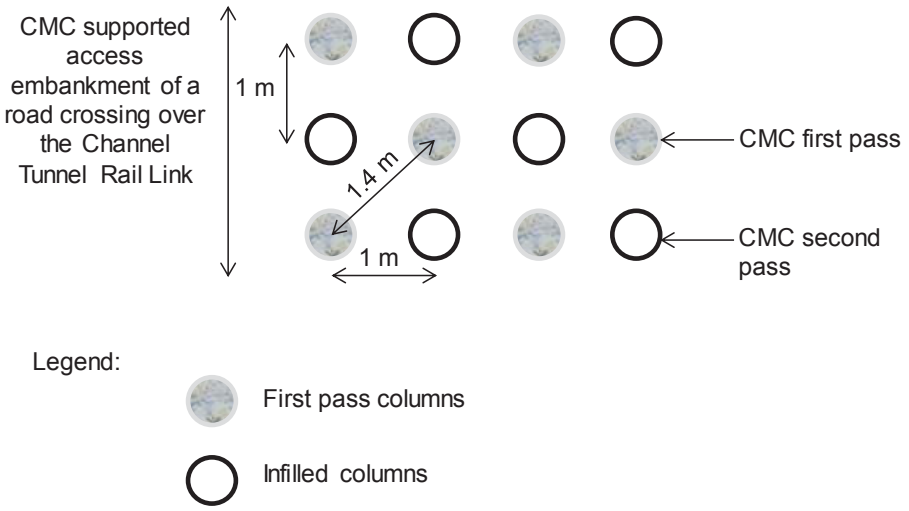

Figure 2.6 Installation sequence to avoid damage to adjacent freshly grouted columns (modified after Plomteux, Porbaha & Spaulding 2004)

Within the area of densely spaced CMCs, Plomteux, Porbaha & Spaulding (2004) highlighted the risk of damaging the freshly grouted columns. As shown in Figure 2.6 the proposed construction method was modified with CMCs installed in two different interleave passes, each with 1.4 m × 1.4 m grids. No integrity tests or load test results were reported by the authors.

2.2.3 Coopernook to Herons Creek Alliance Project

Drilled displacement columns were used to reduce settlement at the bridge approach abutment as part of the Coopernook to Herons Creek Alliance project. The columns had a diameter of 375 mm, and were arranged in a square pattern with column spacing as shown in Figure 2.7. During column installations, Hewitt, Summerell & Huang (2009) adopted a construction sequence similar to Plomteux, Porbaha & Spaulding (2004) to minimise the damage caused to the previously installed columns. The columns were installed in two interleave passes, as shown in Figure 2.7.

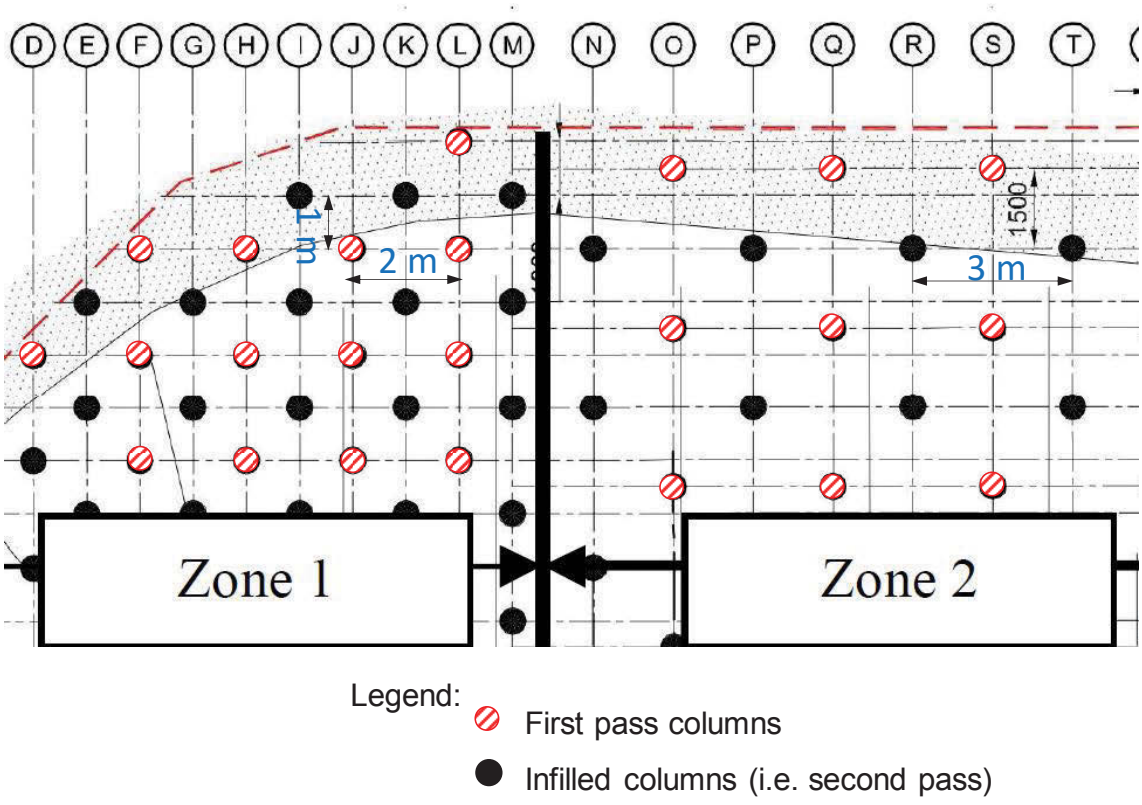

Figure 2.7 Column installation with two different interleave passes at the Camden Haven north bridge approach (after Hewitt, Summerell & Huang 2009)

In this bridge duplication works, the soil heave and lateral displacement induced by new column installations may affect the existing bridge abutment and its approach embankment. The installation sequence allowed columns closer to the existing

embankment to be installed first and then the rig worked away from the existing embankment to avoid accumulated installation-induced stresses. Using the adopted installation sequence, the soil heave of less than 50 mm was observed during column installations. The existing bridge structures and embankment was not affected by the column installations.

Concrete coring and ultrasonic integrity tests were carried out to confirm the quality of the as-built plain concrete columns and to check if any crack was present. Tests results indicated that in some columns, cracking was developed within the upper column shaft but it was unclear about the cause of the cracking. One of the possible reasons could come from the load applied by tracking the rig over the recently completed columns.

2.2.4 Upgrade of a Motorway Interchange in Australia

Larisch, Kelly & Muttuvel (2015) reported a case study involving installations of 450 mm diameter drilled displacement piles at a site underlain by up to 18 m thick soft soil. The near-surface soil was either 1.5 m thick fill platform or by up to 3.5 m thick settled embankment fill. The columns were installed in a 4D or 5D c/c square pattern (where D denotes the diameter of the column). The depth of the columns ranged from 16 m to 25 m, including a 2 m embedment in stiff clay.

As demonstrated by Larisch, Kelly & Muttuvel (2015), trials were requested by the client to investigate the installation effect. As shown in Figure 2.8, four columns were installed in the following sequence: P1, P2, P3 and then P4; and the uplift and horizontal movement of the column head were monitored as installations proceeded. The results shown in the same figure indicated that the uplifts of two out of four columns were substantial and exceeded 100 mm, which was four times greater than the maximum horizontal

displacement of the column heads. It is interesting to note that the horizontal movement of column heads may be superimposed after each subsequently installed column.

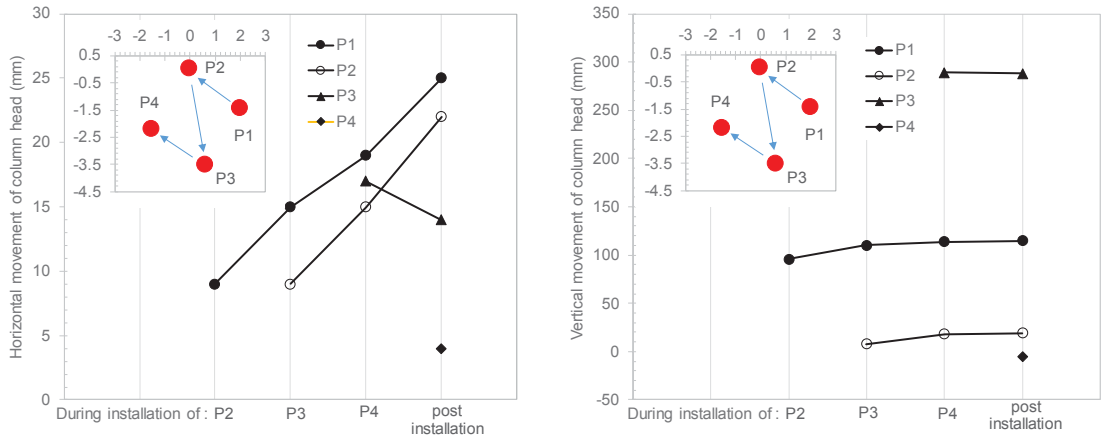

Figure 2.8 Movement of the column head: (a) Horizontal movement, and (b) uplift; (plotted using data from Larisch, Kelly & Muttuvel 2015)

Larisch, Kelly & Muttuvel (2015) also reported trials to optimise the column installation sequence to minimise column deformations induced by the subsequent installations. As shown in Figure 2.9, the installation sequence was: zigzag with AC115 first, then AD116, AC117, AD118, and AC119; then "hit and miss" tactic in a straight line: AD120, AD122 and finally AD124. After installations of these columns (i.e. zigzag pattern), the measured uplift and horizontal movement of the column head ranged from 29 mm to 122 mm and from 6 mm to 14 mm, respectively.

For the pattern (b), the measured uplift and horizontal movement of the column heads ranged from 7 mm to 11 mm and from 5 mm to 10 mm, respectively. The comparison indicated that the zigzag pattern induced greater column head movement than those measured when columns were installed in a straight line, especially with respect to the uplift. Hence, installation sequence as "hit and miss" pattern in a straight line was adopted for the project.

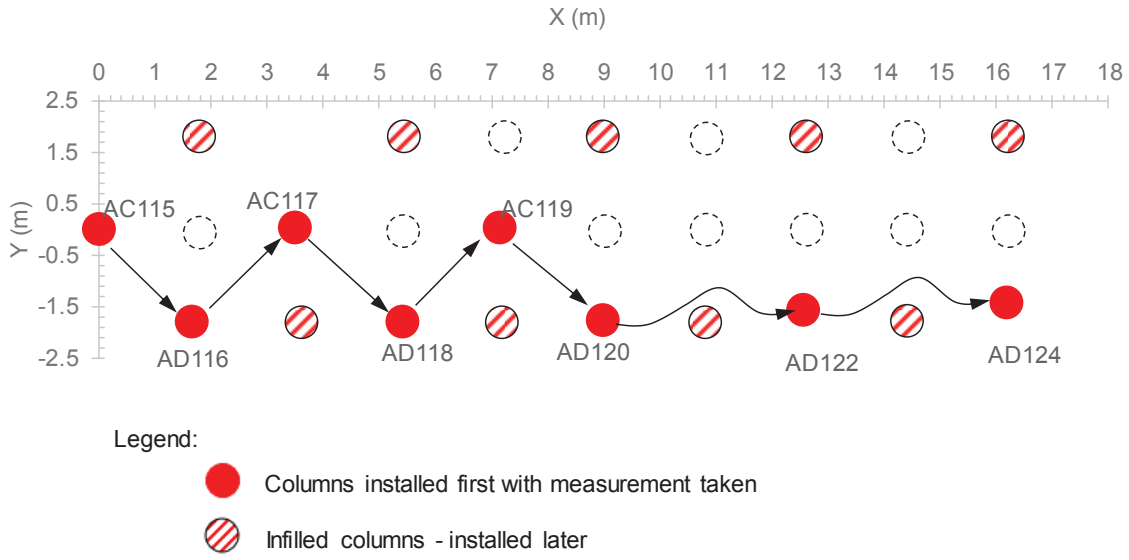

Figure 2.9 Column pattern and installation sequence (after Larisch, Kelly & Muttuvel 2015)

2.2.5 Bridge Approach for a Highway Upgrade Project

This case study involved installing up to 8 m long drilled displacement columns in alluvial deposits with interbedded clay and sands, underlain by extremely weathered bedrock. The thickness of the weak soils within the northern bridge approach ranged from 6 m to 7 m. The adopted column diameter D was 450 mm and the column spacing was 3.5D (i.e. 1.6 m). The concrete overconsumption for the entire project was in the range of 20%.

Trials were carried out to achieve an optimal construction sequence for minimum soil lateral movement. Initially, 17 columns were installed in a trial in a “hit and miss” approach in a straight line. Measured lateral soil movements by inclinometers near the installation site were between 15 mm and 20 mm with visually observed soil heave less than 100 mm. The insignificant ground movements were attributed to the improved drained behaviour due to sand lenses. Therefore, the construction sequence was revised to installations in a straight line continuously, instead of the initially adopted “hit and miss” pattern. The low strain integrity tests for 2% total columns indicated that cracks

and damage were found in two out of 23 columns. The record during installation showed low concrete pressure at depth. However, there was no evidence of column cracking caused by the dynamic load tests.

2.2.6 Large Embankment for Highway Upgrade

The third case study reported by Larisch, Kelly & Muttuvel (2015) involved installing a grid of 450 mm diameter drilled displacement columns at a spacing of 1.3 m c/c (that is less than 3D). The average depth of the column was 12.5 m and embedded into medium-dense sand or stiff to very stiff/hard clay. Due to a very close column spacing, the observed heave was significant. In addition, a pile located at a distance of 5 m from the installation sites moved laterally by 150 mm, which demonstrated the installation effect.

To reduce the risk of the freshly cast columns being damaged by nearby installations, the initial sequential order of installation was to leave at least 10D or 4.5 m spacing between the centres of the freshly cast columns. The infilled columns were installed a few days later. Although no severe crack was detected by integrity tests, the adopted installation sequence caused severe site congestions and construction delays. The final adopted sequence was to install columns in a straight line in a sequence that missed at least one column. With the addition of a single bar of steel reinforcement for each column, no severe crack was observed.

2.2.7 Model Test on Displacement Augers

A small-scale laboratory experiment was conducted by Hird, Ni & Guymer (2011) to study the movement of transparent synthetic soil during the penetration of a miniature displacement auger as shown in Figure 2.10b. The soil was contained in a chamber with observable window, which allowed the displacement field to be captured by photographs.

The movement of the soil around the displacement auger was analysed using "particle image velocimetry" (PIV) technique. PIV allows simulating screw displacement auger without the use of on-sample instrumentation. The following important observations were made:

- The soil beneath and around the tip of the auger was displaced downwards and outwards in a similar manner as would be observed for a cylindrical straight-sided pushed pile.
- The soil displacement depends on the rotation speed of the auger and the penetration rate.
- For the auger used in Figure 2.10b, the soil was transported upwards on the flights away from the tip, then forced to move out around the shoulder of the auger, and finally moved back to the smaller stem of the auger.
- The soil displacement observed agreed well with the shallow strain path method.
- Small-scale models may provide roughly similar trends of lateral displacements in full-scale field tests.

Only soil displacement during auger penetration was considered in this research as the concreting stage could not be simulated realistically. Some boundary effects were present as the model size was relatively small (50 mm by 100 mm in plan and 200 mm high). It is noted that the miniature displacement auger used for this study is shown in Figure 2.10b, as compared to the Menard CMC auger, as shown in Figure 2.10a.

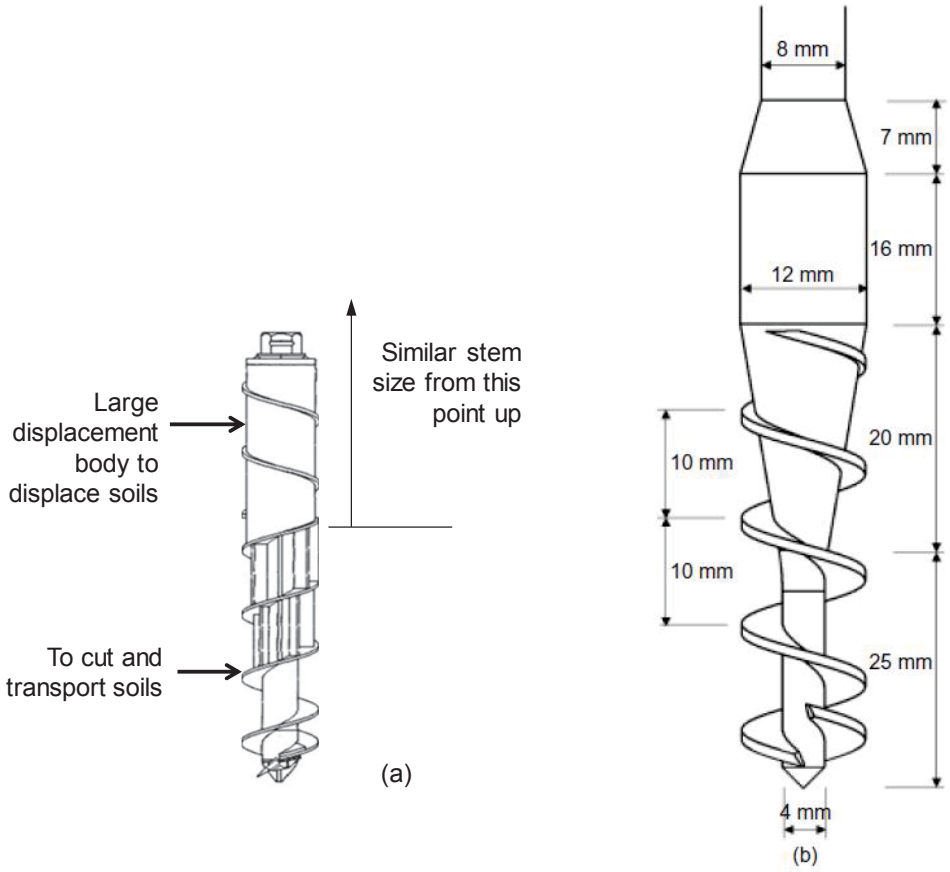

Figure 2.10 Comparison between (a) CMC auger (Cognon 2004; Masse et al. 2017) and the rotary displacement auger with large displacement body (Hird, Ni & Guymer 2011; Skinner et al. 2003)

2.2.8 Summary

As pointed out by Hewitt, Summerell & Huang (2009), the direction of installation progress is important to avoid damage to the existing sensitive structures or newly formed columns. Caution has been taken by practitioners in the past to minimise the unnecessary impact of CMC installations on the existing structures or the freshly cast concrete columns. To account for the site specific geology and project requirements, Larisch, Kelly & Muttuvel (2015) suggested that trials be carried out prior to construction to optimise installation sequence. The following construction practices are often adopted by the piling contractors and building contractors:

- Installing columns initially at a wider grid than design, then progressively filling in to form the design grid; or
- Starting from the centre and working radially outwards in a uniform manner to reduce the risk of causing lateral ground movement in a concentric direction; or
- Starting column installation near the existing structures and then working away from the previously installed columns; or
- Modifying the patterns of installation: The convention of installing columns in the straight line may be modified to become "hit and miss", zig-zag pattern or a combination of both patterns.

A solid justification for the installation sequence may be required and how efficient they were in comparison to other possible installation patterns. Optimisation of the CMC installation patterns requires (1) field trial; (2) accurate assessments of the lateral displacement of the surrounding soils due to column installation, specific to CMC technique; (3) good soil characterisations; and (4) understanding of the soil structure interaction.

2.3 CMC Grout and Properties at Early Age

2.3.1 Grout Mixture

According to Fok et al. (2012), CMC grout mixes typically vary depending on the location of the project and the local availability of the materials, but typically comprise a blend of cement and fly ash, a homogeneous mixture of sands and gravels between 2 and 7 mm and addictive for workability and fluidity. For example, for the Breakwater Road Alignment project in Victoria, Australia the dry component of CMC mix contains fly ash, cement and local sands (Menard Bachy 2012). As a pumpable mix, CMC grout contains

small aggregate or just sands and hence, is termed “lean sand-mix” mortar or pea-gravel concrete (Masse, Brockbank & Pearlman 2004).

2.3.2 Strength and Stiffness

2.3.2.1 Compressive Strength of CMC

Grout specimens after curing periods of 1, 7, 28 and 56 days are tested to determine the cylinder compressive strength (AS 1012.9) and indirect splitting tensile strength (AS 1012.10). The 28 day unconfined compressive strength f_{ck} of CMC grout may vary between 7 and 30 MPa (Cirión et al. 2013; Fok et al. 2012; Masse et al. 2011; Plomteux, Porbaha & Spaulding 2004; Wong & Muttuvel 2012a) for different applications. In a recent CMC project in Poland, according to Michalowski et al. (2018), the concrete used in columns without reinforcement was specified as Class C12/15, with compressive strength f_{ck} = 12 MPa and elastic modulus of E_{cm} = 27 GPa.

Figure 2.11 CMC grout at Gerringong Project site in NSW Australia

Figure 2.12 Drilled displacement columns installed at Camden Haven River bridge, New South Wales, Australia (after Hewitt, Summerell & Huang 2009)

Grout develops its strength from the fresh state (Figure 2.11) to the hardened state (Figure 2.12) and its compressive strength increases with time. As recommended by Eurocode 2 (2015), the compressive strength of concrete at a concrete age of *t* older than 3 days can be estimated using Equation (2.1) and the 28 day unconfined compressive strength f_{ck} of CMC grout.

$$\mathrm{f_{ck}(t)} = exp\left\{\mathrm{s_c}\left[1-\left(\frac{28}{\mathrm{t}}\right)^{\frac{1}{2}}\right]\right\}(\mathrm{f_{ck}}+8)-8 \text{ (in MPa)} \qquad (2.1)$$

where $3 < t < 28$ days and the coefficient $s_c = 0.31$ considering the low strength cement used in CMC grout production. The compressive strength $f_{ck}(t)$ at the concrete age 3 days or earlier can be obtained from the test data or from existing literature (Bazzar, Bouatiaoui & Alaoui 2013; Huang et al. 2013; Lam, Wong & Poon 2000; McCarthy & Dhir 2005; Naik et al. 2003; Siddique 2004; Smith 1991; Yoshitake et al. 2014) applicable to the characteristics of CMC grout (e.g. a 50% replacement of cement with fly ash and a water/binder ratio of approximately 0.5).

2.3.2.2 Tensile strength of CMC

Larisch, Kelly & Muttuvel (2015) reported a case study where Abaqus analyses were carried out with columns subject to vertical loads, possibly equal to the full embankment height. They found that the cracks were flexural and not shear, as shown in Figure 2.13.

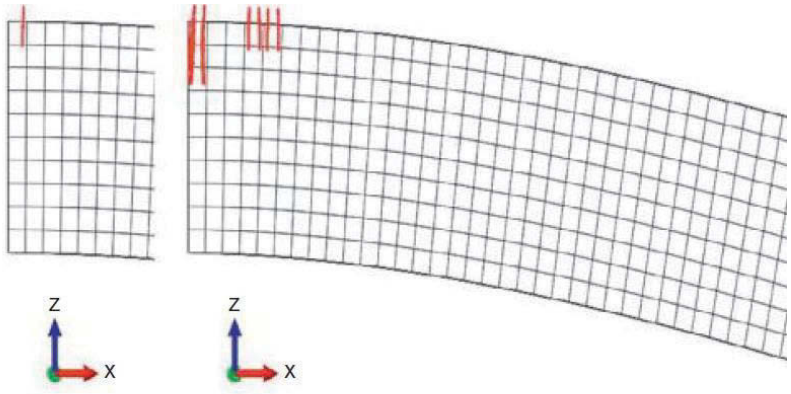

Figure 2.13 Crack initiation and development in DDC columns (after Larisch, Kelly & Muttuvel 2015)

The most important characteristic of CMC grout for lateral column resistance – the CMC tensile strength can be estimated based on Eurocode 2 recommendations for plain concrete. Clough et al. (1981) indicated that the tensile strength of a cemented sand is about 10% of the unconfined compressive strength. The mean tensile strength $f_{ctm}(t)$ at an age of t days can be estimated from Equation (2.2) (2015).

$$\mathrm{f_{ctm}}(t) = exp\left\{\mathrm{s_c}\left[1-\left(\frac{28}{\mathrm{t}}\right)^{\frac{1}{2}}\right]\right\} \times 0.3\mathrm{f_{ck}^{\frac{2}{3}}} \qquad (2.2)$$

The tensile strength of plain concrete (e.g. CMC) can be estimated using Equation (2.3) (BS EN 1992-1-1 2015).

$$f_{ctd,pl} = \frac{\alpha_{ct,pl} \times f_{ctk,0.05}}{\gamma_C \times k_f} \quad (2.3)$$

where $f_{ctk,0.05}$ = characteristic tensile strength of concrete = 0.7× $f_{ctm}(t)$; $\alpha_{ct,pl}$ = is a reduction factor that accounts for the long term effects on tensile strength ($\alpha_{ct,pl}$ = 0.8); γ_C = factor applied for ultimate limit state design (γ_C=1.5); and k_f = factor to obtain the design resistance of cast in place piles (k_f=1.1). In practice CMCs are often designed assuming no tensile stress in the CMC material (Plomteux & Lacazedieu 2007; Wong & Muttuvel 2012a).

2.3.2.3 Stiffness of CMC

Made from low strength concrete, CMC is clearly a quick solution to reduce short-term and long-term post construction settlement and fast-track the bridge construction (Plomteux & Lacazedieu 2007). For comparison, the performance of stone columns depends on the degree of compaction of the materials in the columns (Plomteux, Porbaha & Spaulding 2004; Poorooshasb & Meyerhof 1997).

According to Sideris, Manita & Sideris (2004), Young's modulus (E_c) and Poisson's ratio (ν) values can be estimated from the compressive strength of concrete, which increases with time. The modulus of elasticity of CMC, E_c estimated from f_{ck} based on Eurocode 2 should only be regarded as indicative, especially for geotechnical applications (BS EN 1992-1-1 2015). As recommended by the ASIRI project for rigid inclusions (2012), a long term modulus of elasticity of approximately 10 GPa can be used for concrete inclusions fabricated in-situ with a displacement piling method, for a f_{ck} varying from 12 MPa to 20 MPa. This value can be obtained using Equation (2.4) (Bétons de sable 1994).

$$E_c = 3700 \times f_{ck}^{1/3} \text{ in MPa} \quad (2.4)$$

The modulus of elasticity of concrete at age of t days, $E_c(t)$ was determined based on Equation (2.4) and by adopting the compressive strength $f_{ck}(t)$ at age t in MPa.

2.3.3 Material Models

Concrete structures are often modelled using linear elastic properties, since the applied loading is normally below the yield strength limit. The stress-strain curve is linear and path-independent, with reversible deformations upon unloading. The strain increments generate the stress increments according to the linear and reversible law of Hooke's law, which is described by two elastic parameters: bulk modulus K and shear modulus G (Itasca 2012). However, for low strength concrete, an elastic-plastic model should be used especially when the external load is likely to exceed the yield stress of the concrete. According to ASIRI National Project (2012), besides an elastic model, a material-specific failure criteria should be introduced for the inclusions. According to PLAXIS (Brinkgreve, Kumarswamy & Swolfs 2016), the elastic-perfectly plastic model with Mohr Coulomb yield criteria is the best available option to describe the behaviour of concrete. This model, however, requires determination of the two strength parameters of concrete, cohesion c' and internal friction angle, ϕ', which are not often available. Another constitutive model described in this section is the modified Hoek Brown criterion, and its parameters may be obtained from the conventional laboratory strength tests.

2.3.3.1 Linear Elastic-Perfectly Plastic Model

As shown in Figure 2.14, the plasticity model with Mohr Coulomb yield criterion has the composite yield criteria, consisting of (a) the Mohr Coulomb failure criterion and (b) the tension failure criterion.

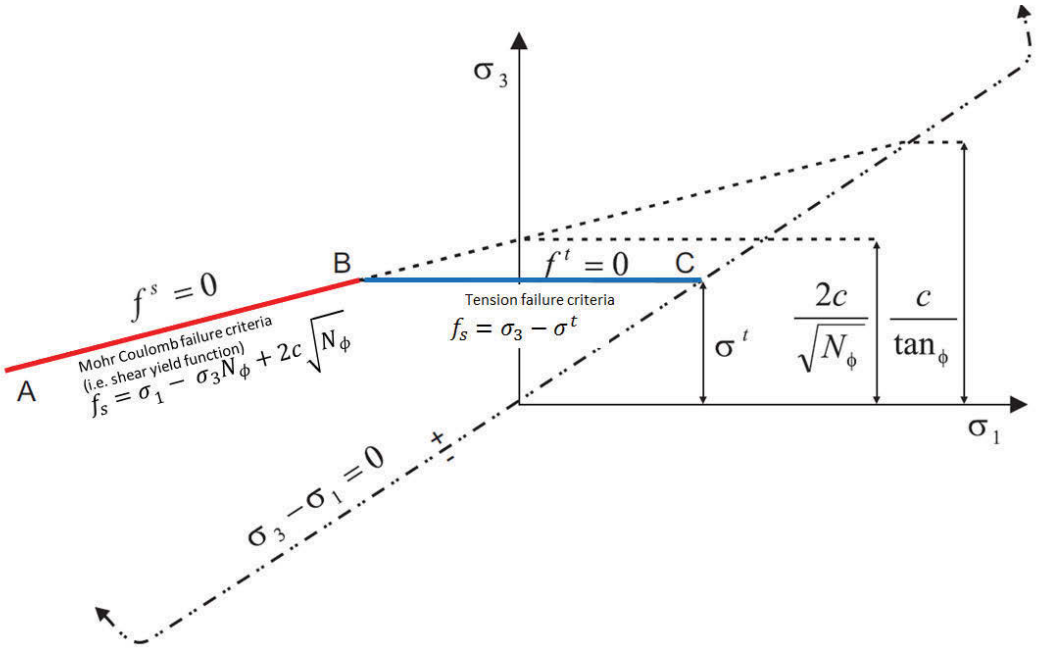

Figure 2.14 FLAC^{3D} Mohr-Coulomb failure criterion (modified after Itasca 2012)

If the stress state does not violate any yield criterion, i.e. stress state lies below the representation of the composite failure envelope in the plane $[\sigma_1, \sigma_3]$ then no plastic flow takes place. If the stress state violates the yield criterion, then either shear failure or tensile failure will take place. The shear yield can be detected if the stress state satisfies Equation (2.5).

$$f_s = \sigma_1 - \sigma_3 N_\phi + 2c\sqrt{N_\phi} < 0 \qquad (2.5)$$

where

$$N_\phi = \frac{1 + \sin\phi}{1 - \sin\phi}$$

σ_3= minor principal stress and σ_1= major principal stress; and

ϕ = friction angle and c = cohesion.

Tensile yield is detected if $f_t = \sigma_3 - \sigma_t > 0$. Tensile strength σ_t cannot exceed the value of σ_3. The maximum value input for the soil tensile strength, σ_{max}^t is shown in Equation

(2.6). Soil tensile strength σ^t defined as the resistance offered by the material to the forces tending to induce cracks is small compared to the compressive strength.

$$\sigma^{t}_{max} = \frac{c}{tan\,\phi} \tag{2.6}$$

If plastic flow occurs, i.e. stress gone beyond yield strength, strain increments can be decomposed into elastic part and plastic part. The direction of the plastic-strain increment vector is specified using a flow rule. Such vectors are normal to the some "potential surface" defined by "potential functions". Shear plastic flow and tensile plastic flow are defined by two potential functions: $g^s = \sigma_1 - \sigma_3 N_\psi$ and $g^t = -\sigma_3$, respectively, where $N_\psi = \frac{1+\sin\psi}{1-\sin\psi}$.

The shear-plastic flow in *FLAC*^{3D} Mohr Coulomb model obeys a non-associated flow rule because the yield envelope function f_s is different to the potential function g_s. On the other hand, the tensile plastic flow obeys an associated flow rule.

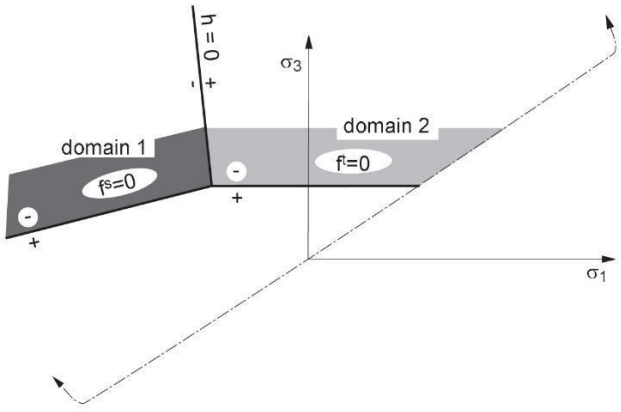

Figure 2.15 Domains used in the definition of flow rule (after Itasca 2012)

If the stress state falls within Domain 1, shear yield failure occurs (Figure 2.15). Stress point is placed on the curve $f_s = 0$ using the flow rule derived using the potential function g^s. The same applied to stress state lies in Domain 2.

The response of the material is modelled via "shear dilatancy", which means volume change occurring with shear distortion. This dilatancy is characterised by the dilation angle, ψ, which relates plastic volume change to plastic shear strain. Dilation angles are typically determined from triaxial or shear-box tests. The default value for dilation angle is zero for all the models in *FLAC*^{3D}.

In addition to the mass density ρ, shear modulus G and bulk modulus K, parameters associated with *FLAC*^{3D} Mohr Coulomb yield criteria include cohesion (c'), angle of shearing resistance (ϕ') and dilatancy angle (ψ) to describe the plastic (failure) part of the model; and soil tensile strength, σ^t. Typical values for dilation angle varies from 0 for normally consolidated clay, 12 for concrete, to 15 for dense sand (Vermeer & De Borst 1984). The model with Mohr Coulomb yield criteria can be used to describe the CMC grout in various stages. Typical elastic modulus and compressive strength of the CMC columns used in practice is summarised in Table 2.2.

Table 2.2 Typical parameters for modelling CMC columns

Reference	***E* (MPa)**	***UCS* (MPa)**	ν	c' **(kPa)**	ϕ' **(º)**
Wong & Muttuvel (2012b)	200 (cracked element)	10 to 15	0.25	50	30
Cirión et al. (2013)	5,000 to 10,000	10 to 15	-	-	-
Plomteux, Porbaha & Spaulding (2004)	11,000	>11	-	-	-
Fok et al. (2012)	5,000	10	-	-	-
Masse et al. (2011)	-	6.9 and 20.7			

Note: E = elastic modulus, UCS = unconfined compressive strength at 28 days, ν = Possion's ratio, c = soil cohesion, and ϕ' = friction angle.

2.3.3.2 Modified Hoek-Brown Material Model

Originally developed for rock mass, the Hoek-Brown criteria (Hoek & Brown 1980) as shown in Equation (2.7) can also be used to model a brittle material such as concrete because it can be considered as one special type of rock, e.g. medium strong claystone, shale or siltstone (Hoek & Brown 1997). In fact, a number of authors adopted the Hoek-Brown criterion to model concrete (Karam & Tabbara 2009; Wu & Zhou 2010).

$$\frac{\sigma_1}{\sigma_c} = \frac{\sigma_3}{\sigma_c} + \sqrt{m\frac{\sigma_3}{\sigma_c} + s} \tag{2.7}$$

where σ_1 and σ_3 = major and minor principal stresses at failure, σ_c = uniaxial compressive strength of intact rock pieces, and m and s = Hoek-Brown material constants.

In *FLAC*^{3D}, the plasticity model incorporates nonlinear Hoek - Brown yield criterion (Hoek & Brown 1980) combined with a tensile yield criterion. *FLAC*^{3D} defines the onset of tensile yielding where the minor principal stresses σ_3 (or the tensile stress) reaches the specified tensile strength. Besides σ_c and dilation angle ψ_c, the Hoek-Brown parameter *s =1* were used, assuming that CMC is intact, and the parameter *m* = 12 may be selected as recommended by Karam & Tabbara (2009). In fact, the adopted m value can be readily justified based on Equation (2.8) and the literature on the uniaxial compressive strength σ_c and tensile strength σ_t of various types of concrete (Hoek & Brown 1980).

$$\frac{\sigma_c}{|\sigma_t|} = \frac{2}{m - \sqrt{m^2 + 4s}} \approx m \quad \text{for } m > 5 \tag{2.8}$$

The $\sigma_c/|\sigma_t|$ ratio calculated for normal concrete ranges from 10 to 25 (ACI Committee 318 2014) and from 9 to 13 for high fly ash concrete (Siddique 2004; Yoshitake et al. 2014). For many practical cases, practicing engineers can derive the m values from the properties of concrete that are readily available.

2.3.4 Quality Control and Testing

CMC column quality is subject to a real-time monitoring system where drill rate, pumping pressure, and volume of grout are recorded and controlled. Besides, static load testing is also a routine form of trial to confirm both the integrity and the performance of both calibration columns during initial stages of construction and production columns throughout the works (Nguyen et al. 2014). Load tests are carried out at 1 to 1.5 times the service load, which may be sufficient as for ground improvement purposes. The European building code requires testing these elements to 1.5 times the working load. If appropriately specified, results of static load tests can provide useful information to the practicing engineers about structural and geotechnical capacities. Typical static load test results for CMC columns are shown in Figure 2.16.

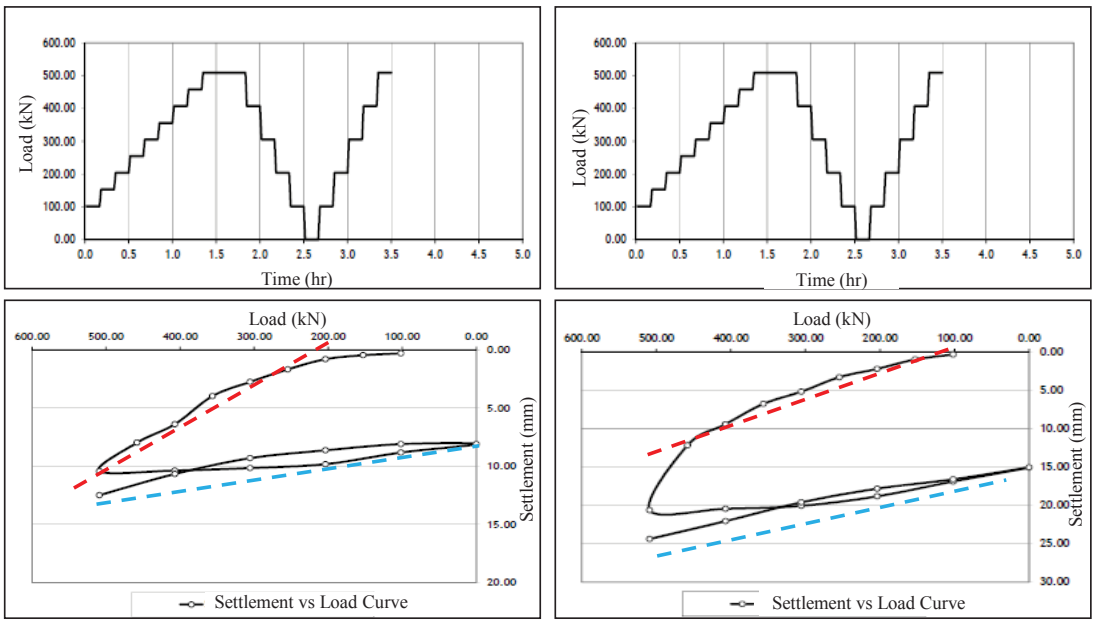

Figure 2.16 Typical static load test results (Nguyen et al. 2014)

According to Michalowski et al. (2018), integrity test is often carried out for CMC using the standard test method for low strain impact integrity testing of deep foundations D5882 − 16 (ASTM 2016a). The durability of the grout columns may be improved with fly ash

as to resist chemic attack and weathering. In fact, grout incorporating high volume fly ash was found to create grout columns with very low permeability and a high resistance to the passage of chloride ions (Bilodeau et al. 1994).

2.4 Existing Analytical Solutions

Most researchers focused on CMC load-deformation analyses (Fok et al. 2012; Ghosh, Fatahi & Khabbaz 2016; Hamidi et al. 2016; Wong & Muttuvel 2012a) or estimating shaft resistance (Basu, Prezzi & Salgado 2013; Rivera et al. 2014). Only a few researchers have assessed the effects of installing CMC or screw displacement columns, and that includes a numerical simulation (Pucker & Grabe 2012), field investigations (Larisch, Kelly & Muttuvel 2015; Suleiman et al. 2016) and small-scale model tests (Hird, Ni & Guymer 2011). There is a crucial need to understand the installation effects of CMCs.

2.4.1 Cavity Expansion Methods

The existing assessment methods used to assess installation effects for various piling and ground improvement techniques that are most relevant to CMC will be discussed herein. Available assessment methods for installation effects include cavity expansion theory (Carter, Randolph & Wroth 1979), strain path method (Baligh 1985) and somewhat more rigorous analyses using numerical modelling. Pile jacking or driving has often been simulated using cavity expansion theory, which is well described by Yu (2000). Unlike jacked and driven piles, the penetration of CMC auger into the ground includes soil loosening by auger flights in addition to the displacement effects. Therefore, CMC installation is not simply a cavity expansion process, but rather affected by the partial flight auger rotation, significantly reducing the normal stress on the column shaft that would be estimated by cavity expansion theory (Basu & Prezzi 2009). The cylindrical cavity expansion theory is more applicable for the middle section of CMC. Closer to the

column tip the installation resembles spherical cavity expansion. Near the ground surface, the confining stress is significantly lower and vertical strain is dominant with the occurrence of heaving effects. Furthermore, since the column is drilled incrementally, the cavity expansion theory cannot simulate the installation process precisely. Despite these limitations, cavity expansion method may be used for preliminary assessment due to its simplicity compared to other sophisticated numerical methods.

2.4.2 Lateral Soil Displacement

As shown in Figure 2.17, for an isotropic homogenous soil medium, a soil element located at a radius *r* from the centre of the cavity will be displaced a radial distance of ρ_r due to undrained cavity expansion from an initial cavity of zero radius to a cylindrical cavity having a radius of r_o. A radius of r_o represents the size of an actual column.

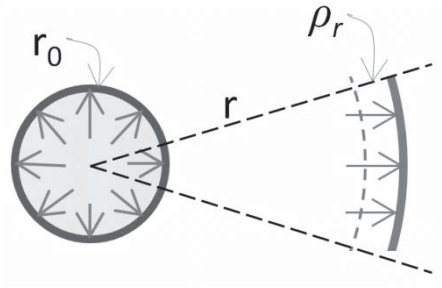

Figure 2.17 Lateral displacement of a soil element at a radius r due to cavity expansion, (after Vesic 1972)

The radial displacement ρ_r at the radial distance *r* from the centre of the cavity can be readily derived by assuming a constant volume of soil before and after undrained cavity expansion, as shown in Equation (2.9).

$$\rho_r = \sqrt{r^2 + r_0^2} - r \tag{2.9}$$

where ρ_r is the displacement at a distance *r* from the centre of column and r_0 is the radius of the column. From some well-known solutions of undrained cylindrical cavity

expansion presented by Yu (2000), Kelly, Muttuvel & Chan (2011) introduced Equation (2.10) to estimate radial soil displacement ρ_r at various depths due to undrained cylindrical cavity expansion from zero initial radius in infinite cohesive soil medium. The undrained finite cavity expansion solution in an infinite soil mass with critical state soils are presented in Yu (2000).

$$\rho_{\mathrm{r}} = s_{\mathrm{u}}/(2G)(1 + \ln(G/s_{\mathrm{u}}))(r_0/r)^2 r \qquad (2.10)$$

where ρ_r is the displacement at a distance r from the centre of the column, s_u is the soil undrained shear strength and r_0 is the radius of the column. This equation allows estimation of soil displacement at various depths with the rigidity index G/s_u obtained from field tests, e.g. Seismic Dilatometer Marchetti Test (SDMT).

2.4.3 Excess Pore Water Pressure

This section reviews the existing analytical solutions for assessing the generation of excess pore water pressure induced by the pile driving (Carter, Randolph & Wroth 1979; Chai et al. 2015; Hill 1950; Randolph, Carter & Wroth 1979; Vesic 1972). In a soil modelled as an elastic-perfectly plastic material, the excess pore water pressure Δu generated around a driven pile, under plane strain conditions and on the assumption of deformation at constant volume, can be determined by the cylindrical cavity expansion solution in Equation (2.11) (Carter, Randolph & Wroth 1979; Hill 1950; Randolph, Carter & Wroth 1979).

$$\Delta \mathrm{u} = 2\mathrm{s_u}\, ln(\frac{\mathrm{R_p}}{\mathrm{r}}) \qquad (2.11)$$

where r_o = radius of the pile; R_p = radial position of the elastic-plastic boundary; $\left(\frac{R_p}{r_0}\right)^2 = G/s_u$; and r = radial distance from the axis of the pile ($r_0 \leq r \leq R_p$). Equation (2.11)

provides a reasonable method to estimate Δu in the plastic region for normally consolidated or lightly overconsolidated soils (Randolph, Carter & Wroth 1979; Yu 2000). Equation (2.12) gives an expression for the excess pore water pressure (Δu_{sp}) induced by spherical cavity expansion below the tip of the column (Chai et al. 2015; Vesic 1972):

$$\Delta u_{sp} = 4 s_u \ln\left(\frac{R_{sp}}{r_{sp}}\right) \tag{2.12}$$

where R_{sp} = radius of the plastic zone around an expanding spherical cavity; r_{sp} = spherical radial distance; and $R_{sp} = r_o \sqrt[3]{G/s_u}$.

2.4.4 Shallow Strain Path Method

Baligh (1985) proposed an approximate analytical technique to predict soil disturbances caused by the installation of various rigid objects in the ground, so-called the Strain Path Method (SPM). The penetrating objects adopted by Baligh (1985) included a simple wall, a simple pile, and a simple tube. For the simple pile, the method has been used to analyses the cone penetration in undrained clay (Teh 1987) and for pile driving (White & Bolton 2004). In this method, the penetration process is treated as a strain controlled problem (Abu-Farsakh, Tumay & Voyiadjis 2003). This method is a more realistic solution for the installation problem, especially at the tip of the cone and deep penetration.

However, similar to the cylindrical cavity expansion method, SPM only applies a deep homogenous clay soil and does not take into account of the presence of the stress-free ground surface (Hird, Ni & Guymer 2011). In other words, those methods apply only to points in the soil, where the cylindrical/spherical cavity expansion model is relevant. It does not provide a prediction of vertical soil movements (Poulos 1994) and more importantly, there are serious concerns about this method disregarding the equilibrium

conditions as pointed out by Randolph (2003) and Huang et al. (2004). Bond & Jardine (1991) pointed out that the simple pile analysis assumed a perfectly smooth boundary between the pile and the soil while there was evidence of large shear stress measured at the pile wall during installation.

Sagaseta, Whittle & Santagata (1997) and Sagaseta & Whittle (2001) modified the strain path method (SPM) to take account of the influence of the stress free ground surface, so the resulting shallow strain path method (SSPM) can be used to predict soil movement when the pile tip is not far below the soil surface. The SSPM solution combines the merit of SPM for deep penetrations, and the method used to compute soil deformations due to near-surface ground loss (Sagaseta 1987). The solutions have been used to estimate the. The closed-form small-strain solutions for soil movement around an axisymmetric closed-ended pile with a rounded tip are shown in Equations (2.13) and (2.14). These equations can be used to reliably predict the ground movements due to column installation (Sagaseta & Whittle 2001). Figure 2.18 shows the geometry of the problem.

$$\delta_{\mathrm{rSS}}(\mathrm{r},0) = \frac{\mathrm{R}^2}{2} \cdot \frac{\mathrm{L}}{\mathrm{r}\sqrt{\mathrm{r}^2+\mathrm{L}^2}} = \frac{\Omega}{2\pi} \cdot \frac{\mathrm{L}}{\mathrm{r}\sqrt{\mathrm{r}^2+\mathrm{L}^2}} \tag{2.13}$$

$$\delta_{\mathrm{zSS}}(\mathrm{r},0) = -\frac{\mathrm{R}^2}{2} \cdot \left(\frac{1}{\mathrm{r}} - \frac{1}{\sqrt{\mathrm{r}^2+\mathrm{L}^2}}\right) = -\frac{\Omega}{2\pi} \cdot \left(\frac{1}{\mathrm{r}} - \frac{1}{\sqrt{\mathrm{r}^2+\mathrm{L}^2}}\right) \tag{2.14}$$

where R is pile radius, L is the embedded length of the pile, Ω = cross-sectional area of the pile = πR^2, SS refers to 'small strain', and r, z are the two cylindrical coordinates (e.g. at the surface $z = 0$).

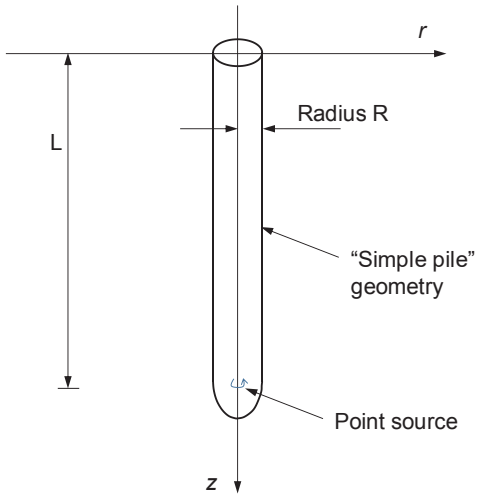

Figure 2.18 Axisymmetric 'simple pile' with geometry and notation used in SSPM analyses (Sagaseta, Whittle & Santagata 1997)

Ni, Hird & Guymer (2009) compared the results of the physical modelling of pile penetration in transparent soils with the predictions using SSPM method. They found good agreements between the modelling and the theory although there are some disparities in terms of magnitudes of soil downward movements. As reported in the literature (Castro & Karstunen 2010; Poulos 1994), the shallow strain path method normally gives slightly higher soil heave near the axis of a pile and less movement away from the axis. The cavity expansion solution, using numerical analyses adopting a non-zero initial cavity as well as the use of limited boundary conditions, may have led to this discrepancy (Castro & Karstunen 2010).

2.4.5 Chai's Method

Chai, Miura & Koga (2005) proposed closed-form equations for estimating the lateral soil displacement caused by the installation of a row of soil–cement columns. The solution was derived based on the cylindrical cavity expansion theory. This solution together with the updated equations (Chai, Miura & Koga 2007; Chai et al. 2009) is currently the only analytical method available for estimating installation effects by installing multiple

columns (Chai & Carter 2012). Equations (2.15) to (2.19) allow the lateral soil displacement for point A in the x-direction, δ_{xA} caused by installing a row of infinitely long columns to be calculated. Figure 2.19 shows the location of point A, and the notations of the parameters used in these equations. It can be seen that in addition to the geometric conditions, the significant parameters controlling the lateral displacement are R_{p} and δ_{p}. In these equations, the point of interest A is on the perpendicular bisector of a row of columns. Chai & Carter (2012) noted that if the point of interest is not on the bisector of the row, then two calculations will be needed, that is using two different values of L and then combining the results.

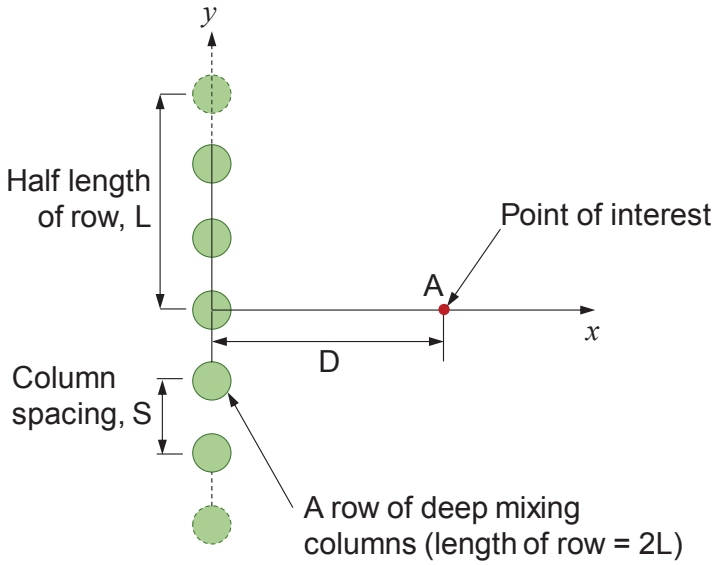

Figure 2.19 Plan view showing Point A, where lateral soil displacement in the x direction to be calculated by Chai et al.'s method (after Chai, Miura & Koga 2005)

Plastic radius, $\mathrm{R_p}$

$$\left(\frac{\mathrm{R_p}}{\mathrm{r_0}}\right)^2 = \mathrm{G/s_u} \tag{2.15}$$

For a clayey deposit, the displacement at $\mathrm{r = R_p}$ is

$$\delta_{\mathrm{p}} = \frac{1+\nu}{\mathrm{E}} \cdot \mathrm{R_p} \cdot s_u \tag{2.16}$$

For $D < R_p$ and $D^2 + L^2 > R_p^2$

$$\delta_{xA} = \frac{2D(2R_p + \delta_p)\delta_p}{S\sqrt{4D^2 + 2R_p\delta_p}} . tan^{-1} \sqrt{\frac{2\left(R_p^2 - D^2\right)}{2D^2 + R_p\delta_p}} + \frac{2R_p}{S}\delta_p \left(tan^{-1}\frac{L}{D} - tan^{-1}\sqrt{\frac{R_p^2}{D^2} - 1} \right) \quad (2.17)$$

For $D < R_p$ and $D^2 + L^2 \leq R_p^2$

$$\delta_{xA} = \frac{2D(2R_p + \delta_p)\delta_p}{S\sqrt{4D^2 + 2R_p\delta_p}} . tan^{-1} \sqrt{\frac{2L^2}{2D^2 + R_p\delta_p}} \quad (2.18)$$

For $D \geq R_p$

$$\delta_{xA} = \frac{2R_p}{S}\delta_p \, tan^{-1}\frac{L}{D} \quad (2.19)$$

where D = offset distance from the centre of a row of columns to Point A of Figure 2.19; S = spacing between two adjacent columns in a row; R_p = the radius of plastic zone around a cylindrical cavity; r_o is the pile radius, δ_p = the displacement at $r = R_p$; and L = the half length of a row.

2.5 Existing Numerical Methods

2.5.1 Remeshing Technique in Numerical Modelling

The rigorous modelling of installation effects with realistic soil model requires the use of finite element method (FEM) or the finite difference method (FDM). For most of the deep penetration problems, it is important to consider the shape of the penetrator. During CMC installation, the soils are displaced vertically, laterally and heavily disturbed by the CMC auger rotation. For modelling CMC, a few problems can be pointed out:

- Very large soil deformation and the heavily distorted mesh
- Soils are strongly affected by the CMC auger rotation
- The auger is asymmetric can only be modelled in a 3D system (Pucker & Grabe 2012) (not possible in a 2D axisymmetric model either)

- Complex contacts between soils and the penetrating tool

Numerical modelling of the penetration of a column/pile or a drill tool into the ground can be done in various ways:

- Arbitrary Lagrangian-Eulerian (ALE) adaptive meshing (ALE available in ANSYS Multi-Material LS/DYNA)
- Coupled Eulerian-Lagrangian (CEL) analysis (available in Abaqus FEA)
- Material Point Method (MPM) analysis

ALE mesh is allowed to move independently of material deformation. In the first step, the distorted mesh caused by the explicit Lagrangian analysis requires a newly improved mesh for the next step. In the second step, the Eulerian analysis is performed, where variables in the previous analysis is transferred into the new mesh. ALE can deal with large deformation problem; however, since elements and connectivity (i.e. topology) do not change, high-quality mesh may not be maintained during extreme deformation. In contrast, CEL (only in Abaqus/Explicit) has spatially fixed mesh. Eulerian and Lagrangian bodies within the same model can interact via a contact definition e.g. a Lagrangian auger travelling into the Eulerian yielding soil.

CEL is more computationally friendly since a fixed mesh means no mesh distortion and less solution convergence (Osthoff & Grabe 2018). Chosen portions of a CEL model can be modelled as Eulerian or Lagrangian. Since the Eulerian mesh is fixed in CEL, soil displacement has to be calculated by integrating node velocities of the Eulerian mesh recorded along a predefined path over time (Pucker & Grabe 2012). The installation of a screw displacement auger into the dry sand was numerically simulated using CEL as in Pucker & Grabe (2012). Abaqus FEA software package has been developed by Dassault Systèmes Corp, a suite of finite element programs used for many general engineering

simulation purposes. The Abaqus/Explicit includes the Coupled Eulerian-Lagrangian formulation, for modelling extremely large deformation (Dassault Systemes 2017). However, Abaqus is not specifically designed for geotechnical analyses, including the limitation in modelling fluid-soil interaction and constitutive material models for soils. Although ALE and CEL analyses are two of the most innovative solutions to the very large strain problems, the analyses seem to offer only single-phase possibility with either fully drained or total stress undrained condition analyses and frictionless contact between bodies (Elkadi, van Lottum & Luger 2014).

According to Phuong et al. (2016), the MPM method is the finite element method (FEM) formulated in an Arbitrary Lagrangian Eulerian (ALE) description of motion. Space discretization consists of (*i*) the computational background mesh, and (*ii*) the collection of material points, which move through the fixed mesh. This method is suitable for modelling large deformation because the state variables are assigned to the material points and are carried independently of the computational mesh. The penetration of a jacked displacement pile into the sand was modelled using MPM method and the results were compared to the centrifuge tests (Phuong et al. 2016). The numerical analyses of the pile installation showed significant differences in the soil stresses and strains around the pile after installation compared with the initial in-situ stress state. The influences of the installation extended to about 8 times pile diameter in the lateral direction from the centre of the pile and 7 times pile diameter below the pile tip. Currently, all simulation of pile installation effects was carried out installing a single CMC column can be modelled using axisymmetric model.

2.5.2 Updated Lagrangian and Update Mesh in *FLAC*^{3D}/PLAXIS

The updated Lagrangian analyses are available in three well known commercially available software packages: *FLAC*^{3D}, Plaxis 3D and Abaqus. The ALE and CEL included in Abaqus have been discussed in the previous section. In Plaxis 3D, the most widely used finite element package for solving geotechnical problems in practice, the "updated mesh" feature (e.g. large strain Lagrangian) is available for modelling large deformation; however, it is not possible to use "updated mesh" feature in a fully coupled flow-deformation analysis (Brinkgreve, Kumarswamy & Swolfs 2016).

FLAC^{3D} (Fast Lagrangian Analysis of Continua) is a three-dimensional explicit finite-difference program for geotechnical analysis with soils and rocks (Itasca 2012). *FLAC*^{3D} can model large displacements and strains and unstable systems. When the soil is soft and large deformation occurs, the influence of the geometry change of the mesh on the equilibrium conditions should be accounted for. The large-strain formulation is the numerical formulation involving large displacements, displacement gradients and rotations; and is termed the large strain mode in *FLAC*^{3D}. The small-strain mode assumes small displacements, displacement gradients and rotations. For small strain, node coordinates are not updated, and stress rotation corrections are not taken into consideration. The material can yield and flow, and the grid can deform (in large-strain mode) and move with the material that is represented. The explicit, Lagrangian calculation scheme and the mixed-discretization zoning technique used in *FLAC*^{3D} ensure that plastic collapse and flow are modelled very accurately. Because no matrices are formed, large three-dimensional calculations can be made without excessive memory requirements. The drawbacks of the explicit formulation (i.e., small time step limitation

and the question of required damping) are overcome by automatic inertia scaling and automatic damping that does not influence the mode of failure.

2.5.3 Numerical Approach and Cavity Expansion Method

Numerical modelling of the installation of a pile into the clay (i.e. created cavity problem) is difficult to implement owing to the initial singularity. According to Carter, Randolph & Wroth (1979), expanding a cavity with an initial radius $r_i = a_o$ to a new cavity radius $r_f = 2a_o$ (i.e. doubling cavity) can be used to give an adequate approximation to what happens in the soil when a cavity expansion from zero radius to the actual column radius (i.e. r_o) occurs (Figure 2.20). According to Carter, Randolph & Wroth (1979), if the deformation occurs at a constant volume i.e. Equation (2.20), then the required relationship between r_o and a_o is:

$$r_o = \sqrt{3}a_o \tag{2.20}$$

Castro & Karstunen (2010) found that quadrupling the initial cavity gives almost identical results compared to doubling the cavity. In fact, an arbitrary value of r_i may be chosen as long as the constant volume expansion is satisfied, as shown in Equation (2.21).

$$r_f = \sqrt{r_i^2 + r_o^2} \tag{2.21}$$

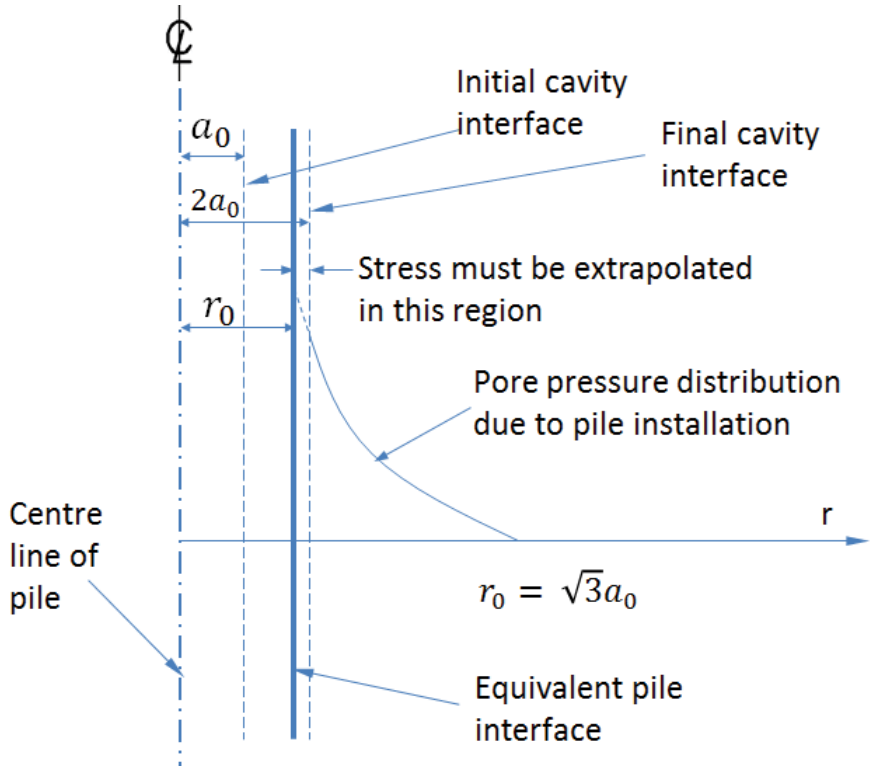

Figure 2.20 Finite cavity expansion for modelling pile installation (after Carter, Randolph & Wroth 1979)

2.5.4 The Two-Stage Approach

As well as needing to simulate the column installation process, a comparison of the effects that installation sequences have on the responses of previously installed columns requires the numerical problem to be treated as a complete 3D model. In fact, this problem involves the soil-column interaction and the presence of multiple columns. An alternative approach to a 3D model called two-stage method has been adopted (Poulos 1994; Tho et al. 2014), and was used to analyse the responses of piles due to loadings induced from the mass movement of soil. In-situ soil movements were obtained from analytical solutions (e.g. the strain path method), and then fed into the pile response analysis.

2.6 Important Features of Model Tests

2.6.1 Single Gravity Modelling and Scale Factor

Under single gravity, the corresponding stress level was low compared to the field condition, hence the scaling laws have implications (Fang & Yin 2007; Kim, Burd & Milligan 1998). According to Bao et al. (2012), in some cases, some compromises have to be made as the model test was performed under a 1*g* condition, and it is not always possible to satisfy all the similarity ratios. Unlike granular materials, due to the expected small volume change in clay during pile installation, the difference in the simulation of column penetration at 1g and at higher g is relatively insignificant (Craig 1985). Kim, Burd & Milligan (1998) performed physical modelling of constructing multiple tunnels under single gravity and reported that in their case the additional complexities of using a centrifuge and the cost outweighed the possible advantages. Table 2.3 shows a summary of scale factors for single gravity modelling on the laboratory floor.

Table 2.3 Scale factors for 1g laboratory physical modelling (modified after Muir Wood 2004)

Quantity	**Ratio of model and prototype values**	**Typical scale factor at 1g (laboratory)**	**Comments**
Length	n_l	$1/n$	Linear length scale shows reduction in dimension to fit in small-scale model test
Mass density	n_ρ	1	-
Acceleration	n_g	1	-
Stiffness	n_G	$1/n^\alpha$	independent scaling factor, with $\alpha \approx 1$ for clay based on experimental experience*
Stress	$n_g n_\rho n_l$	$1/n$	Stresses build up in the ground with depth (i.e. n_l)
Force	$n_g n_\rho n_l^3$	$1/n^3$	-
Force/unit length	$n_g n_\rho n_l^2$	$1/n^2$	-
Strain	$n_g n_\rho n_l / n_G$	$1/n^{1-\alpha}$	-
Displacement	$n_g n_\rho n_l^2 / n_G$	$1/n^{2-\alpha}$	-
Pore fluid viscosity	n_μ	1	-
Pore fluid density	$n_{\rho f}$	1	-
Permeability	$n_{\rho f} n_g / n_\mu$	1	-
Time (creep)	1	1	-
Velocity	$n_g n_l (n_\rho / n_G)^{1/2}$	$1/n^{1-\alpha/2}$	-

Note: * $\alpha = 0$ indicates soil stiffness *G* is identical in prototype and model; $\alpha = 0.5$ indicates that soil stiffness *G* dependent on stress; and $\alpha = 1$ indicates that soil stiffness *G* scales directly with stress.

2.6.2 Penetration Rate

According to Suleiman et al. (2016) and Masse, Brockbank & Pearlman (2004), CMC penetration rate is about 2 m/minute to 6 m/minute (i.e. 0.07 m/s) while the rate of withdrawal is up to 8 m/minute (or 0.13 m/s). The penetration rate for pile driving is 0.01 m/minute to 0.07 m/minute (Roy et al. 1981) while for the jacked piles as reported by Bond & Jardine (1991) the penetration rate ranged from 0.4 to 0.6 m/minute for fast jacking and 0.05 m/min to 0.1 m/min for slow jacking. Hence, the CMC penetration rate is generally much fast than driving and jacking, and it is more likely that the clay behaves under undrained conditions during CMC penetration.

In many laboratory model tests reported in the literature, a small model pile or auger is often used, comparable to the size of a standard penetration cone in CPT testing. The downward penetration rate for CPT was 20 mm/s (or 1.2 m/min). Based on the experimental data, Kim et al. (2008) concluded that the penetration rate between 0.1 mm/s (or 0.006 m/min) to 20 mm/s caused no obvious difference on the measured penetration tip resistance and the generated pore water pressure. On this basis, a penetration rate of 0.025 m/minute was adopted by Chai et al. (2014). Such penetration speed was sufficiently fast to ensure that the soil surrounding the cone would behave in undrained condition during penetration.

The proposed non-dimensional velocity, V, defined by Equation (2.22), has been used by various authors to determine an appropriate velocity so that satisfy the undrained condition of clay during penetration (Finnie & Randolph 1994; Kim et al. 2008; Randolph & Hope 2004). They recommended that when V is greater than 30, clayey soils surrounding the penetrating pile will behave under undrained condition.

$$V = 2 \times v_p \times r_{pile}/c_v \quad (2.22)$$

where v_p is the vertical penetration speed in mm/s, r_{pile} is the model pile radius in mm, and c_v is the coefficient of consolidation of the soil in m^2/year. For example, Li et al. (2017) adopted a penetration rate of 50 mm/min for jacking the model pile into the soil sample to ensure the undrained conditions during pile installation. For auger displacement piles, the penetration speed markedly affects the soil displacement. Hird, Ni & Guymer (2011).

2.6.3 Strain Gauge Embedment in Concrete Pile

Strain gauges give information on bending moments in the compressive and tensile zones along the pile. For linear elastic material behaviour, the bending moment $M(z)$ can be related to the curvature using Equation (2.23) (Comodromos, Papadopoulou & Rentzeperis 2009; Ooi & Ramsey 2003).

$$M(z) = EI\varphi(z) \quad (2.23)$$

where $I = I_x = I_y = \frac{1}{4}\pi r^4$ = the second moment of inertia about the neutral axis of the column. E is the column's modulus of elasticity, and $\varphi(z)$ is the average curvature of the column. The product EI is the flexural rigidity of the column.

If the pile is instrumented with strain gauges along the fibre extreme as shown in Figure 2.21, the curvature $\varphi(z)$ of the pile can be obtained using Equation (2.24) (Doherty et al. 2015; Guo & Lehane 2016; Kovari & Amstad 1982; McVay et al. 2009; Mohamad et al. 2011; Ooi & Ramsey 2003; Rollins et al. 2005; Rollins, Peterson & Weaver 1998; Smethurst & Powrie 2007).

$$\varphi(z) = \frac{\varepsilon_t - \varepsilon_c}{D_{sg}} \tag{2.24}$$

where D_{sg} is the horizontal distance between the two strain gauges positioned at the same depth and spaced at equal but opposite distances from the neutral axis, ε_t is the tensile strain (+) and ε_c is the compressive strain (−).

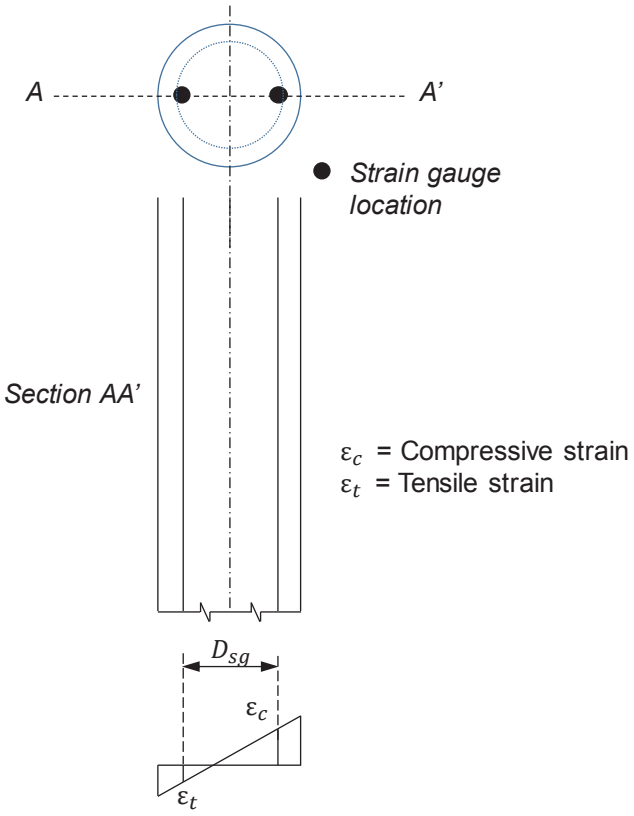

Figure 2.21 Measuring strains along either side of the pile (after Mohamad et al. 2011)

According to Rollins, Peterson & Weaver (1998) and Kovari & Amstad (1982) the strains in Equation (2.24) should include signs + and – for positive and negative strains, respectively. According to Rollins, Peterson & Weaver (1998), this approach cancels out any contribution due to axial strain, and leaves only bending strains. According to Ooi and Ramsey (2003), if only one strain gauge is installed or working at each elevation,

then the curvature is the elongational strain divided by the distance from the strain gauge to the neutral axis.

2.6.4 Soil-Column Interaction

2.6.4.1 Formulae for Elastic Piles and Columns

For elastic pile, Table 2.4 summarise the formulas for the determination of various structural response quantities.

Table 2.4 Integration and differentiation methods in elastic beam

	Parameters included in the functions			
Item	$\mathbf{y(z)}$	$\boldsymbol{\theta}\mathbf{(z)}$	$\boldsymbol{\varphi}\mathbf{(z)}$	$\mathbf{M(z)}$
Pile deflection $y(z)$ =	–	$\int \theta(z)\,dz$	–	$\int\left(\int \frac{M}{E_p I_p}dz\right)dz$
Pile rotation $\theta(z)$ =	$\frac{dy(z)}{dz}$	–	$\int \varphi(z)\,dz$	–
Pile curvature $\varphi(z)$ =	$\frac{d^2y}{dz^2}$	–	–	$\frac{M(z)}{E_p I_p}$
Pile bending moment $M(z)$ =	$-E_p I_p \frac{d^2y}{dz^2}$	–	$EI\varphi(z)$	–
Shear force $V(z)$ =	$-E_p I_p \frac{d^3y}{dz^3}$	–	–	$\frac{dM(z)}{dz}$
Soil-pile pressure $p(z)$ =	$-E_p I_p \frac{d^4y}{dz^4}$	–	–	$\frac{d^2M(z)}{dz^2}$

2.6.4.2 Soil Reaction Deduced from Bending Moment

Shear force $V(z)$ and soil reaction force $p(z)$ (i.e. the force per unit length) can be deduced by differentiating and double differentiating the bending moment profile $M(z)$ of the pile with respect to depth *z* using Equations (2.25) and (2.26) (Dyson & Randolph 2001). To reduce the inaccuracy in determining the *p(z)* by double differentiating *M(z)*, the piecewise polynomial curve fitting method can be used (Qi et al. 2016; Yang & Liang 2006).

$$V(z) = \frac{dM(z)}{dz} \tag{2.25}$$

$$p(z) = \frac{d^2M(z)}{dz^2} \tag{2.26}$$

According to Taghavi et al. (2015), a group of successive moment data points can be fitted to an n-order polynomial using a least-square method. The polynomial can then be differentiated twice and the soil response *p(z)* is evaluated at the central data point. The soil response for the uppermost and lowermost three points may be obtained from n-order polynomials fitted to the highest and lowest data points, respectively.

2.6.4.3 Pile Lateral Deflection Deduced from Bending Moment

According to Weaver, Ashford & Rollins (2005) and Ilyas et al. (2004), double integrating the curvature $\varphi = M(z)/EI$ gives the lateral displacement $y(z)$ of the column.

$$y(z) = \int \left(\int \frac{M}{EI} dz \right) dz \tag{2.27}$$

where $y(z)$ is the lateral pile displacement, and z is the depth below ground level or top of the pile. According to Dyson & Randolph (2001), the experimental bending-moment data can be fitted with a series of equations to evaluate the above equation algebraically. The two integration constants required to derived *y(z)* can be determined from:

- measured displacement at the loading position and an assumed zero deflection condition at the point with zero lateral resistance (Qi et al. 2016)
- matching the measured deflection and rotation at the pile head (Kim et al. 2004)

- assuming zero displacements at the pile tip, and also matching the measured deflection at the pile head. The measured pile head rotation provided some redundancy" (Dyson & Randolph 2001).
- the measured column head displacement as one of the two boundary conditions, and the pile tip displacement relative to the container base of zero as the other condition (Brandenberg et al. 2005). The calculated column displacement profiles contained contributions from curvature along the column and rotation at the column tips. The measured pile head rotation provided an independent check on the reasonableness of the computed shape.
- used measured pile head displacement and zero pile toe rotation as the two boundary conditions (Ong, Leung & Chow 2006).
- lateral displacements measured where the lateral load was applied and the other "assumed to have a zero value where the net soil resistance switched direction – that is, at the inferred point of rotation" (Truong & Lehane 2017).

According to McVay et al. (2009), by integrating the curvature profile, the rotation of the pile can be obtained. According to Sawwaf (2006), the pile rotation (slopes) can be calculated as the ratio of the difference of the two horizontal displacement sensor readings placed at two different levels to the vertical distance between the two measurement points.

$$\theta(z) = \int \varphi(z)\, dz \tag{2.28}$$

2.7 Gap and Limitations in Current Literature

The review of the installation effects of drilled displacement piling method or CMC can be summarised into eight points as follows:

1. The use of full displacement installation methods for ground improvement reduces spoil disposal, prevents borehole collapses and results in cost saving. However, current knowledge and the method of assessing CMC installation effects are very limited.
2. Most researchers focused on CMC load-deformation analyses or estimating shaft resistance. Only a few investigators have assessed the effects of installing CMC or screw displacement columns, and that includes a numerical simulation in the granular soil, a few field investigations and small-scale model tests. There is a crucial need for further advanced and comprehensive study.
3. Field evidence indicated that the lateral soil displacement induced by CMC installation process can be excessive. The excess lateral soil movement is associated with two issues: (*i*) new installations affecting adjacent already-installed CMCs, when columns are closely spaced, and (*ii*) CMC installations may damage nearby existing structures.
4. In the past, model tests only simulated the displacement of the soil during installation of the auger and the concreting stage was not or could not be simulated. Most studies focused on granular materials (i.e. sand), or they simulated one single column.
5. Considering the displacement effects, CMC installation process is analogous to the cavity expansions, which can be simulated in the laboratory and by the numerical method. The jacked pile installation process fulfils the features of a cylindrical cavity

expansion in a way that the surrounding soils are displaced laterally by the penetrating tools.

6. Modelling of pile installation process involves large mesh distortion. Assessing installation effects of multiple columns will requires complex three-dimensional soil-structure interaction, realistic modelling, coupled consolidation mechanical analysis, and construction sequence.
7. Limited investigations on the influence of new column installations on the nearby existing columns for ground improvement purposes, especially when columns have not achieved its 28-day compressive strength.
8. The installation sequence has a considerable influence on the observed lateral displacement on the surrounding soil and adjacent structures. Justifications for adopting these construction practices are often based on simplified analyses and local experience. There exist conflicting ideas on the optimal sequence of installation. While considering the existing construction procedures in place, most of the assessment methods purely involve monitoring during construction. However, solid justification for the installation sequence may be required and how efficient they are in comparison to other possible installation patterns.

CHAPTER 3 Numerical Comparison of Installation Sequences of Plain Concrete Rigid Inclusions

3.1 Synopsis

Soil displacement induced when installing controlled modulus columns (CMC) as ground reinforcement could affect the columns installed close by. Realising numerical analyses may provide useful insights, Chapter 3 describes a numerical approach to investigate how groups of CMC installed in different sequences could affect columns installed previously. Coupled consolidation analyses in large strain mode and incorporating soil-CMC interaction were carried out using the three-dimensional finite difference software package *FLAC*^{3D}. The CMCs were modelled using the advanced non-linear Hoek-Brown plasticity model with a tensile yield criterion while soils with a typical profile were characterised using the modified Cam-Clay and the elastic-perfectly plastic material with a Mohr-Coulomb yield criterion. Where possible, the predicted responses of ground surrounding the CMCs were compared to a number of existing analytical methods and full scale field study. Predictions revealed that lateral soil movement and soil heave near existing CMCs induced by installing new CMCs towards the existing CMCs were approximately 15% and 25% greater than corresponding predictions when a reverse installation sequence was adopted. The maximum excess pore water pressures, induced near existing columns due to installing new columns towards the existing ones, were almost twice more than those caused by the reverse sequence of installation. Moreover, the predicted bending moments generated in the existing columns induced by installing

new columns towards the existing CMCs were almost 22% greater than the corresponding values when the reverse installation sequence was adopted. This shows the importance of selecting an appropriate installation sequence in the CMC construction process as well as considering the initial stress field and bending moments in the surrounding soil and CMCs, respectively when designing embankments on improved soft soils.

3.2 Introduction

Ground improvement using controlled modulus columns (CMC) is one of the most effective ways of reducing long term and short term deformations of weak soil under road embankments, warehouses, and seaports (Fok et al. 2012; Plomteux, Porbaha & Spaulding 2004; Suleiman et al. 2016). A CMC-soil system consists of (a) a grid of columns installed into the weak ground with embedment in a stiff stratum, and (b) a granular load transfer platform. CMCs are built in the ground with a piling rig equipped with a hollow displacement auger that laterally displaces the surrounding soils with minimal spoil return to the ground surface (Plomteux, Porbaha & Spaulding 2004). Variations of this technique in terms of auger shapes or construction process include Controlled Stiffness Columns (CSC), Drilled Displacement Columns (DDC) (Larisch, Kelly & Muttuvel 2015) and Concrete Injected Columns (CIC) (Hewitt, Summerell & Huang 2009; Hsi 2008). The soil deformation induced by CMC installation increases the stresses in the ground such that, in theory, they could enhance the load-bearing capacity of the rigid inclusions. However, loadings associated with the movement of soil due to installation can have an adverse effect on nearby columns installed beforehand (Larisch, Kelly & Muttuvel 2015; Plomteux, Porbaha & Spaulding 2004; Turatsinze & Garros 2008), particularly when the columns are closely spaced. In fact, newly installed CMCs are susceptible to an imposed load, due to the slow strength gain of fly ash concrete at early ages (Mehta 2004), low strength intended for ground improvement purposes (McCarthy & Dhir 2005; Plomteux, Porbaha & Spaulding 2004; Turatsinze & Garros 2008), and pre-existing micro-cracks that naturally develop in most concrete. Unless a proper installation sequence is considered, large cracks and cross-sectional shear failure may develop in the columns, leading to damage, loss of verticality, and reduced flexural stiffness (Larisch, Kelly & Muttuvel 2015).

Most researchers only focused on CMC load-deformation behaviour (Fok et al. 2012; Ghosh, Fatahi & Khabbaz 2016; Hamidi et al. 2016; Wong & Muttuvel 2012a) or estimating shaft resistance (Basu, Prezzi & Salgado 2013; Rivera et al. 2014). Only a few researchers have assessed the effects of installing CMC or screw displacement columns, and that includes a numerical simulation (Pucker & Grabe 2012), field investigations (Larisch, Kelly & Muttuvel 2015; Suleiman et al. 2016) and small-scale model tests (Hird, Ni & Guymer 2011). Suleiman et al. (2016) indicated that the influence zones of CMC installation extend $4r_o$ to $6r_o$ from CMC face (r_o is CMC radius). Larisch, Kelly & Muttuvel (2015) reported the uplifts and lateral movements of the previous columns due to subsequently installed columns and suggested that trials be carried out prior to construction to optimise installation sequence to account for site-specific geology and project requirements.

Since CMCs are installed using a displacement piling method, it is reasonable to relate the effects due to driven piles, jacked piles, stone columns, cement soil mixing, and jet grouted columns. Since the 1950s, the cavity expansion method (Bishop, Hill & Mott 1945; Hill 1950; Yu 2000) has been used to assess the installation effects of driven piles (Randolph, Carter & Wroth 1979; Vesic 1972), jacked piles (Bond & Jardine 1991; White & Bolton 2004), stone columns (Guetif, Bouassida & Debats 2007), jet grouting (Liu et al. 2017; Shen, Wang & Cheng 2017; Wong & Poh 2000), and deep soil mixing columns (Chai, Miura & Koga 2005; Shen, Miura & Koga 2003; Shen & Miura 1999). The response of soil due to column installation is analogous to the creation or expansion of cylindrical and spherical cavities, which can be examined in undrained or drained conditions. The time-dependent soil responses can be evaluated via consolidation analysis (Randolph & Wroth 1979; Zhou et al. 2017). Numerous analytical or semi-analytical solutions have been developed for various soil models, e.g., Tresca model (Hill 1950),

linearly elastic-perfectly plastic Mohr-Coulomb material (Carter, Booker & Yeung 1986; Vesic 1972; Yu & Houlsby 1991), modified Cam-clay (Cao, Teh & Chang 2001; Chen & Abousleiman 2012; Collins & Yu 1996) and bounding surface plasticity (Chen & Abousleiman 2016). The shortcoming of cylindrical cavity expansion is an assumption of plane strain conditions at the mid-depth of a long vertical pile; in other words, the effect of soil heave is ignored. Similarly, spherical cavity expansion simplifies the geometries of various penetrating objects as half-spheres, and hence ignores the complex strain paths near column tip. The strain path method (SPM) (Baligh 1985) was developed to assess the deep penetrating problem, while its modified version – the "shallow strain path method" (SSPM) (Sagaseta, Whittle & Santagata 1997) was used to estimate the movement of soil near the surface. While CEM and SPM have their own merits and limitations, CEM remains the most widely used method for assessing installation effects. Note also that for problems involving complex soil constitutive models and stratigraphy, the analytical solutions of the cavity expansion method would become cumbersome.

Since the 1970s, finite difference and finite element methods have emerged due to the significant improvement in modern computing power. A simplified simulation of pile penetration by expanding a cavity from a finite radius using complex material models has been implemented successfully for various practical cases (Carter, Randolph & Wroth 1979; Guetif, Bouassida & Debats 2007), but modelling the penetration of piles into the ground is a much more complex problem due to heavily distorted mesh. To minimise mesh distortion causing premature numerical termination, several interesting proposals (Dijkstra, Broere & Heeres 2011; Engin, Brinkgreve & van Tol 2015) were reported. However, the most notable advancements so far are as follows: the arbitrary Lagrangian–Eulerian (ALE) method, (Liyanapathirana 2009; Nazem, Carter & Airey 2009; Sabetamal et al. 2014), the coupled Eulerian–Lagrangian (CEL) method (Hamann, Qiu & Grabe

2015; Pucker & Grabe 2012), and the Material Point Method (MPM) (Phuong et al. 2016). However, finite element methods based on mesh free or re-meshing schemes are complex to implement. Furthermore, as well as needing to simulate the column installation process, a comparison of the effects that installation sequences have on the responses of previously installed columns requires the numerical problem to be treated as a complete 3D model. An alternative approach to a 3D model called two-stage method has been adopted (Poulos 1994; Tho et al. 2014), and was used to analyse the responses of piles due to loadings induced from the mass movement of soil. In-situ soil movements were obtained from analytical solutions (e.g. the strain path method), and then fed into the pile response analysis.

The literature review led to the conclusion that to achieve a realistic and innovative simulation of multiple CMC installations and to compare the effects of using differing installation sequences on existing columns, a number of important aspects should be accounted for. Firstly, the numerical analysis should model individual columns to allow the soil to move between and interact with the columns. Secondly, when installing CMC in clay soils, the dissipation of excess pore water pressure in the time lag between installing two successive CMCs must be addressed. Thirdly, the non-linear behaviours of soil and columns and realistic model boundary conditions should be included for practical purposes. Finally, a simulation of CMC installation could utilise the widely accepted cavity expansion method in the numerical model; this would provide a practical compromise for many design situations as well as overcoming the need for more sophisticated analyses such as ALE or CEL schemes. Obviously, field trials are the most accurate way to optimise installation sequences but they are not always cost-effective and it may be difficult to apply the results to other projects where the ground conditions are different.

This chapter presents a 3D large strain numerical model to analyse the response of already installed CMCs subjected to loadings associated with the lateral movement of soil induced by installing a number of nearby CMCs. This chapter focuses on investigating the effects of using two different installation sequences on nearby CMCs in short and long terms. An undrained cavity expansion analysis to simulate the installation process of each CMC was followed by a consolidation analysis to allow excess pore water pressure dissipation during the lag between any two successive columns being installed. A modified Hoek-Brown model with a tensile yield criterion represents the non-linear behaviour of CMCs while the modified Cam-Clay and the elastic-perfectly plastic material with a Mohr-Coulomb yield criterion were used to characterise the soils. The numerical analyses were initially carried out using the properties of CMC grout at an early age, but to investigate how the curing periods affected the behaviour of existing CMCs subjected to nearby installations, the analyses were repeated by assigning the existing CMC with the properties of grout after 28 days. The response of soil to the installation of nearby columns was examined along their length and where possible the predictions were then compared to existing analytical methods. The responses of the existing CMCs in the long and short terms were also reported.

3.3 Numerical Simulation

3.3.1 Finite Difference Mesh and Boundary Conditions

In this chapter, the column installation process simulated with 3D numerical modelling using *FLAC*^{3D} v5.01 (Itasca 2012) in large strain mode, is explained. A 3D grid as shown in Figure 3.1 was created to represent the soils and an arrangement of 9 columns consisting of three already installed (denoted as CMC E1 to E3, aligned along Row 1) and six proposed columns (denoted as CMCs 1 to 6 of Rows 2 and 3). This block of

columns is located in the centre of the 3D model. The installation of CMCs along Rows 2 and 3 was simulated and their influence on the existing CMCs (Row 1) was studied. Each column had a diameter D = 450 mm and a length of 7.2 m, which includes 1 m deep socket into the stiff clay. The columns are arranged in a square pattern at 1.8 m centre to centre intervals to correspond to 4D column spacing, thus capturing closely spaced columns in practice.

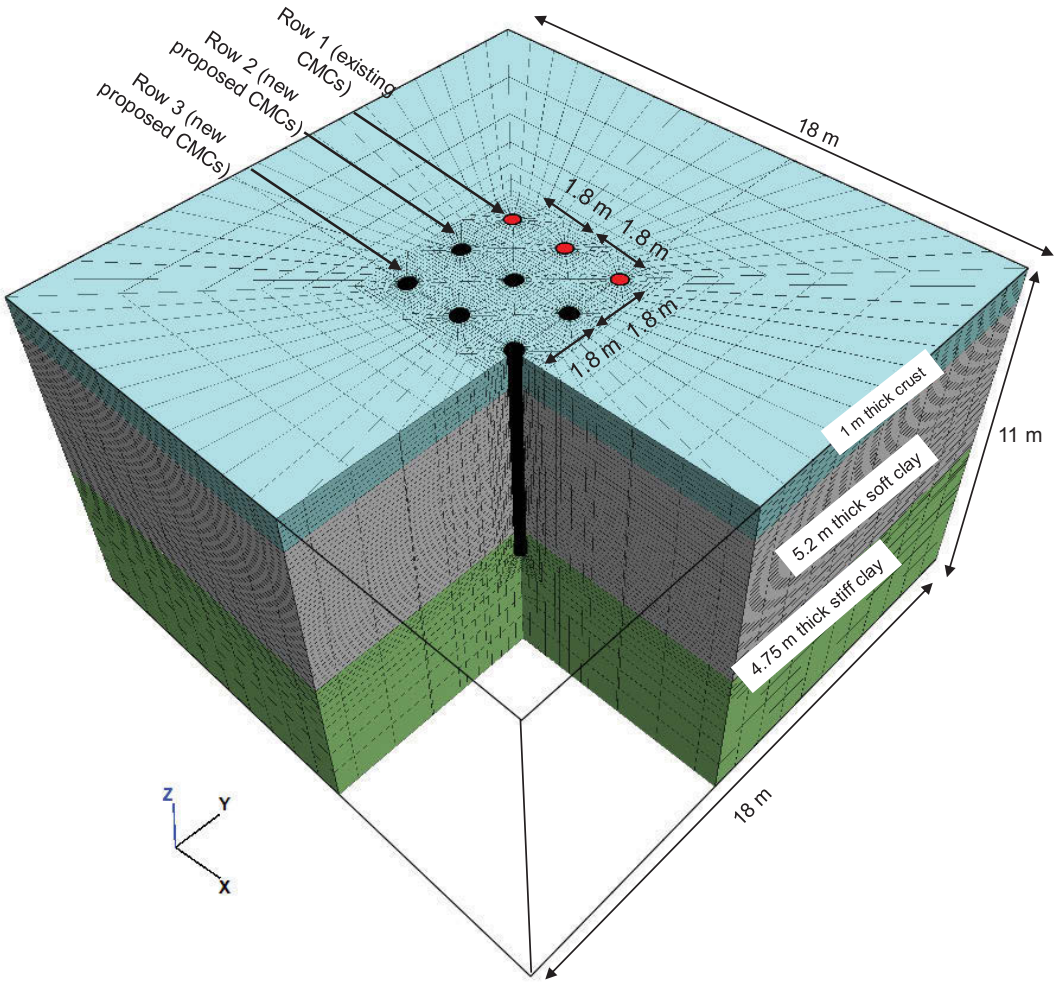

Figure 3.1 Model geometry in 3D view

The soil and CMC regions were created from solid elements such as brick, wedge and pyramid zone types. The *FISH* program language embedded in *FLAC*^{3D} enables geometric shapes that are not readily available to be created. For example, a hemispherical

mesh was formed to simulate spherical cavity expansion at the tip of the column while a circular grid was created to model the cross section of the columns. The model grid has 127,611 zones and 137,667 grid points. Each *FLAC*^{3D} analysis took almost 12 weeks to run using a 3.40 GHz core i7 CPU computer.

Referring to Figure 3.1, the top boundary of the grid (z = 11 m) represents the stress-free ground surface and the assumed water table, while the remaining boundaries were assumed to be impervious. The lateral boundaries were extended to 30 times the radius of the column from the outmost column to minimise the boundary effects. The soil at the vertical side boundaries was fixed against the normal displacements at the boundary planes. As shown in Figure 3.1, the bottom boundary was extended by almost 18 times the radius of the column and was restrained against movement in all directions to simulate competent bedrock.

3.3.2 Adopted Installation Sequences

To assess the effects of installing new columns beside existing ones, two different installation sequences as shown in Figure 3.2 were used. Installation Sequence No. 1 in Figure 3.2 shows that the CMC rig starts close to the existing columns and then moves farther away as installation continues, whereas Sequence No. 2 is a reversal of Sequence No. 1 (i.e. installation begins further away and then comes closer to existing CMCs).

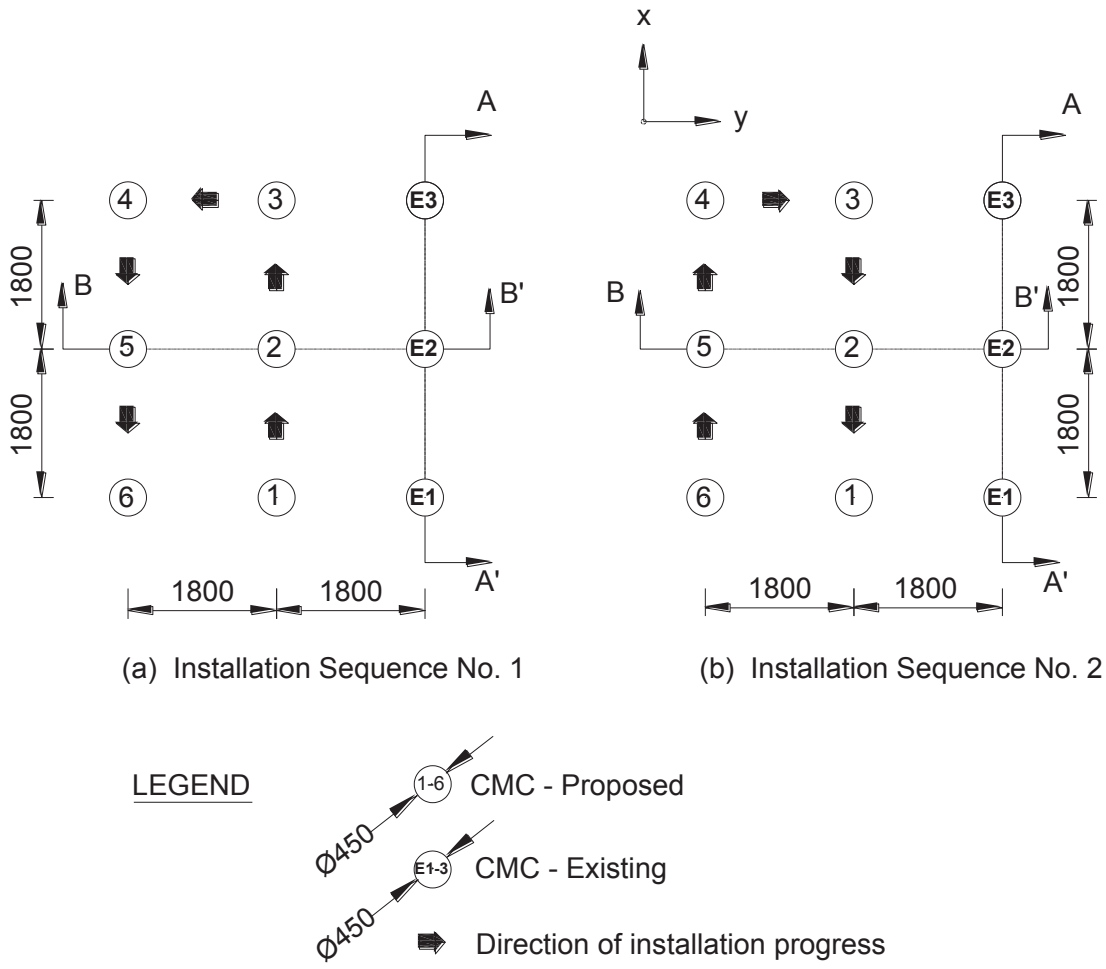

Figure 3.2 Plan view of (a) installation Sequence No. 1 and (b) installation Sequence No. 2, used in numerical models (all dimensions in millimetres)

The analysis commenced with the CMCs along Row 1, which are already in the ground (i.e. "wish in place"). In each installation sequence, the construction of six CMCs was modelled. Each CMC is installed in three stages, (*i*) cavity expansion to simulate penetration by the CMC displacement auger, (*ii*) grouting phase to build CMC, and (*iii*) the consolidation phase to model the evolution of excess pore water pressure with time. A time lag of approximately 30 minutes was allowed between two CMCs installed in succession. When all the CMCs have been installed, consolidation analyses were performed to investigate the long-term response of existing CMCs and the surrounding ground.

3.3.3 Ground Profile and Properties

Table 3.1 summarises the model parameters of the soil layers, as shown in Figure 3.1. The soil properties were derived from the site investigation and laboratory data, which were undertaken for a highway upgrade in New South Wales, Australia. The modified Cam-Clay (MCC) material model (Roscoe & Burland 1968) was used to represent the behaviour of the highly over-consolidated crust and the layer of soft clay, while the underlying stiff ground was characterised by the linearly elastic-perfectly plastic material with a Mohr-Coulomb (MC) yield criterion.

During the initial stage of the modelling process, other soil model types were also considered, such as Hardening Soil or Soft Soil models (Brinkgreve & Vermeer 1999). It is noted that such soil models are the built-in constitutive models in the PLAXIS software package (Brinkgreve & Vermeer 1999). In the adopted numerical tool for this research project, i.e. *FLAC*^{3D} by Itasca (2012), the best and most practical model option for soft soils was the MCC model. While it was possible to create users' own constitutive model, the focus of the thesis was the installation effects of CMC column, where the modelling of concrete column was a primary concern, rather than soils alone. Furthermore, most of the cavity expansion analyses have been carried out using modified Cam Clay model or Mohr Coulomb material model rather than hardening soil model or other recent material models.

Referring to the existing literature, the elastic-perfectly plastic MC model can be adopted for the simulation of stiff clays (Chaiyaput, Bergado & Artidteang 2014; Kelesoglu & Springman 2011; Lee 2013; Voottipruex et al. 2011), while the soft clay is often modelled using the MCC model. However, it should be noted that when the emphasis of the research is on the behaviour stiff clay (in this study CMCs are mainly in soft clay deposit),

more advanced and rigorous soil constitutive models such as the elasto-plastic cap model presented by Reul & Randolph (2003) can be used to simulate stiff clay deposit.

The laboratory test results for estuarine deposits (i.e. soft and firm soils) sampled from the site (south of Sydney, Australia) indicate that soft to firm soils have an effective friction angle, ϕ' , varying between 27.5° and 36°. A value closer to the lower bound was adopted for the crust and the soft soil (i.e. 28°, as given in Table 3.1). It should be noted that in the real practice, most often, no laboratory testing results are provided for the mechanical properties of the crust layer.

The strength of the stiff soil deposit at the base of the model, which is characterised by the elastic-perfectly plastic model with MC yield criterion (Brinkgreve, Swolfs & Engin 2011), is controlled by both the effective friction angle $\phi' = 28°$ and the effective cohesion $c' = 10$ kPa. On the other hand, for soft clay represented by MCC model, the effective friction angle ϕ' is the sole strength parameter and is directly related to the critical state frictional constant *M*. It should be noted that Phutthananon et al. (2018) also used the same effective friction angle for the crust, soft soil and stiff clay, but with varying soil effective cohesion.

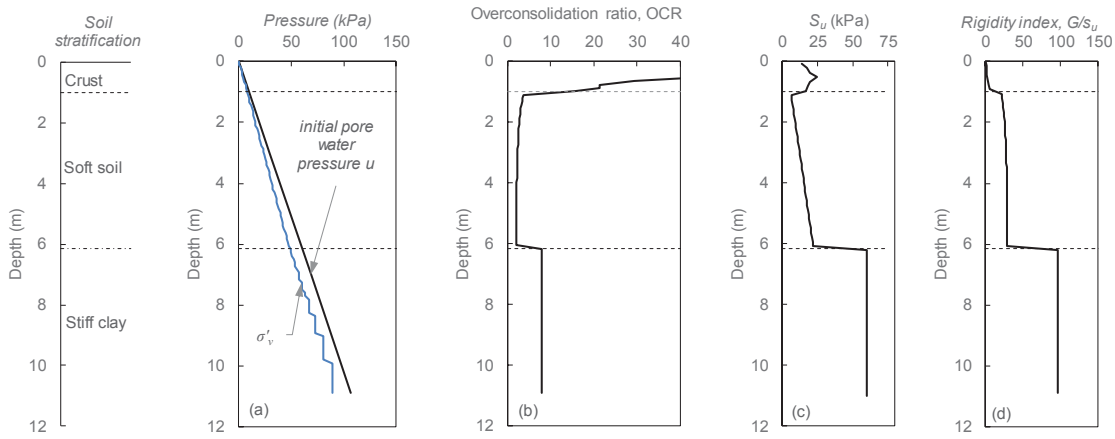

Figure 3.3 Profiles of (a) initial pore water pressure and vertical effective stresses, (b) over-consolidation ratio (c) undrained shear strength, and (d) rigidity index of soil

The initial ground conditions adopted are: *(i)* the initial hydrostatic pore water pressure, u_o, *(ii)* the groundwater table to be at the ground surface, and *(iii)* the initial in-situ vertical effective stresses, $\sigma'_{\mathrm{v,o}}$, to be induced by the weight of the soil, while the horizontal effective stresses, $\sigma'_{\mathrm{h,o}}$, are directly proportional to the vertical stresses σ'_{vo} using the K_0 values presented in Table 3.1. It is noted that the K_0 values for the soft clay and stiff clay were estimated using Equation (3.1) as recommended by Mayne & Kulhawy (1982). Based on the authors' past experience with the soils in the region and the design approach adopted in the literature (Indraratna, Balasubramaniam & Sivaneswaran 1997; Jenck, Dias & Kastner 2009; Tan, Tjahyono & Oo 2008), a uniform K_0 was adopted for the firm crust soil and the soft soil. The K_0 value for stiff clay calculated from Equation (3.1) compares well with the typical values for stiff clay from the literature (Bolton & Powrie 1987; Chen & Abousleiman 2012; Chou & Bobet 2002).

$$K_0 = (1 - \sin\phi') \times \mathrm{OCR}^{0.5} \tag{3.1}$$

The profiles of the initial stresses of the soil deposit, the isotropic overconsolidation ratio $\mathrm{OCR} = p'/p'_{\mathrm{o}}$, the undrained shear strength s_{u}, and the rigidity index G/s_{u} are shown in

Figure 3.3. The soil modulus G is correlated to the mean effective stress p' of the soil (Cao, Teh & Chang 2001; Zytynski et al. 1978), and is an important parameter for estimating the excess pore water pressure and stresses induced during the cavity expansion process.

Table 3.1 Selected soil model parameters adopted in the 3D finite difference analysis

Parameters	**Firm crust**	**Soft clay**	**Stiff clay**
Depth range (m)	0 - 1	1 - 6.15	6.15 – 10.9
Adopted soil constitutive model	Modified Cam-Clay	Modified Cam-Clay	Linearly elastic-perfectly plastic
Saturated unit weight, γ_s (kN/m^3)	17.8	17.6	19.6
Poisson's ratio, ν'	0.3	0.3	0.3
Recompression index, κ	0.073	0.073	-
Compression index, λ	0.29	0.29	-
Critical state stress ratio, M	1.1	1.1	-
Reference pressure, p'_{ref} (kPa)	74	74	-
Reference specific volume, υ_{ref} †	2.55	2.55	-
Initial in-situ coefficient of permeability, k_h (m/s)	7×10^{-9}	7×10^{-9}	3×10^{-8}
In-situ undrained shear strength, s_u (kPa)	25	7 - 22	60
Elastic modulus, E' (MPa)	-	-	15
Effective cohesion, c' (kPa)	-	-	10
Effective friction angle, ϕ'_{cs} (°)	28	28	28
OCR	15 - 350	2 – 3.6	8
Coefficient of lateral earth pressure at rest, K_0	0.75	0.75	1.2
Initial in-situ void ratio, e_o	1.1	1.5	1.0

Note: † υ_{ref} = specific volume for a K_0 normally consolidated sample at p'_{ref}.

3.3.4 CMC Properties

Concrete structures are often modelled using linear elastic properties, but an elastic-plastic model should be used for low strength concrete, especially when the external load is likely to exceed the yield stress of the concrete. In this study, CMC was modelled using the Hoek-Brown material model, following recommendations from Karam & Tabbara (2009) and Wu & Zhou (2010). The linear elastic-perfectly plastic model with Mohr Coulomb yield criteria (MC model) was initially considered (Section 2.3.3.1). However, a review conducted in this study shows that the friction angle and cohesion of the concrete required for MC model are difficult to be determined from the conventional laboratory testing schemes. The adopted Hoek-Brown model is therefore an innovative and essential aspect in CMC modelling. A summary of the adopted CMC parameters are presented in Table 3.2 and the procedures used to obtain these parameters are described below:

3.3.4.1 Compressive Strength of CMC

The 28 day unconfined compressive strength f_{ck} of CMC grout may vary between 7 MPa and 30 MPa (Cirión et al. 2013; Fok et al. 2012; Masse et al. 2011; Plomteux, Porbaha & Spaulding 2004; Wong & Muttuvel 2012a) for different applications. In this study, a f_{ck} = 20 MPa was used because it is common practice in Australia. As recommended by Eurocode 2 (2015), the compressive strength of concrete at an age of *t* days was estimated using Equation (3.2).

$$f_{ck}(t) = exp\left\{s_c\left[1-\left(\frac{28}{t}\right)^{\frac{1}{2}}\right]\right\}(f_{ck}+8)-8 \text{ (in MPa)} \quad (3.2)$$

where $3 < t < 28$ days and the coefficient s_c = 0.31 considering the low strength cement used in CMC grout production. The continuous line in Figure 3.4 shows the design uniaxial compressive strength of concrete changing with time. For the concrete age

between 3.5 days and 28 days, Equation (3.2) was used to obtain the time-dependent strength of concrete. For the concrete age between 1 day and 3.5 days, the best fit to the experimental data available in the literature (Bazzar, Bouatiaoui & Alaoui 2013; Huang et al. 2013; Lam, Wong & Poon 2000; McCarthy & Dhir 2005; Naik et al. 2003; Siddique 2004; Smith 1991; Yoshitake et al. 2014) was used. The concrete in the referenced literature was applicable to the characteristics of CMC grout (e.g. they were made with a 50% replacement of cement with fly ash and a water/binder ratio of approximately 0.5). The adopted values of f_{ck} at various curing ages are given in Table 3.2.

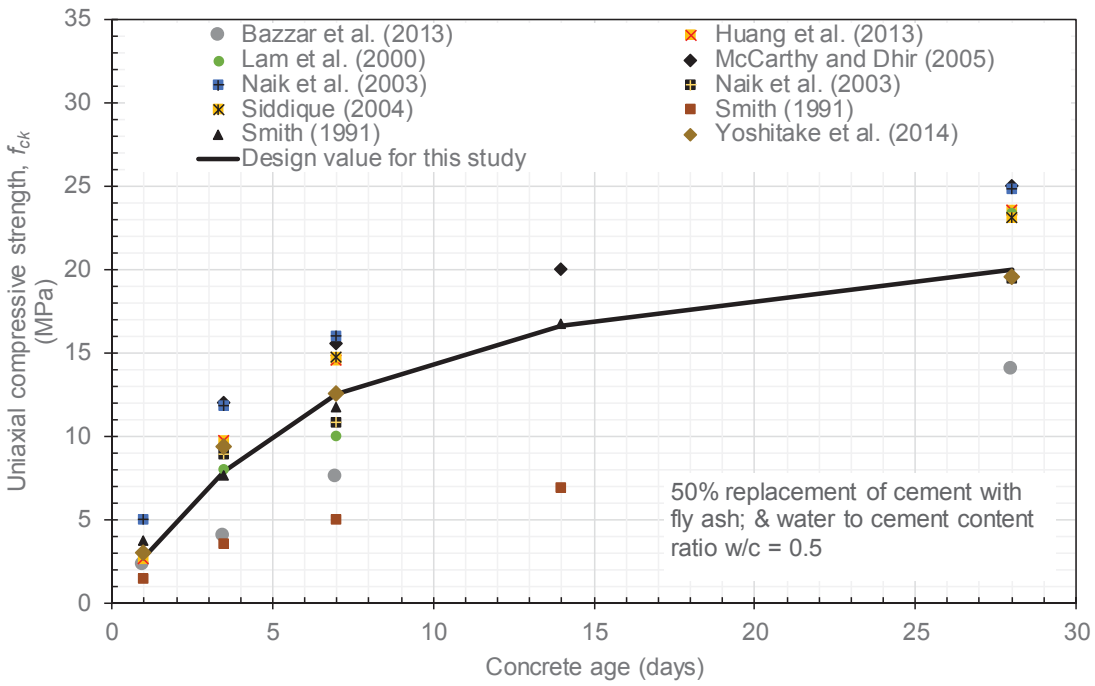

Figure 3.4 Development of the uniaxial compressive strength of fly ash concrete with time

3.3.4.2 Tensile strength of CMC

The most important characteristic of CMC grout for lateral column resistance – the CMC tensile strength was estimated based on Eurocode 2 recommendations for plain concrete.

The mean tensile strength $f_{ctm}(t)$ at an age of t days was estimated from Equation (3.3) as recommended by Eurocode 2 (BS EN 1992-1-1 2015).

$$f_{ctm}(t) = exp\left\{s_c\left[1-\left(\frac{28}{t}\right)^{\frac{1}{2}}\right]\right\} \times 0.3 f_{ck}^{\frac{2}{3}} \quad (3.3)$$

The tensile strength of plain concrete (e.g. CMC) can be estimated using Equation (3.4) from Eurocode 2 (BS EN 1992-1-1 2015).

$$f_{ctd,pl} = \frac{\alpha_{ct,pl} \times f_{ctk,0.05}}{\gamma_C \times k_f} \quad (3.4)$$

where $f_{ctk,0.05}$ = characteristic tensile strength of concrete = 0.7× $f_{ctm}(t)$; $\alpha_{ct,pl}$ = is a reduction factor that accounts for the long term effects on tensile strength ($\alpha_{ct,pl}$ = 0.8); γ_C = factor applied for ultimate limit state design (γ_C=1.5); and k_f = factor to obtain the design resistance of cast in place piles (k_f=1.1). The adopted values may not necessarily be conservative, as in practice CMCs are often designed assuming no tensile stress in the CMC material (Plomteux & Lacazedieu 2007; Wong & Muttuvel 2012a).

3.3.4.3 Stiffness of CMC

The modulus of elasticity E_c estimated from f_{ck} based on Eurocode 2 should only be regarded as indicative, especially for geotechnical applications (BS EN 1992-1-1 2015). As recommended by the ASIRI project for rigid inclusions (ASIRI National Project 2012), a long-term modulus of elasticity of approximately 10 GPa can be used for concrete inclusions fabricated in-situ with a displacement piling method, for a f_{ck} varying from 12 MPa to 20 MPa. This value can be obtained using Equation (3.5) (Bétons de sable 1994).

$$E_c = 3700 \times f_{ck}^{1/3} \text{ in MPa} \quad (3.5)$$

The modulus of elasticity of concrete at age of *t* days, $E_c(t)$ was determined based on Equation (3.5) and by adopting the compressive strength $f_{ck}(t)$ at age t in MPa, as shown in Table 3.2.

3.3.4.4 Adopted Parameters for Modelling CMC

Originally developed for rock mass, the Hoek-Brown criteria (Hoek & Brown 1980) as shown in Equation (3.6) can also be used to model a brittle material such as concrete because it can be considered as one special type of rock, e.g. medium strong claystone, shale or siltstone (Hoek & Brown 1997). In fact, a number of authors adopted the Hoek-Brown criterion to model concrete (Karam & Tabbara 2009; Wu & Zhou 2010).

$$\frac{\sigma_1}{\sigma_c} = \frac{\sigma_3}{\sigma_c} + \sqrt{m\frac{\sigma_3}{\sigma_c} + s} \tag{3.6}$$

where σ_1 and σ_3 = major and minor principal stresses at failure, σ_c = uniaxial compressive strength of intact rock pieces, and m and s = Hoek-Brown material constants. In this study, CMC material was modelled using a plasticity model that incorporates nonlinear Hoek - Brown yield criterion (Hoek & Brown 1980) combined with a tensile yield criterion. The modified Hoek Brown criterion in *FLAC*^{3D} defines the onset of tensile yielding where the minor principal stresses σ_3 (or the tensile stress) reaches the specified tensile strength. Besides σ_c and dilation angle ψ_c, the Hoek-Brown parameter *s =1* were used, assuming that CMC is intact, and the parameter *m* = 12 was selected as recommended by Karam & Tabbara (2009). In fact, the adopted m value can be readily justified based on Equation (3.7) and the literature on the uniaxial compressive strength σ_c and tensile strength σ_t of various types of concrete (Hoek & Brown 1980).

$$\frac{\sigma_c}{|\sigma_t|} = \frac{2}{m - \sqrt{m^2 + 4s}} \approx m \quad \text{for } m > 5 \tag{3.7}$$

The $\sigma_c/|\sigma_t|$ ratio calculated for normal concrete ranges from 10 to 25 (ACI Committee 318 2014) and from 9 to 13 for high fly ash concrete (Siddique 2004; Yoshitake et al. 2014). For many practical cases, practicing engineers can derive the m values from the properties of concrete that are readily available. Table 3.2 shows a summary of all the input parameters for CMC grout adopted in this study.

Table 3.2 Concrete parameters for numerical modelling of CMC

Concrete age, t (days)	**1 day**	**3.5 days**	**7 days**	**14 days**	**28 days**
Concrete density, ρ_c (kg/m^3)	2400				
Modulus of elasticity at age t days, $E_{cm}(t)$ (MPa)	5,100	7,400	8,600	9,400	10,040
Mean tensile strength at age t days, $f_{ctm}(t)$ (MPa)	0.57	1.25	1.62	1.94	2.21
Design tensile strength, σ_t (MPa)*	0.193	0.426	0.55	0.66	0.75
Poisson's ratio, ν'_c	0.2				
Cylinder compressive strength at t days, $f_{ck}(t)$ (MPa)	2.6	7.9	12.5	16.6	20
Dilation angle, ψ_c (°)**	12				
Hoek-Brown constant *m*	12				
Hoek-Brown constant *s*	1				

Note: * $\sigma_t = f_{ctd,pl}$= tensile strength for plain concrete cast-in-situ piles, ** recommended by Vermeer & De Borst (1984) .

3.3.5 Initial Conditions and CMC-Soil Interface

Once the in-situ soil stresses described in Section 3.3.3 were established, the three CMCs along Row 1 were installed by changing the material properties in the existing CMC zones from soils to CMC ("wished-in-place"). CMCs were considered to be impermeable and they were modelled using solid elements. Existing columns E1, E2 and E3 were given the properties of grout that corresponded to either an age of 1 day or 28 days, whichever was

relevant to short and long curing periods, before new columns were installed close by. Although CMCs 1-6 were installed in a period of 3 hours, the properties of one-day old grout was adopted for simplicity.

Interface elements were used to simulate the interaction between CMC and soil, including any possible gapping or sliding. In addition, the constraining effects of previously installed columns on the lateral displacement can be considered, which otherwise may not be possible with analytical methods (Chai, Miura & Koga 2005). For each CMC, the interface between the soil and column consists of an upper portion that represents the interaction between soft soil and CMC, and a lower portion that models the interface between stiff clay and CMC. The Mohr-Coulomb criterion was used to capture the shear strength at the soil and CMC interface. The strength of the tensile bond at the interface was assumed to be zero. The cohesion and friction angle of the clay and concrete interface were calculated based on the relationship given in the literature (Bowles 1997; Potyondy 1961). The normal stiffness and shear stiffness for the interface k_n and k_s were estimated using Equation (3.8), as recommended by Itasca (2012).

$$\mathrm{k_n} \approx \mathrm{k_s} \approx 10 \times max\left[\frac{\mathrm{K} + \frac{4}{3}\mathrm{G}}{\Delta \mathrm{z_{min}}}\right] \tag{3.8}$$

where, K and G = bulk and shear moduli of surrounding soil, and Δz_{min} = smallest width of zone adjoining interface in the normal direction. The adopted parameters are presented in Table 3.3.

Table 3.3 CMC-soil interface parameters adopted in this numerical modelling

Parameters	**Values**	
Types of interaction	CMC - soft soil	CMC - stiff soil
Interface shear and normal stiffness values, $k_s = k_n$ (kPa/m)	3×10^5	2×10^6
Cohesion of interface element, $c_i^{'}$ (kPa)	1	6
Friction angle of interface element, $\phi_i^{'}$ (°)	18	18

3.3.6 Cavity Expansion to Simulate Column Installation

For a simplified simulation, the process of drilling holes for CMC ground improvement is assumed to consist of *(a)* cylindrical cavity expansion along the shaft, and *(b)* spherical cavity expansion near the tip (Figure 3.5a). Note that the analytical solutions using this combined cylindrical and spherical cavity expansion for cone penetration testing by Chai et al. (2015) agreed reasonably well with the laboratory measurements. The creation of a hole was followed by backfilling with CMC grout, and consolidation analyses.

Numerical modelling of the installation of a pile into the clay (i.e. created cavity problem) is difficult to implement owing to the initial singularity. According to Carter, Randolph & Wroth (1979), expanding a cavity with an initial radius r_i to a new cavity radius $r_f = 2r_i$ can be used to give an adequate approximation to what happens in the soil when a cavity expansion from zero radius to the actual column radius (i.e. r_{CMC}) occurs. If the deformation occurs at constant volume i.e. Equation (3.9), then the necessary relation between r_i and r_{CMC} is $r_{\mathrm{CMC}} = \sqrt{3}r_i$ (Carter, Randolph & Wroth 1979). For example when r_{CMC} = 225 mm, then the adopted initial radius of the cavity would be r_i = 130 mm. However, the required final radius of the cavity would be r_f = 260 mm which is notably

larger than the radius of the actual CMC (r_{CMC}) and is not desirable. Parametric study conducted by Castro & Karstunen (2010) found that quadrupling the initial cavity gives almost identical results compared to doubling the cavity as presented by Carter, Randolph & Wroth (1979). Hence, a smaller initial cavity r_i = 65 mm was chosen for this study, which results in a more realistic case as the final radius r_f = 234 mm determined based on Equation (3.9) is much closer the actual CMC radius (only 4% difference). It should be noted that an initial cavity radius smaller than 65 mm would result in excessive mesh distortion and could not be adopted successfully in this study.

$$r_f = \sqrt{r_i^2 + r_{CMC}^2} \tag{3.9}$$

The adopted initial and final radii were applied to the cylindrical and spherical cavity expansions, as shown in Figure 3.5a. Note that concrete over-break and the effect of concrete pumping pressure was not considered in this study.

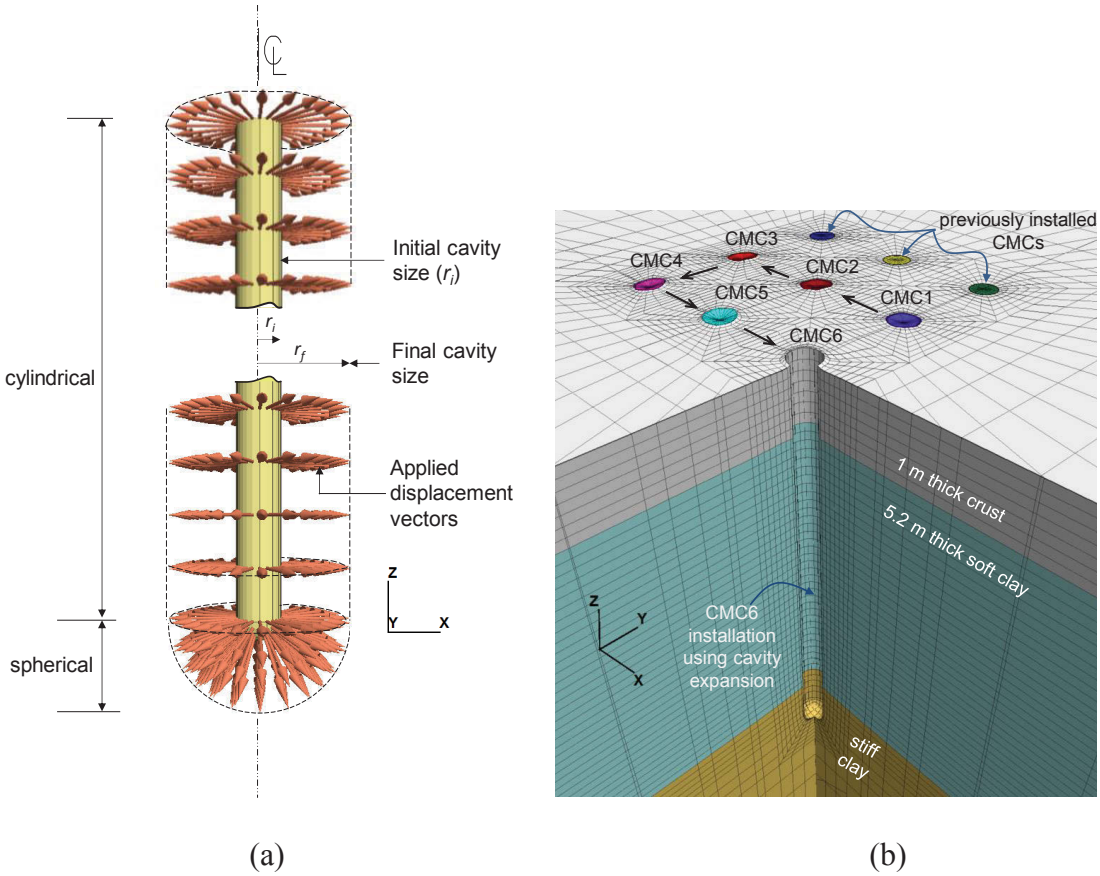

(a) (b)

Figure 3.5 (a) Simplified model for CMC installation, and (b) Deformed mesh after undrained cavity expansion at CMC 6 in Sequence No. 1

The first step in creating a small initial cavity ($r = r_i$) is to turn the soil inside the initial cavity into "null" material, and then apply outward normal velocities to the cavity wall so that when mechanical stepping in large strain mode is used, the wall would be displaced in a normal direction until achieving the final cavity r_f = 234 mm. After creating the CMC cavity, concrete material (see Table 3.2) was assigned to the elements inside the cavity to simulate the placement of CMC grout. After installation of each CMC, a coupled hydraulic and mechanical simulation was conducted to allow the excess pore water pressure to dissipate within a 30-minute lag between two successive CMC installations. The starting conditions for consolidation analysis corresponded to those immediately after cavity expansion (Randolph, Carter & Wroth 1979). The next CMC in the sequential

order was installed in the same way as the first CMC. Figure 3.5b shows the deformed mesh of soil and columns, after creating the hole at CMC 6. The changes in model variables in the soil and CMCs were recorded with time.

3.4 Results and Discussion

3.4.1 Response of Soil to CMC Installation

3.4.1.1 Lateral Soil Movement

Figure 3.6a shows the contours of lateral soil displacement at the ground surface (in x direction) induced by the complete penetration of the first CMC (i.e. CMC 1 of installation Sequence No. 1). Note that the existing CMCs are well within the radius of influence of the new column installation. Figure 3.6b shows the contours of the lateral soil surface displacement in y direction where as expected, the existing columns restrained movement, and the displaced soil moved past the clear space between the two existing columns.

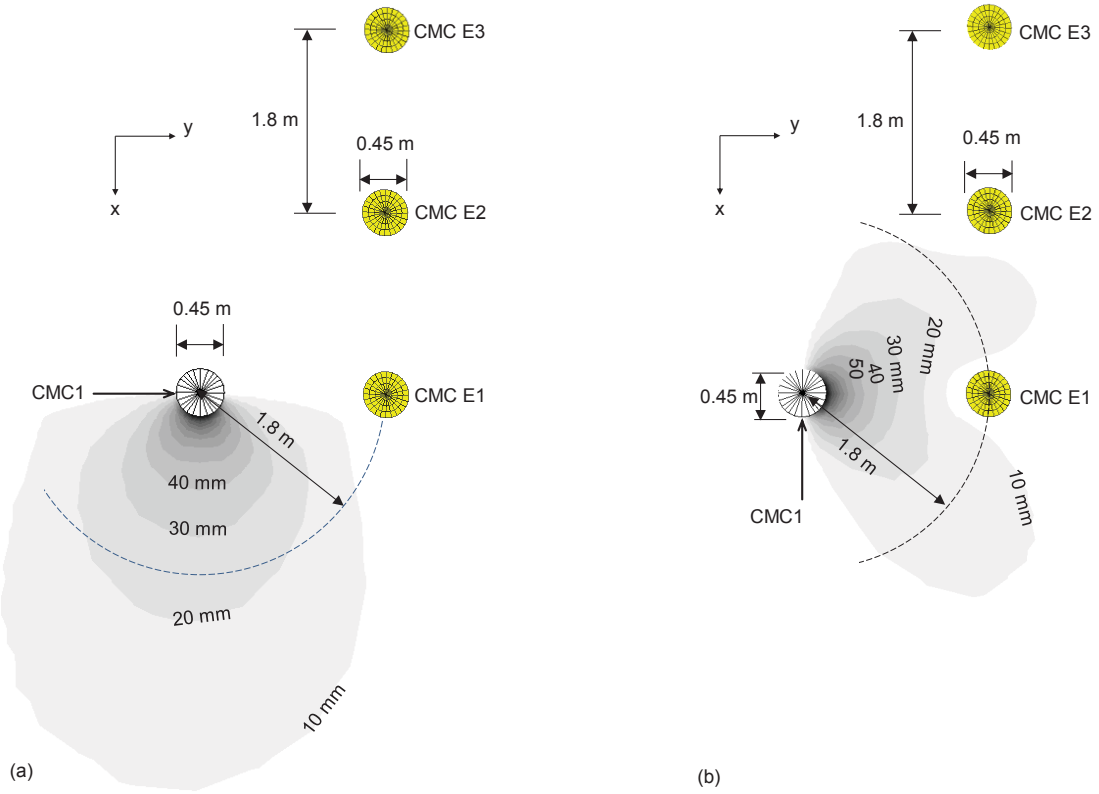

Figure 3.6 Contours of lateral surface soil displacement (a) in x direction and (b) in y direction, induced by installing the first CMC

The lateral displacement of soil due to installation plotted with depth in Figure 3.7 reveals that a single CMC installation may affect the next two adjacent columns in the row. Assuming that $\frac{\delta}{r_{CMC}} = 2\ \%$ represents the outer boundary of the zone of influence (or beyond where lateral displacement δ is less than 5 mm), Figure 3.7 shows that the zone of influence had extended by approximately 24 times of the CMC radius. It can be noted that the lateral soil displacement in soft clay was greater than in the underlying stiff clay.

Figure 3.8 shows a cross section through CMC 2 and CMC E2, and the accumulated lateral soil displacement induced by the installation of the first two CMCs (i.e. CMC1-2). The contours shown in Figures 3.7 and 3.8 indicate that the installation of CMC2 increased the movement of accumulated soil; thus, the radius of the influence zone

($\frac{\delta}{r_{CMC}} \approx 2\%$) increased from 24 r_{CMC} to 28 r_{CMC} when the second CMC was installed. Figure 3.8 also shows that the existing CMC E2 modified the pattern of lateral soil movement with denser contours in front of the column and much wider contours around the back face.

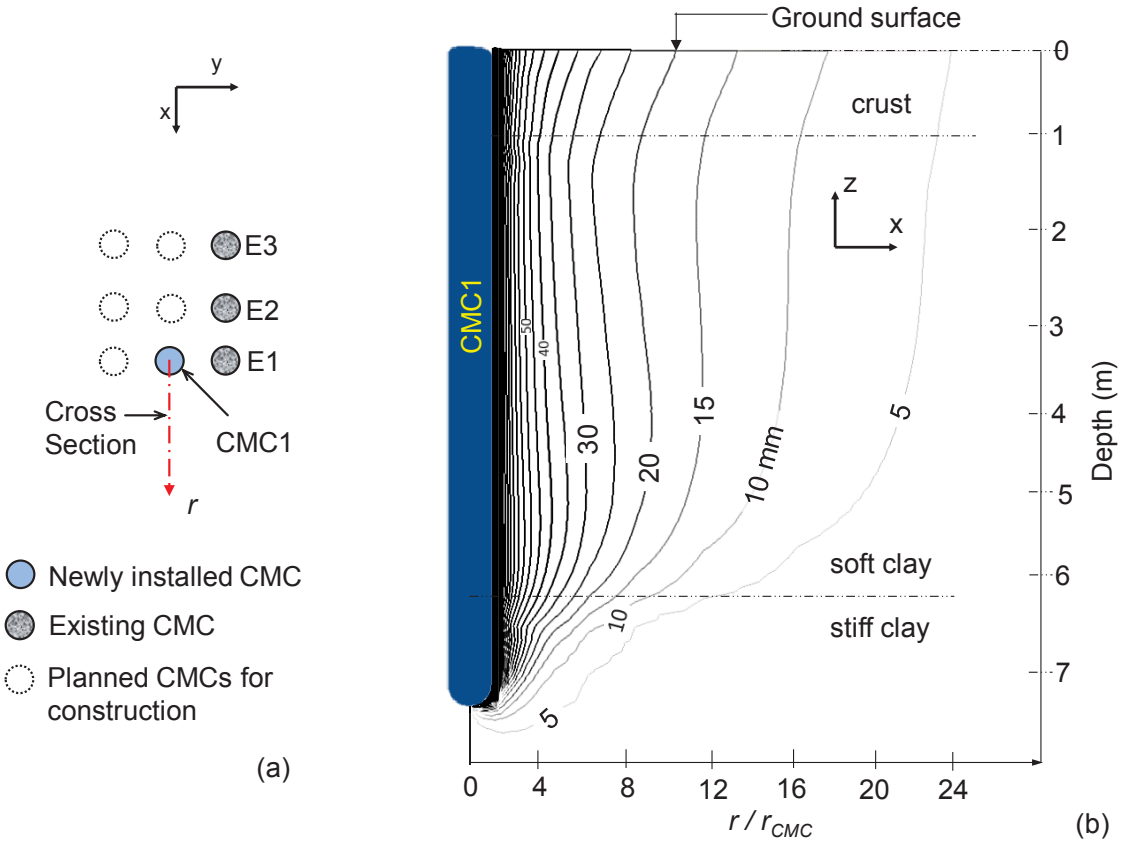

Figure 3.7 Magnitude of lateral soil displaced by the installation of CMC1 (a) plan view, and (b) cross section through CMC1 axis

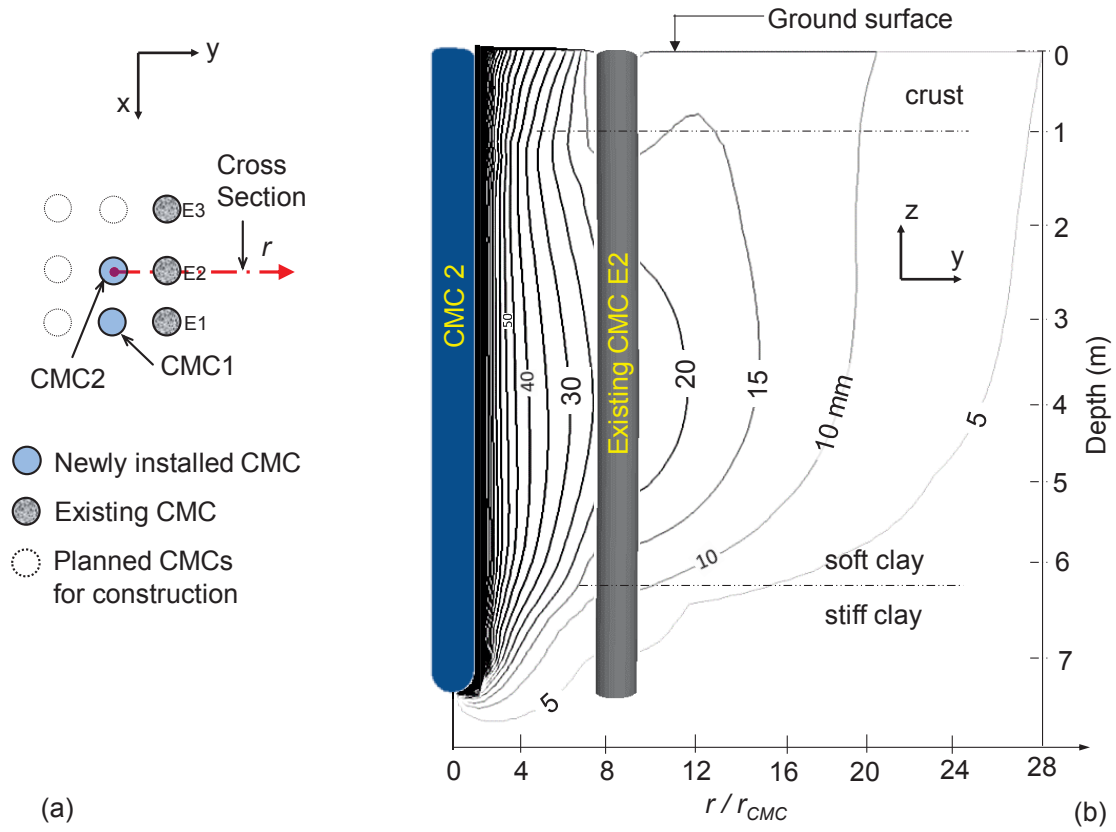

Figure 3.8 Accumulated lateral soil displacement induced by two CMCs installed in succession: (a) plan view, and (b) cross section through the axis of CMC 2 and CMC E2

Chai et al. (2009) proposed closed-form equations for estimating the lateral soil displacement caused by the installation of a row of soil–cement columns derived based on cylindrical cavity expansion theory. This solution is currently the only analytical method available for estimating installation effects induced by installing multiple columns (Chai & Carter 2012). Figure 3.9 shows the lateral soil displacement in *y* direction induced by installing CMC 1 to CMC 3 in a row at the mid-depth of the soft clay layer. The comparison shows that there is good agreement between the adopted numerical approach in this study and the Chai et al. (2009) analytical method.

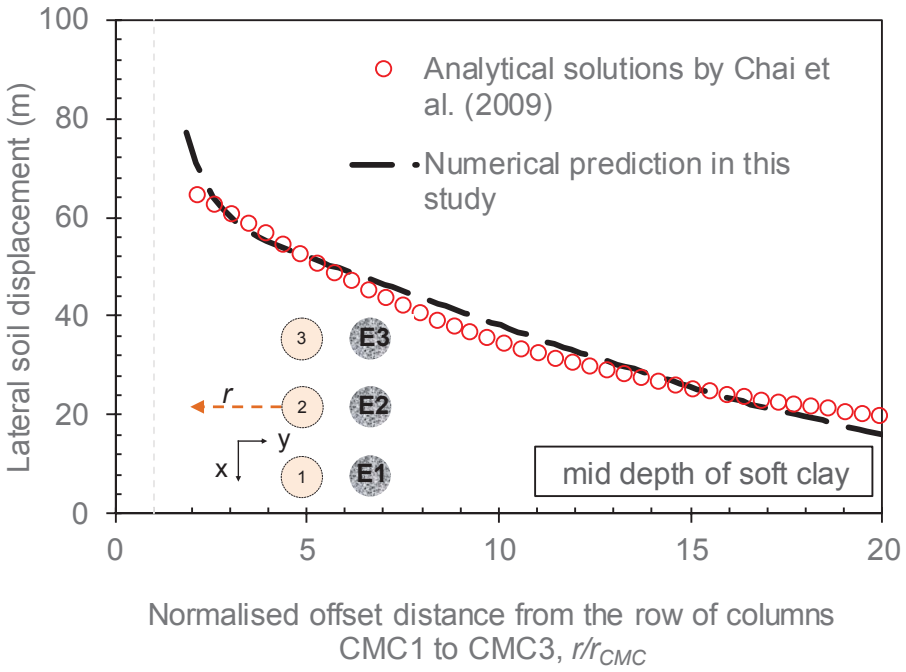

Figure 3.9 Comparisons of Chai's method (Chai et al. 2009) and this numerical study for lateral soil movement induced by installing columns of the first row

The affected columns were traditionally assessed using the estimated lateral displacement of soil in an in-situ soil field (Poulos 1994), so it is also interesting to estimate the accumulated lateral displacement of displaced soil that moved past the clear space between two existing columns, induced by the installation of new CMCs (Figure 3.10a). At Point A in Figure 3.10a, located at an offset distance of $8\times r_{CMC}$ from CMC Row 2, the lateral soil movement induced by installing two new rows of columns was approximately 47 mm, which is almost twice of the lateral soil movement induced by a single CMC installation as shown in Figure 3.7. Although the difference in lateral soil movements within the upper 2 m of soil was insignificant between the two installation sequences, the differences between depths of 2 m and 6 m are notable because of different installation sequences. Figure 3.10a shows that the predicted lateral soil movement in the soft clay layer is 15% greater when Sequence No. 2 is used rather than Sequence No. 1. In the stiff clay, the lateral soil movement induced by both installation sequences was

between 5 mm and 10 mm, and is of the same order of magnitude compared to the corresponding values for a single CMC. Considering the overall profile of lateral soil movement with depth, it can be seen that the general pattern of lateral soil displacement was similar to the field measurement reported by Chai, Miura & Koga (2005) for the soil-cement column installations at the Kubota site in Saga, Japan.

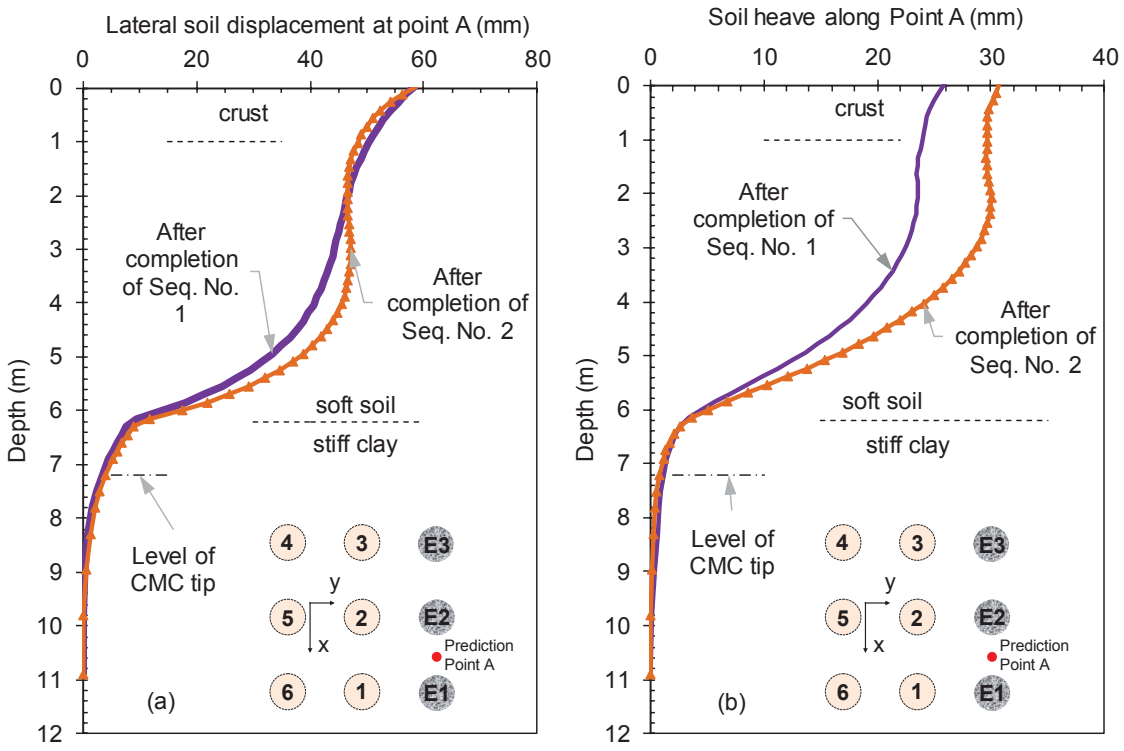

Figure 3.10 Induced soil movement: (a) Lateral displacement of soil in y direction, and (b) Soil heave between two adjacent existing CMCs after installing new CMCs

The predicted lateral soil displacement as shown in Figure 3.10a was compared to the measured values taken from a field case study in Melbourne, Australia (King et al. 2017). It is noted that the diameter and the quantities of the columns reported by King et al. (2017) and those adopted in this study were similar. In addition, at both sites the soils were over-consolidated clays; and the soil layerings and stiffnesses were also similar. Due to the difference in the thicknesses of the soil layers between the two studies, the depth was normalised by the depth to the hard stratum, at which the lateral soil movements

induced by CMC installations were almost zero. Figure 3.11 shows the comparison between the measured lateral soil movements and the numerically predicted values at depths in the soil induced by the adjacent soil-displacement column installation activities. The observed trends as shown in the figure indicate that the predicted lateral soil displacement matched well with the measured data.

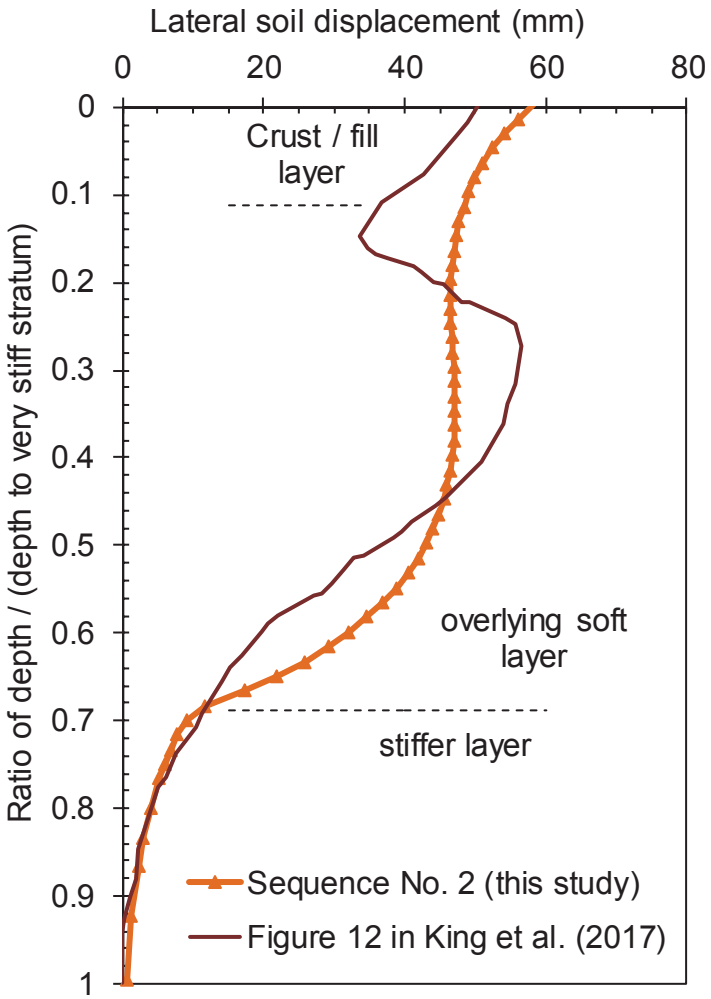

Figure 3.11 Comparison of measured and numerically predicted lateral soil movements in the soil induced by the adjacent column installation site

3.4.1.2 Vertical Soil Heave

Sagaseta, Whittle & Santagata (1997) published the Shallow Strain Path Method (SSPM) solution to estimate the soil movement around an axisymmetric closed-ended pile with a rounded tip. This solution combines the merit of the strain path method (Baligh 1985) for deep penetrations, and the methods used to compute soil deformations due to near-surface ground loss (Sagaseta 1987). The closed-form small-strain solutions of SSPM method (Sagaseta, Whittle & Santagata 1997) for the pile penetration can be used to reliably predict the ground surface heave due to column installation (Ni, Hird & Guymer 2009; Sagaseta & Whittle 2001). Soil heave induced by the installation of CMC 1 was plotted against the normalised radial distance, as shown in Figure 3.12, in which the prediction by the finite difference analysis in this study shows reasonably good agreement with the predicted values using the SSPM method. The SSPM method, however, yielded greater soil heave within a radial distance of 4 times the CMC radius, but as reported in the literature (Poulos 1994), the SSPM method normally gives slightly higher soil heave near the axis of a pile and less movement away from the axis. Referring to Figure 3.12, around paths CE and CD, the existing CMCs E1 and E2 led to a localised reduction in soil heave due to friction between the soil and the columns.

Figures 3.13a and 3.13b show the accumulated soil heaves at the ground surface and the vertical uplift of three existing CMCs (i.e. E1 to E3), due to the installation of nearby CMCs (i.e. CMCs 1 to 6). In particular, Figure 3.13a plotted the predictions corresponding to Sequence No. 1 and clearly indicates that soil heave between CMC E1 and E2 increased rapidly as installation proceeded from CMC 1 to CMC 3, whereas the pattern for Sequence No. 2 was the reverse, as shown in Figure 3.13b. In fact, the soil heave induced by the installation of the first row accounted for approximately 85% of the

total soil heave near the existing CMCs induced by Sequence No. 1, compared to only 20% for Sequence No. 2. However, at the completion of all installations, the maximum soil heave at the surface recorded between the two adjacent existing CMCs was 26.5 mm and 31 mm for installation Sequences No. 1 and No. 2, respectively (a difference of 17%). Hence, predicted progressive soil heave as the installation progresses clearly indicated that the first three installed columns along Row 2 of Sequence No. 1 acted as the stiff barrier preventing further soil heave built-up towards CMCs E1-E3. Due to the soil heave, the CMC E2 was uplifted by 9.1 mm and 9.7 mm after installation Sequences No. 1 and No. 2, respectively, representing a 6% difference. It should be noted that, referring to Figures 3.13a and 3.13b, the predicted soil heave for both installation sequences was approximately three times the column uplift.

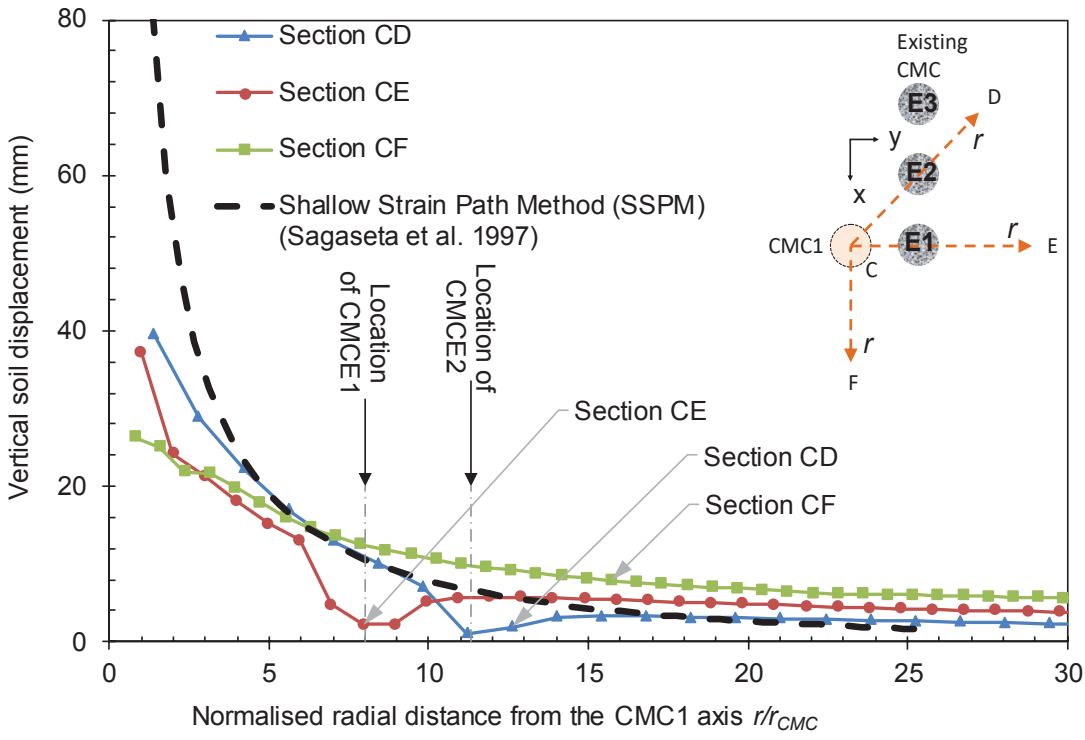

Figure 3.12 Comparisons of Sagaseta, Whittle & Santagata (1997) analytical method and this numerical study for soil heave induced by installation of CMC 1

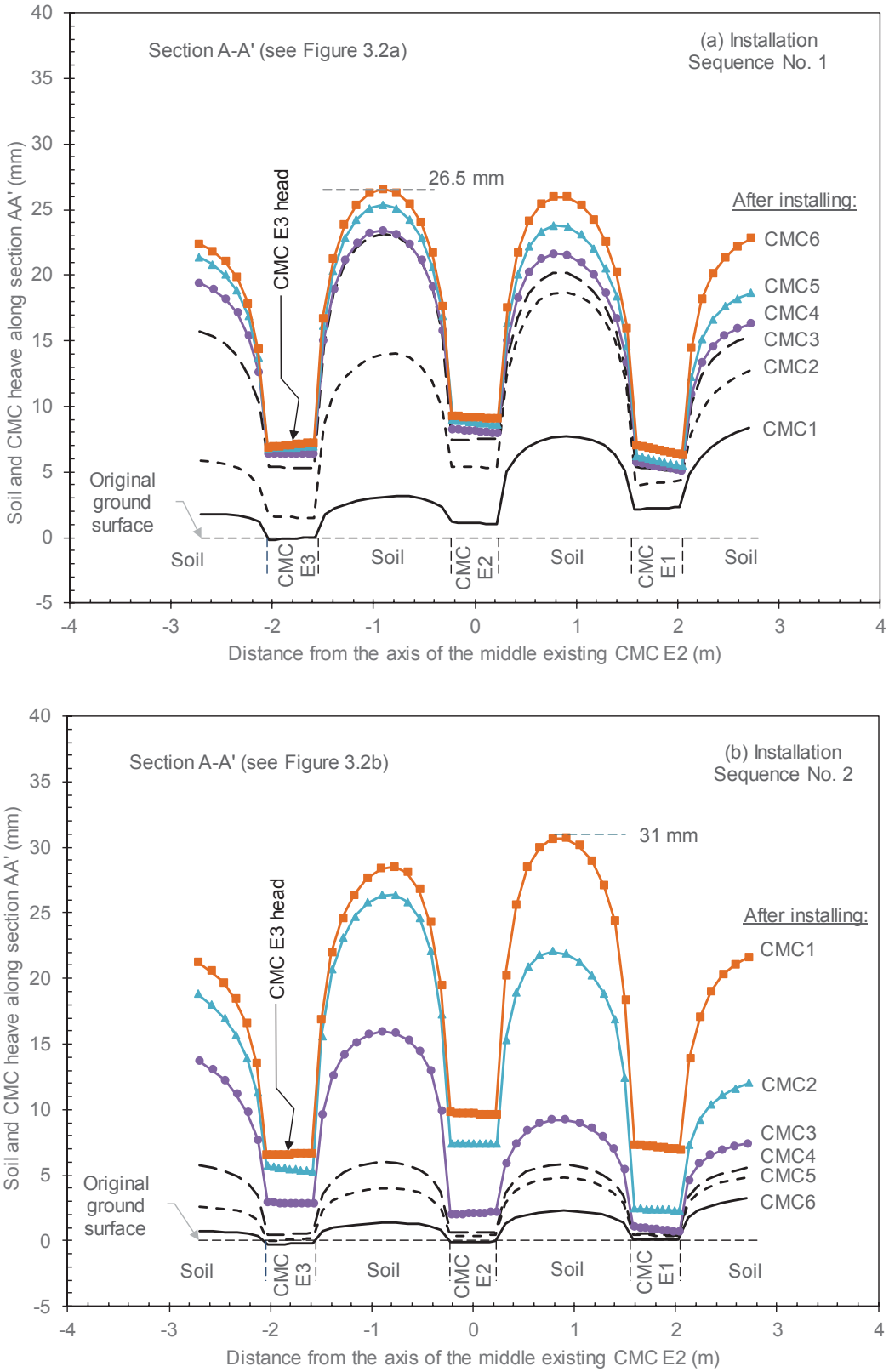

Figure 3.13 Soil heave and CMC uplift due to new installations (a) Sequence No. 1 and (b) Sequence No. 2

When a site involves installation of a large number of CMCs such as those reported by Michalowski et al. (2018), estimating induced soil heave may be useful in planning subsequent earthworks to achieve the required finished platform level. The contour plots of predicted ground surface heaves are shown in Figures 3.14a and 3.14b for installation Sequences No. 1 and No. 2, respectively; the predicted ground surface heave ranged from 20 mm (near the edge of the existing CMCs and outside the newly installed columns at a distance of 8D) to 100 mm (near the edge of CMCs 1-6). Figure 3.14b shows that the contour lines of soil heave at the front face of the existing CMCs were more concentrated due to the installation Sequence No. 2. Note that unlike installation Sequence No. 1, the contour line corresponding to 30 mm soil heave induced by installation Sequence No. 2 extended beyond the front face of the existing CMCs.

The use of different sequential orders for CMC installation also results in different amounts of soil heave with depths. Soil heave at location A between CMCs E1 and E2, is plotted with depth in Figure 3.10b. Most of the calculated soil heave occurred in the upper half of the soft soil where Sequence No. 2 induced 25% more heave than Sequence No. 1. As expected, there was a rapid decrease in heave at the interface of the soft soil and stiff soil near the tip of the CMC.

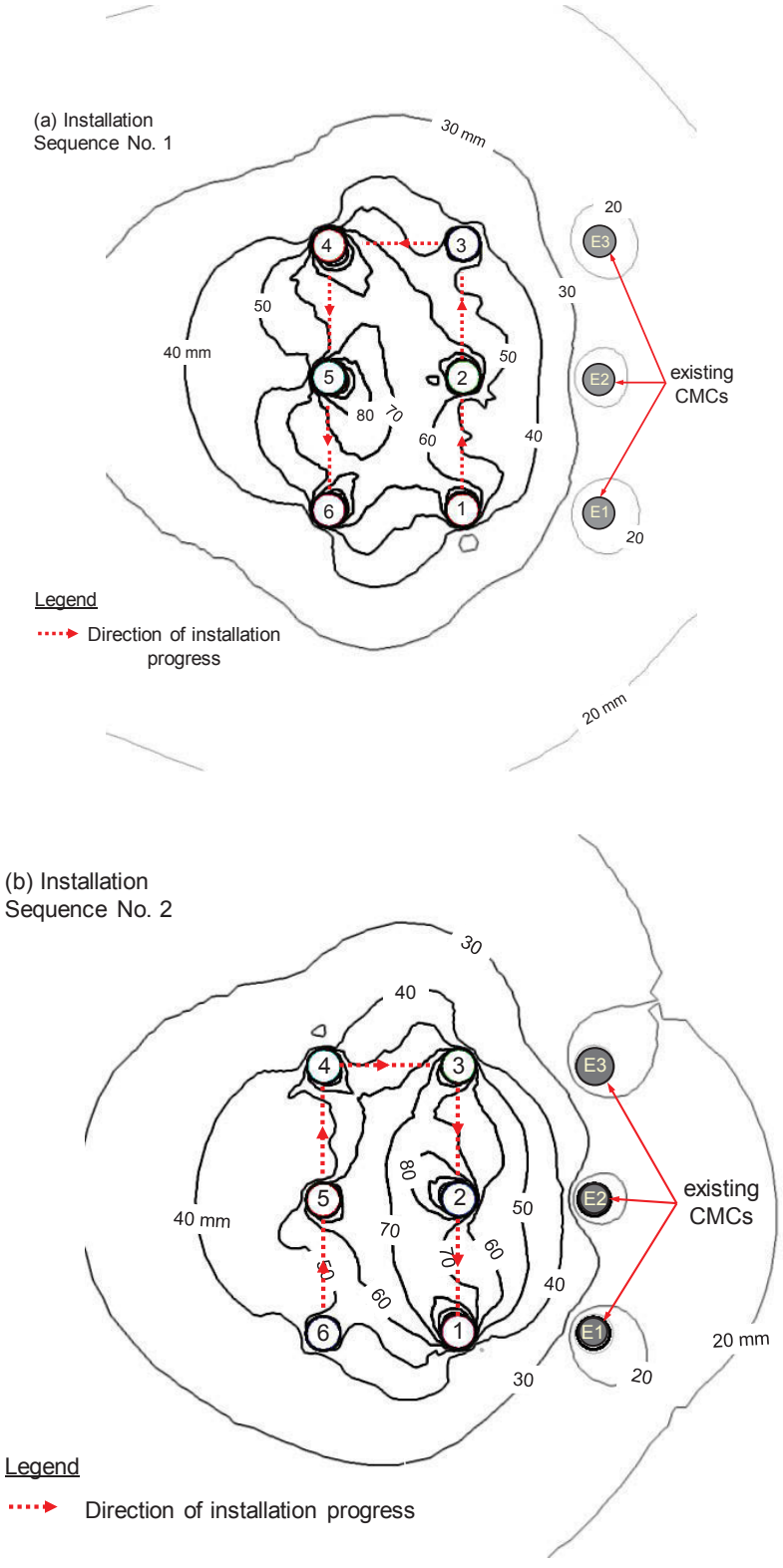

Figure 3.14 Contour plot of the vertical movement of soil at the surface after installing all the CMCs: (a) Sequence No. 1 and, (b) Sequence No. 2

After installing CMCs, the fluid flow and distribution of stress in the soil cause time-dependent movement due to the consolidation process. Figures 3.15a and 3.15b show that the soil surface continued to heave after installing the CMCs and the existing column heads rose accordingly. Four weeks after installation, post-installation soil heave was 2.9 mm and 3.4 mm for Sequences No. 1 and 2, respectively. The predicted post-installation soil heaves were approximately 10% of the predicted ground heave during CMCs 1-6 installation, which were 26.5 mm and 31 mm for installation Sequences No. 1 and No. 2, respectively (see Figures 3.13a and 3.13b). The results presented in Figures 3.15a and 3.15b are in good agreement with the past field observations reported by Randolph, Carter & Wroth (1979) and Hagerty & Peck (1971) for driven piles; indicating that the soil heave continues a long time after pile installation. Figure 3.16a shows the change in soil surface heave predictions at Point A between CMCs E1 and E2 from the installation time of CMCs1-6 to over one month after installation. The rate of soil heaving over time as shown in Figure 3.16b decreased substantially three weeks after completion of the installation.

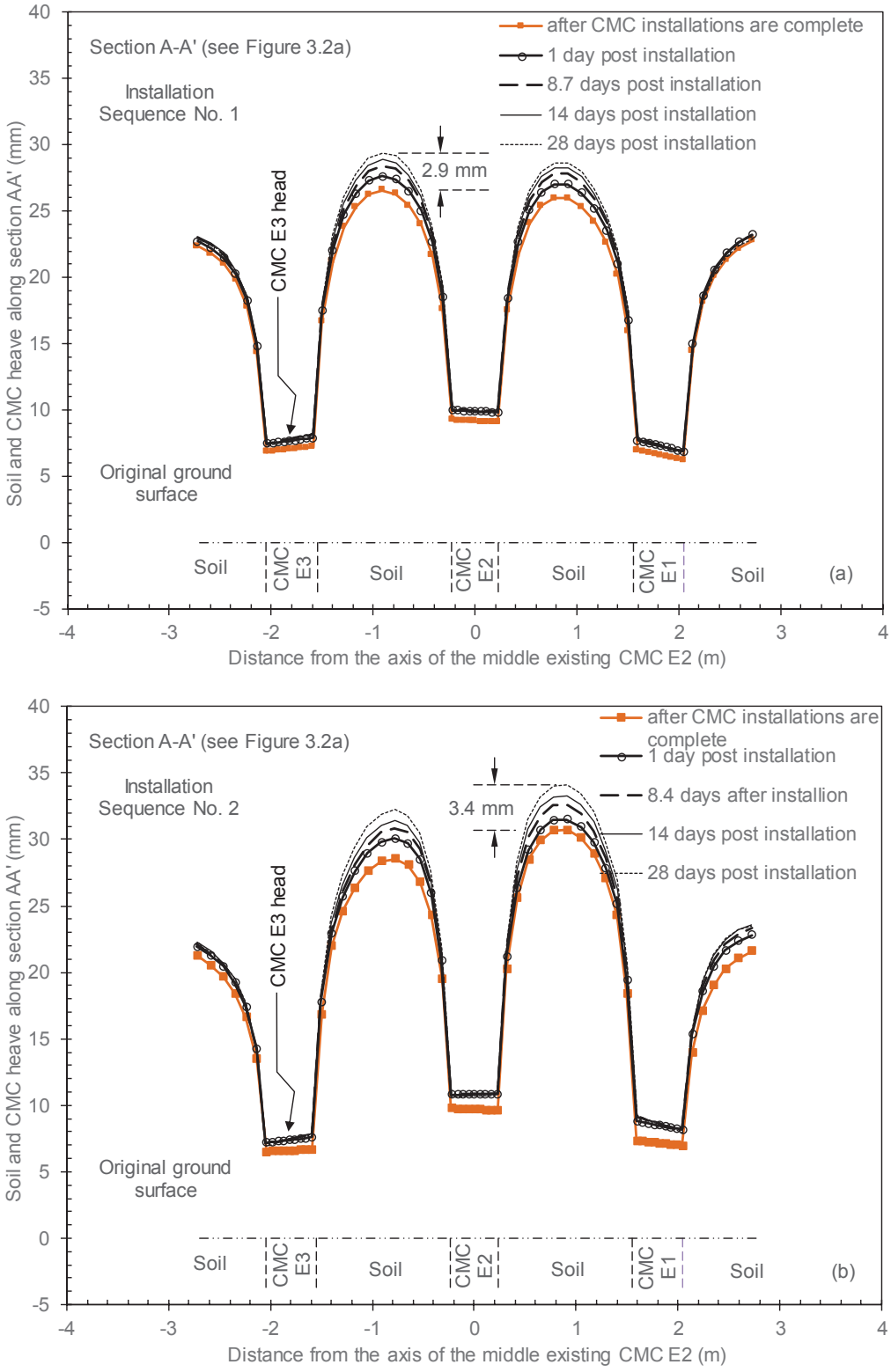

Figure 3.15 Time-dependent uplift of CMCs and soil heave: (a) Sequence No. 1 and, (b) Sequence No. 2

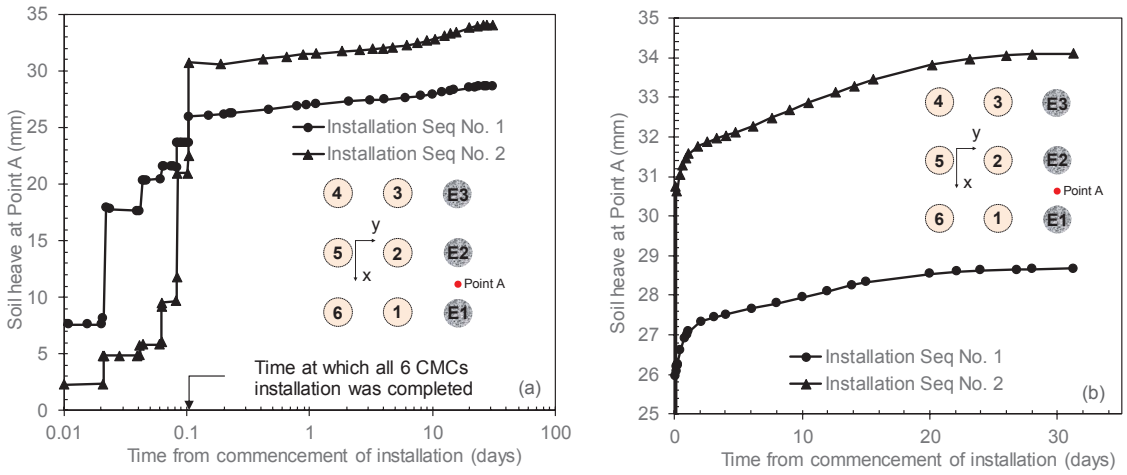

Figure 3.16 Soil heave between two existing CMCs during and after installing CMC1-6 with the time axis plotted: (a) on a logarithmic scale and (b) on a normal scale

3.4.1.3 Excess Pore Water Pressure

The existing analytical solutions (Vesic 1972) for assessing the generation of excess pore water pressure induced by the pile driving was used to compare with the results of the numerical model. In a soil modelled as an elastic-perfectly plastic material, the excess pore water pressure Δu generated around a driven pile, under plane strain conditions and on the assumption of deformation at constant volume, can be determined by the cylindrical cavity expansion solution in Equation (3.10) (Vesic 1972).

$$\Delta \mathrm{u} = 2\mathrm{s_u}\, ln(\frac{\mathrm{R_p}}{\mathrm{r}}) \tag{3.10}$$

where r_o = radius of the pile ; R_p = radial position of elastic-plastic boundary; $\left(\frac{R_p}{r_0}\right)^2 = G/s_u$; and r = radial distance from the axis of the pile ($r_0 \leq r \leq R_p$). Equation (3.10) provides a reasonable method to estimate Δu in the plastic region for normally consolidated or lightly overconsolidated soils (Randolph, Carter & Wroth 1979; Yu 2000). The excess pore water pressure (Δu_{sp}) induced by spherical cavity expansion below the tip of the column is (Vesic 1972):

$$\Delta u_{sp} = 4 s_u \ln\left(\frac{R_{sp}}{r_{sp}}\right) \quad (3.11)$$

where R_{sp} = radius of the plastic zone around an expanding spherical cavity; r_{sp} = spherical radial distance; and $R_{sp} = r_o \sqrt[3]{G/s_u}$.

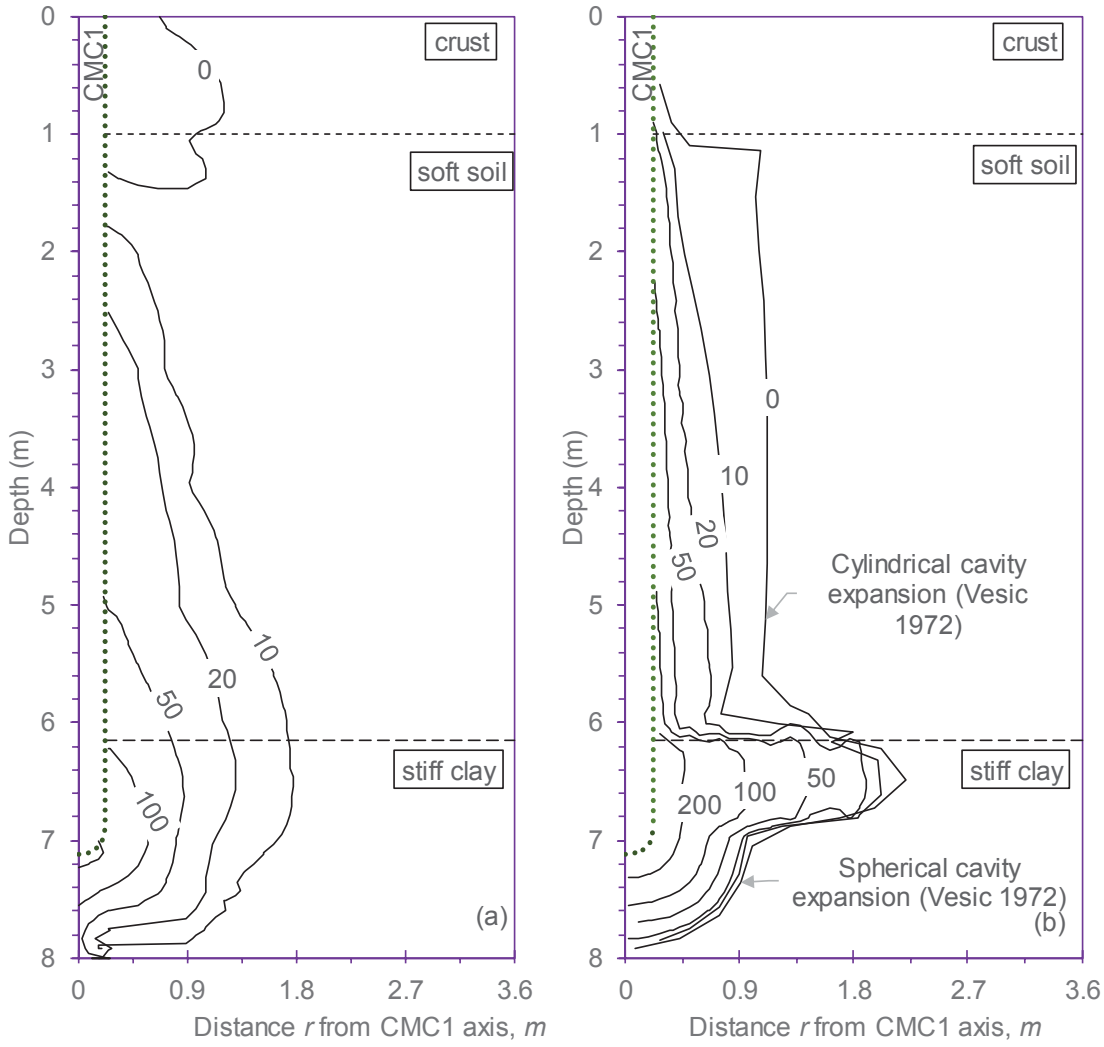

Figure 3.17. Excess pore water pressure generated by installing CMC 1: (a) current numerical prediction, and (b) existing analytical solutions by Vesic (1972)

Figure 3.17 shows the distributions of Δu in the soil obtained from the current numerical simulation and the existing analytical solutions presented in Equations (3.10) and (3.11) with some reasonable agreement. The discrepancy in the predicted values can be

attributed to uncertainty in the adopted values of G/s_u for use in Equations (3.10) and (3.11), and to the isotropic soil stress conditions assumed in the analytical solutions. While the analytical solutions yield excess pore water pressures at discrete points based on a plane strain assumption, the numerical methods can describe the cavity expansion in layered soils and the complex strain paths that soil follows near the tip of the pile.

The consolidation analysis included at the end of each CMC installation indicated that the excess pore water pressure had largely dissipated. Immediately adjacent to the front face of CMC E2 (i.e. Point C), the variation of accumulated excess pore water pressure (Δu) induced by installation Sequences No. 1 and 2 is shown in Figures 3.18 and 3.19. The Δu value at the end of installation Sequence No. 2 was approximately 42 kPa, almost twice the Δu induced by installation Sequence No. 1 (i.e. 24 kPa). In fact, after a peak Δu value induced by the installation of CMC 2 in installation Sequence No. 1, the consolidation time available during the installation of subsequent columns (i.e. 0.5 hours per column) largely reduced the accumulated excess pore water pressure. Referring to Figure 3.19, an opposite trend was observed for installation Sequence No. 2 where the first four columns did not induce considerable excess pore water pressure, compared to the last two columns (i.e. CMC 2 and 1). Therefore, it can be concluded that the time lag between the installations of two successive CMCs is an important factor because it directly affects the amount of excess pore water pressure build-up as construction proceeds.

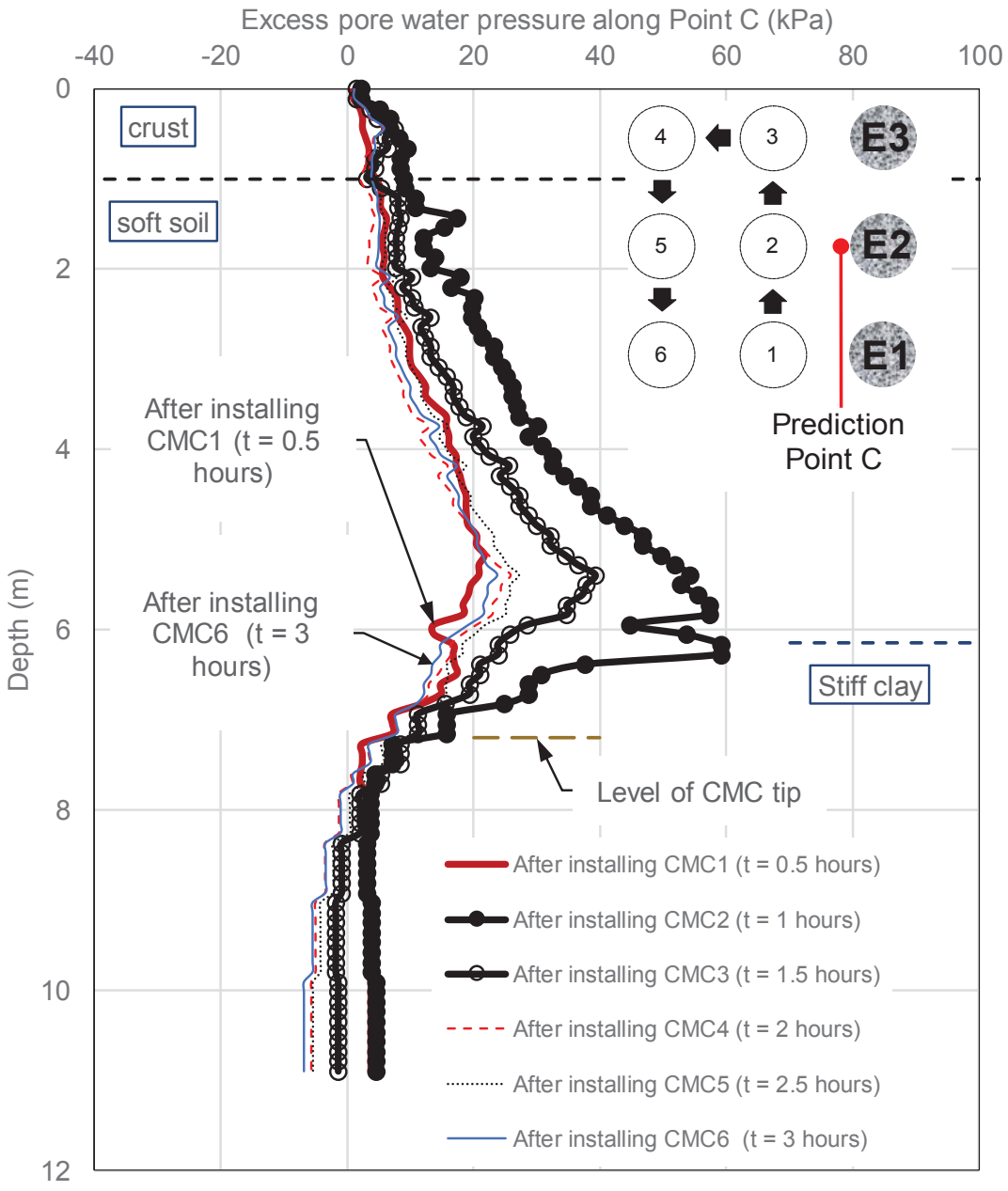

Figure 3.18 Accumulated excess pore water pressure along the front face of CMC E2, induced by installing nearby CMCs (Sequence No. 1)

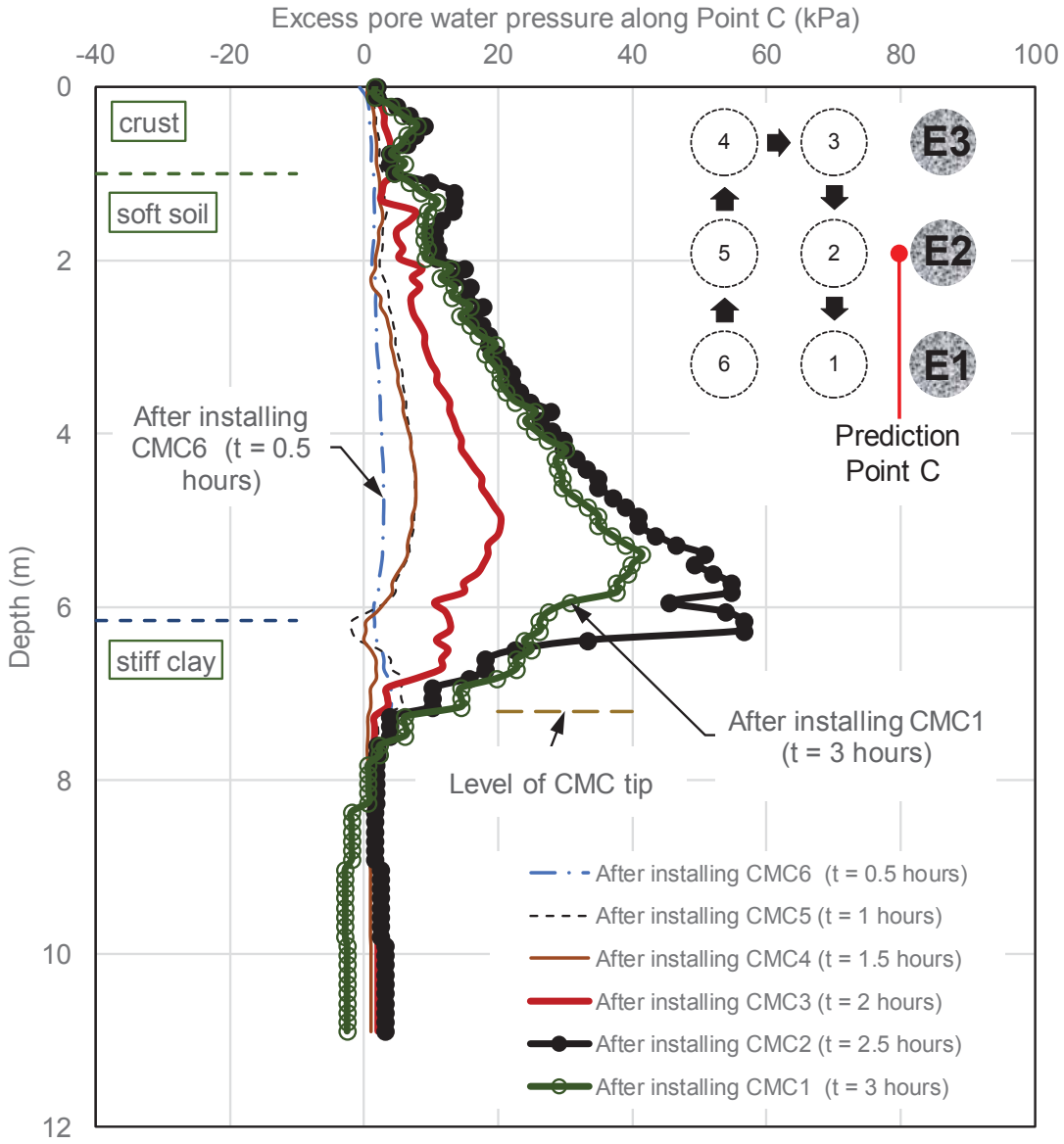

Figure 3.19 Accumulated excess pore water pressure along the face of CMC E2, induced by installing nearby CMCs (Sequence No. 2)

A comparison was made between the predicted excess pore water pressures (Figure 3.19) with the measured values reported by King et al. (2017). The comparison indicates a reasonable agreement in terms of the excess pore water pressures generated in the soil near the installation site. In particular, an increase in the pore water pressure (Δu) of 70 kPa was measured at a depth of 8 m below the ground level by King et al. (2017) while

this study predicted a maximum excess pore water pressure of approximately 60 kPa at a depth of approximately 6.2 m.

The variation of excess pore water pressure (Δu) was monitored at three locations near the front face of CMC E2 as shown in Figures 3.20a, 3.20b, and 3.20c. Cross section BB' (see Figure 3.2) was included in Figure 3.20 to identify these monitoring points. Referring to Figure 3.20, the following observations can be made:

- At point D in Figure 3.20a (i.e. near the mid-depth of soft soil), the maximum Δu generated during CMC installations was approximately 20 kPa. As CMC installations were completed, the excess pore water pressure at this point fell rapidly to 6 kPa, and seven days after installation Δu rose to 9 kPa before dissipation.
- At Point E in Figure 3.20b (i.e. 6 m depth), the maximum Δu generated due to CMC installation was 55 kPa, but two weeks after installation Δu at Point E dropped to 5.5 kPa (i.e. 90% excess pore water pressure had dissipated).
- At Point F in Figure 3.20c, during installation both construction sequences generated negative excess pore water pressure in the soil. The maximum negative Δu at Point F was -11 kPa and -16 kPa for Sequences No. 1 and No. 2, respectively, but one day after all the CMCs had been installed, Δu increased to approximately 9 kPa before dissipation.

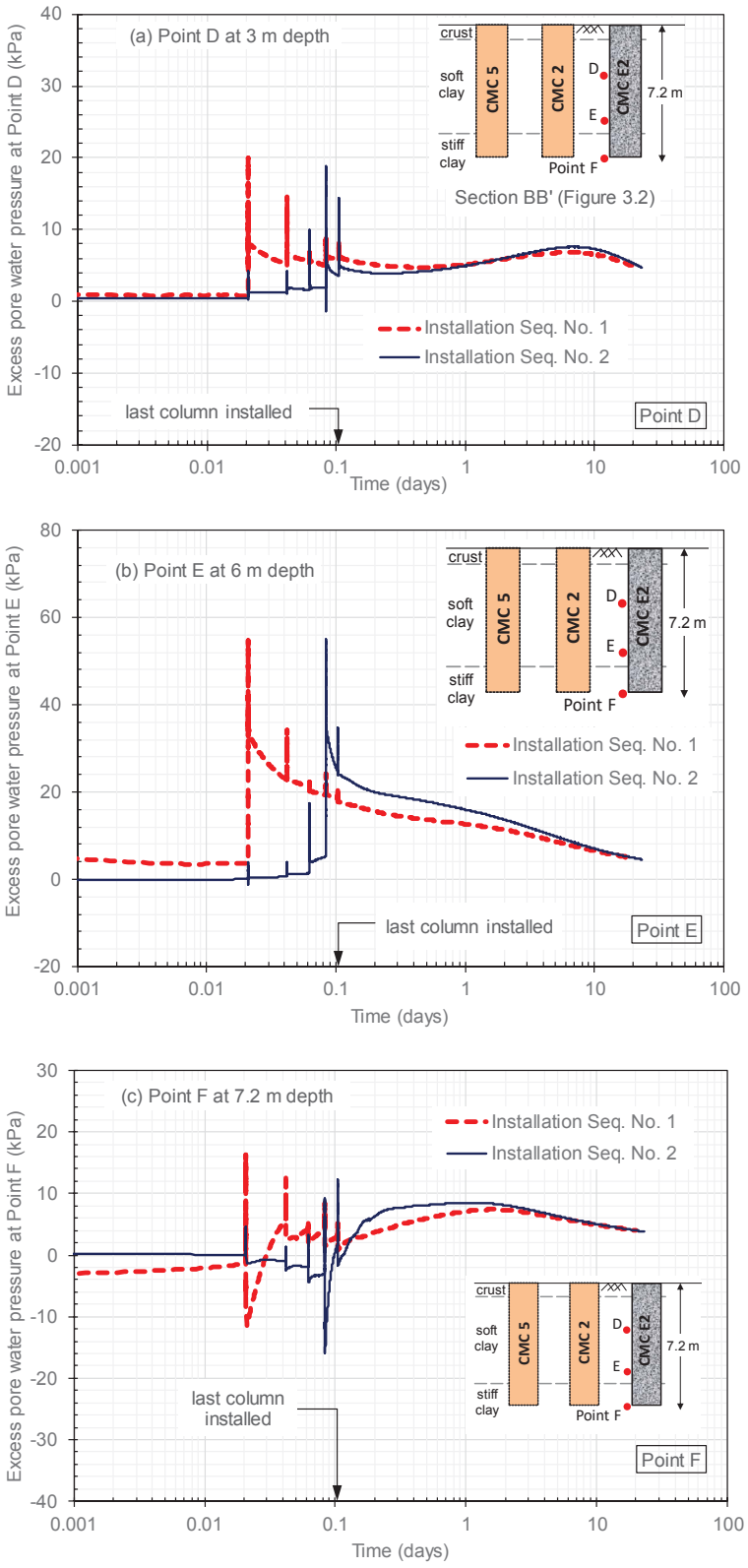

Figure 3.20 Excess pore water pressure along CMC E2 front face: (a) Point D, (b) Point E, (c) Point F

3.4.1.4 Mean Effective Stress

Figure 3.21a shows the evolution of the excess pore water pressure (Δu) and mean effective stress p' in the soil near the face of CMC 2 and CMC E2 at 2.0 m depth. The mean effective stress in the soil near the face of CMC 2 increased by 13 kPa, which is almost twice as large as the in-situ p'_o. Four weeks after installation, the rise in p' mainly occurred in the soil within a radius of $3 \times r_{\mathrm{CMC}}$ from CMC 2. The effect of installing CMC 2 on the stress state of the soil adjacent to CMC E2 was evident due to the increase in the mean effective stress p' at 2 m depth by 25% and 50% on the front and back face of CMC E2, respectively. During the soil consolidation process, although there was a slight increase in p' on the back face, a marginal decrease in p' of the soil occurred on the front face of CMC E2. A slight reduction in p' of the soil on the front face of CMC E2 can be attributed to small excess pore water pressure Δu generated at this location by the time all installations were completed (Figure 3.21a), and is likely to be the result of the lateral deflection of CMC E2 away from CMCs 1-6 (Figure 3.24a). In fact, although the predicted net lateral soil resistance was rather small at 2 m depth (see Figure 3.25d, installation Sequence No. 1), careful inspection shows that the back face of CMC E2 actually carried the soil resistance, rather than the front face.

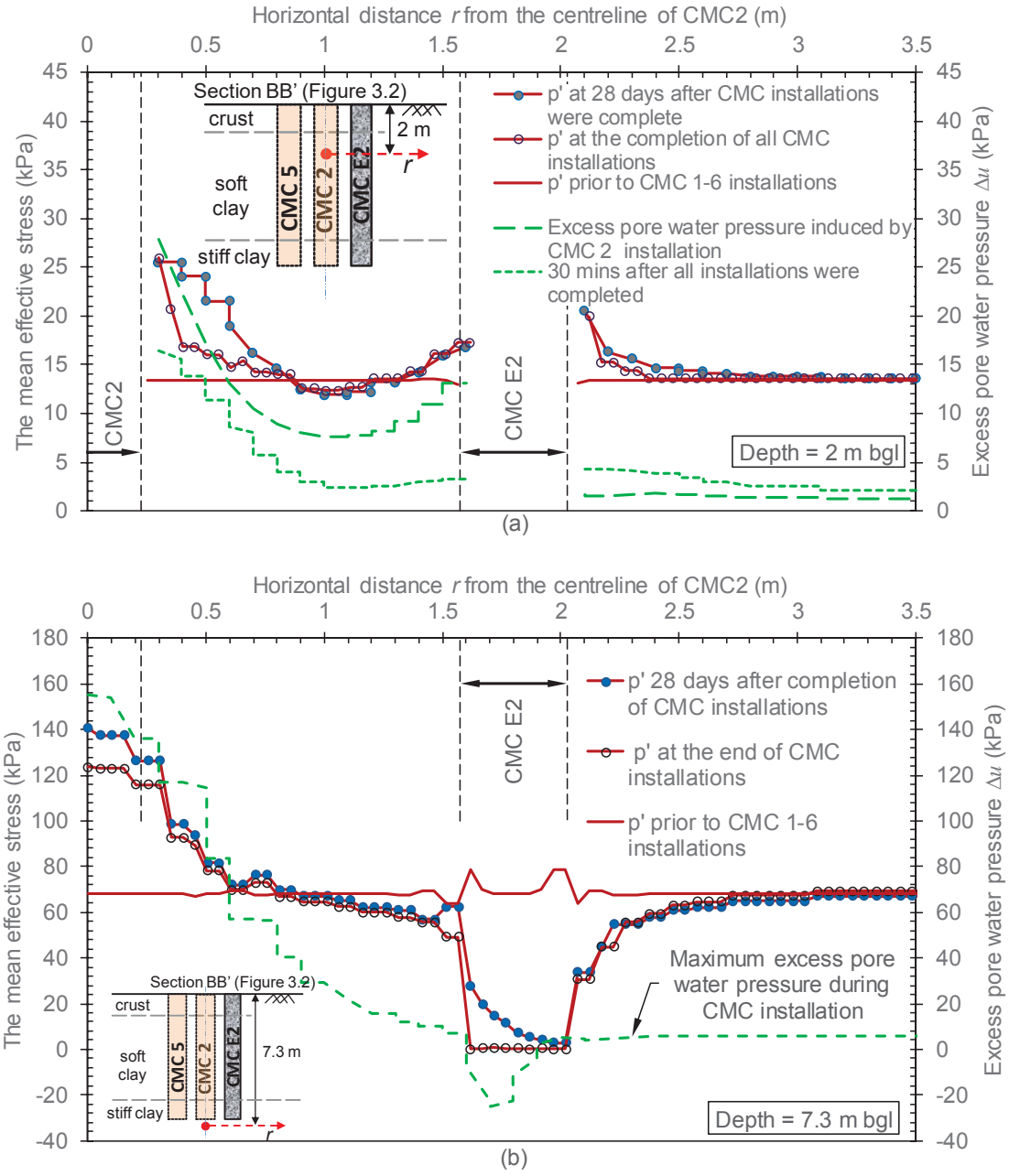

Figure 3.21 Excess pore water pressure and mean effective stress of soil: (a) at 2m depth, and (b) below the base of CMC E2 and CMC2

Figure 3.21b shows the development of the excess pore water pressure (Δu) and the mean effective stress (p') in the soil below the tip of CMC 2 and CMC E2 at depth of 7.3 m. During CMCs 1-6 installations, the excess pore water pressure at the base of CMC 2 rose significantly by approximately 155 kPa while the mean effective stress p' in the soil also increased from 69 kPa to 122 kPa (an increase of 53 kPa). Four weeks after installation

there was a further increase in p' of approximately 18 kPa due to soil consolidation below CMC 2. A reverse trend, however, is observed in terms of the soil state near the affected CMC E2. As shown in Figure 3.21b, a negative excess pore water pressure of approximately - 25 kPa ($\Delta u/u_o = -0.36$) was generated in the soil below column E2, which is most likely related to the uplift of the column E2 discussed later in Section 3.4.2.2. It is also noted that, since column E2 tilted away from CMC 2 and rotated about its toe, negative pore water pressure was only generated within one half of the column base, closer to CMC 2. The mean effective stress in the soil fell to zero, and tension was generated in the soil near the tip of CMC E2. Two weeks after installation, the dissipation of negative pore water pressure led to an increase in p' of up to 25 kPa.

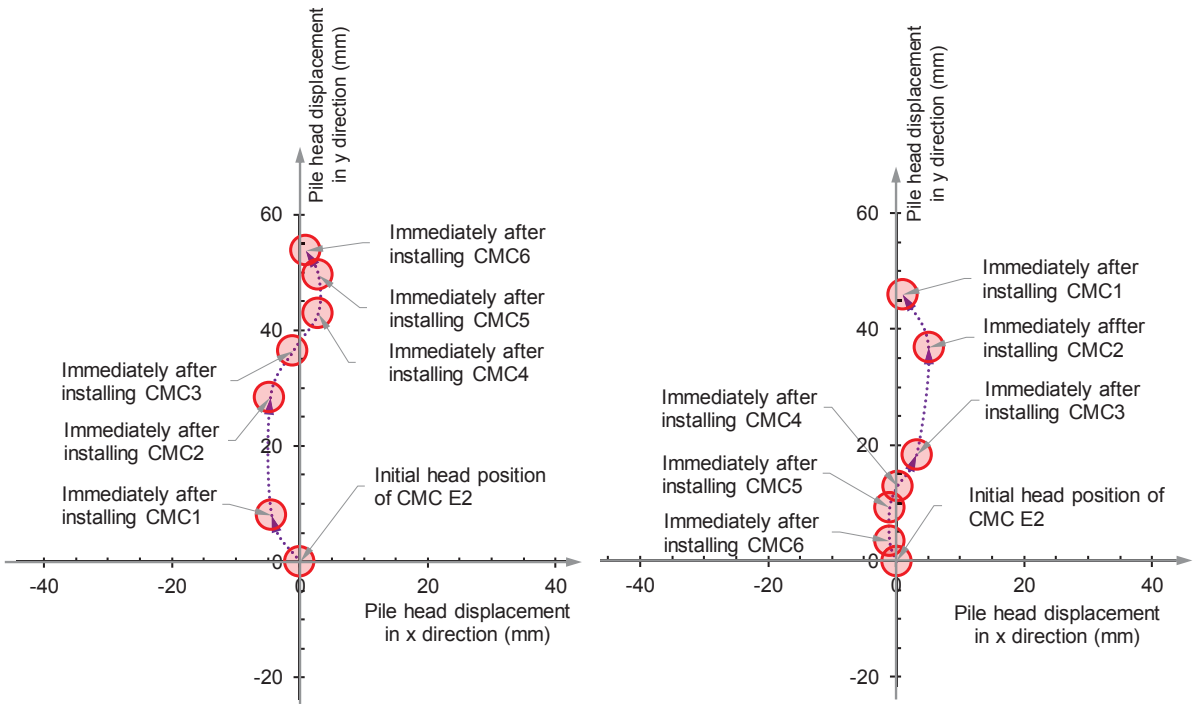

(a) Installation Sequence No. 1 (see Figure 3.2a) (b) Installation Sequence No. 2 (see Figure 3.2b)

Figure 3.22 Schematic diagram of head movements of CMC E2: (a) installation Sequence No. 1 and (b) installation Sequence No. 2

3.4.2 Responses of Previously Installed CMC to New Nearby CMCs

3.4.2.1 Movement of Existing CMC Head

For both sequential orders of installation (i.e. Sequences No. 1 & No. 2), the induced displacements of the soil moved the head of CMC E2 away from the new CMCs in y direction, which are plotted schematically in Figure 3.22. Because different CMCs in the group were installed in different (x, y) coordinates, CMC E2 also moved sideways in x direction. The movements of the CMC head due to installation Sequences No. 1 and No. 2 in y direction were approximately 55 mm and 46 mm, while the corresponding head movements in x direction were approximately 4.6 mm and 5.1 mm, respectively. Although the paths of the existing CMC head movement were different for the two adopted installation sequences, the column head returned to its original x coordinate at the completion of all CMC installations in both cases, due to the symmetric arrangement of CMCs. While CMCs are socketed in the stiff stratum, the displacement of the CMC head often leads to loss of verticality. The Australian Standard for Piling – Design and Installation (Standards Australia 2009) recommends that adequacy of the columns be assessed when the lateral movements of the previously installed piles is in excess of acceptable limits. According to the Australian practice for concrete inject columns (Roads and Maritime Services NSW 2017), the maximum permissible deviation of the column axis from its design plan position at its cut off level is 75 mm in any horizontal direction while the maximum permitted deviation of the finished column from the vertical axis at any level should not exceed 1:100 (H:V).

3.4.2.2 CMC Uplift

The soil heave shown in Figures 3.10–3.16 interacted with the existing CMCs and caused column uplift. Figure 3.23a shows the accumulated uplift of CMC E2 at its head (i.e.

Point I) and tip (i.e. Point J) due to different sequences of installing CMCs 1-6. The predicted uplifts of CMC E2 head at the end of both installation sequences are similar and were approximately 9.5 mm (i.e. 0.02D). Since the column was embedded in stiff clay rather than in a rock socket, the base was expected to rise during nearby installations. The uplift of the CMC tip (i.e. Point J) is approximately 0.01D. According to Figure 3.23a, the difference in predicted uplifts at the head and tip indicated that CMC E2 had stretched approximately 6.0 mm due to the installation of adjacent CMCs, or an average axial strain of 0.085% (Figure 3.23b). The maximum axial strain of 0.55% occurred at the depth of 6.4 m, slightly below the interface of soft and stiff clay. Approximately 5.0 m deep, the maximum axial strain of CMC E2 in the soft soil was 0.2% and 0.25%, for installation Sequences No. 1 and No. 2, respectively (Figure 3.23b).

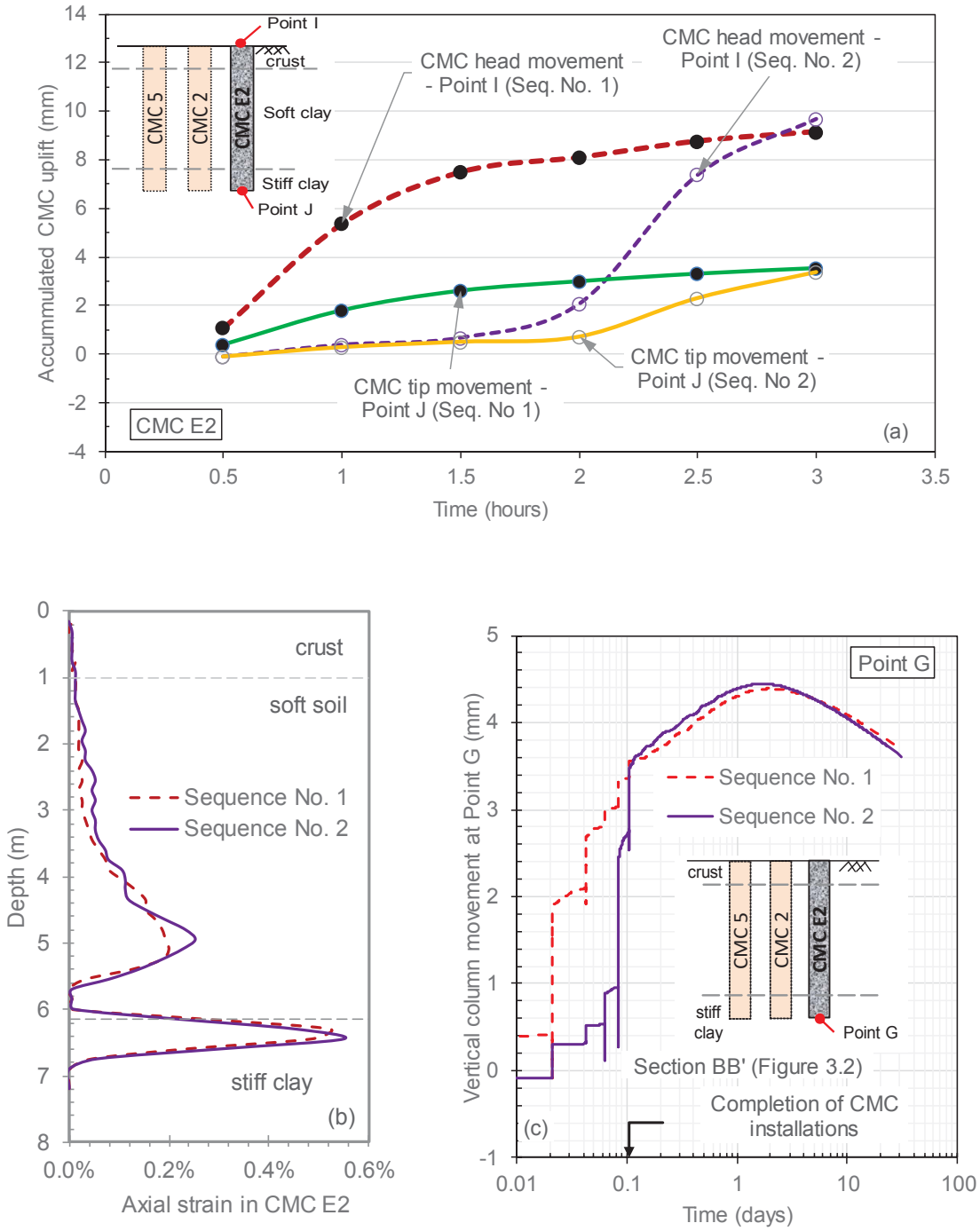

Figure 3.23 (a) Uplift of existing CMC E2 due to installing new CMCs, (b) Axial strain in CMC E2, and (c) Displacement of CMC E2 tip during and after CMC installations

In Figure 3.23c, the tip of CMC E2 experienced continuing uplift during and after the installation of CMC1-6. The subsequent downward movement of the column tip two days

after commencing the nearby installations was attributed to the dissipation of excess pore water pressures as presented in Figure 3.20. Referring to Figure 3.23c, one month after nearby installations, the tip of column E2 settled to the level immediately after nearby installations. The column heave that occurred during nearby installations may seriously impair its load carrying capacity and is likely to increase the long and short-term settlement of the composite ground at a later stage. When the installation site is loaded, significant settlement will occur as the heave induced gap between the CMC tip and the bearing stratum is closed. In fact, short-term surcharge may need to be applied onto the CMC reinforced ground to compensate for uplifts induced by the nearby installations.

3.4.2.3 Lateral Deformation of Existing CMCs

Figure 3.24 shows the accumulated lateral deflection of CMC E2 with depth after each subsequent CMC installation. In the installation Sequence No. 1, the lateral deflection of CMC E2 increased quickly after installing CMCs 1 - 3. These new CMCs formed a barrier that partially restrained the movement of soil near CMCs E1-E3 due to the installation of CMCs 4-6. Obviously, this restraining effect relies mainly on how quickly the CMC grout sets.

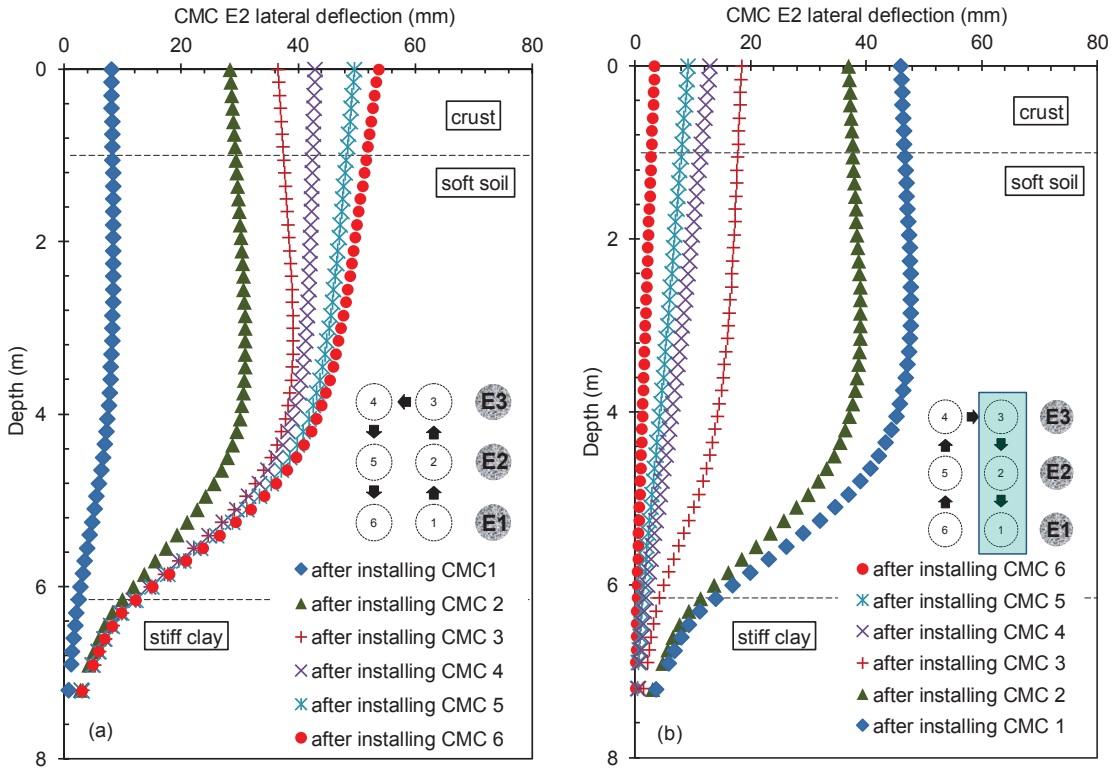

Figure 3.24 Lateral deflection of existing CMC E2 induced by new installations nearby: (a) Installation Sequence No. 1, and (b) Installation Sequence No. 2

As shown in Figure 3.24b, in the installation Sequence No. 2, the deflection of CMC E2 increased slightly due to installing CMCs 6 – 4, but the subsequent installation of CMCs 3-1 significantly increased the deflection in CMC E2. In fact the installation of CMCs 6-4 (Row 3) increased the total stress and pore water pressure in the ground between (shaded area in Figure 3.24b), and therefore the subsequent installation of CMCs 3-1 (Row 2) further increased the excess pore water pressure and the corresponding soil displacement, especially near CMC E2.

3.4.2.4 Bending Moments, and Shear Forces in CMC and Soil-CMC Interaction

The effects that two installation sequences had on the lateral deflection of column E2 were replotted for comparison purposes in Figure 3.25a. The lateral head movement of CMC E2 due to installation Sequence No. 2 was 8 mm less than that induced by Sequence

No. 1, indicating that the head of CMC E2 had less freedom to displace laterally. In fact, within the upper 3 m of the soil, Sequence No. 2 induced 25% more soil heave (Figure 3.10b) and less lateral movement than Sequence No. 1 (Figure 3.10a). Figure 3.25a also indicates that the lateral deflection of column E2 at depths between 3 m and 6 m in Sequence No. 2 was much more than that induced by Sequence No. 1. The combination of head restraint due to soil heave near the surface, column deflection at lower depths, and the loosely socketing effect in stiff clay, resulted in slightly greater column bending associated with installation Sequence No. 2.

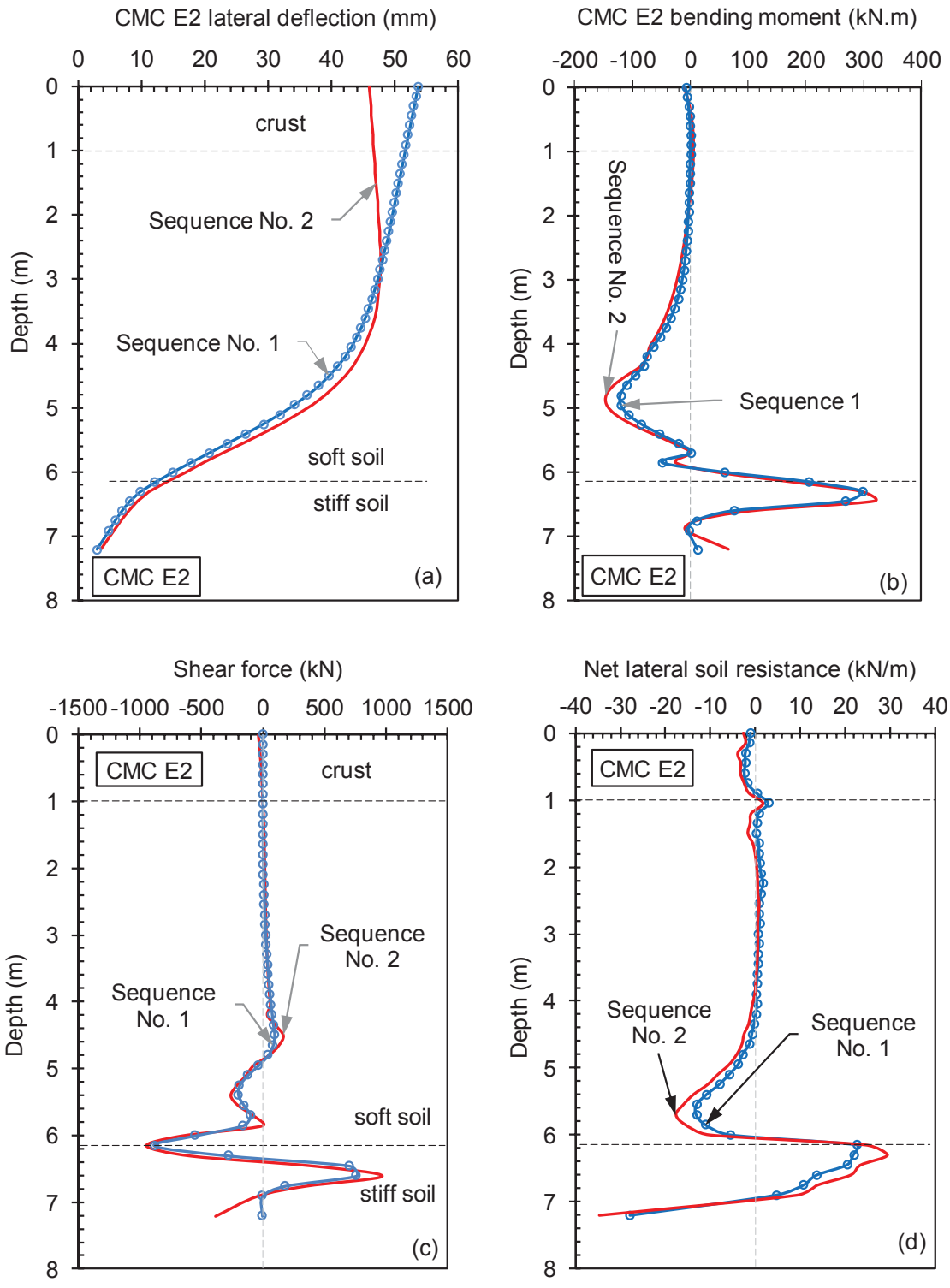

Figure 3.25 Profile of CMC E2 in terms of: (a) lateral deflection (b) bending moment (c) shear force and (d) net lateral soil resistance following installation Sequences No. 1 and No. 2

The bending moment, M and shear force, V can be computed by successive derivations of column deflection δ using Equations (3.12) and (3.13), respectively; the results are reported in Figures 3.25b and 3.25c. The piecewise polynomial curve-fitting method was used to calculate the derivatives.

$$M(z) = \frac{d^2\delta}{dz^2} E_c I \tag{3.12}$$

$$V(z) = \frac{dM(z)}{dz} \tag{3.13}$$

where I is the area moment of inertia of the column section and z is the depth of the column. In Figure 3.25b, a negative bending moment means that tensile stresses were induced along the CMC shaft facing away from the newly installed CMCs. The bending moment profile of CMC E2 reported in Figure 3.25b has a double curvature with negative and positive peaks near the interface between the layers of soft and stiff soil:

- At approximately 4.9 m deep, local maximum bending moments induced by installation Sequences No. 1 and No. 2 were - 120 kN.m and - 146 kN.m, respectively (i.e. a difference of 22%).
- At approximately 6.4 m deep, maximum positive bending moments were 298 kN.m and 318 kN.m for installation Sequence No. 1 and No. 2, respectively (a 7% difference).

The difference in the maximum bending moments in CMC E2 induced by the two adopted installation sequences are due to the difference in lateral CMC deflections, as explained earlier (i.e. the larger curvature in CMC E2 induced by installation Sequence No. 2 was associated with larger soil heave near the surface and greater lateral soil movement at lower depths).

As expected, the largest shear stress induced in CMC E2 occurred between the soft and stiff layers, as shown in Figure 3.25c. The peak shear forces in CMC E2 are 880 kN and 968 kN for installation Sequences No. 1 and No. 2 (i.e. a difference of 10%). These large shear forces are closely related to the rapid variation of soil and CMC pressure at depth (i.e. net lateral soil resistance), as shown in Figure 3.25d. The net lateral soil resistance at the soil and CMC interface induced by installation Sequence No. 2 was greater than installation Sequence No. 1 by approximately 35%. The net lateral soil resistance predictions, as shown in Figures 3.25d, 3.31d and 3.32d, were determined by summing the y components of the forces predicted at the nodes of the interface elements between the soil and column E2. This calculation was performed via a subroutine written in $FLAC^{3D}$ as part of this study. The net lateral soil resistance is an important parameter in the analysis of a passive pile (Pan et al. 2000) and for the estimation of the $p - y$ curves for the analysis of laterally loaded piles.

As Randolph & Wroth (1979) pointed out, as the soil consolidates it experiences unloading in shear. It was expected that after completing the nearby installations, CMC E2 would begin to relax as the soil particles moved towards the installation site; indeed the bending moment in the column E2 decreased by approximately 8% by utmost over time, as shown in Figure 3.26b.

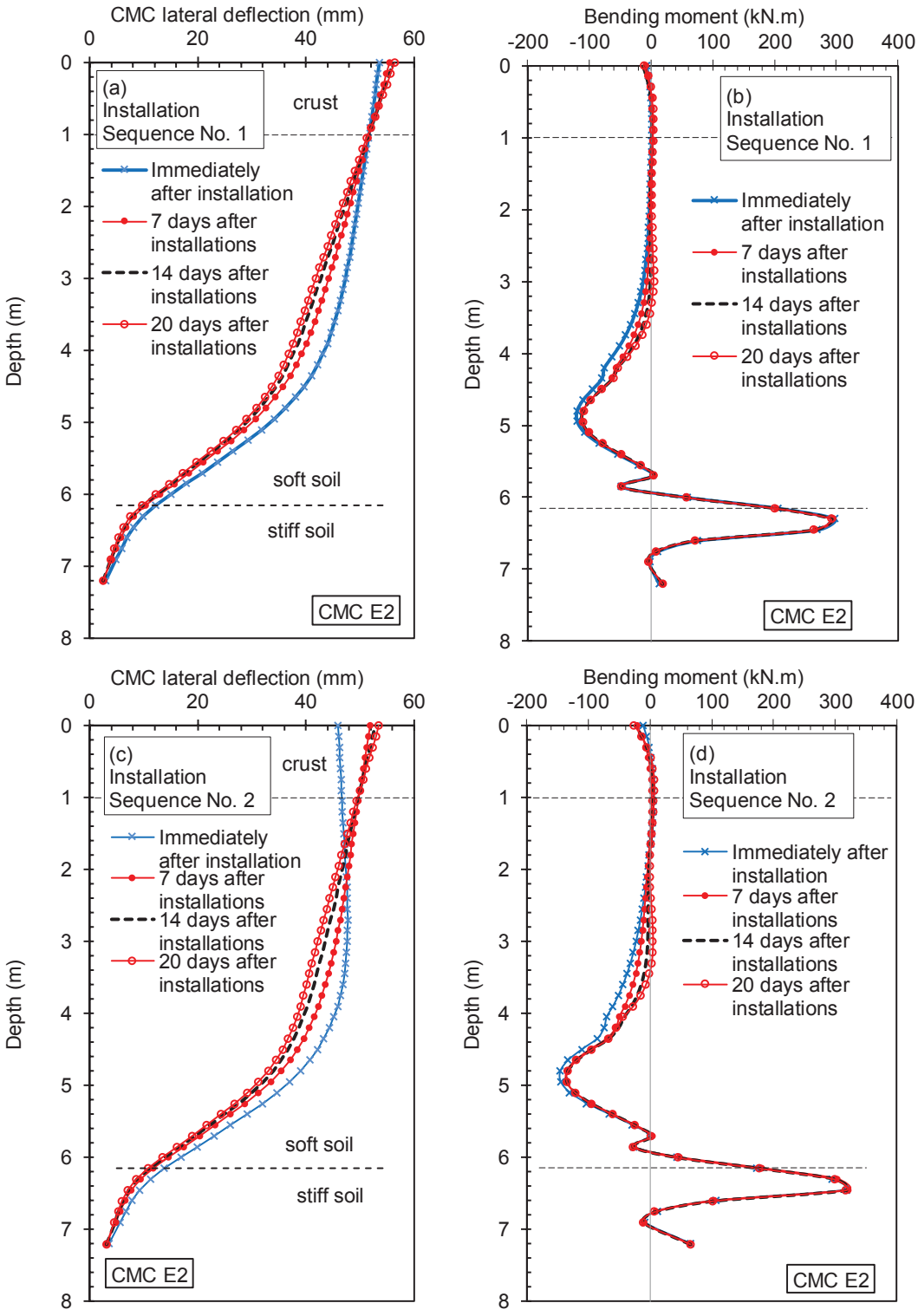

Figure 3.26 Time-dependent responses of column CMC E2: (a) lateral deflection and (b) bending moment due to installation Sequence No. 1; and (c) lateral deflection and (d) bending moment due to installation Sequence No. 2

3.4.2.5 Installation-induced Tension Plasticity in Existing CMCs

The tensile strength of CMC is the determinant factor for crack development in the column. Figure 3.27 shows the major and minor principal stresses (σ_1 and σ_3) along the back of column E2 (i.e. Point K), as it was subject to nearby installations. The installation of the nearest column (i.e. CMC 2 of Sequence No. 1) caused the yielding of CMC E2 as the induced stress met the yield criteria (i.e. indicated by red dot points lying on the tensile yield surface in Figure 3.27). Referring to Figure 3.30, the minor principal stresses (σ_3) in CMC E2 indicated that the largest tensile stresses occurred between 3.5 m and 4.5 m deep in the layer of soft clay and between 6 m and 6.5 m deep in the stiff clay layer.

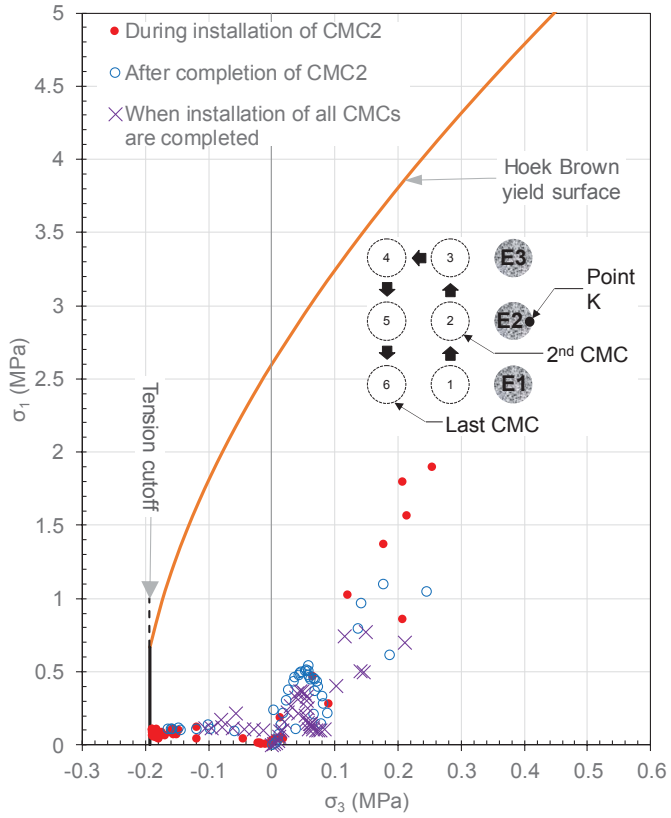

Figure 3.27 Hoek-Brown yield surface and stress state in CMC E2 along point K

Figure 3.28 and Figure 3.29 show the development of tensile yielding in column E2 during installation Sequences No. 1 and 2. As shown in Figure 3.28a and Figure 3.29a, when column E2 had only been cured for one day, tensile yielding occurred along almost its entire length. However, much less yielding occurred when CMC E2 had been cured for 28 days (Figure 3.28b and Figure 3.29b). The adopted tensile yield strength of CMC in this study is about 8% to 4% of the unconfined compressive strength at 1 and 28 day age, respectively. In the current practice, columns are rarely used to resist tensile stresses.

Figure 3.30 shows the evolution of tensile stress in CMC E2, and are well illustrated using the results of the analysis for installation Sequence No. 2, where column E2 had been cured for 28 days prior to nearby installations. The installation of the final two columns caused tensile yielding in CMC E2 at depths between 2 m and 5 m and between 6.5 m and 7 m. The installation of the first four columns (CMC 6-3) increased the tensile stress in CMC E2 to some extent, but was not sufficient to cause tensile yielding. In fact, the installation of CMC 5, located at a distance of 8× D from CMC E2, induced a substantial tensile stress at the mid length of the existing CMC, equal to approximately 85% of the tensile yield stress, calculated using Equation (3.4) and reported in Table 3.2. The relaxation of this tensile stress can be seen during the installation of the subsequently installed CMCs 4 and 3, which only caused greater tensile stresses within the lower portion of the existing CMCs.

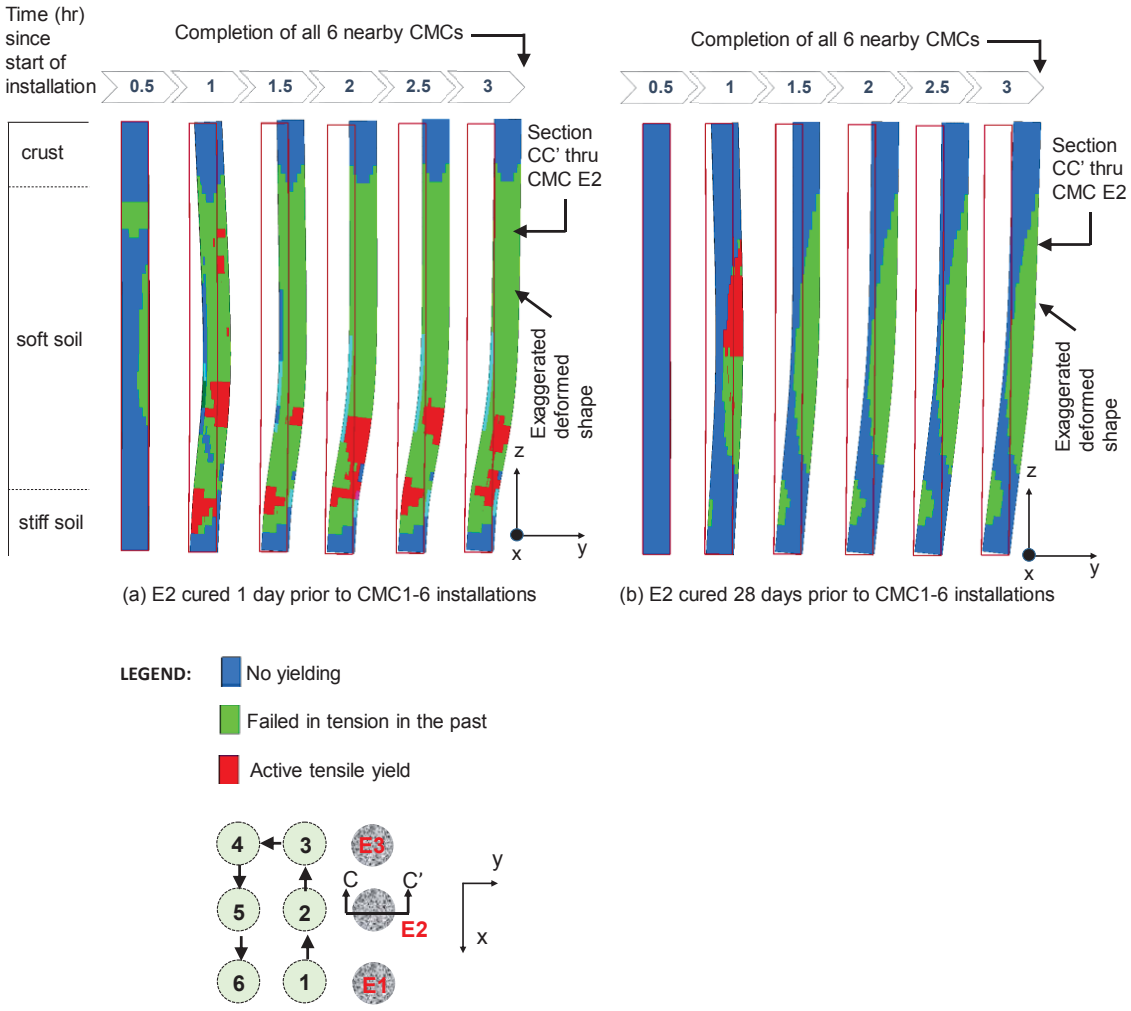

Figure 3.28 Evolution of tension plasticity in CMC E2 at: (a) one day old and (b) 28 day old, subject to CMC1-6 installations using Sequence No. 1

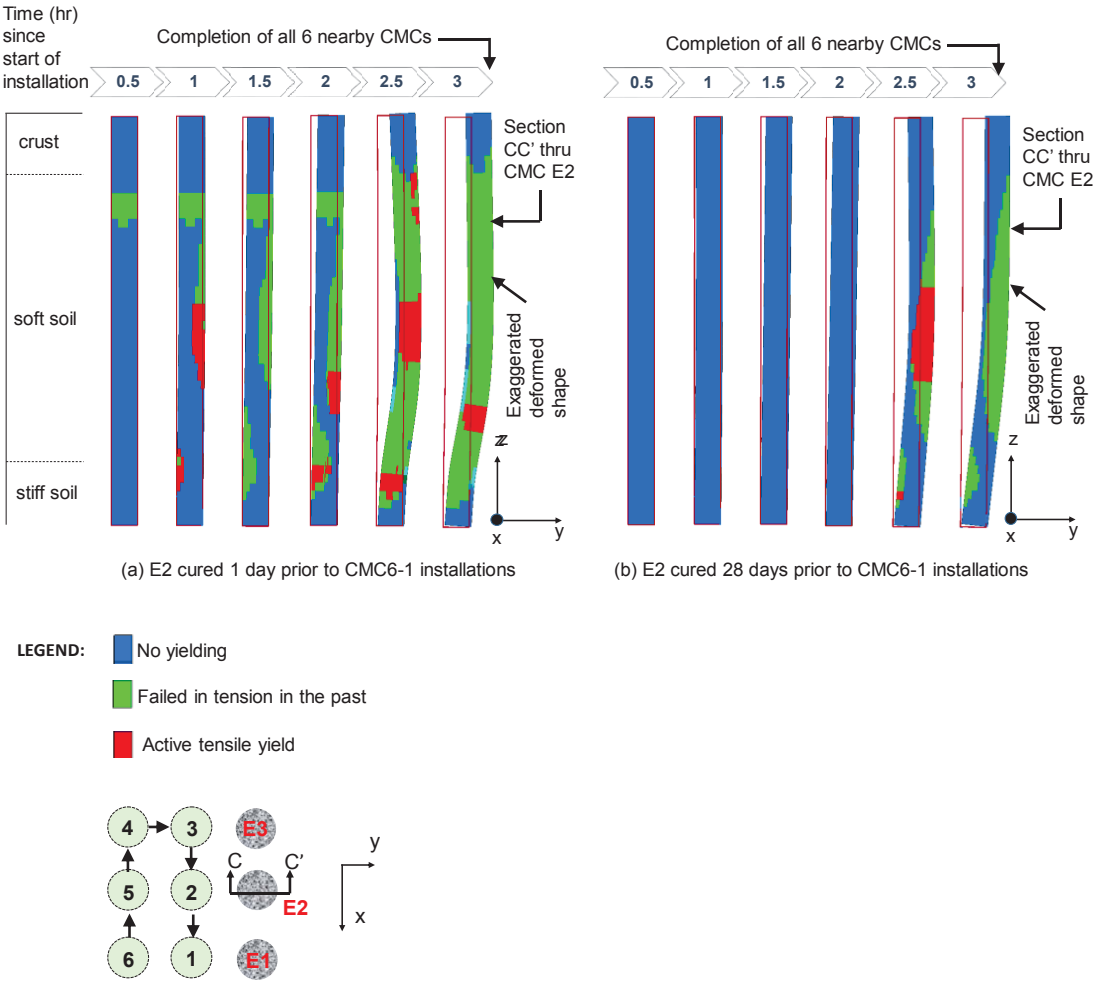

Figure 3.29 Evolution of tension plasticity in CMC E2 at: (a) one day old, and (b) 28 day old, subject to CMC6-1 installations using Sequence No. 2

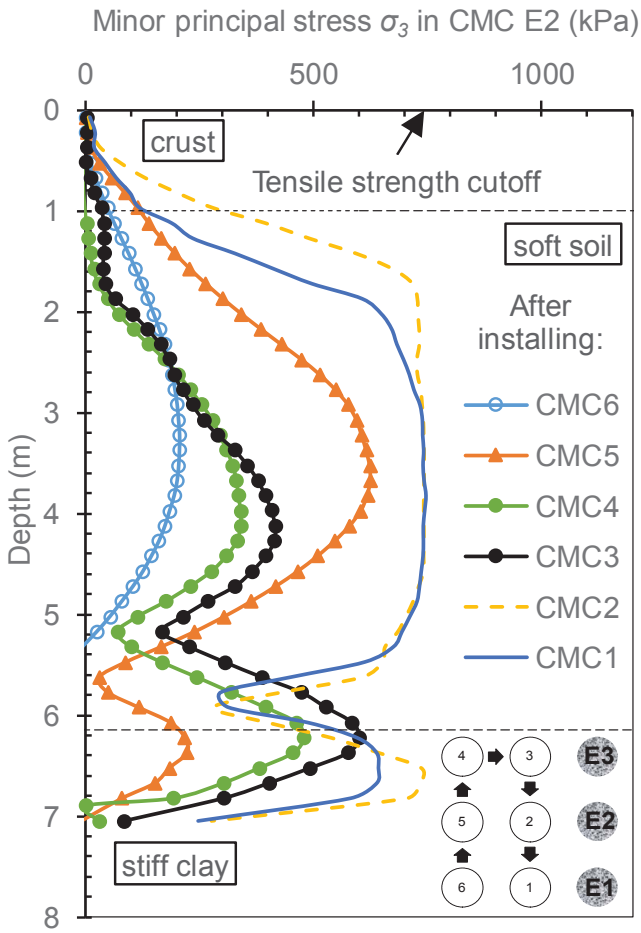

Figure 3.30 Maximum tension stress generated in CMC E2 (after 28 days of curing), induced by installation Sequence No. 2

3.4.2.6 Effects of Curing Period on Performance of CMC during Nearby Installation

New CMCs may sometimes be installed next to a row of existing columns that have cured for more than 24 hours, and thus have gained most of the standard 28-day strength. As the stiffness increased over a longer curing period, CMCs will respond differently to the effect of installation, so two more analyses were carried out by assuming that CMCs E1-3 had achieved their 28-day strength and stiffness, as reported in Table 3.2. Figure 3.31 and Figure 3.32 illustrate installation Sequence No. 1 and No. 2 to reveal the effect of

using two different curing periods on responses of CMC E2 to column installations nearby. At both curing periods, CMC E2 has a double curvature with positive and negative peaks of bending moment, but there are three notable differences:

- Firstly, referring to Figures 3.31b and 3.32b, for existing CMC with a short curing time, maximum induced bending moment occurred at the interface between soft and stiff soils, but when existing CMC cured for longer periods the maximum induced bending moment shifted up towards the mid-depth of the soft soil (i.e. at ~4 m deep). Indeed Figure 3.31b shows that the absolute value of the maximum negative bending moment (- 95 kN.m) was 3 times greater than the maximum positive bending moment of CMC E2 (34 kN.m), when the CMC had been cured for 28 days. Column E2 at 28 days was much stiffer than the stiff clay (i.e. $E_{c,28d}/E_{st}$ = 670 versus $E_{c,1d}/E_{st}$ = 340) so the layer of embedment soil had less restraint against the lateral movement of CMC E2, and an insignificant induced bending moment developed in the column at this depth.
- The second notable difference is that CMC E2 at one day old experienced much more (~ 10 times) severe responses than CMC E2 at 28 days old (see Figure 3.31b, c). In the former case, the maximum induced bending moment of 300 kN.m and the maximum shear force of 800 kN occurred near the interface between soft and stiff soils, while the corresponding *M* and *V* in CMC E2 after 28 days were 34 kN.m and 72 kN, respectively.
- In Figure 3.31c and Figure 3.32c the net lateral soil resistance in the stiff clay surrounding the existing CMC after 28 days was almost three times larger than the corresponding values after one day. Within the soft soil, the effect that curing time had on the net lateral soil resistance was only marginal because the response of

laterally loaded pile was governed mainly by the relative stiffness of the column to the soil.

The effect of using different sequences of installing CMCs 1-6 after the CMCs E1-E3 had cured for 28 days can be compared using Figure 3.31b and Figure 3.32b. The maximum negative bending moments developed in the CMC E2 for Sequences No. 1 and No. 2 occurred at a depth of 4.2 m and were -95 kN.m and -142 kN.m, respectively; this is a difference of 49% in the predicted negative bending moments. As shown on the same figures, the effect of using different installation sequences on the one-day-old CMC E2 is not noticeable, when compared with the case of the 28-day curing period, where the maximum induced bending moment due to Sequence No. 2 is just 21% greater than that due to Sequence No. 1. Therefore, for the economic and realistic design of CMC, it is crucial to consider the effect of installation sequence as well as the curing time of CMC on the bending behaviour of the columns.

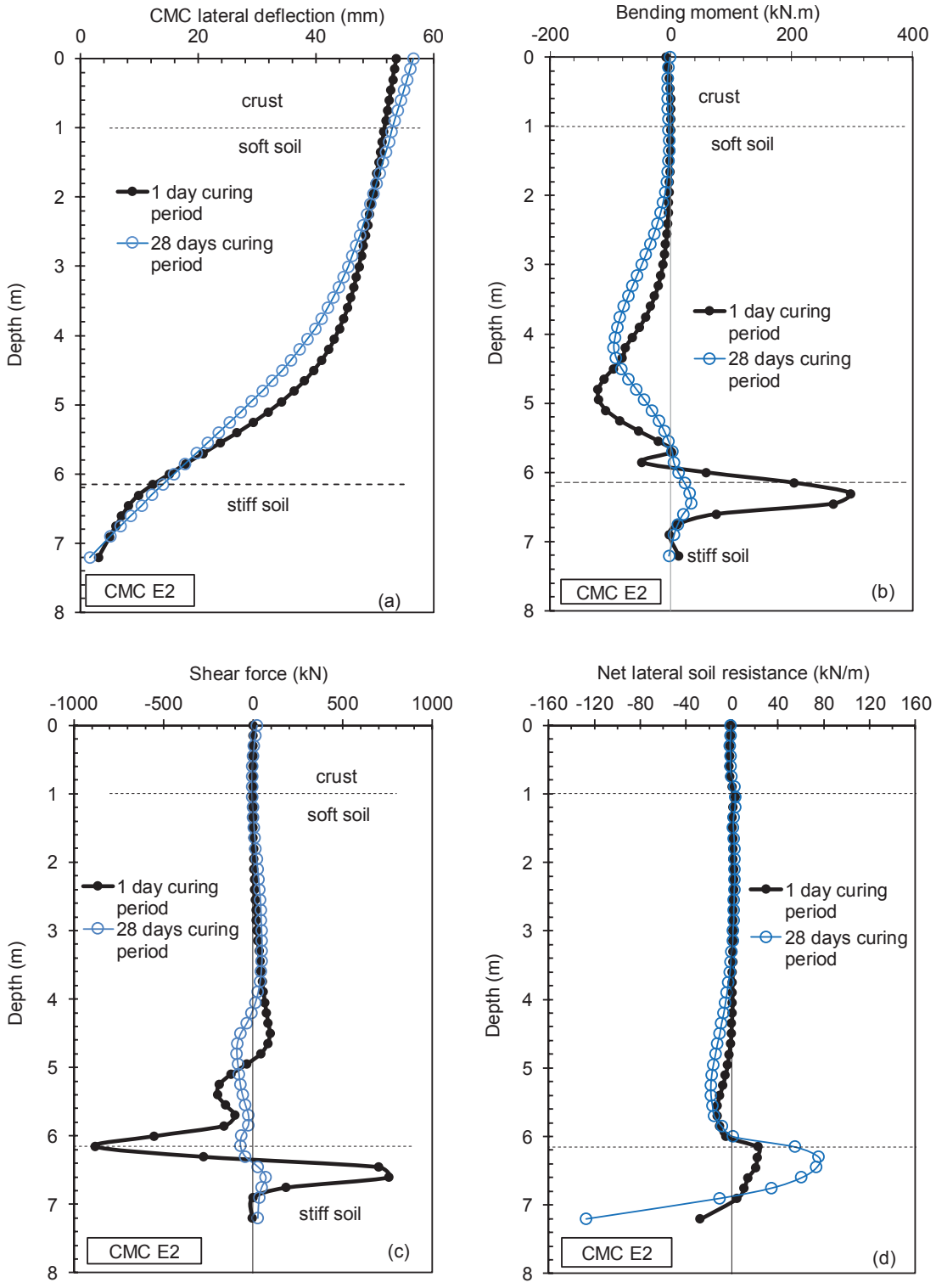

Figure 3.31 Effect of curing periods on behaviour of CMC E2: (a) lateral deflection, (b) bending moment, (c) shear force, and (d) lateral soil resistance (Sequence No. 1)

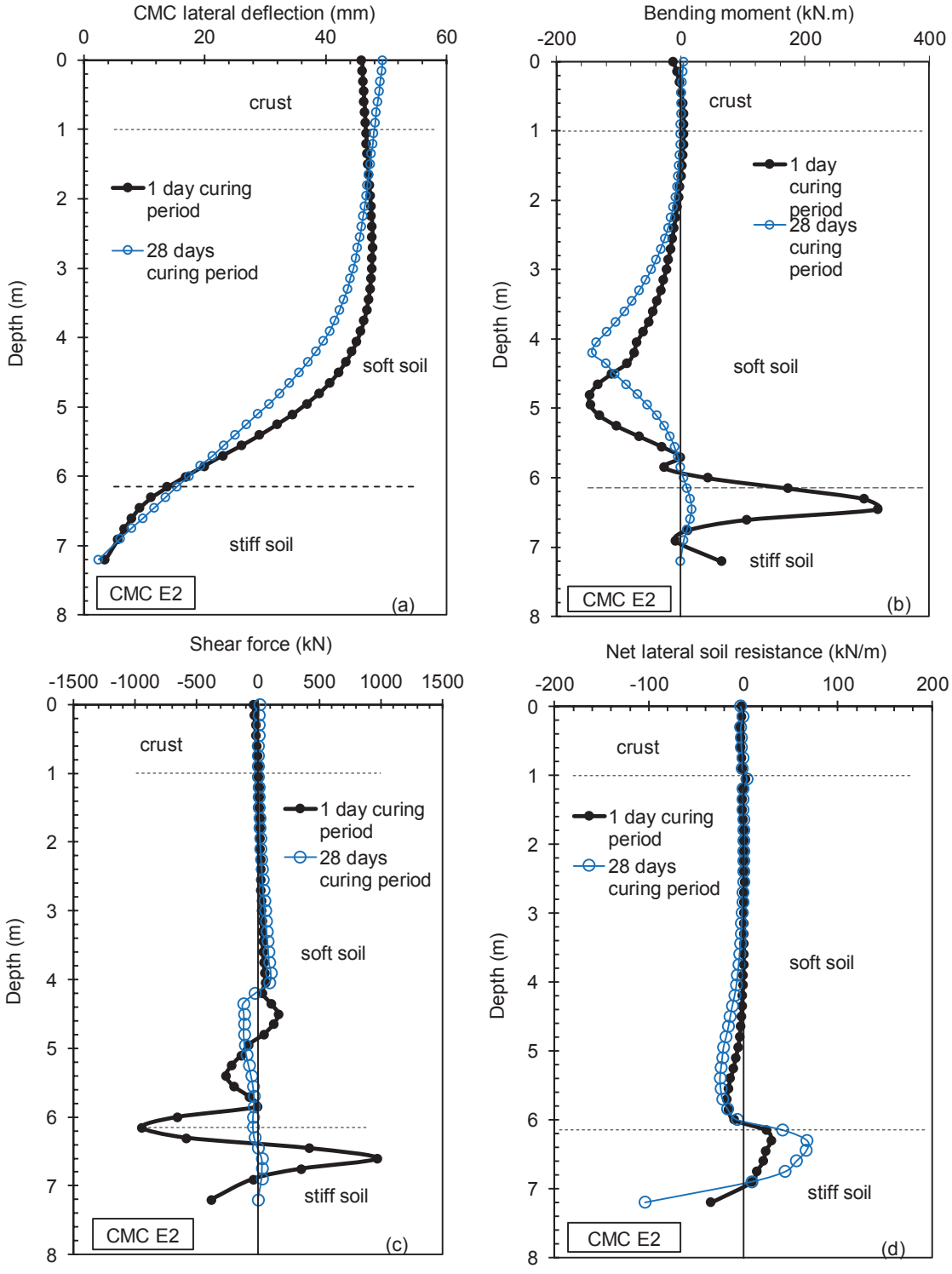

Figure 3.32 Effect of curing periods on behaviour of CMC E2: (a) lateral deflection (b) bending moment, (c) shear force, and (d) lateral soil resistance (Sequence No. 2)

3.5 Summary

Large strain numerical analyses were carried out using *FLAC*^{3D} to examine the long and short-term effects of installing new CMCs close to previously installed CMCs using two different sequences. Installation Sequence No. 1 was denoted for when the CMC rig starts close to the existing columns and then moves farther away as installation continues, whereas Sequence No. 2 is a reversal of Sequence No. 1 (i.e. installation begins further away and then comes closer to existing CMCs). Installing each CMC was modelled with a combination of undrained cavity expansion and consolidation analysis to include a 30 minute lag between successive CMCs while allowing for soil consolidation and strength gain. The results revealed the following aspects of column installation that are difficult to observe by regular field and laboratory means:

- The lateral displacement of soil induced by installing a single CMC extends beyond the two CMCs previously installed in a row nearby. Thus if two adjacent columns are constructed in quick succession, the induced lateral displacement could accumulate and extend to the next three adjacent columns.
- The profile of the predicted accumulative lateral soil displacement induced by adjacent CMC installations plotted with depth was similar to the measurement profile reported in a selected published field study.
- The lateral movement of in-situ soil and soil heave near the existing CMCs due to installation Sequence No. 2 were greater than Sequence No. 1 by approximately 15% and 25%, respectively.
- During the installation of adjacent CMCs, most of the soil heave near the existing CMCs occurred in the upper half of the soft soil layer, and continued for weeks after

installation. In fact, four weeks after installation, post-installation surface heave accounted for 10% of ground heave generated during installation.

- The maximum induced excess pore water pressure generated in the front face of existing CMCs due to installation Sequence No. 2 was almost twice that caused by installation Sequence No. 1. The influence zone of excess pore water pressure induced by CMC installation was narrower than the lateral displacement and soil heave.
- Consolidation analysis should be included when assessing the effect of installation and the build-up of excess pore water pressure as construction proceeds to account for the lag between the installations of two successive CMCs.
- During installation, the soil surface heave was approximately three times more than the column head uplifts.
- The ground movement induced by the installation of new CMCs can cause an uplift of existing CMCs by approximately 2% of their diameter (D) at the column head and approximately 0.01D at the tip. CMCs continued to heave for a couple of days after installation and then settled as the soil consolidated. The ensuing uplift may require a short-term surcharge to allow the column to settle back to the depth specified in the design.
- The predicted bending moments generated in existing CMCs due to installation Sequence No. 2 were almost 22% more than the corresponding values from Sequence No. 1. The bending moment induced in existing CMC due to nearby installation decreased by almost 8% after three weeks of stress equilibrium and soil consolidation.
- Subject to loadings from nearby installations, the maximum bending moment induced in a one-day old CMC occurred at the interface of soft and stiff clay, but when cured for 28 days the maximum bending moment of CMCs shifted up towards the soft clay layer.

- The 28-day old CMC E2 experienced approximately 50% more maximum bending moments due to Sequence No. 2 than the corresponding value predicted due to Sequence No. 1 when installing away from the existing CMCs. CMC E2 is presented in Figure 3.19.

The bending moments in existing CMCs induced by the lateral movement of soil due to the installation of nearby CMCs similar to this study can exceed their bending capacity and thus the structural integrity of CMCs should be checked after installations. It is recommended that practicing engineers consider the effects of installation by applying the initial stress field, bending moments, and shear force to soft soil and CMCs when designing embankments on improved soft soil. Moreover, for closely spaced CMCs the installation sequence must be optimised because specific site geology and project requirements can lead to various installation induced impacts. The hope is that the general conclusions drawn from comparing two different installation sequences on the same soils that are presented here may be applied to similar soil conditions.

CHAPTER 4 Laboratory Model Test on the Responses of Early Age Concrete Inclusions in Soft Ground Subject to Nearby Installations

4.1 Synopsis

Soil movement induced by installing grouted columns using soil-displacement piling method for ground improvement may have an adverse impact on the previously installed columns. This chapter describes a laboratory model test to study the response of a newly formed concrete column subjected to ground movement induced by installing subsequent surrounding new columns. Seven concrete columns were cast in-situ in soft soil from low strength concrete for ground improvement using a displacement piling method. Strain gauges were cast inside the concrete inclusion to measure column bending moment. An innovative electrical circuit was coined to reduce the number of strain gauge lead wires employed inside the reduced-scale concrete column. Accumulated soil heave measured by 3D scanning, stress change and excess pore water pressure in the soil, together with the uplift and bending moment of the affected column are reported. The results indicate that the one-day-old concrete column uplifted during the subsequent installation of the adjacent columns, and the total uplift halved the heave of the surrounding soft soil. For the newly formed plastic concrete column (i.e. cured for less than 2 hours), the column uplift induced by the subsequently installed columns was similar to the heave of the surrounding soft soil. It was also found that lateral loadings generated by the installation

of the surrounding columns could affect the integrity of the existing column, in particular at their early age.

4.2 Introduction

Piled embankments were traditionally constructed from driven or bored piles (Hewlett & Randolph 1988). However, the installation of such rigid inclusions is costly, time-consuming, and often generates excessive noise, spoils, and vibration. In the past 60 years, alternative solutions have been developed to install concrete columns for ground improvement, where soils are displaced laterally leaving a cavity for concrete placement. Examples of such application include the drilled displacement columns (DDC) and concrete injected columns (CIC) as discussed in Section 2.1.1. For ground improvement purposes, low strength concrete with a characteristic strength ranging from 5 MPa to 35 MPa is often used to cast the rigid inclusions (Masse et al. 2017). The typical diameter of such concrete columns and the nominal centre to centre spacings were discussed in 2.1.3.

During column installation process by a soil-displacement piling method, the ground generally experiences an increase in horizontal soil stresses and lateral soil movement (Suleiman et al. 2016). Hence, the method enhances production rate, increases bearing capacity of the columns and minimises the chance of borehole collapses (Michalowski et al. 2018; Plomteux, Porbaha & Spaulding 2004). However, loading arising from soil movements induced by the installation process, if becoming excessive, could adversely affect the performance of the nearby existing columns. In fact, at early concrete age, the plain concrete, which forms the rigid inclusions, can yield when subjected to excessive lateral loadings (Michalowski et al. 2018; Turatsinze & Garros 2008; Zhang & Choi 2015). There is a need to investigate the behaviour of columns during its early strength

development under influence of subsequently installed columns. This aspect has not been considered in the existing design methods.

The review of the current literature has indicated that investigations on installation effects of concrete rigid inclusions using displacement-piling techniques for ground improvements are currently limited. As discussed in Section 2.4, most researchers only focused on load-deformation analyses or estimating shaft resistance; and only a few researchers have assessed the effects of installing drilled displacement columns. Such investigations indicated that the horizontal stresses gradually increased until the piling tools reached the elevation of the pressure-measuring device, which was followed by a horizontal stress decrease. The soil zone influenced by the column installation extended to 2*D* to 3*D* (*D* = column diameter) from the outer surface of the column.

The review of the current literature also indicated that previous model tests for soil-displacement piles did not provide a detailed means to construct the concrete columns (Hird, Ni & Guymer 2011). Currently, no in-depth investigation was carried out to study the influence of new column installations on the nearby existing columns for ground improvement purposes, especially when the existing grouted columns are developing their concrete strength. In such problems, the difference in stiffness between concrete columns and the surrounding soils play an important role. For example, according to Chow & Teh (1990), assessing the uplift of the previously installed columns induced by surrounding soil heaves becomes more difficult when columns are installed in soft soil.

This chapter presents the results of a laboratory model test in which a group of concrete rigid inclusions was cast in-situ in an overconsolidated clay using a soil-displacement installation method for ground improvement. The objective of this study is to provide an initial insight into soil responses to the column installation process as well as the

behaviour of an existing concrete column subject to soil movement induced by surrounding subsequent installations. In this study, an instrumented soil tank, a penetration system, and a repeatable column installation method was developed. Established from multiple preliminary trials, the method for installing columns was able to generate a similar stress and displacement field in the soil. Soil heave occurring during column installations were captured by a 3D laser scanner. Horizontal and vertical stress changes due to soil displacement were recorded by pressure sensors installed in the soil tank. The bending moment developed in the grouted column by multi-directional lateral loadings, induced by soil movements due to installing various adjacent columns, was measured by multi-level embedded strain gauges. The arrangement of embedded strain gauges in the column and the design of a circuit connection to minimise the occupation of strain gauge lead wires inside a reduced scale concrete column are described in the chapter.

4.3 Model Test Set-up and Material Properties

4.3.1 Equipment

The lateral soil displacement induced by drilled displacement columns and jacked pile installations are both analogous to the cylindrical cavity expansion. However, unlike jacked piles, drilled displacement columns were formed by cast in-situ grouting. Hird, Ni & Guymer (2011) conducted a small-scale experiment to study the movement of transparent synthetic clay during the penetration of a miniature displacement auger. They demonstrated that the movement of the soils around the displacement auger was found to be similar to those observed around a cylindrical straight-sided pushed pile. Hence, in this study, to simulate the installation process of a drilled displacement column in the

laboratory, the idea of jacked pile installation as a soil-displacement piling technique was combined with the cast in-situ grouting using a specially designed piling probe.

The description of equipment and instrumentation used in the experiment is given below. The penetration system as shown in Figure 4.1 consisted of a reaction frame, a motorised linear actuator and a piling assembly, which allow installing multiple columns into the soil bed prepared inside a large cylindrical strong box.

As shown in Figure 4.1, the Servomech electric linear actuator with a 3-phase 0.25 kW motor was used to push and pull the piling assembly into and out of the ground in a linear fashion. The maximum push and pull capacity of the actuator was 5 kN and the maximum piston travel distance was 500 mm. The linear speed of the actuator was controlled by a Bosch variable speed drive. The actuator was equipped with electric switches, which limit the actuator movement and guarantee motor switch-off. A laser displacement sensor was used to log the vertical movement of the actuator push rod. The actuator and the motor were mounted on the reaction frame, which was approximately 1.8 m in width and 2 m in height. The soil penetration resistance was recorded using a 5 kN tension-compression MeasureX load cell, which was attached in line with the actuator push rod (Figure 4.1).

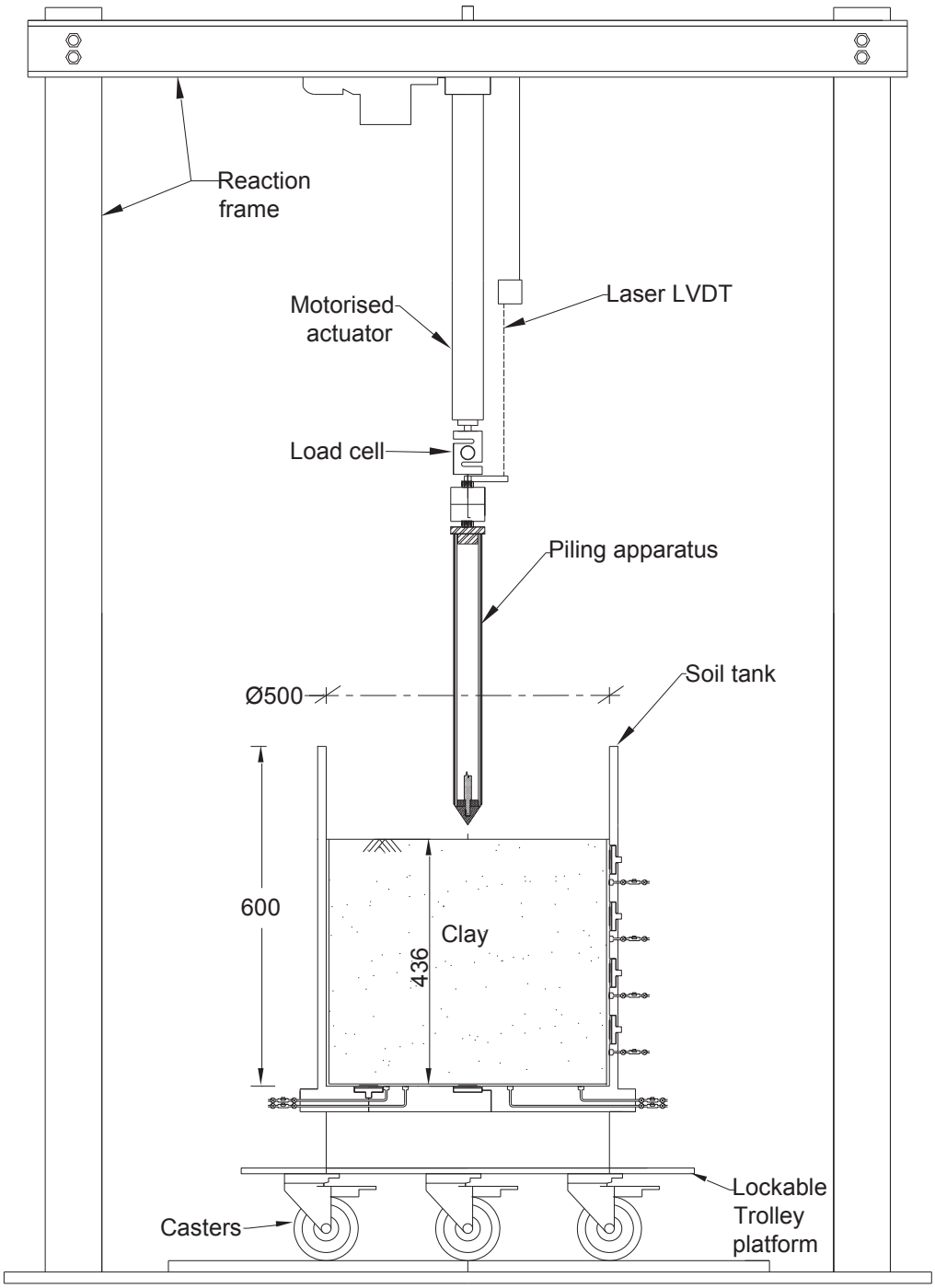

Figure 4.1 Schematic set-up for column installation simulation (all dimensions in mm)

Referring to Figure 4.1, the piling assembly was positioned below the motorised actuator and the load cell. The assembly was designed to form cast in-situ soil-displacement columns. The design of the apparatus is shown in details in Figure 4.2, which aimed for repeatable displacement effects due to each column installation. This piling tool has a similar concept to the installation poker adopted for installing stone columns in the past (Black et al. 2007; Noor Muneerah PG Haji Jeludin et al. 2015), but was tailored to form concrete rigid inclusions. To minimise the suction pressure induced by retraction of the inner tube during column installations, the cone tip can be loosely detached from the upper inner tube.

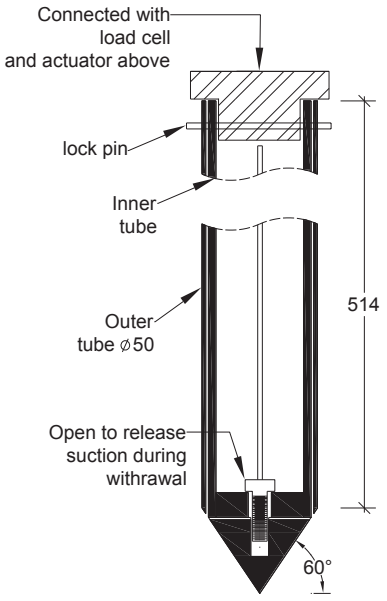

Figure 4.2 Piling assembly for soil displacement and grouting (all dimensions in mm)

The piling assembly was fabricated from an aluminium alloy, consisting of an external 1.6 mm thick tube having an outside diameter of 50 mm and a smaller inner tube with an outside diameter of 44.4 mm. A reasonably tight fit between the tubes was provided by

wrapping a thin plastic sleeve around the inner tube. The lower end of the inner tube was attached to a cone of 60°– apex angle, which is typical for the cone penetration test.

Another important component of the model test was the stainless steel cylindrical soil tank (Figure 4.3), which was used to prepare the soil bed. The cell has an internal diameter of 500 mm and an interior wall height of 600 mm. The cell was originally fabricated and supplied by GDS Instruments; however, for this study, the modification was made to the tank to include six pressure sensors (PS1 to PS6 in Figure 4.3). The soil tank assembly consisted of a top lid, a 15 mm thick wall and a rigid base, which can be held together by twelve stainless steel tie rods (Figure 4.3a). A watertight seal was provided at the connections of the cell parts by a nitrile O-ring sitting in a specially machined groove, which encircles either ends of the cell wall. Five strong steel casters as shown in Figure 4.1 allowed the soil tank to be manually manoeuvred during the installations of various columns.

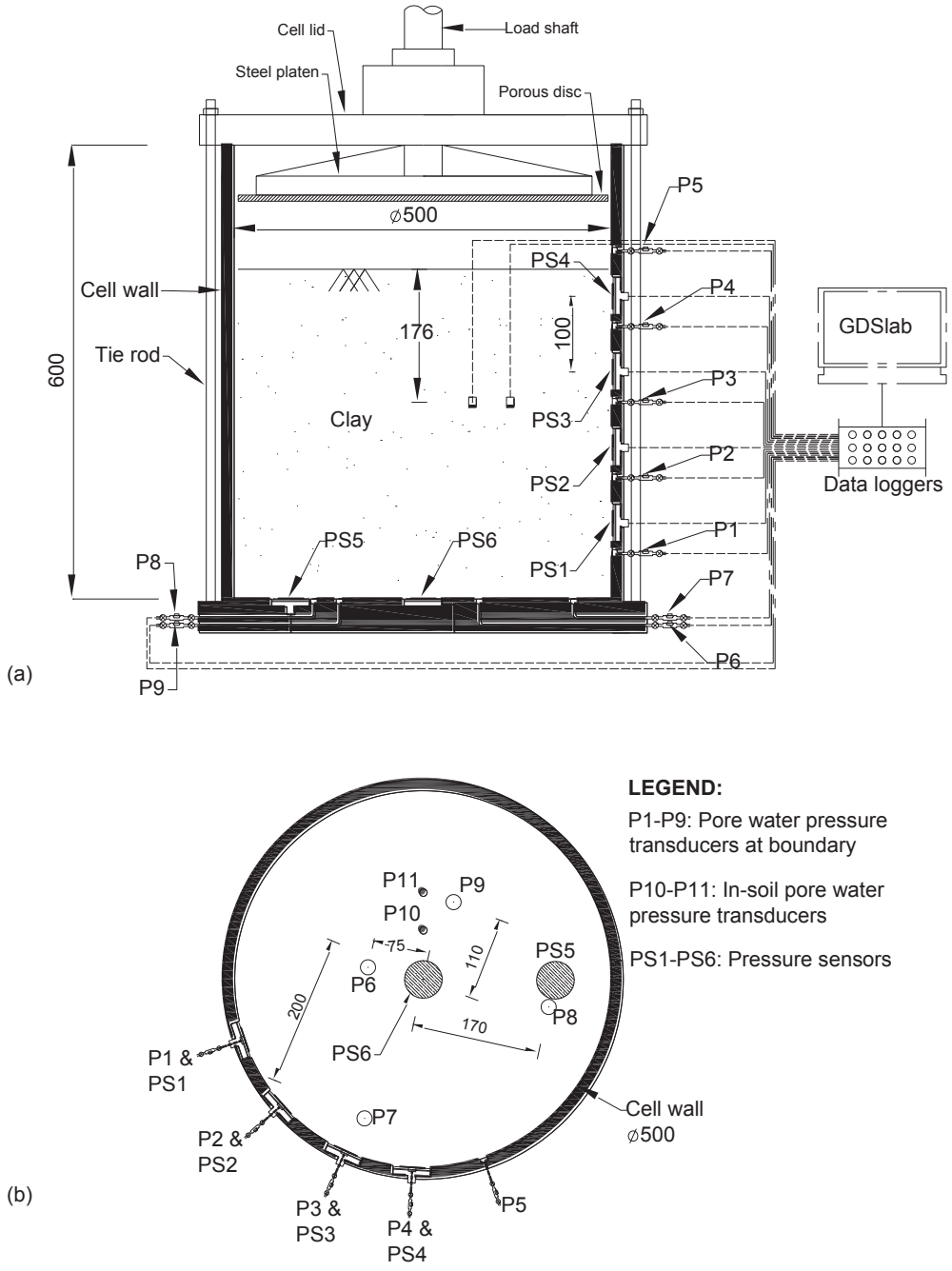

Figure 4.3 Schematic diagram of the consolidation cell: (a) cross-sectional view, and (b) plan view (all dimensions are in mm)

As shown in Figure 4.3, the soil tank had nine pore water pressure transducers installed along its boundaries (denoted as P1 to P9). Transducers P1 to P5 were mounted flush with the interior surface of the cell wall, at a spacing of 100 mm in the vertical direction, and at the same spacing in the horizontal direction (Figure 4.3a). At the bottom of the cell, transducers P6 to P9 were located at various radial distances from the base centre (Figure 4.3b). In addition, two miniature transducers P10 and P11 were embedded at a depth of 176 mm to measure the excess pore water pressure in the soil. The schematic diagrams of these miniature transducers and their specifications are shown in Figure 4.4a and Table 4.1.

Table 4.1 Technical specifications for pressure sensors & pore water pressure transducers

Instrument ID Adopted for This Study	**PS1 – PS4**	**PS5**	**PS6**	**P10 and P11**
Model – Capacity	Pressure Sensor KDF 200 kPa	Pressure Sensor KDF 500 kPa	Pressure Sensor KDE 1 MPa	Pore Water Pressure Transducer KPE-PB 200 kPa
Rated output (RO)	~ 0.3mV/V (600×10^{-6} strain)	~ 0.5mV/V (1000×10^{-6} strain)		+1026 μV/V ($+2052\times10^{-6}$ strain)
Non-linearity	2% RO			0.3% RO
Input/output resistance	350 Ω			~353.5 Ω
Temperature range	-20 ~ +60°C			-
Weight	160 g			-
Cable core	4-core shielded chloroprene cable			0.035 mm^2

Note: Data obtained from Tokyo Sokki Kenkyujo Co., Ltd.

Boundary pressure sensors were installed at six locations in the cell, denoted as PS1 to PS6 in Figure 4.3. Two models of the sensors with different cable connection layouts are shown in Figures 4.4b and 4.4c while their technical specifications are shown in Table

4.1. Pressure sensors model KDF-PA (Figure 4.4b) were installed in the tank wall (PS1 to PS4) and at location PS5 while model KDE-PA (Figure 4.4c) was installed at location PS6. Each sensor was built waterproof with an environmental protection IP rating 68. During installation of the sensors, circular holes and slots were precisely machined in the cell wall and base to host the pressure sensor and to allow an exiting path for wiring. The sensing surface of the sensor was installed flush with the cell interior while the body of the sensor was held securely in place. A rubber O-ring positioned in a radial groove between the pressure sensor and the machined hole provided a watertight seal at the installation location of the sensor.

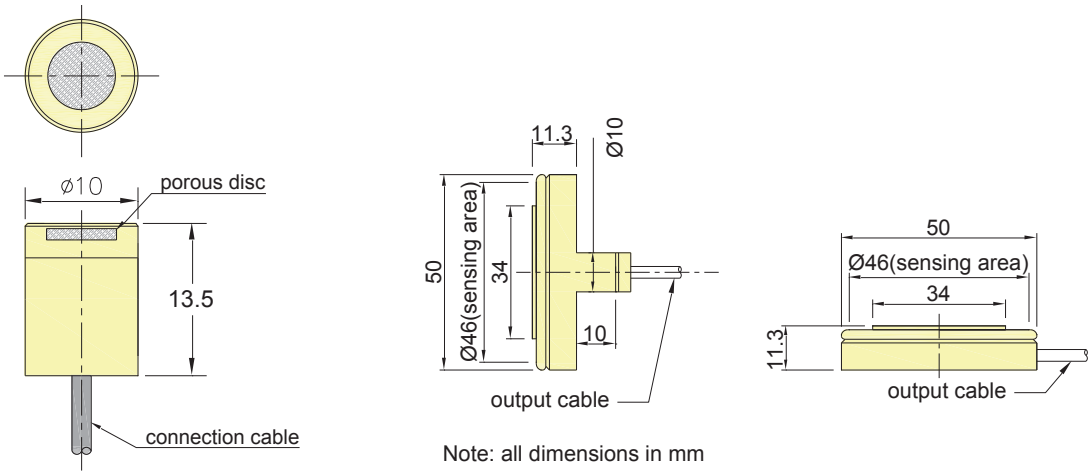

(a) KPE-PB (b) KDF-PA (c) KDE-PA

Figure 4.4 Miniature instrumentation: (a) in-soil pore water pressure transducers, (b) pressure transducers with cable exiting at the back of sensor (c) pressure transducers with cable exiting at the side of the sensor (courtesy of Tokyo Sokki Kenkyujo Co., Ltd)

Soil stress and pore water pressure data were collected by an automatic GDS data-logging system, which consisted of three nine-channel portable data loggers. Signal data from contactless laser displacement transducers, linear variable differential transformers

(LVDT) and strain gauges were logged using three programmable data loggers. Calibration via fluid pressure was carried out for all the pore water pressure transducers and pressure sensors prior to testing. Using an external pressure controller, calibration was made by matching the applied pressures and those registered by the monitoring instrumentation.

4.3.2 Soil Bed Preparation

The soil mixture, previously formulated by Le, Fatahi & Khabbaz (2015), was used to form the clay bed for the laboratory simulation of column installations. The dry portion of the mixture consisted of 70% of dry Q38 kaolinite, 15% of Active Bond 23 bentonite, 15% of fine to medium sand, by the total dry mass. The particle size distribution of the sand was characterised by 99%, 40%, 0.85% and 0.16% finer than 0.6 mm, 0.3 mm, 0.15 mm, and 0.075 mm, respectively. The sand was added to increase the permeability, while the bentonite increased the liquid limit of the mix. The dry components were mixed with water to form a slurry of an initial water content of 125%.

The interior surface of the cell wall was coated with silicone grease to reduce side friction before slurry placement. The slurry was then filled layer by layer to a total thickness of 520 mm. Free drainage condition at the top of the soil bed was provided by 8 mm thick porous brass disc. A layer of separation geotextile was laid between the soil and the brass disc to minimise drainage blockage. The surcharge was then applied incrementally using a 250 kN GDS axial loading system as shown in Figure 4.5.

Figure 4.5 The 250 kN axial loading system for consolidating slurry in the soil tank

The surface of the soil bed was sprayed with water until the completion of the model test to prevent desiccation of the surface soil. The evolution of the excess pore water pressure of the soil, the change in soil stress and the consolidation settlement of the soil with time was monitored. At the end of pre-consolidation period, the surcharge pressure and the lid of the cell were removed, leaving a soil thickness of approximately 436 mm.

The average pre-consolidation pressure $p'_{c,o}$ and the degree of consolidation of the soil sample at the end of the soil preparation period were estimated using the Asaoka and hyperbolic methods (Asaoka 1978; Tan, Inoue & Lee 1991). The details and the steps to construct the plots are shown in Appendix A. The predicted final settlement ρ_f was approximately 150 mm based on the Asaoka method while a higher ρ_f value of 195 mm was based on the hyperbolic method. Hence, the averaged degree of consolidation was approximately 60%. The average calculated $p'_{c,o}$ value of the soil sample using two methods was approximately 70 kPa.

The undrained shear strength profile of the soil was estimated using the measured soil penetration resistance during column installations (see Section 4.5.1.1) and was confirmed at the end of the main test by the laboratory miniature shear vane testing (ASTM 2016b).

Table 4.2 provides a summary of the soil properties. In particular, the Atterberg limits were obtained from a previous investigation by Le, Fatahi & Khabbaz (2015). According to Australian Standard AS 1726 (2017), the soil can be classified as high plasticity clay (CH). The bulk unit weight of the soil was measured using specimens extracted by U50 sampler after the model test. A Rowe cell consolidation test on sample 75 mm in diameter was carried out to determine the compression index C_c, the recompression index C_r, the coefficient of consolidation c_v and the coefficient of permeability k of the soil. The variation of void ratio e with the vertical effective stress $\sigma'_{o,v}$ obtained from the Rowe cell test is shown in Figure 4.6. This gave a compression index, C_c in the range of 0.98–1.3 and a C_r = 0.22.

In addition to the 75 mm diameter Rowe cell consolidation test, a large soil specimen 250 mm in diameter and 200 mm in height was consolidated under a vertical effective stress of σ'_v = 15.8 kPa until primary consolidation was completed to estimate the c_v (Figure 4.7). The c_v of the soil computed using the settlement time data obtained from this exercise was also included in Table 4.2. Figure 4.8 shows the variation of the permeability k with the void ratio e derived from the results of the Rowe cell consolidation test. The permeability change index C_k shown in Figure 4.8 was derived from Equation (4.1) (Taylor 1948).

$$k = k_0 \times 10^{-\frac{e_0 - e}{C_k}} \tag{4.1}$$

where e_0 is the initial void ratio, k_0 is the permeability at the initial void ratio e_0, and e and k are the void ratio and permeability at the condition considered, respectively.

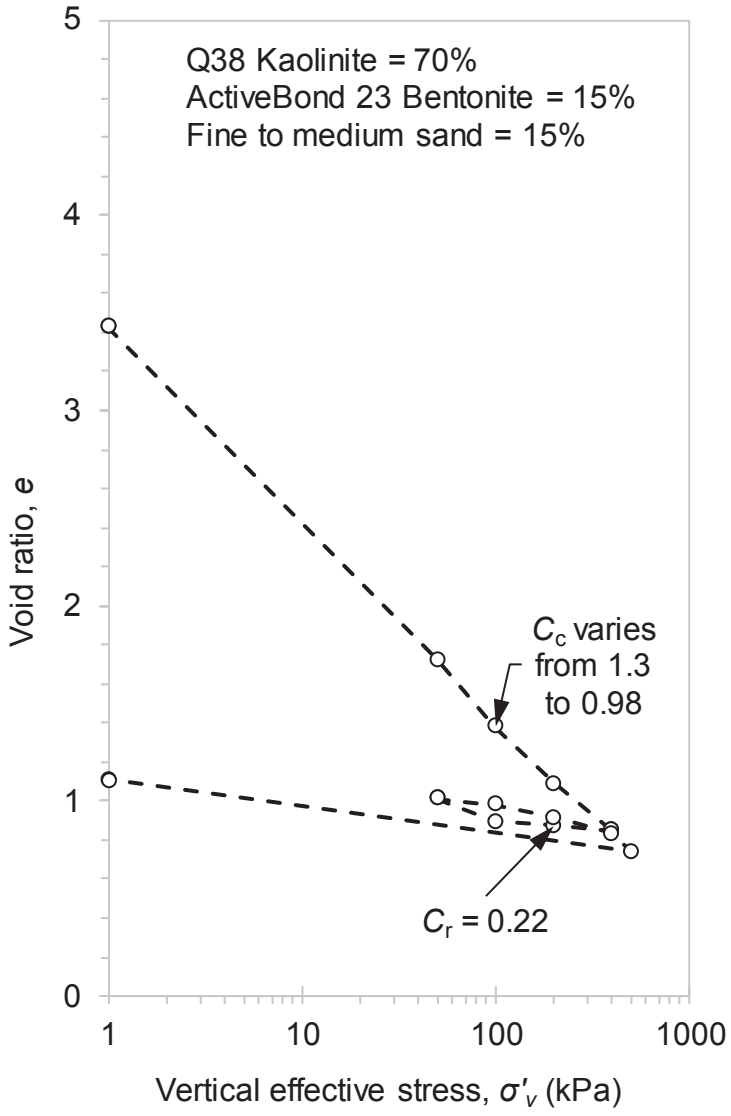

Figure 4.6 Void ratio versus vertical effective stress

The slope $M = q/p'$ of the critical-state line (CSL) presented in Table 4.2 was calculated using the plot of the deviatoric stress q against the mean effective stress p' on the p':q

stress plane, which was obtained from the undrained triaxial compression tests with pore pressure measurement (Figure 4.9).

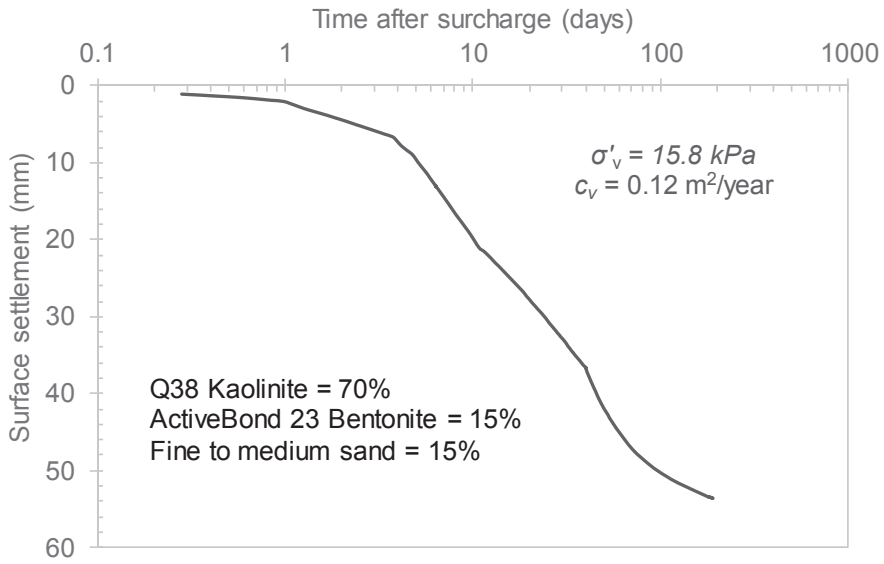

Figure 4.7 Consolidation settlement versus time during consolidating a soil sample 250 mm in diameter and 200 mm high

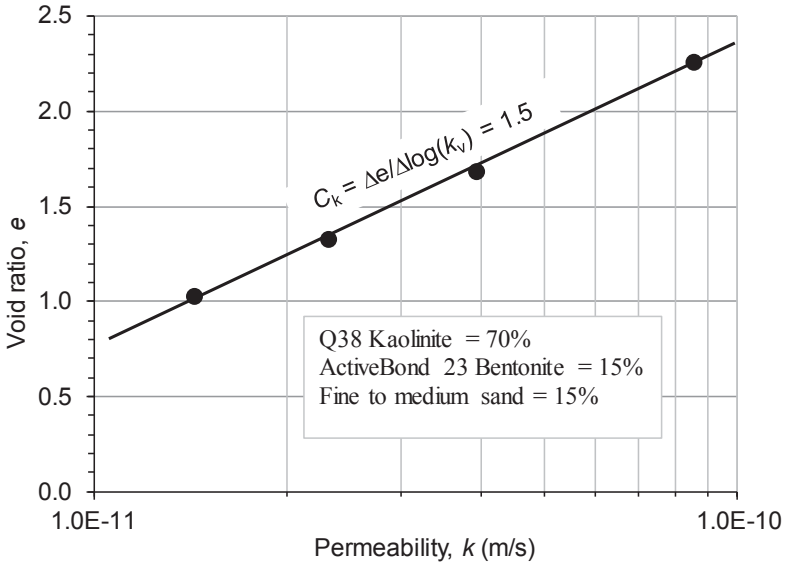

Figure 4.8 Permeability and void ratio relationship of soft soil used in the model test

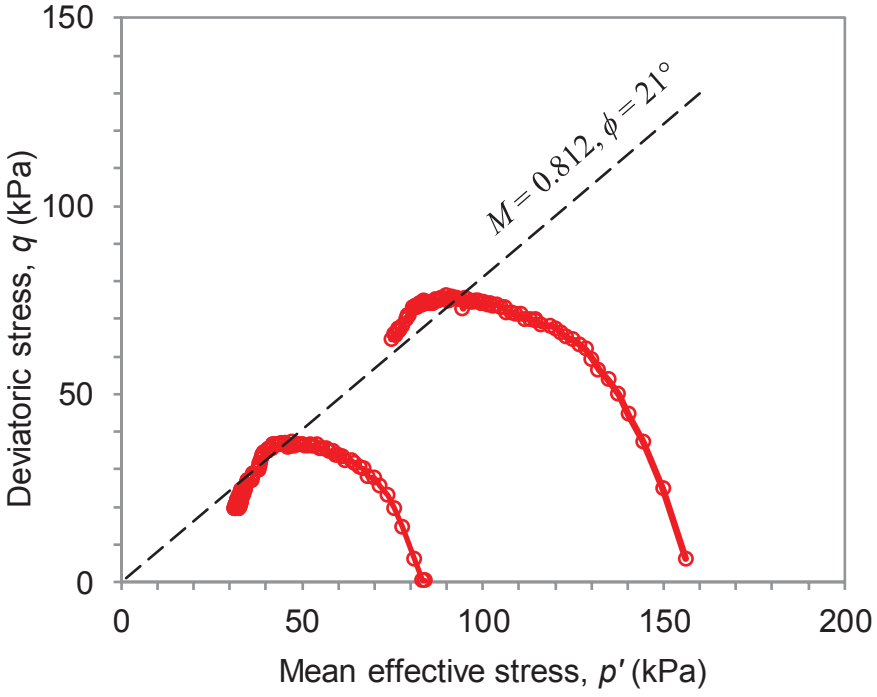

Figure 4.9 Results of consolidated undrained triaxial compression tests

Table 4.2 Properties of soft soil used in model test

Soil Properties	**Values**
Plastic limit, w_P[§] (%)	22
Liquid limit, w_L[§] (%)	80
Specific gravity, G_s	2.65
Saturated unit weight, γ_{sat} (kN/m^3)	14.7
Permeability change index, C_k	1.5
Effective Poisson's ratio, ν'	0.3
Internal friction angle at the critical state, ϕ' (°)	21
Slope of critical state line, M	0.812
Average initial in-situ void ratio, e_o	2.2
Vertical coefficient of consolidation at various stress levels, c_{v} (m^2/year)	0.12 when σ_v' = 16 kPa; from 0.1 to 0.07 when σ_v' between 50 kPa and 100 kPa
Compression index, C_{c}	1.3 to 0.98 (σ_v' = 50 kPa to 400 kPa)
Recompression index, C_{r}	0.22
Average initial coefficient of permeability, k (m/s)	4×10^{-11} (at stress level between 50 kPa and 400 kPa); 9×10^{-11} at σ_v' = 50 kPa
Initial undrained shear strength, s_u (kPa)	$8 - 12$
Average pre-consolidation pressure, p_c' (kPa)	70

Note: [§]Atterberg limits obtained from Le, Fatahi & Khabbaz (2015).

4.3.3 Concrete Column Properties

According to Fok et al. (2012), grout mixes for ground improvement purposes typically vary depending on the location of the project and the local availability of the materials, but typically comprise a blend of cement and fly ash, a homogeneous mixture of sands and gravels between 2 mm and 7 mm and addictive for workability and fluidity. In this study, the grout mix as described by Fok et al. (2012) was used to cast the columns, however, the aggregate was sensibly sized to account for scale effect. Grout specimens after curing periods of 1, 7, 28 and 56 days were tested to determine the cylinder compressive strength in accordance with AS 1012.9 (Standards Australia 2014a) and

indirect splitting tensile strength in accordance with AS 1012.10 (Standards Australia 2014b). The stiffness of the concrete was determined via strain gauges during the compressive strength tests in accordance with AS 1012.17 (Standards Australia 2014c). The average mass density of concrete column ρ_c was approximately 2300 kg/m^3. The strength test results are summarised in Table 4.3, which indicates an increase in the mechanical characteristics of the grout over time. The one-day age grout specimen had an unconfined compressive strength of 3.7 MPa, which was 14% of the 28-day unconfined compressive strength. The measured indirect split tensile strength, σ_{st}, was approximately 20% to 24% of the corresponding measured unconfined compressive strength, f'_{ck} for the range of curing ages considered in this study. The ratio of the one-day stiffness of the grouted specimen, E_c, to that of the soft soil, E_s, is approximately 4700, considering $E_s \simeq 200\times s_u$.

Table 4.3 Strengths and stiffness of grouted columns

Age of grout (days)	Unconfined Compressive Strength, f'_{ck} (MPa)	Elastic Modulus, E_c (GPa)	Indirect Tensile Strength, σ_{st} (MPa)
1	3.7	9.4	0.9
7	11.9	25.3	2.4
28	26.9	-	5.3
56	28.3	-	6.4

4.4 Method of Installing Columns

4.4.1 Column Layout and Sequence of Installation

The layout of the concrete columns and their positions relative to the monitoring instrumentation attached to the soil tank are shown in Figure 4.10. The central column was denoted as C1, while the six perimeter columns were denoted as C2 to C7. The plan

dimensions of the model were smaller than the authors would have liked but were limited by the available cell. Therefore, some boundary effects had to be tolerated. In this configuration, the installation of any perimeter column inside the soil tank implied a concurrent installation of the mirror image column outside the tank wall, considering the soil tank wall as the symmetrical boundary. Each concrete column in the model test was 50 mm in diameter (D) and the centre to centre spacing, s, of the columns was 180 mm ($\simeq 3.6D$).

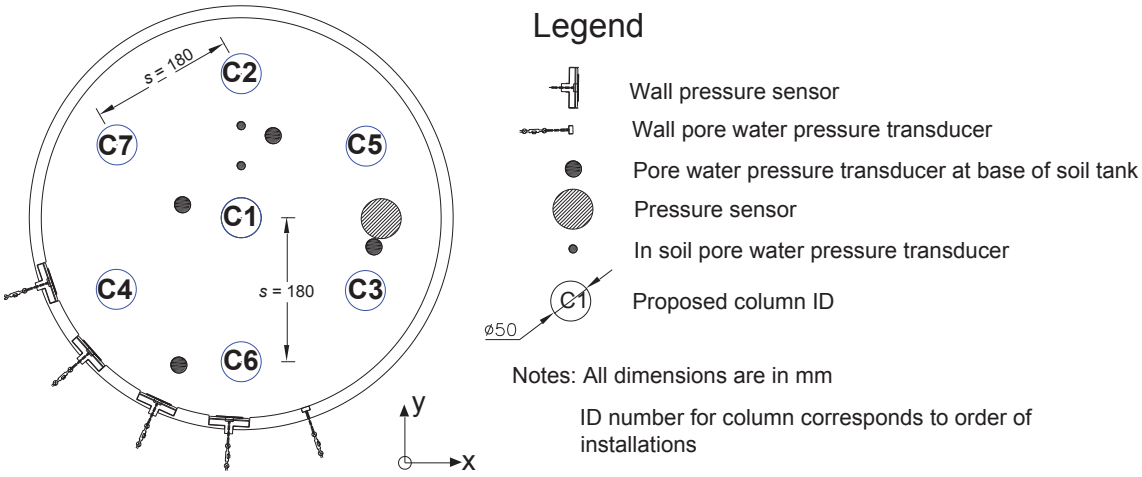

Figure 4.10 Plan view and the layout of columns

The arrangement of the columns in a triangular pattern corresponded to an area replacement ratio of 7%. It can be noted that the area replacement ratio in the Dutch practice for piled embankments is between 4.5% and 12% (Van Eekelen, Bezuijen & van Tol 2013). All columns were extended to the full depth of the soil. In particular, the length of the as-built central column was 440 mm, while the remaining columns were longer by approximately 20 mm due to the generated soil heave. The model dimensions were selected based on the scaling ratio given in Table 4.4. It is noted that some compromises were made as the model test was performed under a 1g condition, and it was not possible to satisfy all the similarity ratios. Unlike granular materials, due to the expected small

volume change in clay during pile installation, the difference in the simulation of column penetration at 1*g* and at higher *g* is relatively insignificant (Craig 1985).

Table 4.4 Column properties in the model test and scaled dimension for prototype

Item	**Size (prototype)**	**Size (model test)**	**Similarity Ratio**
Column diameter, D (m)	0.45	0.05	9
Column length, L (m)	3.96	0.44	9
Column spacing, s (m)	1.62	0.18	9
Second moment of area, I (m^4)	2.01×10^{-3}	3.07×10^{-7}	-
Bending stiffness of column, EI ($N.m^2$)	1.81×10^{7}	2.76×10^{3}	6.56×10^{3}
Elastic modulus of column E_c (kPa)[§]	-	9×10^{6}	-
Density of column, ρ_c (kg/m^3)	-	2300	-

Note: [§] Concrete strength at 1 day old.

The column IDs as shown in Figure 4.10 were numbered in accordance with the sequential order of installations (i.e. C1, C2, C3, C4, and then C5, C6 and C7). Column C1 was installed first, during which strain gauges were embedded in the grout. The installation of the perimeter columns (C2 to C7) commenced one day after the installation of column C1. The one-day lag allowed column C1 to harden, which resulted in a developed bonding of embedded strain gauges to the grout host.

4.4.2 Installing the Central Column

The penetrating system, as shown in Figure 4.1, was used to install the columns. For the central column, the installation process involved three steps: (*i*) creating a lined borehole by a displacement method; (*ii*) inserting strain gauges inside the borehole; and (*iii*) grouting to form the concrete columns. The steps for installation of column C1 are shown schematically in Figure 4.11.

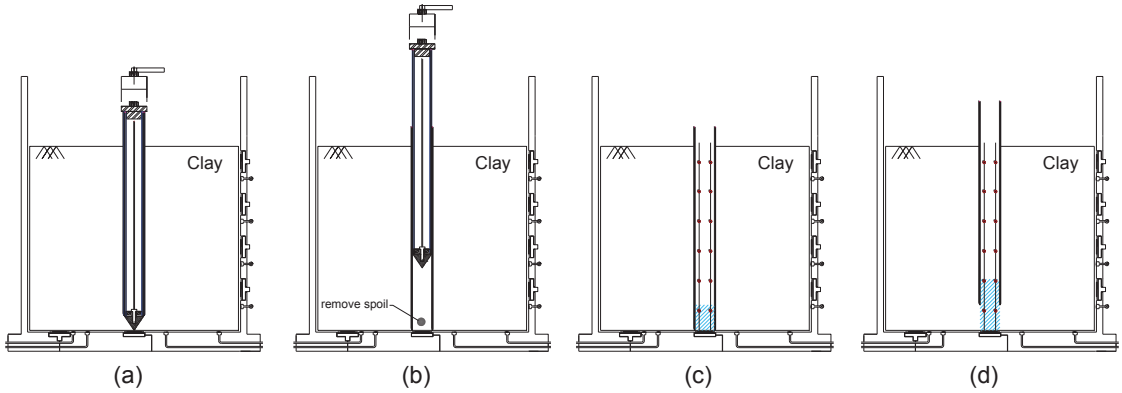

Figure 4.11 Graphical representation of the test procedures: (a) jacking until full penetration (b) outer tube advancing downward, inner core retract, and spoil removal; (c) insertion of strain gauges and pouring first lift of grout (d) pouring second grout lift and retracting outer tube

4.4.2.1 Creating a Lined Borehole

Referring to Figure 4.11a, the piling apparatus was jacked into the soil in a monotonic mode at a downward penetration rate, v_p, of 3.4 mm/s (compared to 20 mm/s for CPT) until full penetration was achieved. Such penetration speed was sufficiently fast to ensure that the soil surrounding the pile would behave in undrained condition during penetration. In fact, the calculated normalised penetration velocity, V, defined by Finnie & Randolph (1994) using Equation (4.2), is much greater than the recommended value of 30, as a minimum velocity to satisfy the undrained behaviour of clay during penetration (Kim et al. 2008; Randolph & Hope 2004).

$$V = 2 \times v_p \times r_{pile}/c_v \tag{4.2}$$

where v_p is the vertical penetration speed in mm/s, r_{pile} is the model pile radius in mm, and c_v is the coefficient of consolidation of the soil in m^2/year.

As the conical tip of the piling probe reached the cell base, the outer tube was advanced further to the cell base, which remained in place as the temporary casing until the

completion of the subsequent grouting process (Figure 4.11b). Next, while restraining the outer tube against uplift, the inner tube and the conical tip was then retracted slowly upwards to provide an unobstructed passage for concrete injection. A small amount of spoils left inside the outer tube were removed, leaving a clean borehole ready for insertion of strain gauges and subsequent grouting.

4.4.2.2 Embedding Strain Gauges

In the next step (i.e. Figure 4.11c), a cage with the attached strain gauges, as shown in Figure 4.12a, was inserted into the created borehole. The embedment of the strain gauges inside column C1 was to measure the bending moments induced in the column due to soil movements generated by the installation of the perimeter columns. This section describes the arrangement of strain gauges in the column and the design of the circuit connections to minimise the volume of strain gauge lead wires inside the reduced-scale concrete column.

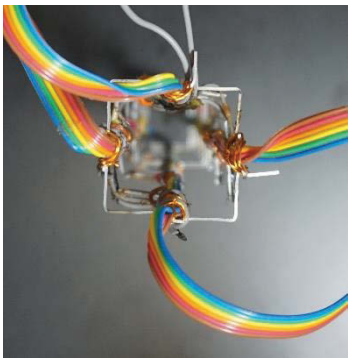

(a)

(b)

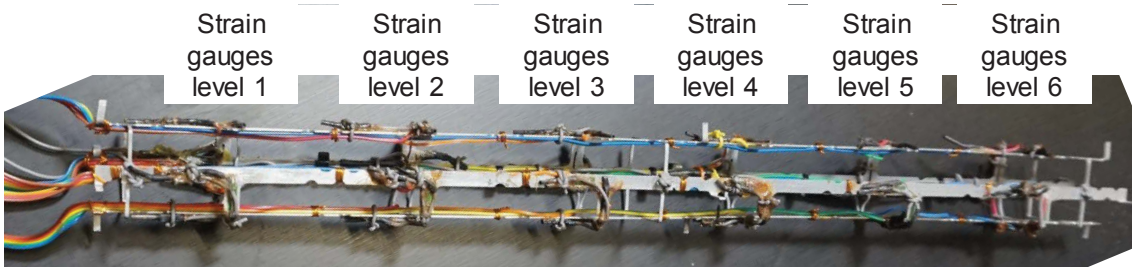

(c)

Figure 4.12 Strain gauge holding cage: (a) cage hosting strain gauges, (b) cage placed inside the created borehole, and (c) side view

Due to expected multi-directional lateral loadings induced by soil movements resulting from the installation of different columns in the (*x*,*y*) coordinates (see Figure 4.13a), two pairs of strain measuring locations at each level were arranged in the cross-sectional area of the concrete column (Figure 4.13a). Each pair were embedded onto the opposite sides of the column. This configuration allowed strain measurements to be taken, from which bending moments about two axes *x* and *y* were estimated. The orientation of the strain gauges inside the borehole relative to the (*x*,*y)* coordinates are shown in Figure 4.13a.

As shown in Figure 4.13c, forty-eight foil strain gauges (model FLA-5-23 fabricated by TML, Japan) were embedded at six levels along the length of the column C1. The longitudinal strain near the fibre extreme (i.e. near the surface of the column), or bending strain, was ensured by attaching strain gauges onto four (4) 0.6 mm thin holding strips (440 mm long × 5 mm wide) fabricated from aluminium. Horizontal stirrups were used

to hold these four vertical strips in place, at three levels (Figure 4.13c). Bonding between the aluminium strips and the column body was enhanced by adding a tread pattern to the strips (Figure 4.13d).

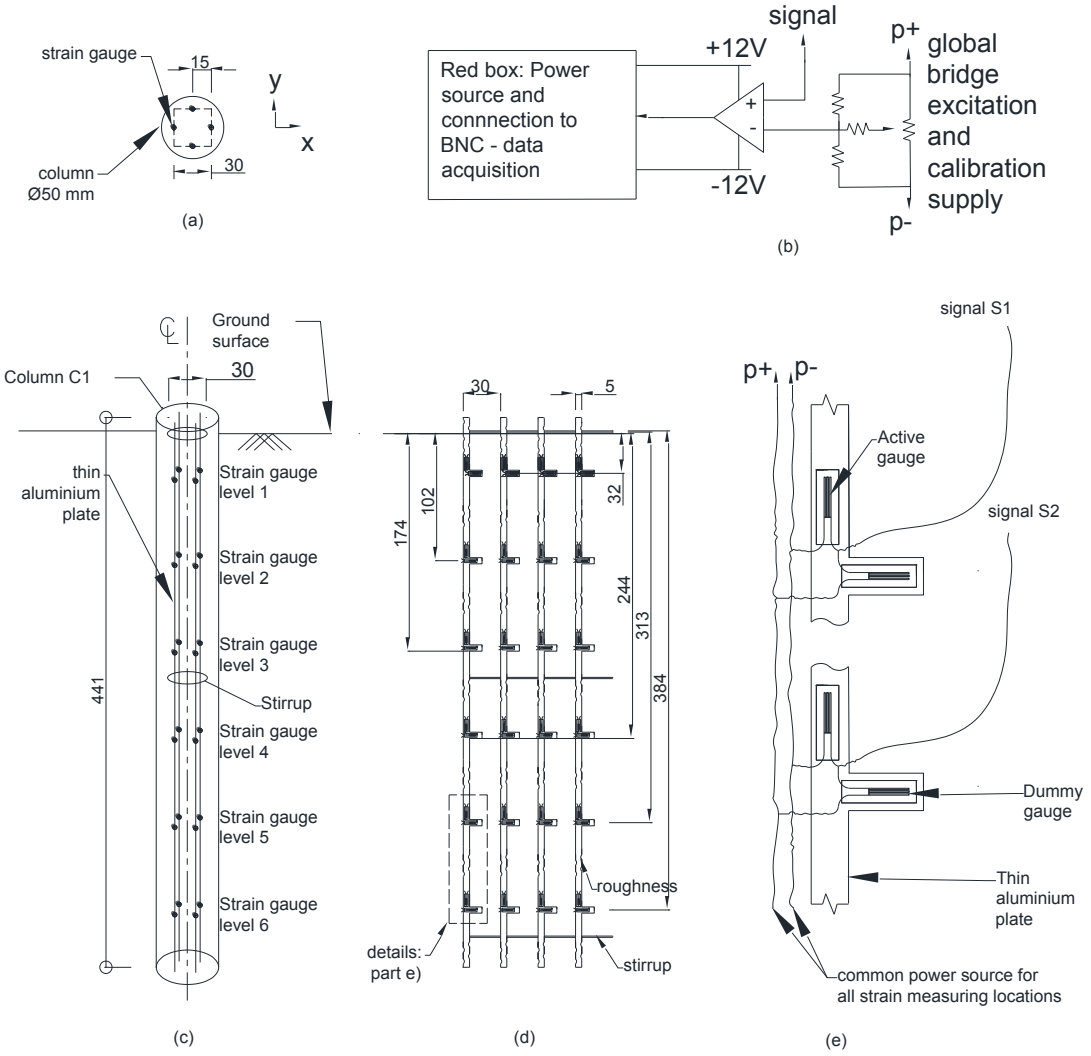

Figure 4.13 (a) Columnar sectional area, (b) amplification and bridge completion, (c) embedded strain gauges in column C1, (d) locations of strain gauges when column C1 is unfolded, and (e) half bridge strain gauge layout and connection; all dimensions are in mm

The two strain gauges formed a location on the aluminium material of the holding strips. Each strain gauge has a gauge length of 5 mm and a width of 1.5 mm, while the gauge backing is 3 mm wide by 10 mm long, with the nominal resistance of 120 Ω. While it was

desirable to position each strain measurement point as close as possible to the outer surface of the column, it was also necessary to leave sufficient concrete cover over the gauges and aluminium holding strips (Figure 4.13a). To maintain a small concrete cover, the cage was centred in the hole by spacers.

At each strain measuring location, a half bridge circuit configuration consisted of an active gauge and a dummy gauge. The dummy gauge was thermally coupled to the active gauge, which provided compensation for resistance changes due to temperature. The placement of the dummy gauge in a strain neutral position caused the circuit to behave in a similar manner as a quarter-bridge configuration (Figure 4.13e). However, the routing of the bridge excitation supply to each half-bridge pair would result in an excessive volume of lead wires inside the concrete column. Therefore, a common power supply consisting of two lead wires (P+ and P-) was used to power all of the strain measuring locations, this almost halving the number of wires needed. A single signal lead wire was then used to convey the gauge signal from each strain measuring location to the outside. All strain gauges were waterproofed and protected with a coating material. During grouting and the early stage of the hydration period, strain gauge wires were disconnected from the amplifiers and power sources to avoid damage by electrolysis induced by excessive fluid in the soil and the grout.

4.4.2.3 Grouting Process

The grouting process was carried out lift by lift for each column as shown in Figures 4.11c and 4.11d. The process was carried out in quick succession so that the grout would not harden quickly and hence block the piping that took the grout to the required location. Each lift involved filling 60 ml grout prepared by a Hobart mixer, and hence the grouting process was completed after nine lifts. After each filling lift, the tubular liner was slowly

retracted upward while restraining the embedded strain gauges against uplift. The grouted material was compacted to reduce air void and a downhole camera was used to check the column consistency. Multiple trials carried out prior to the main test indicated that grouted columns had a consistent geometrical profile with unnoticeable void and defects. A typical grouted column is shown in Figure 4.14.

(a)

(b)

Figure 4.14 (a) Typical cast in-situ concrete column at one-day age, recovered from soft soil; and (b) exposed soil and columns after excavation

After an initial setting period of 24 hours, signals from the strain gauges embedded in column C1 were amplified and collected through the PC-based data loggers. The vertical movement of column C1 head was monitored by an LVDT (Figure 4.15). The rotation of

the column head C1 in the *y* direction was monitored by a pair of non-contact laser displacement transducers T1 and B1, while the rotation in the *x* direction was measured by transducers T2 and B2. Transducers T1 and T2 were positioned 95 mm above the column head and the other two transducers were positioned 55 mm above the column head.

4.4.3 Installing Perimeter Columns

The installation of columns C2 to C7 commenced after column C1 had been cured for 24 hours, using a similar procedure to those adopted for installing column C1. Test results of concrete specimens sampled during column installations indicated consistent concrete strength and stiffness despite using separate concrete batches for different columns. The grouted columns and soil surface after each column installation are shown in Figure 4.16. As shown in Figures 4.16g and 4.16h, the non−contact laser displacement transducers were relocated to allow rooms for installations of columns C6 and C7.

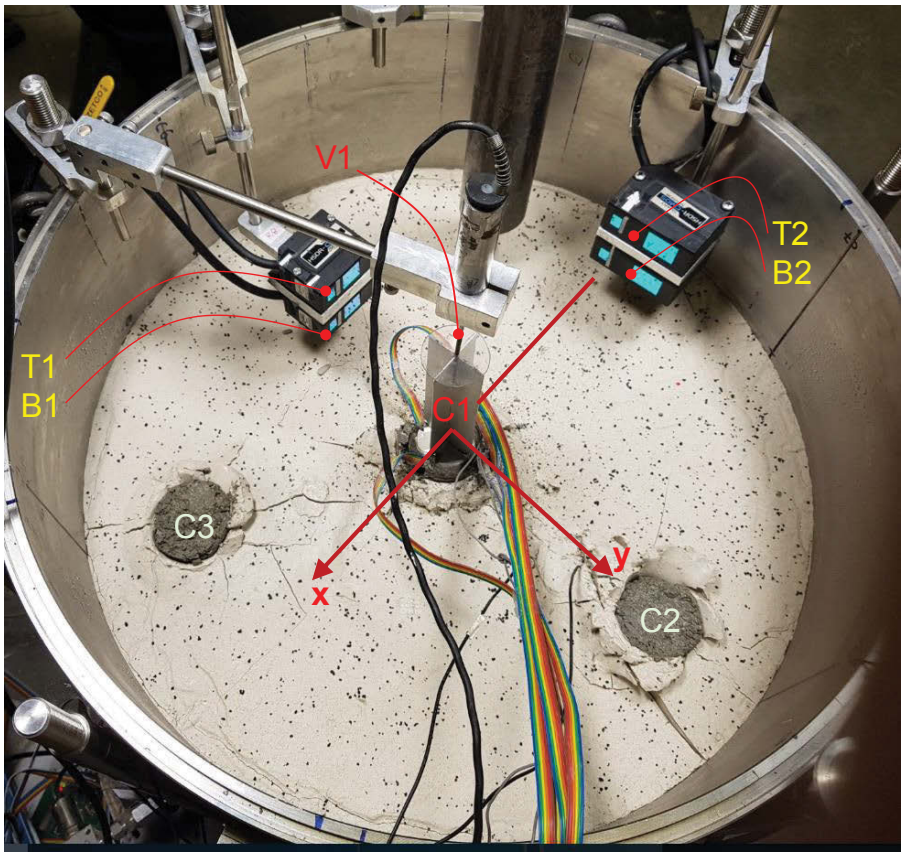

Legend

T1, B1, T2, and B2: Laser displacement sensors
V1: Linear variable displacement transducer (LVDT)
C1 to C3: concrete columns

Figure 4.15 Arrangement of monitoring instrumentation for column C1

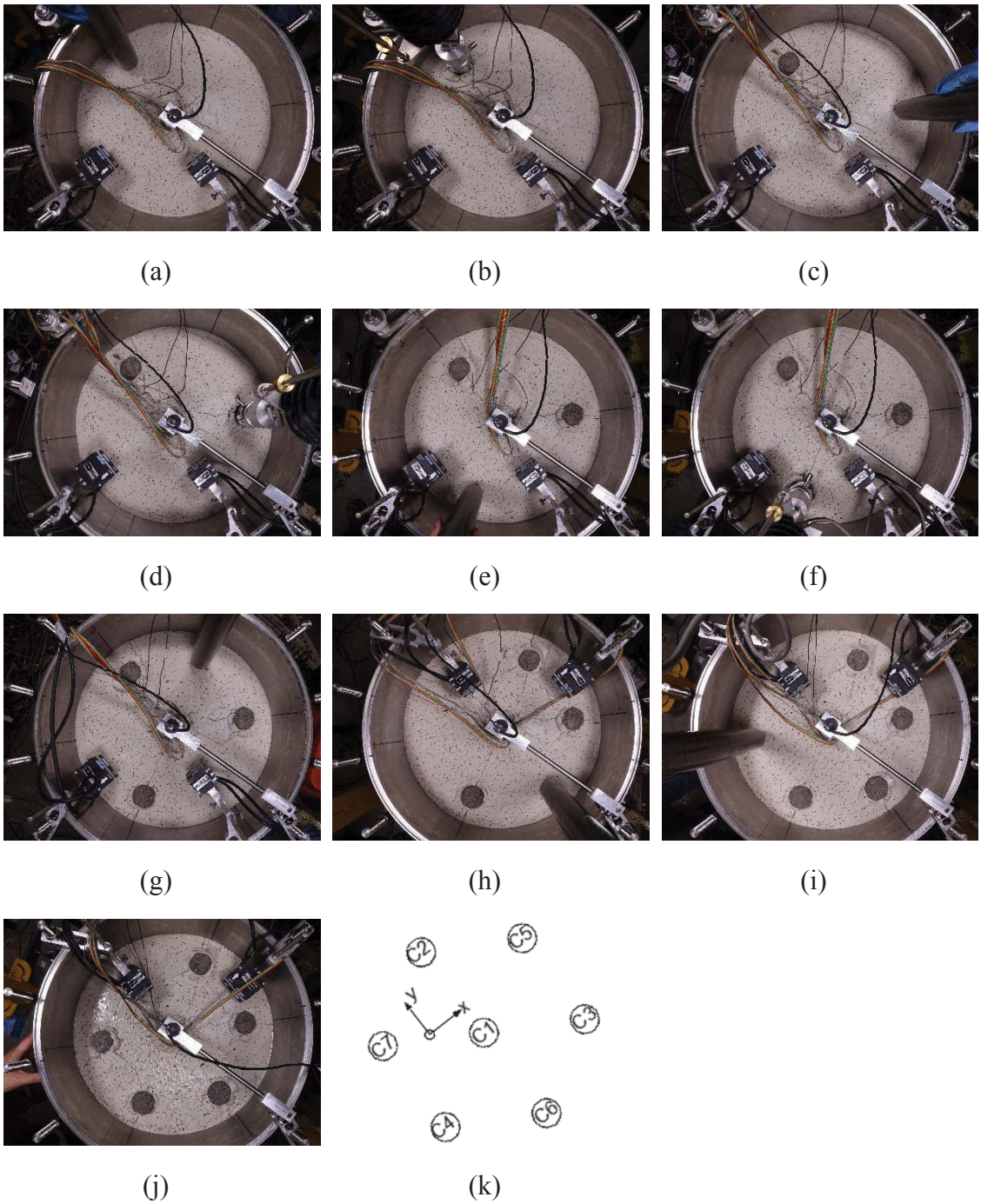

Figure 4.16 Plan view of installations: (a) initial conditions; (b) installing C2; (c) completing C2; (d) jacking to full depth at column C3; (e) C1 to C3 installed; (f) full penetration at column C4; (g) grouting completed at C4; (h) grouting completed at C5; (i) complete installation at C6; (j) all columns installed; and (k) orientation of all columns

4.5 Results and Discussion

4.5.1 Responses of Soil to Column Installations

4.5.1.1 Soil Resistance to Jacking

As shown in Figure 4.17, the measured penetration resistance during jacking the model pile into the soft soil at columns C1 to C7 was approximately 130 N. The penetration resistance remained almost constant with depth. Since the conical pile used in this study has a similar diameter to a 1500-mm^2 piezocone or 43.7 mm in diameter (ASTM 2012), the measured penetration resistance was used to correlate with the undrained shear strength s_u of the soil. The estimated s_u of the soft soil ranged from 7 kPa to 12 kPa, assuming a typical friction ratio (i.e. skin friction over tip resistance) for soft clay between 1% and 3% (Kelly et al. 2017; Nash, Powell & Lloyd 1992; Pestana, Hunt & Bray 2002). Slight variation in the measured soil resistance may be attributed to the complex unloading and reloading conditions, induced by installations of various columns. The results of the miniature shear vane tests conducted at the completion of the main test indicated that the averaged undrained shear strength was approximately 5.5 kPa.

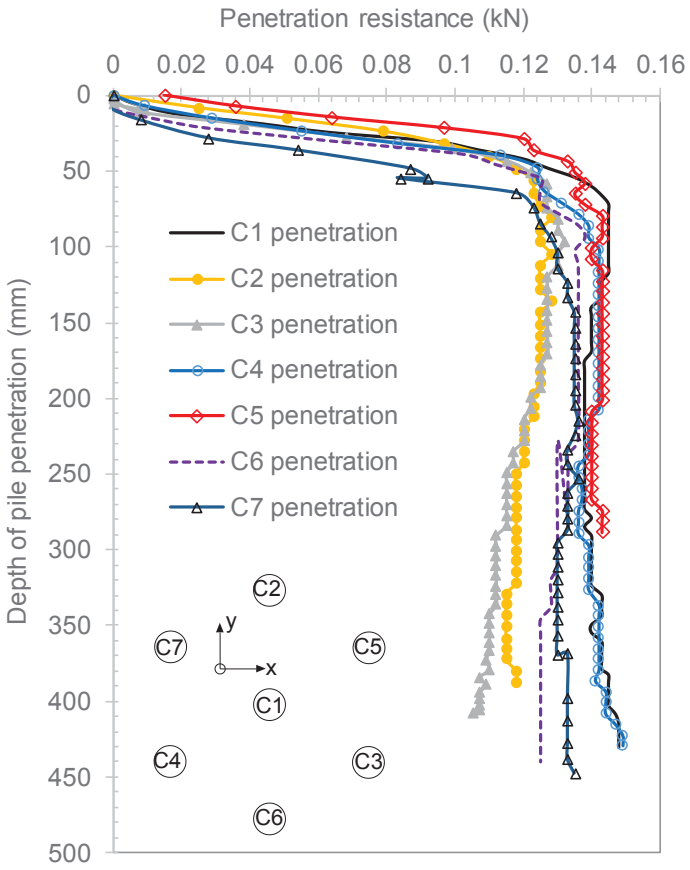

Figure 4.17 Measured penetration resistance during jacking for installing columns C1 to C7

4.5.1.2 Heave of Surface Soil

Throughout the model test, the deformation of the soil surface was captured by a handheld 3D laser-scanning device (Metris ModelMaker MMDX100, Figure 4.18). This scan model was able to measure the surface level of the soft soil accurately since the laser scanning technology is non-contact (Figure 4.18b). The 3D cloud data was then processed using the 3D surface mapping software Surfer 15.1 (Golden Software 2017). Figure 4.19 portrays the 3D contour of the soil surfaces during the installation of seven columns. The results show that the soil heave accumulated after each column installation.

(a)

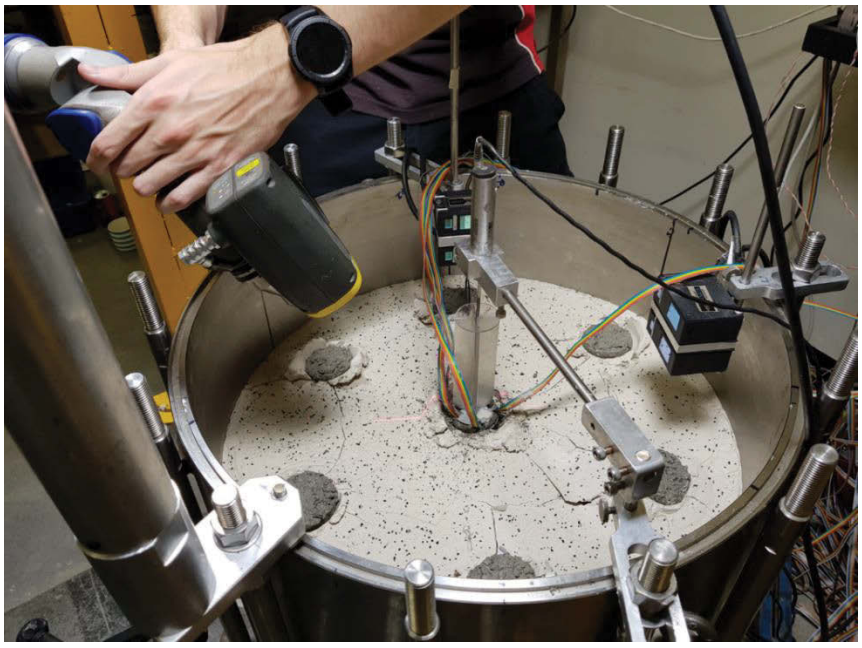

(b)

Figure 4.18 3D scanning: (a) the set-up of the handheld 3D laser scanning device (b) scanning operation during column installations

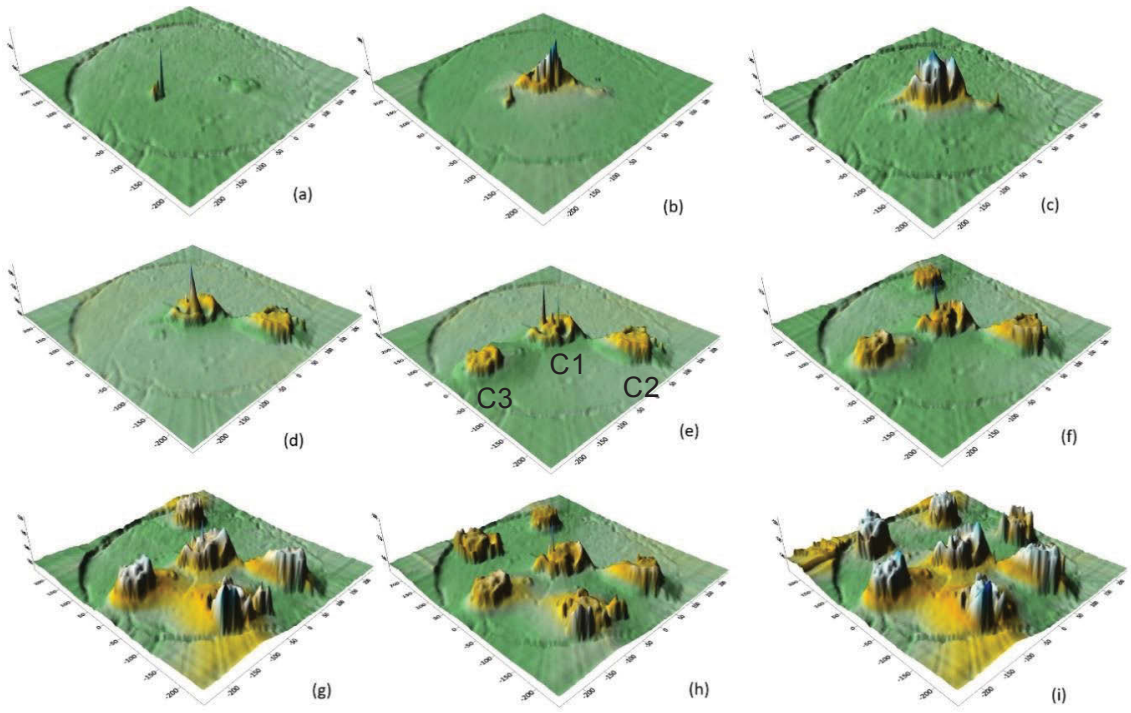

Figure 4.19 3D scans of surface soil and column heads: (a) initial condition, (b) C1 installation, (c) a day after C1 installation, (d) after C2 installation, (e) after C3 installation, (f) after C4 installation (g) after C5 installation, (h) after C6 installation, and (i) after C7 installation

Referring to Figures 4.19g to 4.19i, a concentration of soil heave illustrated by the yellow fill contour occurred between columns C1, C2, C5 and C3. During the undrained cavity expansion (or column installation by full displacement piling), the combined volume of soil displaced radially and vertically would be equal to the volume of concrete inserted to build the column, which was approximately 0.856 litre per column. Figure 4.20 shows the volume of soil surface heave induced by each subsequently installed column, calculated using the Surfer software. The averaged incremental increase in the soil heave volume was similar to the volume of a grouted column.

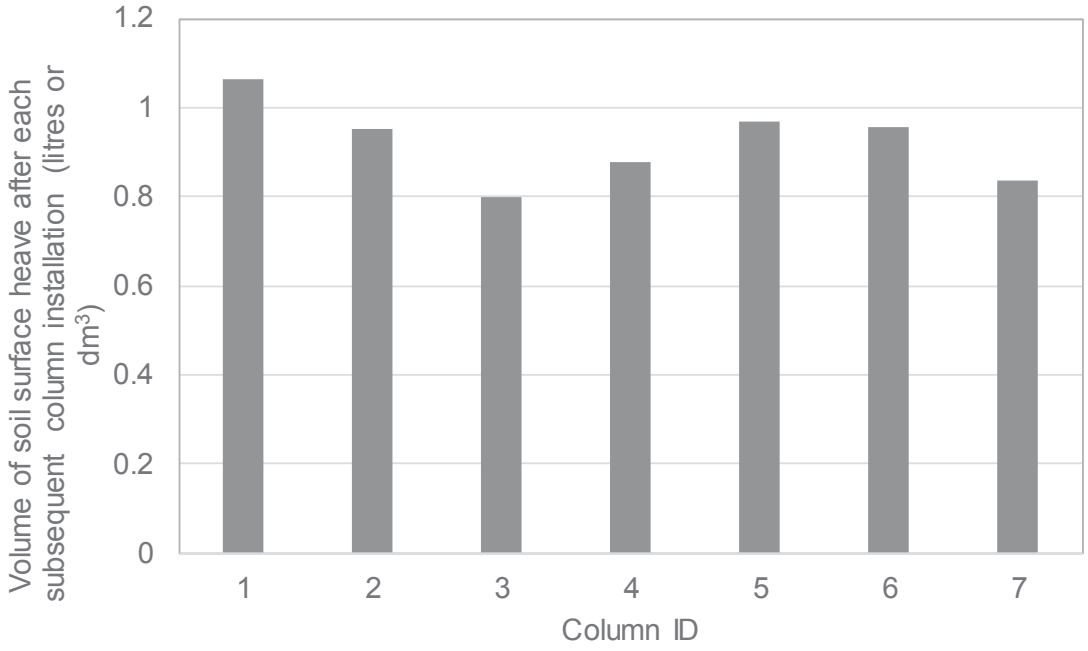

Figure 4.20 Volume of soil surface heave induced by each subsequent column installation

Figure 4.21 shows the contour of the soil surface heave at the end of all column installations. Midway between the columns the soil heave varied from 22 mm (occurring near C1, C6, C4 and C7) to 27 mm (occurring near columns C1, C2, C5 and C3). Immediately around the edge of the columns, the maximum soil heave ranged from 32 mm to 37 mm. Figure 4.22 shows the evolution of the topography of the surface soil and column along Section AA′ of Figure 4.21, as the installations progressed. The figures indicated that column C2 uplifted as the result of the remaining installations. According to Figure 4.22e, it is interesting to note that column C2 uplifted the similar amount as the surrounding soft soil heaved. This observation agreed very well with the theoretical assumption made by Chow & Teh (1990). They believed that for a given pile and soil conditions, the heave at the pile head increases as the pile stiffness decreases; and if it is assumed that the pile stiffness was equal to soil stiffness then the pile heave would be equal to the soil surface heave.

Referring to Figure 4.22 the 3D scanning device was not intended to record the lateral movement and uplift of column C1. The precise monitoring of column C1 movement was provided by an LVDT and four non-contact laser displacement sensors, which will be described in later sections.

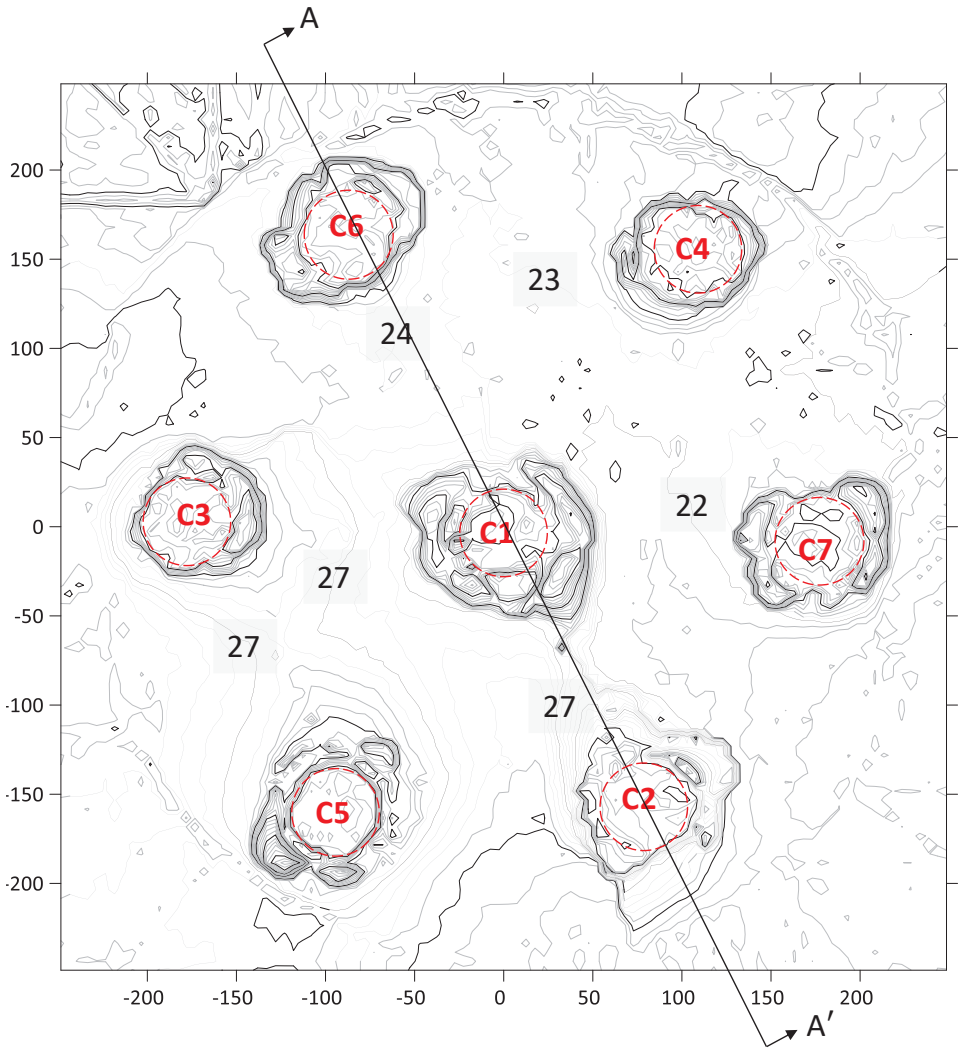

Figure 4.21 Contour of soil surface heave after all installations were completed

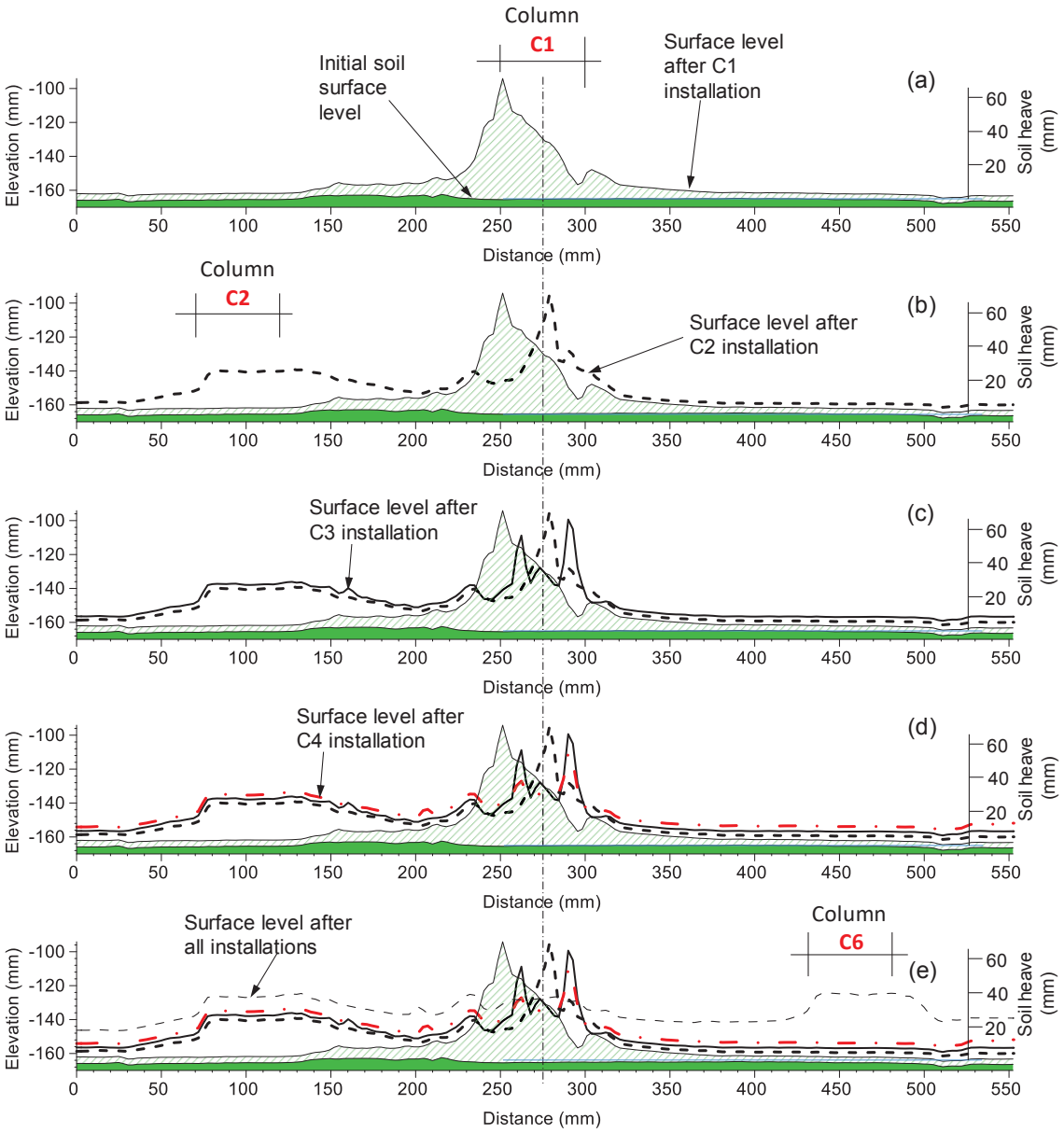

Figure 4.22 Soil surface heave along Section AA′ of Figure 4.21: (a) the initial ground surface level and surface level after C1 installation (b) after C2 installation (c) after C3 installation (d) after C4 installation and (e) after all 7 columns were installed

4.5.1.3 Stress Change Induced by Column Installations

The stress changes imposed in the soil during the installation process of any given displacement column may have a considerable effect on the capacity of nearby columns. Figures 4.23, 4.24, and 4.25 illustrate the variation of measured soil horizontal stresses at the soil tank boundary during the installations of columns C1 to C7. The figures clearly

show that the changes of the horizontal stress in the soil continued to occur throughout the installation process. The variation of the soil stresses measured by the sensors indicates that the effects induced by the installation procedure for every single column were consistent.

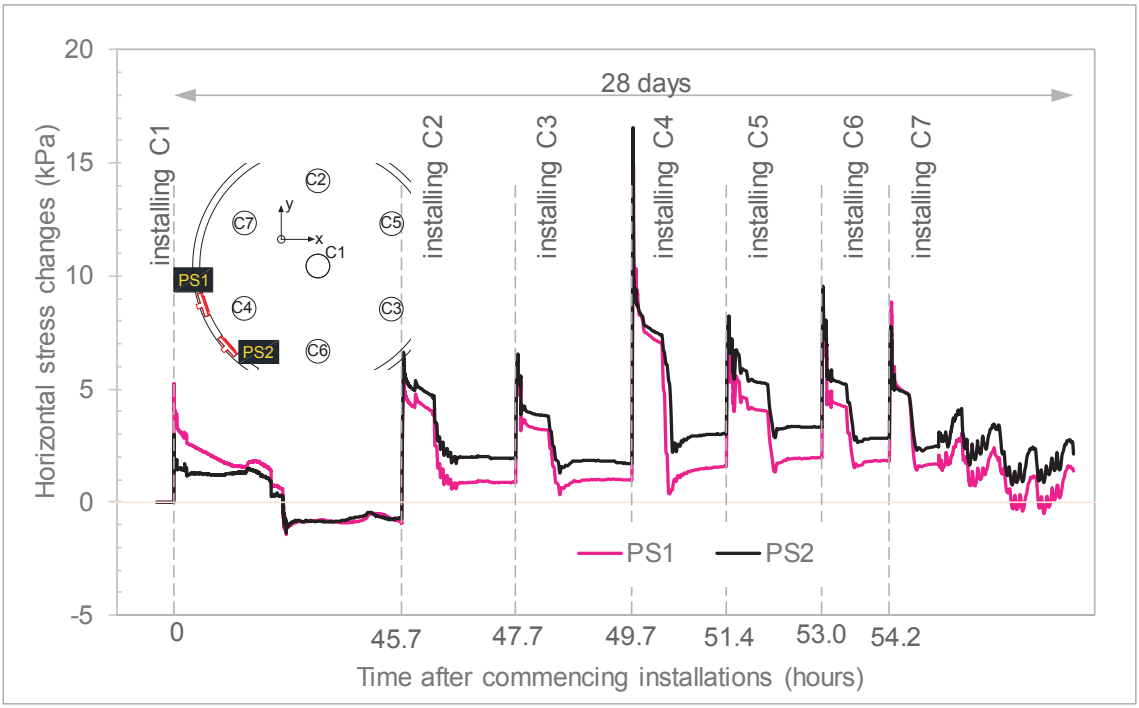

Figure 4.23 Changes in total horizontal stresses in the soil at depths of 236 mm (PS2) and 336 mm (PS1)

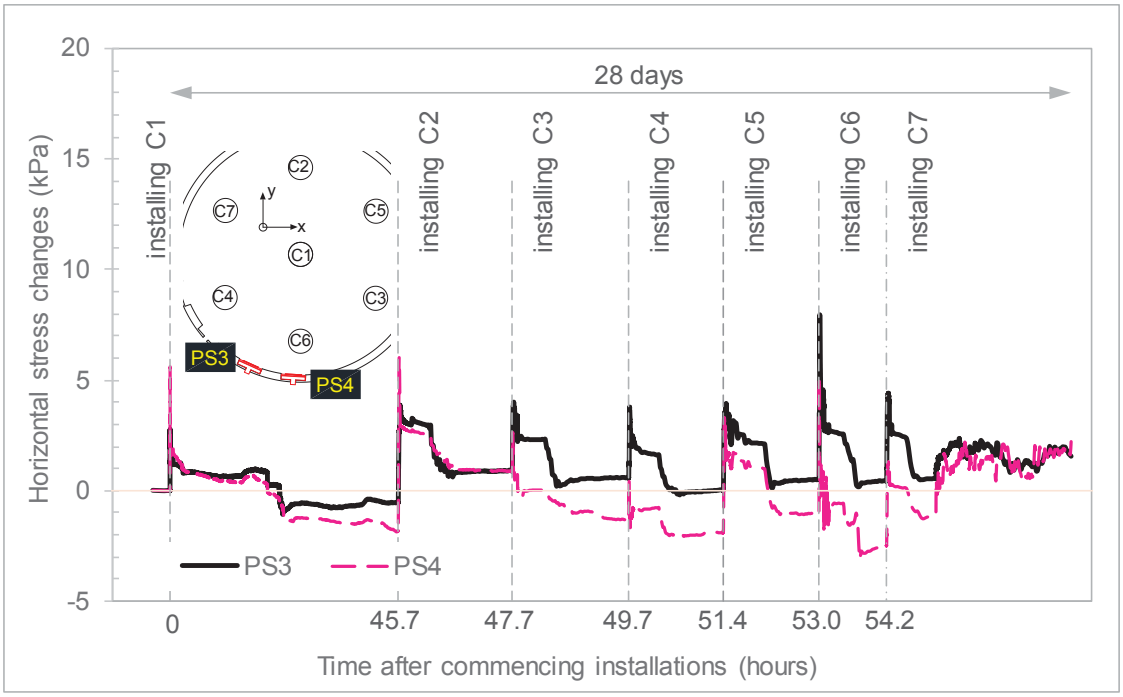

Figure 4.24 Changes in total horizontal stresses in the soil at depths of 36 mm (PS4) and 136 mm (PS3)

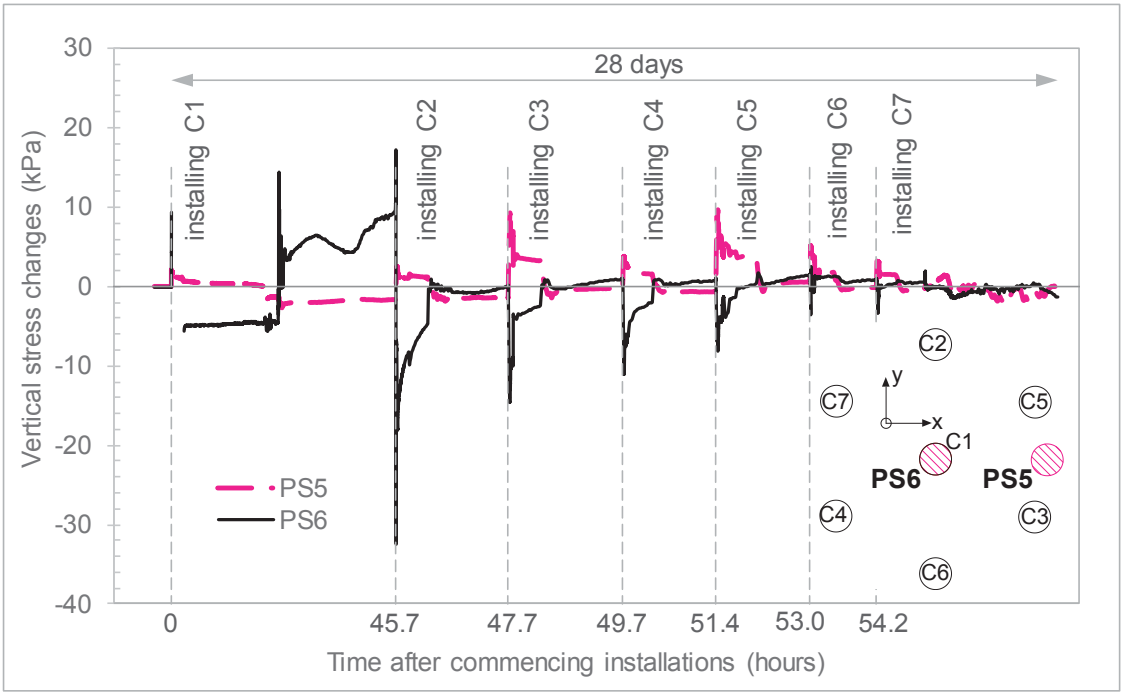

Figure 4.25 Changes in total vertical stress at the base of the soil tank at pressure sensor PS6 (beneath column C1) and PS5 (between columns C5 and C3)

The stresses in the soil were generally affected by the soil heave at depths. Referring to Figure 4.24, at the location of PS4, which was 36 mm below the soil surface, the negative change in the measured horizontal stress indicates that the induced soil stress was less than the in-situ horizontal value. This reduction in stress can be attributed to the soil surface heave occurring at a shallow depth. On the other hand, at the location of PS3, 136 mm deep below the soil surface, the measured change in the horizontal soil stress was positive, indicating that the installation-induced stress was greater than the in-situ value. The positive changes in the soil stress at PS3 was also observed at PS2 and PS1, which were located 236 mm and 336 mm deep below the soil surface, respectively (Figure 4.23). Pressure sensors PS1 to PS3 were much less influenced by the soil heave than PS4.

The installation of the perimeter columns induced stress changes near the tip of column C1, where pressure sensor PS6 was located (see Figure 4.10). Prior to column installations, the measured vertical total pressure recorded at PS6 was approximately 7 kPa. After column C1 installation was completed, the vertical stress at this location increased by 9.5 kPa (Figure 4.25), which approximates the applied vertical stress induced by the self-weight of the newly formed concrete column C1. During penetration process for installations of adjacent columns, especially column C2, the measured total vertical stress at sensor PS6 dropped below the initial stress value and became negative (- 32 kPa). This large stress reduction below the in-situ value can be attributed to the uplift of the tip of column C1, a subject of discussion in Section 4.5.2.1. Since no drainage path was allowed at the bottom of the soil tank, the uplift of column C1 was likely to result in a large amount of suction at the tip of C1 column. However, shortly after penetration at column C2, the negative suction at the tip of C1 increased towards zero, which indicated that column C1 had settled and hence closed the gap created previously below the tip of column C1. Due to the partial closure of the uplift-induced gap, the reduction in the

magnitude of the suction was recorded at PS6 during the installations of the remaining columns. On the other hand, the vertical stresses recorded at PS5 located midway between columns C3 and C5 was greater than the in-situ vertical stresses throughout the test (Figure 4.25).

Referring to Figure 4.23, after all column installations were completed, PS2 and PS1 recorded a steady reduction in the horizontal stress, in response to the stress equilibration and soil consolidation process. On the other hand, referring to Figure 4.24, the horizontal soil stresses measured at the two shallower sensors PS3 and PS4 were found to fluctuate heavily, which may be attributed to the movement of the preceding upheaved soils and the variation in the moisture of the surface soil.

4.5.1.4 Evolution of Excess Pore Water Pressure

Figure 4.26 shows the evolution of the excess pore water pressure in the soil at the locations of P10 and P11 throughout the installations of columns C1 to C7. The excess pore water pressure was estimated by deducting the measured total pore water pressure from the initial (i.e. in-situ) pore water pressure in the soil. The maximum excess pore water pressure at location P10 due to pile jacking for installation of column C1 was 5 kPa, which was three times greater than that observed at the location P11. Predicted excess pore water pressure using the cavity expansion theory by Vesic (1972) matches reasonably well with the measurement at P10, considering the soil rigidity index G/s_u of 15 and the soil undrained shear strength s_u of 8 kPa. After jacking, the maximum excess pore pressure at both measuring locations decreased significantly. During the grouting period after the jacking stage, the excess pore water pressure at both locations become negative, which was likely to be associated with soil unloading. It is noted that during the

grouting period, the progressive withdrawal of the lined casing may have resulted in some soil stress relief in the surrounding soil.

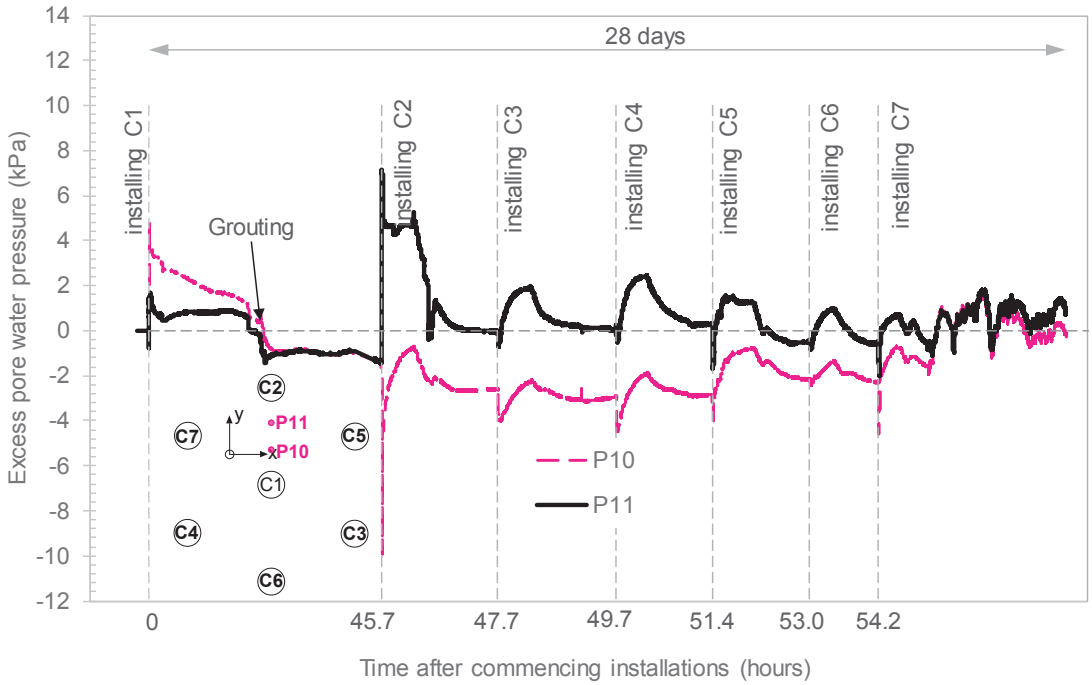

Figure 4.26 Evolution of excess pore water pressure between columns C1 and C2, and 176 mm below the soil surface (P10 and P11)

Figure 4.27 Displacement of transducer P11 and P10 due to the installation of C1

Prior to commencement of jacking for column C2 installation, transducer P11 may have been displaced laterally by a distance of at least 2.6 mm in the positive *y* direction as a result of installing column C1 (Figure 4.26). This lateral soil displacement was estimated based on the recommendation by Kelly, Muttuvel & Chan (2011). In fact, excavation of the soil after the test revealed that transducer P11 moved laterally by up to 14 mm away from its original location towards column C2 due to the installations of the remaining columns (see Figure 4.27).

During jacking at column C2, 24 hours after formation of column C1, the excess pore water pressure at location P11 rose by 8 kPa. Compared to the measured excess pore water pressure at P10 due to the installation of column C1, this measured value at P11 was found reasonable since the transducer had been moved closer to C2 column, and hence endured greater impact. At location P10, it is worthwhile to mention that a negative excess pore water pressure of -10 kPa was recorded. This could be attributed to the movement of column C1 during the installation at C2 position. In fact, as shown later in this chapter, column C1 head initially moved away from C2 location, which induced possible open cracks in the soil and associated suction pressure at P10. However, as soon as the installation was completed at column C2, the pore water pressure at P10 rose again because column C1 head moved backward toward C2.

In addition to the excess pore water pressure measurements made at P10 and P11, the evolution of the excess pore water pressure throughout the installations of columns C1 to C7 was also reported in the soil near the wall of the soil tank (P1 to P4) and at the base (P6 to P9) (Figures 4.28, 4.29 and 4.30). Referring to Figure 4.28, although the measured excess pore water pressure near the wall at locations P3 and P4 (276 mm and 176 mm deep) appeared to increase gradually as the column installations progressed, the trivial

excess pore water pressure as measured was more likely affected by the open cracks in the soil, becoming unsaturated during the installation process. On the contrary, as shown in Figure 4.29, transducers P1 and P2 (376 mm to 276 mm deep) responded well to the column installations, evidenced by the gradual dissipation of the excess pore water pressure after all installations were completed.

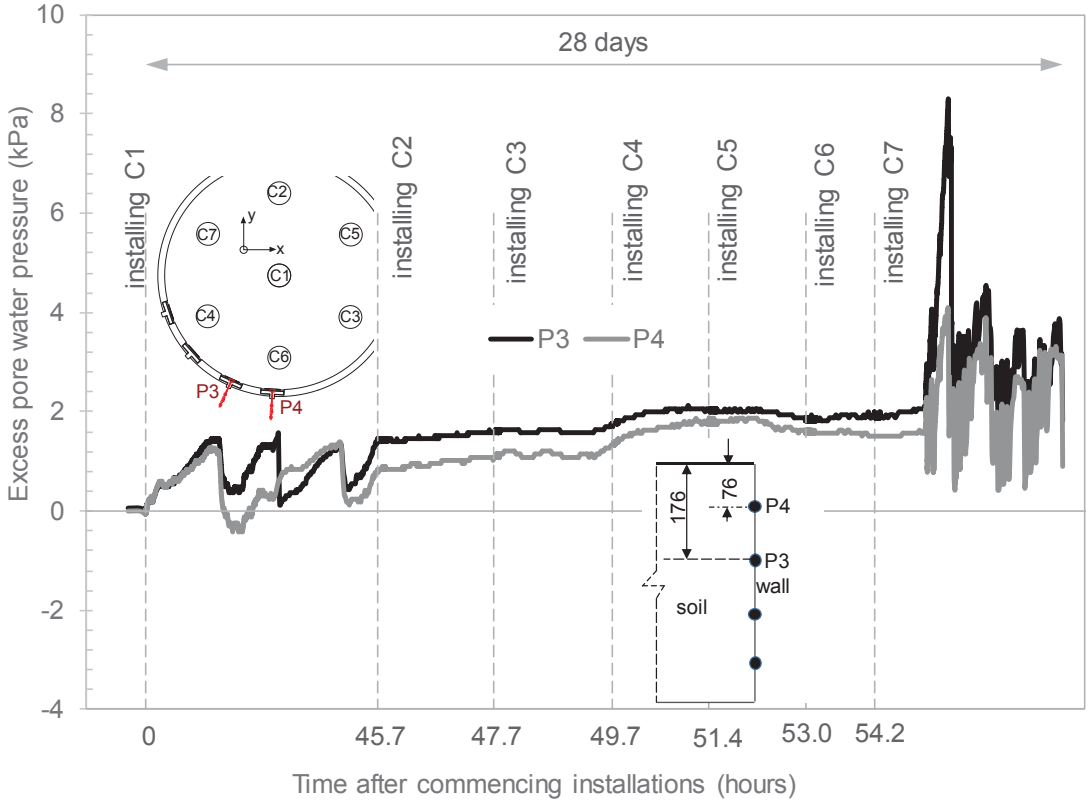

Figure 4.28 Excess pore water pressure at the boundary at locations of P3 & P4

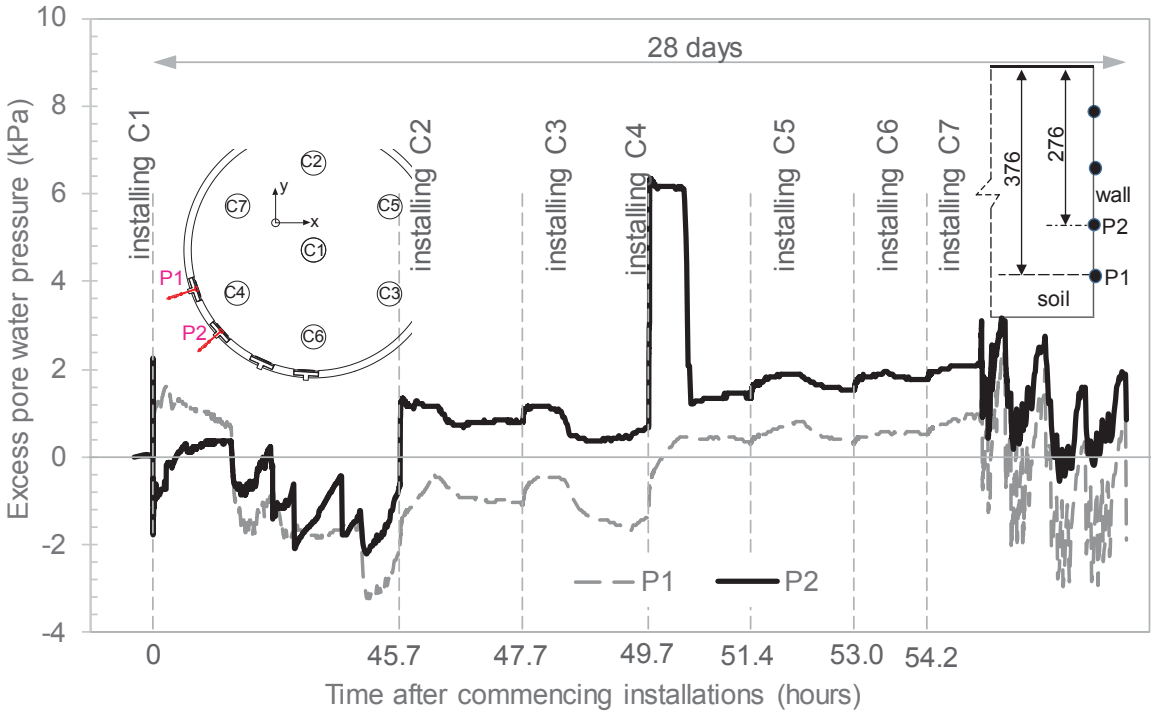

Figure 4.29 Excess pore water pressure at the boundary at locations of P1 & P2

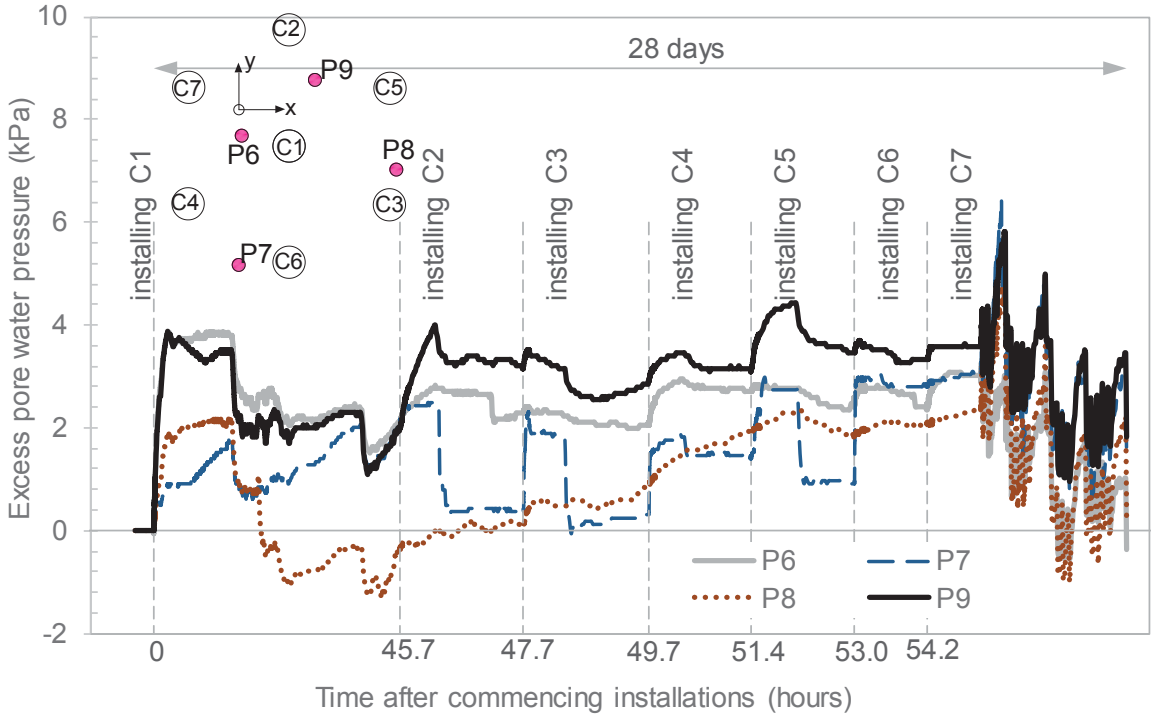

Figure 4.30 Excess pore water pressure at the base of the soil tank at locations of P6 to P9

4.5.2 Response of Column C1 to Nearby Installations

4.5.2.1 Uplift of Column C1

Installation of grouted columns C2 to C7 caused heave of the ground surface, which was accompanied by the uplift of the existing column C1. Figure 4.31 shows that column C1 head uplifted during the jacking of subsequently installed columns. The rise of column C1 induced by each subsequent installation was about 2 to 3 mm and the average uplift was 2.3 mm or 5% of the column diameter. Following the jacking phase of each subsequent column installation, due to soil consolidation and stress equilibrium, column C1 head settled slightly by approximately 0.7 mm on average, which was about 30% the preceding column uplift (Figure 4.31).

As shown in Figure 4.31, the total uplift of column C1 head at the end of all installations was 14 mm, which was about a half of the maximum measured soil heave midway between the columns as illustrated in Figure 4.21. Once all seven installations were completed, column C1 settled slightly due to the soil consolidation. As shown in Figure 4.31, the 28-day post-installation settlement of column C1 was approximately 8% of the total column uplift during column installation or 2% of the column diameter. As shown in Figure 4.31b, the uplift of column C1 head was normalised to become non-dimensional by the column area, Ω, and the column length, L, as suggested by Sagaseta & Whittle (2001). The results shown in Figure 4.31b indicated that the measured uplift of column C1 in this study in the recommended non-dimensional format, $\delta_z \pi L/\Omega$, was consistent with the range of pile uplifts due to adjacent pile driving as reported by Sagaseta & Whittle (2001).

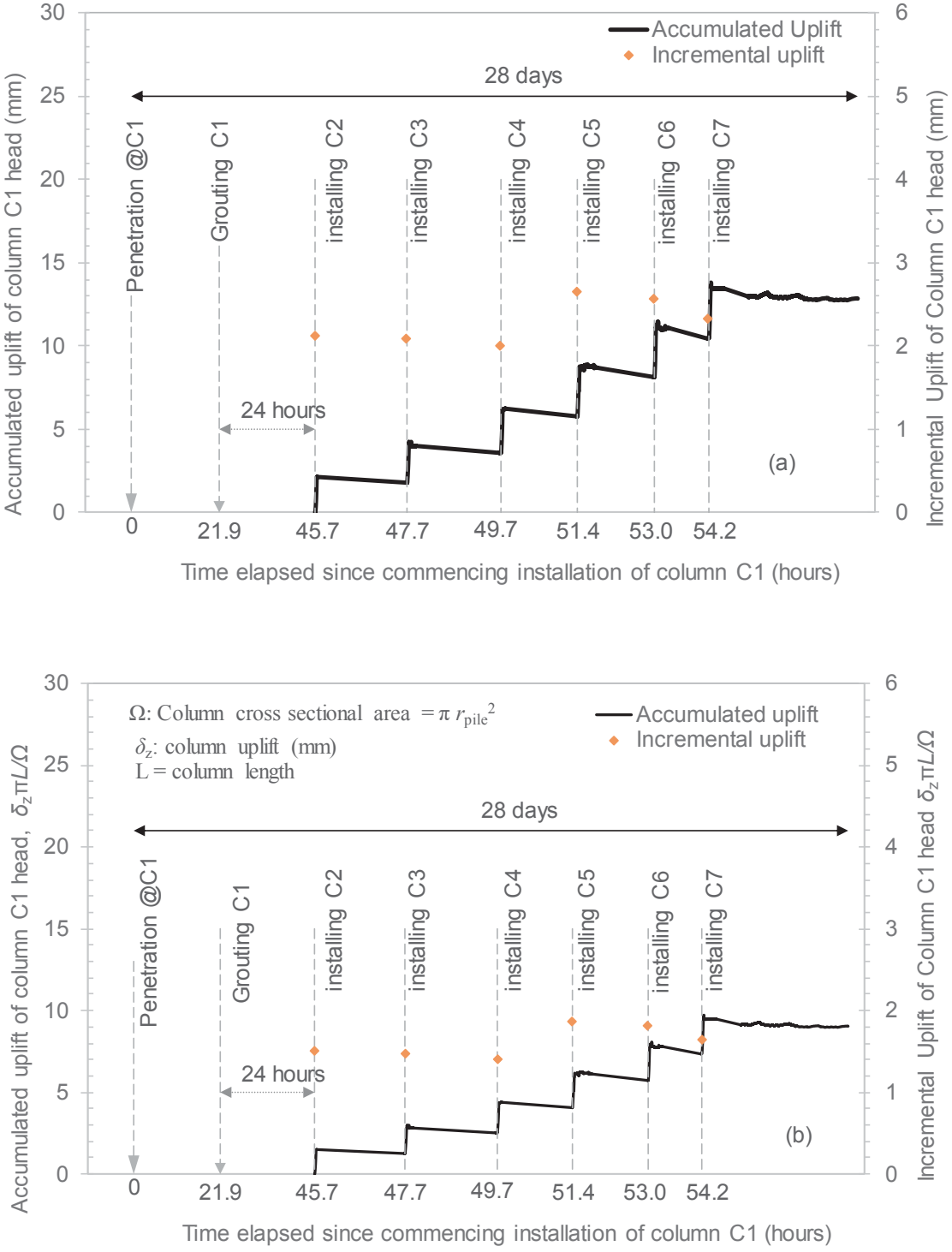

Figure 4.31 Accumulated and incremental uplift of column C1 head due to installation of subsequent columns and (a) column uplift in mm, and (b) normalised column uplift with column length and cross-sectional area

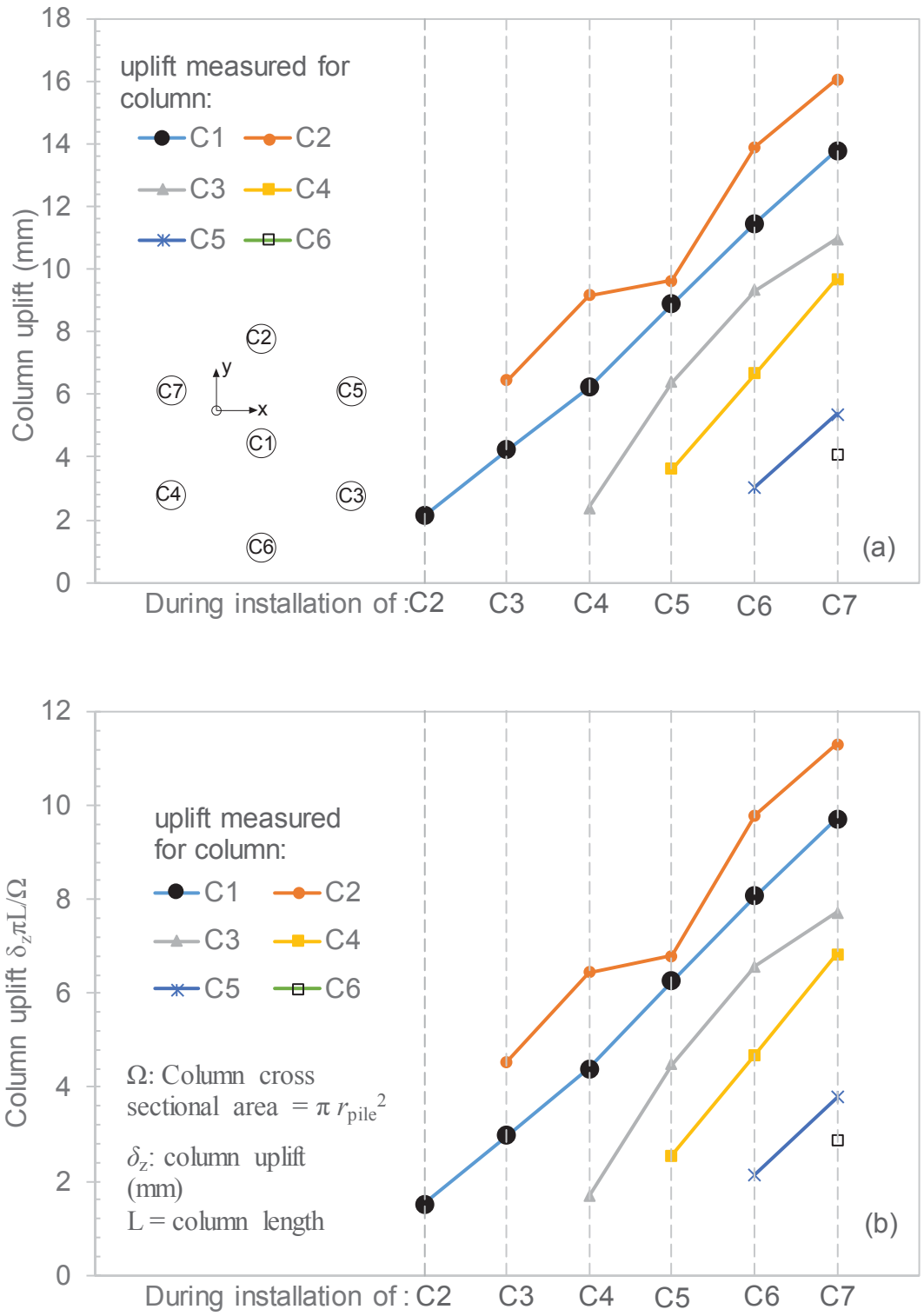

Figure 4.32 (a) accumulated uplift of each individual column as installations progressed, and (b) normalised accumulated uplift with a non-dimensional format ($\delta_z \pi L/\Omega$)

As illustrated in Figure 4.32, the uplift of column C1 increased almost linearly as more perimeter columns were added. It is interesting to note that the uplift of column C1 was less than the uplift of column C2. One possible explanation of this observation is that in comparison to the one-day old column C1, column C2 was still in a plastic state during the installation of the subsequent columns, and hence was more likely to be uplifted (Chow & Teh 1990).

4.5.2.2 Column Head Rotation and Induced Bending Moment of Central Column

First, the rotation of column C1 head during the installation of column C2 was examined based on the results of the non-contact laser displacement sensors T1 and B1. As illustrated in Figure 4.33, during the initial stage of jacking at column C2, the head of column C1 moved away from column C2 (i.e. in the negative y direction). Once the jacking at C2 approached full penetration, column C1 head moved closer to C2 (i.e. in the positive y direction) and the rotation of column C1 was $\theta(z) = 0.36°$ (see Figure 4.33). If the calculated bending moment in column C1 induced by installation of column C2 had a single curvature, it would be sensible to conclude that the tension side of the column was facing C6 and the compression side was facing C2.

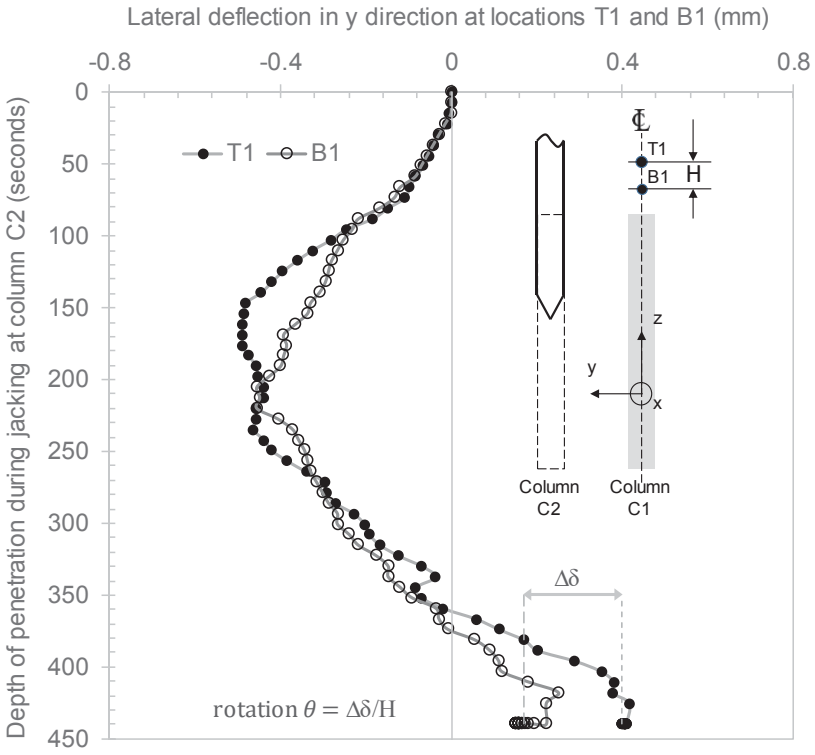

Figure 4.33 Rotation of column C1 head during the installation of column C2

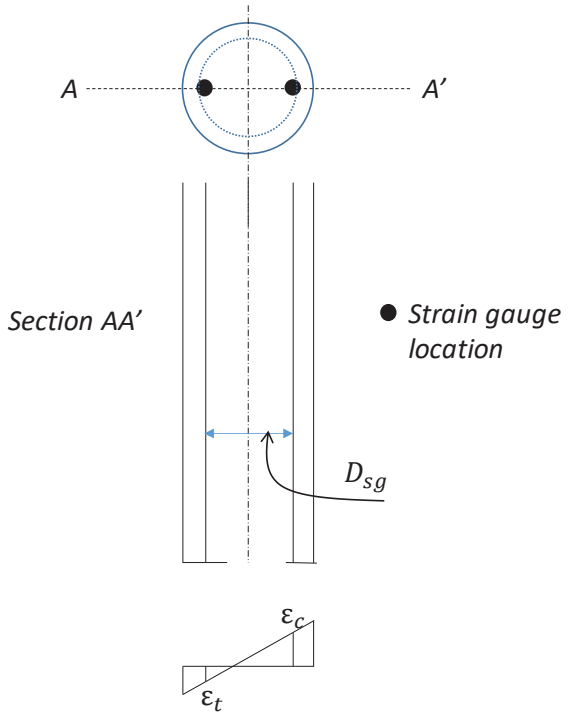

Figure 4.34 Measuring strains ε_t and ε_c along either side of the pile (after Mohamad et al 2011)

The bending moment $M(\mathrm{z})$ of column C1 due to lateral loadings induced by the surrounding installations was estimated using Equation (4.3) (Doherty et al. 2015; Ooi & Ramsey 2003). The tensile strain ε_t and compressive strain ε_c as measured by the strain gauges were used to calculate the curvature $\varphi(z)$ shown in Equation (4.3).

$$M(z) = EI\varphi(z) = EI\frac{\varepsilon_t - \varepsilon_c}{D_{sg}} \tag{4.3}$$

where D_{sg} is the horizontal distance between the two strain gauges positioned at the same depth and spaced at equal but opposite distances from the neutral axis, ε_t is the tensile strain (+) and ε_c is the compressive strain $(-)$ (Figure 2.21). The calculation approach for $M(\mathrm{z})$ using Equation (4.3) cancels out any contribution due to axial strain, and leaves only bending strains (Rollins, Peterson & Weaver 1998). It is noted that + and – signs should be included for the positive and negative strains used in Equation (4.3), respectively (Kovari & Amstad 1982; Rollins, Peterson & Weaver 1998).

During the column installations, strain gauges at two strain-measuring locations (out of 48 locations) malfunctioned. One was located in the *x*-axis and the other was in the *y*-axis. With only one strain gauge in working condition, the curvature $\varphi(z)$ at that location was calculated as the single available elongational strain (either ε_t or ε_c) divided by the distance from the strain gauge to the neutral axis as recommended by Ooi & Ramsey (2003). The calculated bending moments induced in column C1 about the *x* and *y* axes as the surrounding installations progressed are shown in Figures 4.35a and 4.35b. It is noted that the induced bending moment in these figures was calculated after full jacking of piling assembly at each column position was completed. The sign conventions for the calculated bending moment is also shown in Figures 4.35a and 4.35b. In this convention, the bending moment in the column was treated as positive when the tension side of the

column was facing towards column C6 as in Figure 4.35a. Figure 4.35a shows that the maximum bending moment induced in column C1 about the *x*-axis was 16.9 N.m. The corresponding value about the *y*-axis was 9.4 N.m (Figure 4.35b). Using the similarity ratio provided in Table 4.4, for use in a prototype model, the bending moments induced in column C1 about *x* and *y* axes could be roughly projected to 111 kN.m and 61 kN.m, respectively.

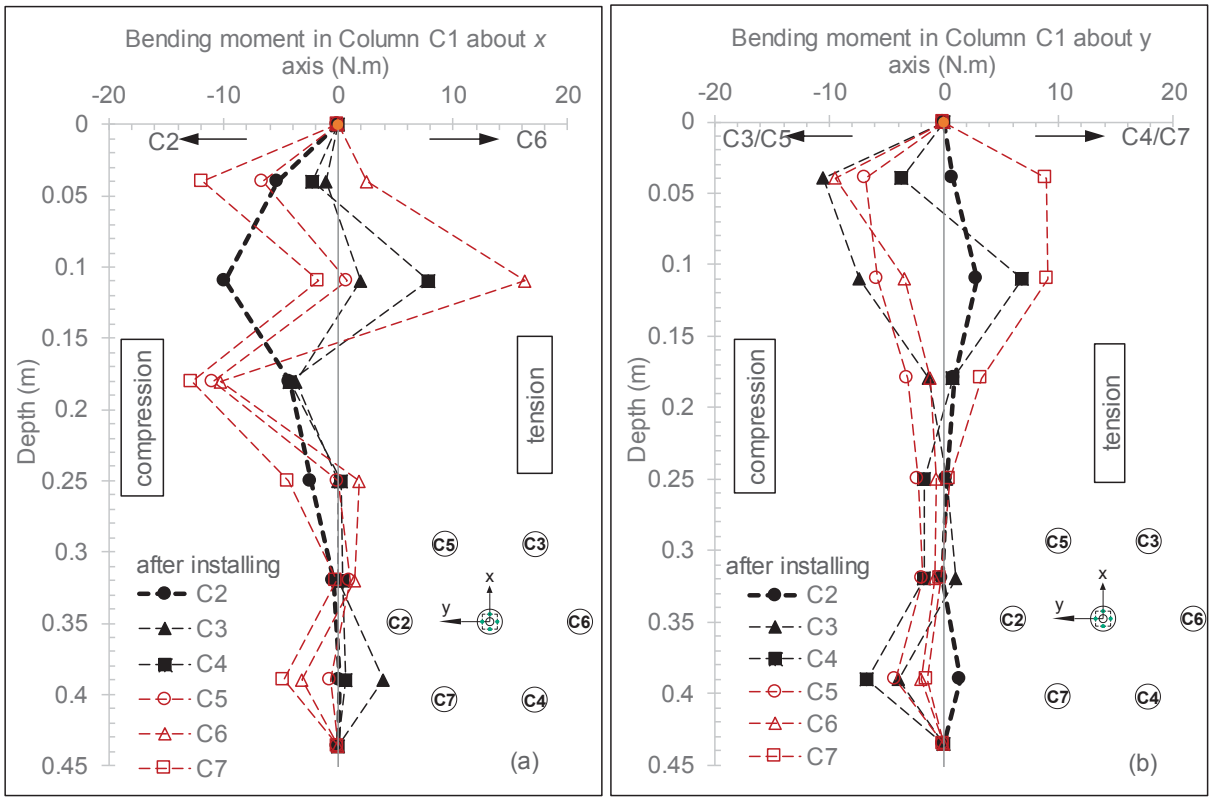

Figure 4.35 Bending moments induced in column C1 due to installing C2-C7: (a) about x axis, and (b) about y axis

The induced bending moment in column C1 can be compared to the theoretical cracking moment of the column, M_{cr} determined using Equation (4.4), which corresponds to the maximum tensile stress that the concrete can accommodate.

$$M_{cr} = f_r I / y_t \tag{4.4}$$

where I is the second moment of area of the concrete column section (Table 4.3), y_t is the distance from the centroid to the edge of the section = ½D, and $f_r = 0.62\sqrt{f_c'}$ is the modulus of rupture as recommended by ACI Committee 318 (2014). The measured unconfined compressive strength at one-day f_c' of 3.7 MPa corresponds to a calculated modulus of rupture f_r of 1.2 MPa, which is reasonably consistent with the measured splitting tensile strength of 0.9 MPa obtained from the laboratory test results shown in Table 4.4. The cracking moment of the column M_{cr} calculated from Equation (4.4) is 10.5 kN.m. The calculated cracking bending moment is much less than the bending moments induced in column C1 as shown in Figures 4.35a and 4.35b. This result implies possible yielding in the central concrete column during the field installation of the surrounding columns.

4.6 Summary

This chapter describes a model test to study the effects of installing concrete columns by a soil-displacement method for ground improvement on the behaviour of the soft soil and existing columns. The behaviour of the central column subject to the surrounding columns was meticulously investigated. Based on the results of the laboratory model test, the following conclusions can be drawn:

- The uplift of the existing concrete column after 1-day curing induced by the surrounding installations halved the amount of soil heave induced midway between the columns. However, the amount of uplifting of the existing concrete column at its very early concrete age (i.e. plastic state/ initial setting time) induced by the surrounding installations was similar to the surrounding soil surface heave.

- The magnitude of the measured uplift experienced by the central column induced by each subsequent column installation was similar.
- The uplift of a column base was associated with a large amount of suction at the base of the column. However, as the installation progressed, the suction reduced.
- Excess pore water pressure increased as more columns were installed, but reduced during the time lag between two columns.
- Lateral loadings generated by the installation of the surrounding columns could affect the integrity of the existing column, especially at their early age.
- Complex interactions were observed between the soil and the columns, which are otherwise often difficult to observe in the field.

The results of the model test can be used as suitable data for future computer modelling. Although the model test was performed at $1g$ and at corresponding low stress level, it is believed that the observation of mechanisms of the response of the rigid inclusions and soils, which was the prime emphasis of this study, will still be relevant.

CHAPTER 5 Effects of Pile Penetration in Comparison with Combined Cylindrical and Spherical Cavity Expansions: Experimental and Numerical Studies

5.1 Synopsis

Installations of piles by jacking, driving or drilled displacement piling techniques are effective geotechnical solutions to improve the load-bearing capacity of piles in the weak ground. However, numerical simulation of the soil behaviour affected by the pile installation remains challenging and is of special interest among the geotechnical community. This chapter presents a laboratory model test to study the responses of the soft soil subject to the installation of a jacked-in closed-ended displacement pile and the soil consolidation after pile installation. A theoretical study for the test was also conducted. The model test shows that the arrival of the peak pore water pressures experienced a noticeable hysteresis. The large strain numerical analyses were carried out using the finite difference code *FLAC*^{3D} to simulate the model test, taking into account the boundary effects and tip end effects of the model pile. The pile penetration was simplified as the combined use of the cylindrical and spherical cavity expansions. The lightly overconsolidated soft soil was modelled by the modified Cam-clay model and the evolution of the soil permeability during consolidation was taken into account. The results of the coupled consolidation analyses were compared with the results of the model test in terms of the soil surface movement and the evolution of the excess pore water pressure.

A reasonably good overall agreement was observed between the numerical and experimental results, demonstrating the suitability of using the cavity expansion theory for solving such problems. However, the pitfalls using this solution scheme are also pointed out.

5.2 Introduction

The construction of deep foundations using displacement piling techniques such as driven piles, jacked piles, auger displacement piles and jet grouted columns have been investigated intensively in the past (Almeida, Danziger & Lunne 1996; Cooke, Price & Tarr 1979; He, Wang & Hong 2016; Lehane & Jardine 1993; Randolph, Carter & Wroth 1979; Steenfelt, Randolph & Wroth 1981; Suleiman et al. 2016). However, installation effects of such deep penetrations are still some of the most complicated and challenging topics in the field of geotechnical engineering (Baligh 1985; Engin, Brinkgreve & van Tol 2015; Zhou, Liu & Yuan 2018). The pile installation induces soil movement, generates excess pore water pressures and increases stress in the surrounding soils. At shallow depths, the soils are displaced downwards and sideways, and likely to heave upwards. At lower depths, less soil heave is generated while the lateral soil movement is dominant, especially for full displacement piles.

Since the 1950s, cavity expansion method (CEM) has been developed to model the pressuremeter tests and deep foundations (Chadwick 1959; Hill 1950; Ladanyi 1964; Palmer 1972; Vesic 1972). The response of soils due to the installation process is analogous to the creation or expansion of cylindrical and spherical cavities. On that basis, CEM has been used to assess the installation effects of driven piles (Randolph, Carter & Wroth 1979; Vesic 1972), jacked piles (Bond & Jardine 1991; White & Bolton 2004), stone columns (Castro & Karstunen 2010), jet grouting (Shen, Wang & Cheng 2017), the

cone penetration (Chai et al. 2015; Pournaghiazar, Khalili & Russell 2012), and deep soil mixing columns (Chai, Miura & Koga 2005; Shen, Miura & Koga 2003). Undrained cavity expansion for saturated clays has been studied (Cao, Teh & Chang 2001; Chen & Abousleiman 2012) together with the long-term consolidation analyses assuming radial consolidation (Randolph & Wroth 1979). Analytical or semi-analytical cavity expansion solutions have been developed for various soil constitutive models e.g. Tresca model (Hill 1950), Mohr-Coulomb (Carter, Booker & Yeung 1986; Vesic 1972; Yu & Houlsby 1991), modified Cam Clay (Cao, Teh & Chang 2001; Chen & Abousleiman 2012; Collins & Yu 1996). The anisotropic stress state in the soil recently is included in some of the cavity expansion solutions (Chen & Liu 2018; Han et al. 2011; Jaeger, DeJong & Boulanger 2011; Li, Li & Sun 2016; Zhou et al. 2014). The shortcoming of the cylindrical cavity expansion applied in the deep penetration is that the plane strain condition is assumed at the mid-depth of a long vertical cylindrical pile and hence the effect of soil heave is ignored (Baligh 1985; Chai et al. 2009). On the other hand, the spherical cavity expansion simplifies the geometries of various penetrating objects as half spheres in an approximate way.

Modelling the penetration of piles into the ground is an extremely complex problem due to heavily distorted mesh. A number of interesting proposals were reported for solving such problem (Dijkstra, Broere & Heeres 2011; Engin, Brinkgreve & van Tol 2015). Notable advancements in the simulation of pile installation include Arbitrary Lagrangian–Eulerian (ALE) method (Liyanapathirana 2009; Nazem et al. 2008; Tolooiyan & Gavin 2011), Coupled Eulerian–Lagrangian (CEL) method (Hamann, Qiu & Grabe 2015; Ko, Jeong & Lee 2016; Sabetamal et al. 2014), and the Material Point Method (MPM) (Ceccato, Beuth & Simonini 2016; Phuong et al. 2016; Tehrani et al. 2016). While the finite element re-meshing schemes have significantly advanced the field of geotechnical

engineering, the code implementation is sophisticated in any daily engineering practice. In addition, the effective stress analyses and the consolidation analyses are not yet established for these methods.

For ground improvement purposes, cavity expansion theory remains the popular method due to its simplicity and its long development history. Due to the initial singularity problem, cavity creation from a zero radius is not possible in the continuum mechanics. A simplified simulation of pile penetration by expanding a cavity from a finite radius using complex material models has been implemented successfully for various practice cases (Carter, Randolph & Wroth 1979; Chen et al. 2009; Guetif, Bouassida & Debats 2007). However, in developing these solutions, the development of a truly rational approach to pile installation simulation has been hampered by a lack of reliable data regarding the physical processes that govern soft soil behaviour. Specifically, there has been only a limited amount of the laboratory test data available for verification especially when jacked piles intersect soft soil layers. According to Chow & Teh (1990) and others, when the surrounding soil is very soft to soft, the interaction behaviour between soils and jacked piles is often very complex.

This chapter presents the results of a laboratory model test to simulate the jacked pile penetration and the subsequent soil consolidation. In addition, a theoretical model for the model test was provided by a large strain numerical approach to study the soil responses due to jacked pile installation, based on the idea of combined use of the cylindrical and spherical cavity expansions. In the laboratory model test, the closed-ended cylindrical pile was jacked into the lightly overconsolidated soft soil. The soft soil was subjected to a surcharge pressure during the pile penetration. After penetration, the consolidation settlement of the soils and the dissipation of excess pore water pressures were monitored.

Although this model test was performed at a single gravity, the investigation of the undrained and drained mechanism of a soft soil around a displacement pile has been the prime purpose of the present investigation.

The results of the 3D numerical model, on the other hand, provide insights into the laboratory model test. The jacking of a model pile was simulated by expanding cavities in the medium of a lightly overconsolidated soft clay based on the combined use of the cylindrical and spherical cavity expansion methods (Cao, Teh & Chang 2001; Carter, Randolph & Wroth 1979; Ladanyi 1964; Yu 2000). The simulation was implemented in a 3D finite difference code *FLAC*^{3D} v5.01. The soft soil was numerically modelled by the modified Cam-clay material model. The variation of soil permeability with the void ratio during soil consolidation was taken into account. Undrained cavity expansion analysis was first conducted to simulate the installation process of the pile, which was then followed by a coupled hydraulic-mechanical analysis (i.e. soil consolidation) to allow excess pore water pressure to dissipate. The code incorporated large strain mode via the updated Lagrangian formulation. The numerical approach was compared with the results of the laboratory model test in terms of the soil surface movement and the dissipation of excess pore water pressures in the soil surrounding the penetrating pile. This type of pile installation simulation utilises the widely accepted cavity expansion methods; this would provide a practical compromised approximation for many design situations as well as overcoming the need for more sophisticated analyses such as ALE or CEL schemes in many practical cases.

5.3 Laboratory Model Test

5.3.1 Soil Tank

The laboratory model test was performed in a soil tank, which was originally designed as a large Rowe consolidation cell. This soil tank has an internal diameter of 250 mm, and a wall height of 204 mm (Figure 5.1). For the purpose of this experiment, only the wall and the base of the cell were used. They were fastened together with steel bolts, and sealed by a rubber O-ring for water-tightness at the joint. As shown in Figure 5.1, pore water pressure measurement can be recorded at three locations along the interior wall surface (denoted as PWPB2, PWP-B3 and PWP-B4) and at other three locations at the base level of the soil tank (denoted as PWP-A2, PWP-A4 and PWP-A5). At each measuring location, a porous disc was embedded flush with the interior surface of soil tank, and the pore water pressure can be measured by an externally fitted pore-water pressure transducer. Each transducer was calibrated using a volume pressure controller prior to testing. All readings from the transducers were recorded on a GDS computer controlled data logger.

5.3.2 Soil Bed Preparation

The soft soil bed was prepared in the soil tank by a slurry-based soil deposit. The dry portion of the slurry consisted of 70% of dry Q38 kaolinite, 15% of Active Bond 23 bentonite, 15% of fine to medium sand, by the total dry mass. The dry materials were mixed with de-aired water to have a moisture content of 127%. Details of this soil mixture were obtained from Le, Fatahi & Khabbaz (2015).

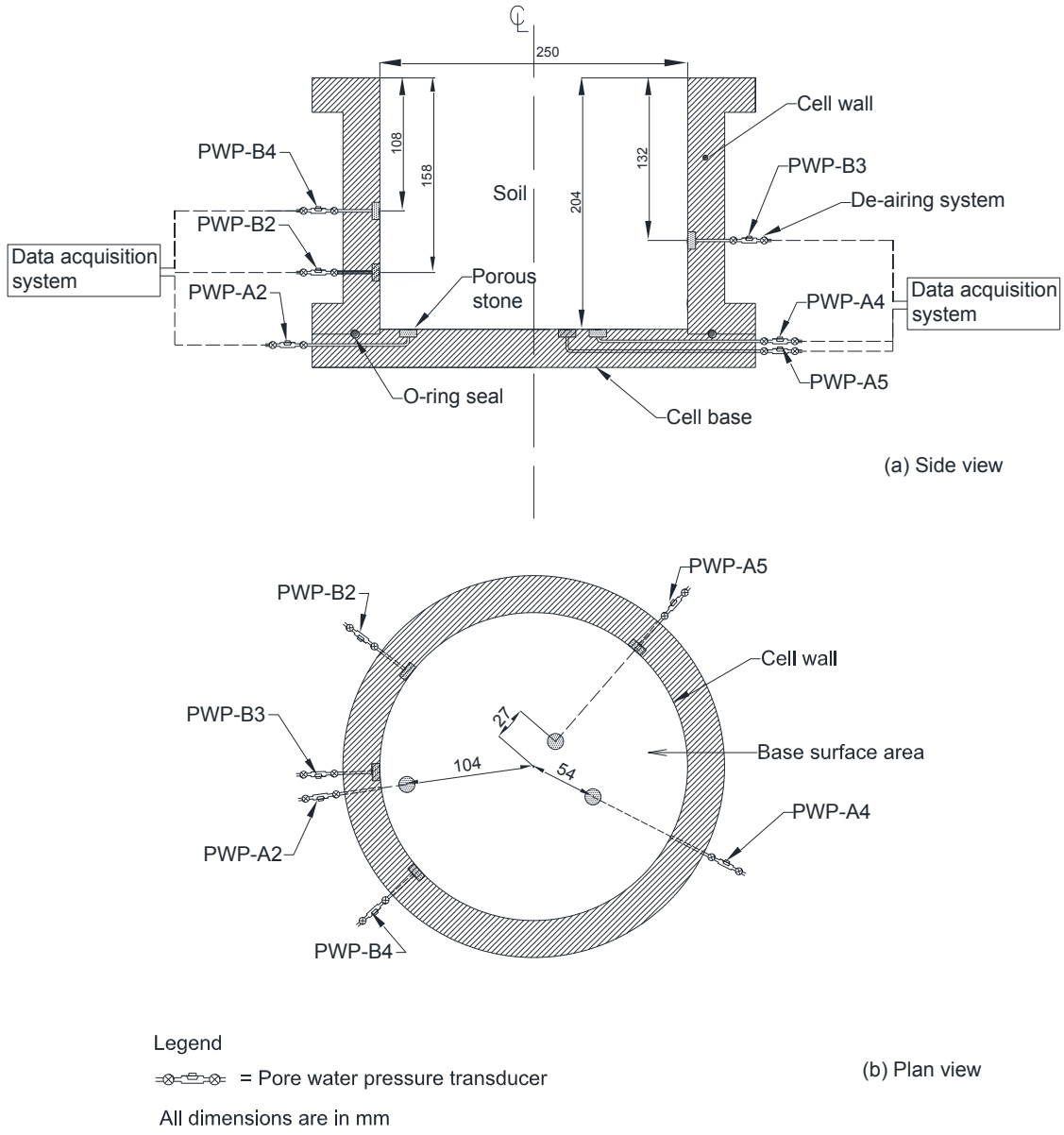

Figure 5.1 Diagrams of the soil tank and the arrangement of pore water pressure transducers: (a) side view, and (b) plan view

(a)

(b)

(c)

Figure 5.2 Soil bed preparation: (a) Slurry prepared in the soil tank (b) placement of the first surcharge weight plate and (c) full surcharge pressure applied

After the interior wall surface had been smeared with silicone grease, the slurry was then filled slowly into the soil tank in layers until a slurry thickness of 200 mm was achieved (Figure 5.2a). According to the literature (Cao, Teh & Chang 2001; Chen & Abousleiman 2012), the over-consolidation ratio (OCR) of the soil is an important parameter in assessing the changes in soil stresses and pore water pressure around an expanded cavity. In this model test, the soil was pre-consolidated one-dimensionally under a vertical surcharge pressure of 15.8 kPa. This pressure was achieved by stacking a number of steel plates, fully covering the surface of the slurry. The surcharge was added in small increments to avoid soil shear failure (Figure 5.2c). One-way upward drainage towards

the soil surface was allowed via a layer of separation geotextile between the surcharge and the soil surface. In addition, the bottommost steel plate of the surcharge was perforated to allow dissipation of the generated excess pore water pressure, as shown in Figure 5.2b. A thin water layer above the upper surface of the sample was maintained throughout the test to keep the soil saturated. The excess pore water pressure dissipated completely after approximately two months. The final thickness of the soil specimen after the preconsolidation was approximately 150 mm.

5.3.3 Soil Properties

Table 5.1 provides a summary of the soil properties. In particular, the Atterberg limits were obtained from a previous investigation by Le, Fatahi & Khabbaz (2015). The bulk unit weight of the soil was measured using soil specimens recovered at the completion of the main test. The Rowe cell consolidation tests on soil samples 75 mm in diameter were carried out to determine the compression index C_c, the recompression index C_r, the coefficient of consolidation c_v and the coefficient of permeability k of the soil. The variation of void ratio e with the vertical effective stress $\sigma'_{o,v}$ obtained from the Rowe cell consolidation test is shown in Figure 4.6 as part of Chapter 4. In addition to the Rowe cell consolidation test, a large soil specimen 250 mm in diameter and 200 mm in height was consolidated under a vertical effective stress of σ'_v = 15.8 kPa until primary consolidation was completed (Figure 4.7). The c_v value of the soil computed using the settlement time data obtained from this exercise was also included in Table 5.1. It is noted that the c_v value is usually about 2 to 3 fold higher for soil specimens in an overconsolidated state (Lo et al. 2008). The soil is classified as high plasticity clay (Standards Australia 2017).

The variation of the permeability k with the void ratio e was derived from the results of the Rowe cell consolidation test (Figure 4.8). The evolution of the permeability with

consolidation process is represented by the permeability change index C_k which was derived from Equation (4.1) (Taylor 1948) in Chapter 4.

The slope $M = q/p'$ of the critical-state line (CSL) presented in Table 5.1 was calculated using the plot of the deviatoric stress q against the mean effective stress p' on the p':q stress plane, which was obtained from the undrained triaxial compression tests with pore pressure measurement (Figure 4.9). The coefficient of lateral earth pressure at rest K_o for lightly overconsolidated clay was estimated from Equation (5.1) (Alpan 1967).

$$K_o = (1 - \sin\phi') \times \mathrm{OCR}^N \tag{5.1}$$

where $N = 0.5$ as suggested by Mayne & Kulhawy (1982) for clay soils, ϕ' is the effective friction angle correlated with the M value (see Table 5.1) and an OCR = 1.9. The miniature shear vane tests conducted for the soil indicated an undrained shear strength s_u value of 3.5 kPa.

Table 5.1 Physical and index properties of soft soil used in the model test

Soil properties	**Interpreted Value**	**Back Calculated Value in *FLAC*^{3D}**
Plastic limit*, w_{P} (%)	22	
Liquid limit*, w_{L} (%)	80	
Plasticity index, I_p	58	
Specific gravity, G_{s}	2.65	
Saturated unit weight, γ_{sat} (kN/m^3)	14.7	
Permeability change index, C_{k}	1.5	
Effective Poisson's ratio, ν'	0.3	
Effective friction angle, ϕ' (°)	21	
Slope of CSL, M	0.812	0.85
Initial in-situ void ratio, e_{o}	2.32 when $\sigma'_{\mathrm{v,o}}$ is 1 kPa	2.2
Compression index, C_{c}	1.3 to 0.98 when σ'_v = 50 kPa to 400 kPa	
Slope of NCL, λ	0.348 assumed $\lambda \simeq 0.6I_p$; 0.39 assumed $C_{\mathrm{c}} = \lambda \ln 10$	0.5
Recompression index, C_{r}	0.22	
Slope of URL, κ	0.096 assumed $C_r = \kappa \ln 10$	0.11
Vertical coefficient of consolidation at various stress levels, c_{v} (m^2/year)	0.12 when σ'_v = 16 kPa; from 0.1 to 0.07 when σ'_v is between 50 kPa and 100 kPa	
Reference pressure, p'_{ref} (kPa)	46	
Specific volume at reference pressure, v_{ref}	2.88	
Coefficient of permeability at various stress levels, k (m/s)	9×10^{-11} when normal consolidated at σ'_v = 50 kPa; 0.7×10^{-9} when normal consolidated at σ'_v = 15.8 kPa.	0.7×10^{-9} to 0.7×10^{-9} and c_k = 1.5
Coefficient of earth pressure at rest, K_{o}	0.88	
Preconsolidation pressure, p'_{c} (kPa)	15.8	

Note: * obtained from Le, Fatahi & Khabbaz (2015); URL = unloading and reloading line; NCL = normal consolidation line; CSL = critical state line.

5.3.4 Jacked Pile Penetration

At the end of the initial surcharging period, the surcharge and the separation geotextile were removed from the soil. The clay sample was then subjected to a new surcharge pressure of 8.4 kPa, which halved the initial surcharge during soil bed preparation. Therefore, the soil became lightly overconsolidated and the OCR of the soil at this state was approximately 1.9. This surcharge was applied throughout the model test. It is noted that free drainage condition was maintained at the interface of the soil and the upper surcharge via a separation geotextile layer and a perforated steel plate. Each surcharge dead weight and the separation geotextile layer had a circular vertical opening of approximately 63.5mm in diameter, which formed a passage of the model pile through the surcharge into the soft soil (Figures 5.3a and 5.3b).

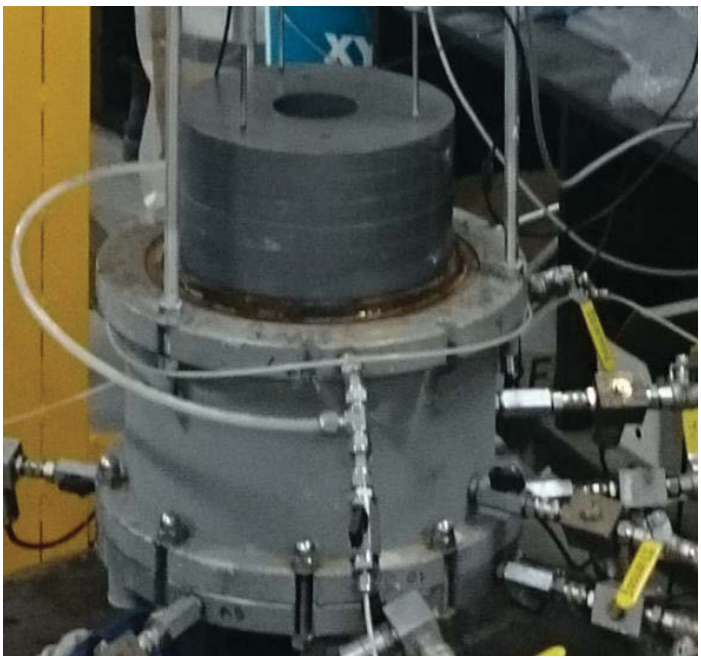

Figure 5.3 Soil specimen with surcharge placement prior to the jacked in pile installation

Figure 5.4 shows a schematic diagram of the experimental set-up for the jacked pile penetration. The miniature closed-ended model pile had a diameter (d_{pile}) of 63.5 mm

and was fabricated from an aluminium alloy. The conical tip of the mode pile had a 95° apex angle. The lower end of the model pile was initially positioned above the soil surface, along the centre line of the soil tank. The upper end of the model pile was connected to a linear displacement motorised actuator, which was mounted on a steel reaction frame (Figure 5.4). This actuator has a push-and-pull capacity of 5 kN. The speed of the actuator was controlled by a Bosch speed control unit. During pile penetration, the soil penetration resistance and the movement of the pile were recorded using a 5 kN tension-compression load cell placed atop the model pile, and a linear variable differential transformer (LVDT). During the pile penetration and thereafter, the other three LVDTs were set-up above the steel weights to measure the vertical movement of the soil, as shown in Figure 5.5. The laboratory set-up and the data acquisition system are shown in Figure 5.6.

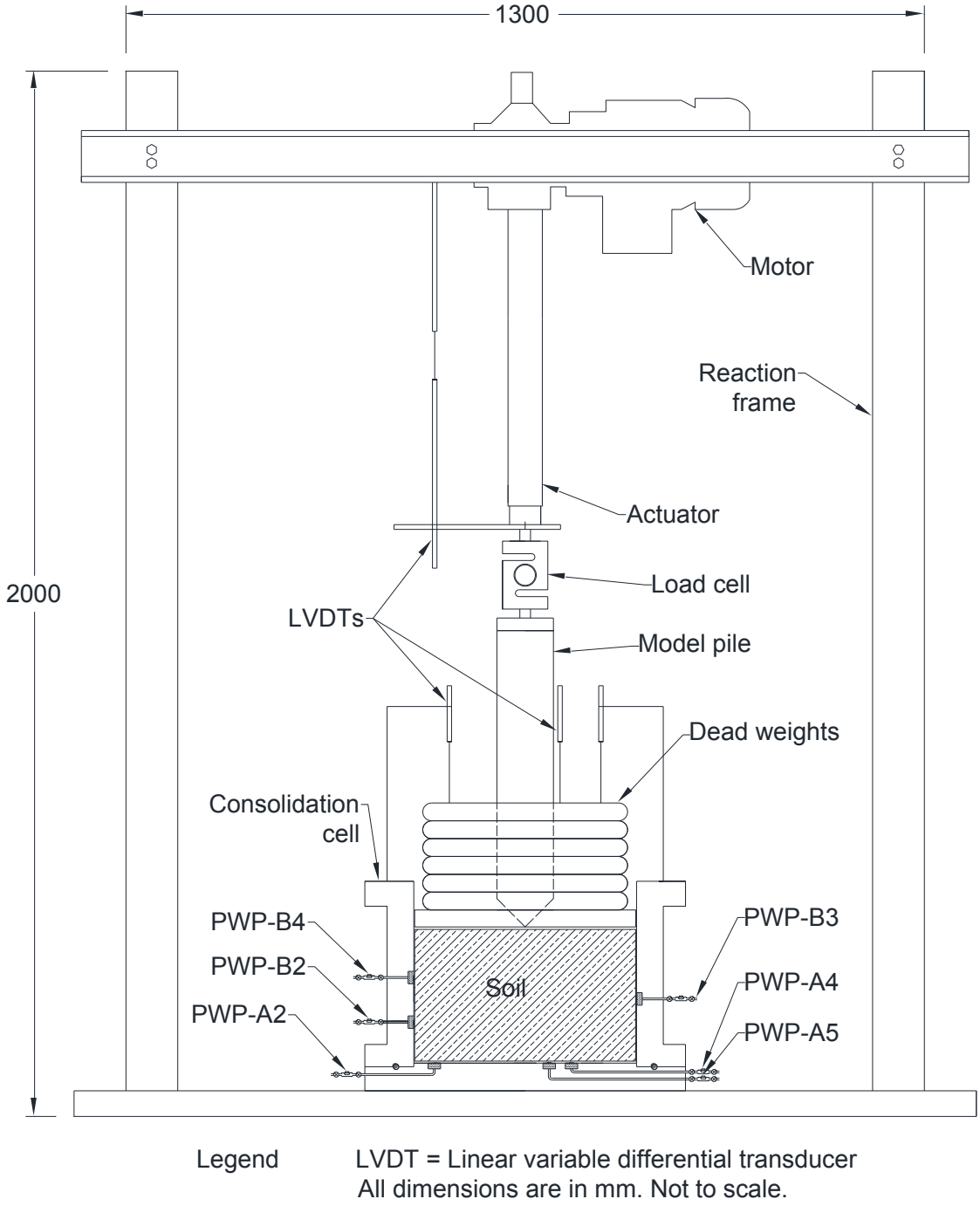

Figure 5.4 Schematic diagram of the experimental set-up for jacked pile penetration

The model pile was jacked into the soft soil in a monotonic mode at a downward penetration rate v_p of 3.8 mm/s. The adopted penetration speed was sufficiently fast to ensure that the soil surrounding the pile would behave in undrained condition during penetration. To relate the penetration speed to the drainage conditions in the soil surrounding the penetrating pile, Finnie & Randolph (1994) normalised the penetration speed with the pile radius r_{pile} and the coefficient of consolidation of the soil c_v, using Equation (5.2).

$$V_{norm} = 2 \times v_p \times r_{pile}/c_v \tag{5.2}$$

The normalised penetration velocity V_{norm} calculated from Equation (5.2) for this model test was much greater than 30, a minimum normalised velocity to ensure undrained behaviour of the soft soil surrounding the pile (Kim et al. 2008; Randolph & Hope 2004).

At the end of pile jacking, the model pile was held in place and the soil underwent consolidation under a constant surface stress. Once the generated excess pore water pressure dissipated, the set-up was dismantled. Vane shear tests, moisture content determination and unconfined compression tests were carried out on specimens extracted from the soil bed. The next section presents the results of the numerical analyses to simulate the laboratory model test.

Figure 5.5 Experimental arrangement above the soil tank

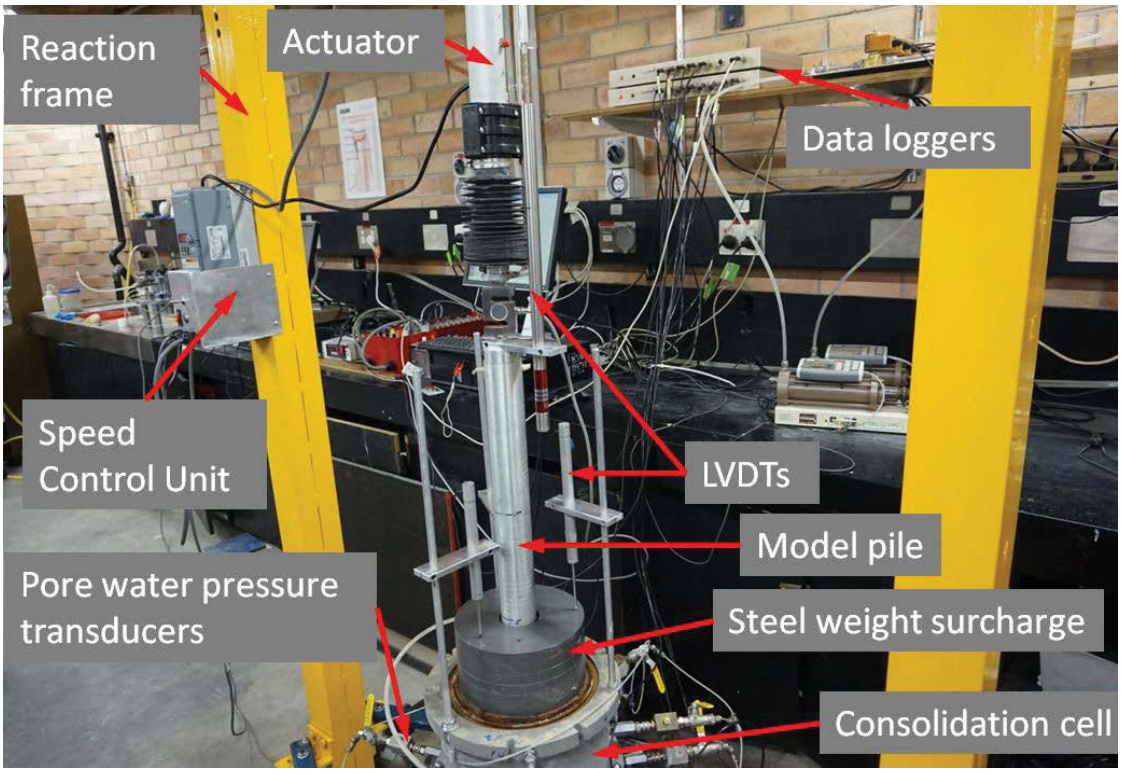

Figure 5.6 Data acquisition system in the laboratory

5.4 Finite Difference Analysis

5.4.1 Geometry and Boundary Conditions

Numerical analyses of the laboratory model test were performed using *FLAC*^{3D} v5.01 in large strain mode to provide a theoretical approach to the problem. The undrained analyses were conducted for the pile penetration stage, followed by the coupled hydraulic and mechanical analysis performed to simulate the subsequent soil consolidation after the completion of the pile penetration. Although the problem was essentially axisymmetric, the quarter-symmetry 3D model was utilised because the expected computation cost relative to the modern computers is minimal. A 3D grid shown in Figure 5.7 represented

the soft soil and the surcharge in the laboratory model test. The soil and column regions were created from solid elements such as brick, wedge and pyramid zone types. The mesh was generated using *FISH* programming language to facilitate the simulation of the quasi-static penetration of the jacked pile. For example, a hemispherical mesh was formed to simulate spherical cavity expansion at the tip of the column. The 3D grid as shown in Figure 5.7 consisted of 3528 zones and 4574 grid points. The runtime was approximately 48 hours for a *FLAC*^{3D} analysis on a 3.40 GHz core i7 CPU computer.

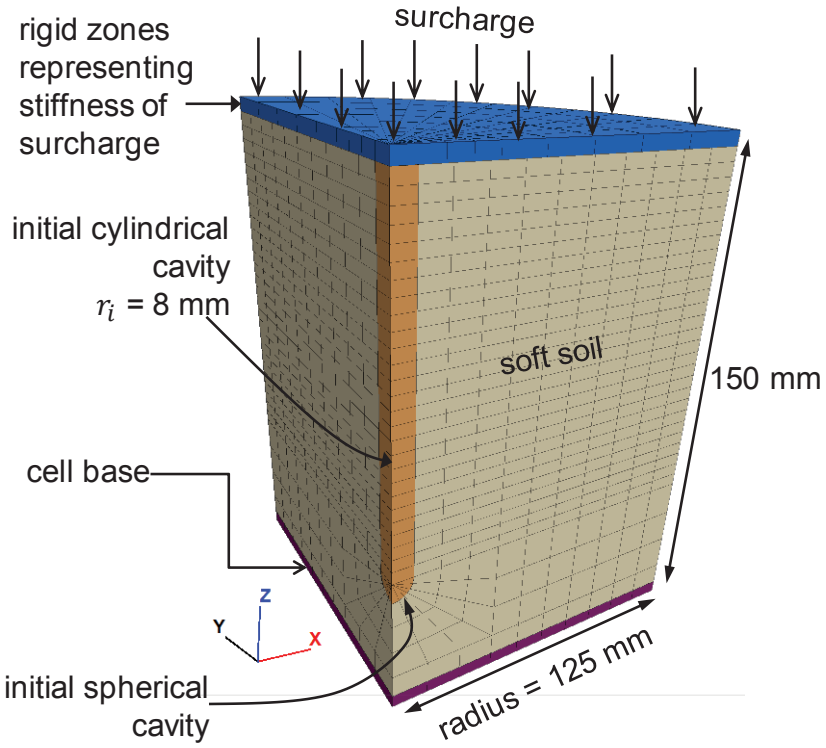

Figure 5.7 The FLAC^{3D} *finite difference mesh*

The boundary conditions for the model are illustrated in Figure 5.8. A free draining boundary was modelled at the interface of the soil and the surcharge while the side and bottom boundaries were considered impermeable. The dead weight overlying soft soil was numerically modelled by applying a uniform vertical pressure of 8.4 kPa on a thin

layer of rigid *FLAC*^{3D} zones. These zones were fixed against horizontal movements and their bottom face interacted with the underlying soft soil by an interface element. While the interface stiffness has to be stiff to prevent soft soils from penetrating into the zones of *FLAC*^{3D}, a high interface stiffness would increase the computation time significantly. The interface normal stiffness and shear stiffness, k_{n} and k_{s}, were estimated using Equation (3.8) as recommended by Itasca (2012).

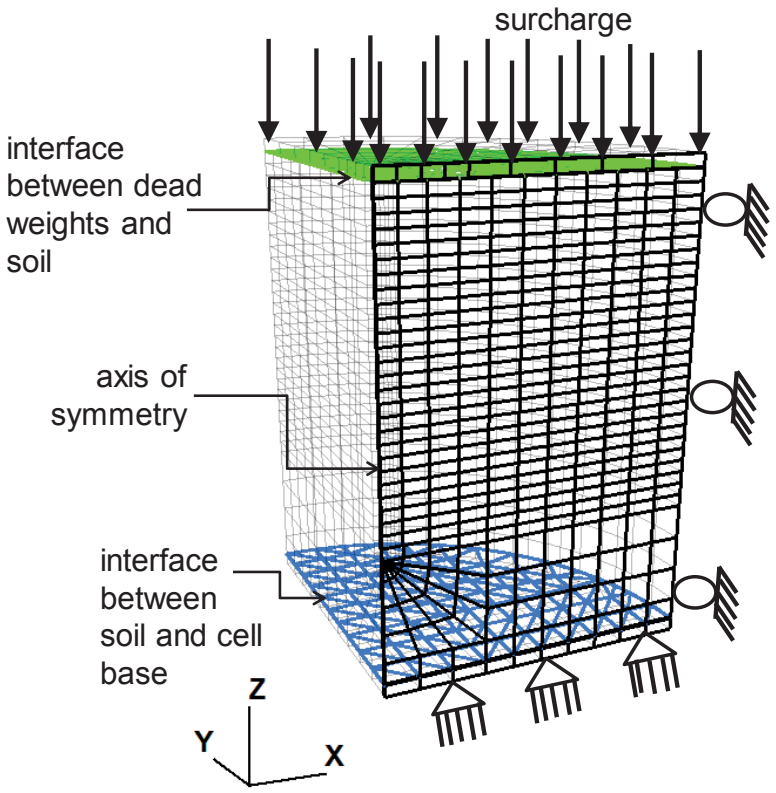

Figure 5.8 Boundary conditions and modelling of surcharge

The rigid base of the soil tank was also modelled as a thin layer of rigid *FLAC*^{3D} zones, which were fixed against displacement in all directions and their top face interacted with the upper soft soil via an interface element. The wall of the soil tank was not explicitly modelled and roller boundaries were used instead, considering that the soil-wall friction in the model test was insignificant.

5.4.2 Material Model for Soft Soil

The modified Cam-Clay (MCC) material model was adopted to represent the elastic-plastic behaviour of the soft clay (Muir Wood 1990; Roscoe & Burland 1968). The *FLAC*^{3D} zones representing the surcharge and the base were characterised by the linear elastic material model. The modified Cam-clay model parameters adopted for soft clay is shown in Table 5.1, which were derived from laboratory test results presented in Section 0. The slopes of the normal compression line (NCL), λ and the unloading and reloading line (URL), κ in the semi-logarithmic compression plane v - lnp' were derived from C_c and C_r. The NCL line was defined by a specific volume v'_{ref} at the reference pressure p'_{ref}. The effective friction angle ϕ' was derived from the frictional constant M estimated from the undrained triaxial shear test results.

The excess pore water pressure and stresses induced during the cavity expansion process is highly dependent on the rigidity index G/s_u of the soil. The soil modulus G is correlated to the mean effective stress p' of the soil (Cao, Teh & Chang 2001; Zytynski et al. 1978). A function of volumetric strain via a *FISH* function was written to update the permeability during the calculation cycle for the soil consolidation analysis.

5.4.3 Numerical Simulation of Cavity Expansion

The initial conditions included the initial hydrostatic pore water pressure u_o, assuming the groundwater table to be at the ground surface and the initial vertical effective stresses $\sigma'_{v,o}$ due to the unit weight of the soil and the applied surcharge. The horizontal effective stresses $\sigma'_{h,o}$ were derived from the vertical effective stresses and the value of K_o reported in Table 5.1.

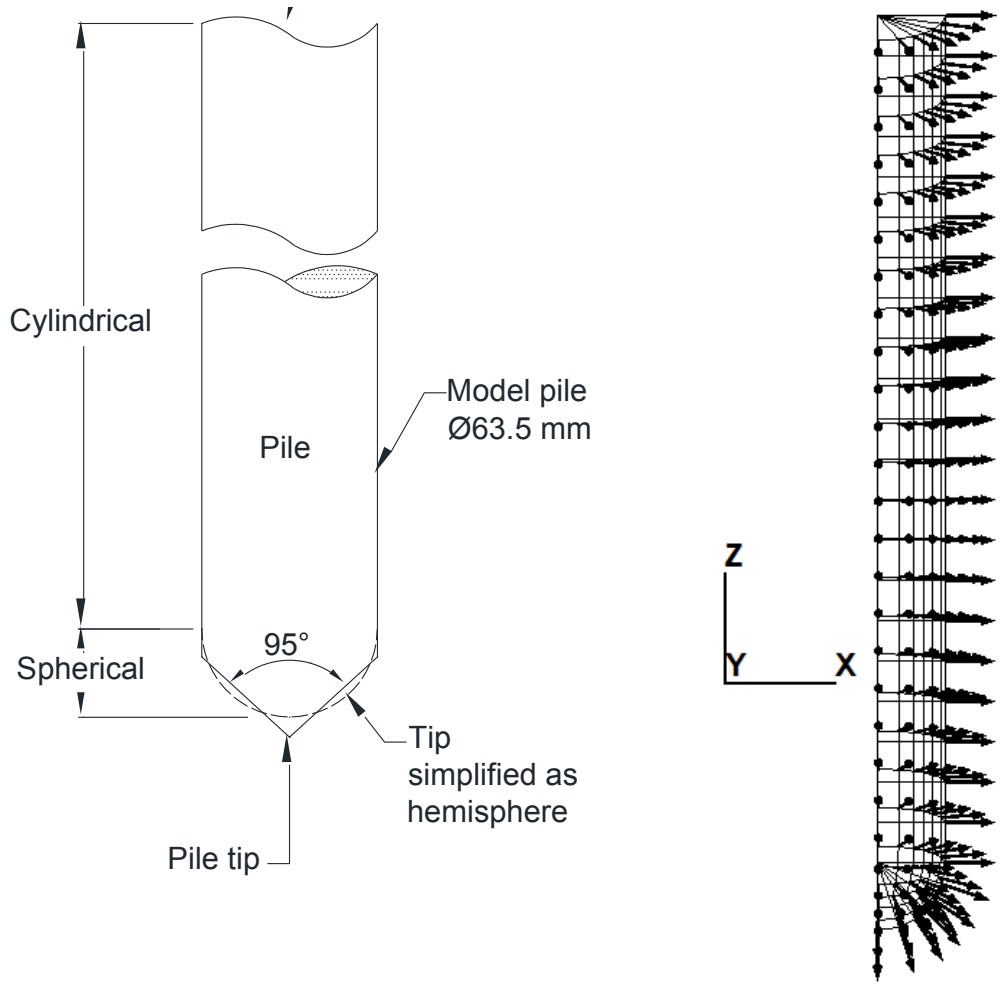

Figure 5.9 Simplified simulation of jacked piling: (a) cavity expansion modelling, and (b) displacement velocity applied to the initial cavity (1/4 of model pile); all dimensions are in mm

The numerical simulation of the jacked pile penetration process was simplified as creating a borehole in the soil with a final radius equivalent to the model pile. As illustrated in Figure 5.9, the volume of the model pile was approximated as a cylinder atop a half sphere; hence, the process of jacked pile penetration may be approximated as expansions of cylindrical and spherical cavities. It is noted that the analytical solutions using this

combined cylindrical and spherical cavity expansion for cone penetration testing by Chai et al. (2015) agreed reasonably well with the laboratory measurements. As shown in Figure 5.10a, the mesh prepared for this simulation comprised soil grid surrounding a cylindrical cavity (i.e. for cylindrical cavity expansion) fitted with a hemisphere (i.e. for spherical cavity expansion). The use of the hemisphere was to produce the correct stress and pore water pressure conditions at the tip of the pile. The creation of the cavity (i.e. the volume of the pile replaced the space of the soil) was followed by the consolidation analysis.

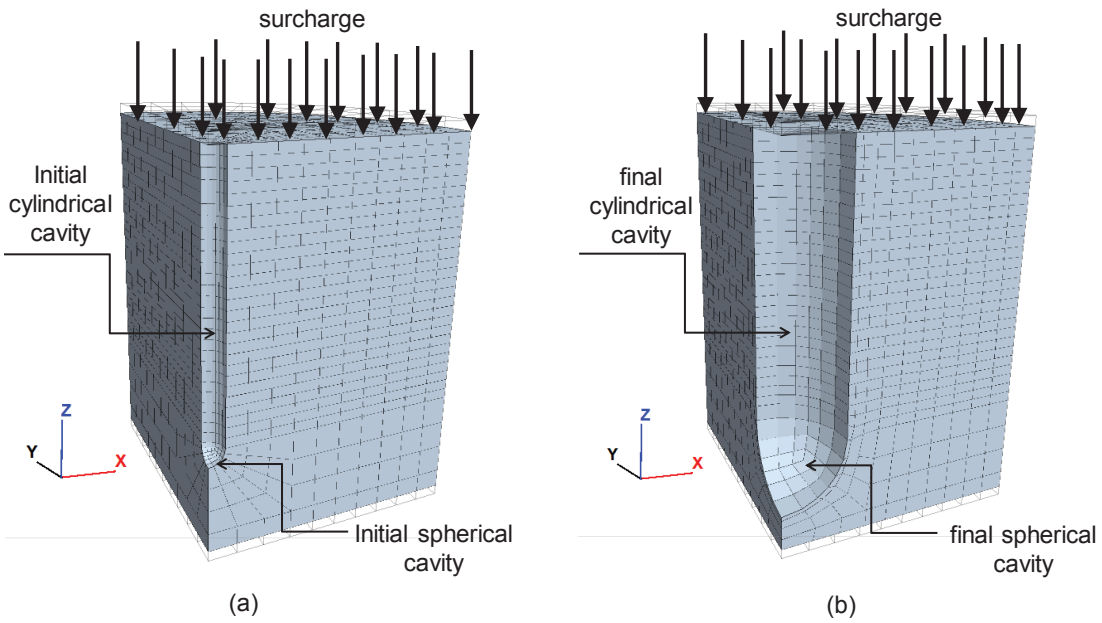

Figure 5.10 Deformed mesh before and after cavity expansion: (a) initial cavity, and (b) after cavity expansion

Numerical simulation of the penetration of a pile into the soil (i.e. creating a cavity) is challenging owing to the initial singularity problem. As recommended by Carter, Randolph & Wroth (1979), expanding a cavity with an initial radius r_i to a new radius $r_f = 2r_i$ can approximate what happens in the soil when a cavity expansion from zero radius to the actual pile radius (i.e. r_{pile}) take places. The required relation between r_i and r_{pile}

for a constant volume deformation in Equation (5.3) is $r_{pile} = \sqrt{3} r_i$ (Carter, Randolph & Wroth 1979). For example when the pile radius r_{pile} is 31.75 mm, the initial radius of the cavity would be r_i = 18.33 mm. However, the required final radius of the cavity after doubling the size would be r_f = 36.67 mm, which is notably larger than the radius of the actual pile (r_{pile}) and is not desirable. Parametric study performed by Castro & Karstunen (2010) indicated that quadrupling an initial cavity gives nearly identical results compared to doubling the cavity as presented by Carter, Randolph & Wroth (1979). On that basis, a smaller initial cavity r_i = 8 mm was chosen for this study, which results in a more realistic case as the final radius r_f = 32.74 mm determined based on Equation (5.3) is much closer to the actual radius of the model pile (only 3% difference). Excessive mesh distortion was encountered using an initial cavity radius smaller than 8 mm.

$$r_f = \sqrt{r_i^2 + r_{pile}^2} \tag{5.3}$$

The adopted initial and final radii were applied to the cylindrical and spherical cavity expansions. First, the material inside the initial cavity r_i was turned to "null". Then outward normal velocities were applied to the cavity wall so that when mechanical stepping in large strain mode was used, the wall would be displaced in a normal direction until achieving a final cavity of r_f = 32.74 mm. The deformed mesh after the cylindrical and spherical cavity creations is shown in Figure 5.10b. At the end of the cavity expansion, the applied velocities at the cavity wall were reduced to zero and the model was stepped to equilibrium. A coupled hydraulic and mechanical simulation was conducted to allow excess pore water pressure to dissipate. The starting conditions for consolidation analysis corresponded to those immediately after cavity expansion (Randolph, Carter & Wroth 1979). The changes in model variables such as vertical and

horizontal effective stresses, excess pore water pressure and displacements in the soil were recorded with time. The next section describes the experimental test results and the comparison with the finite difference analyses.

5.5 Comparison between Results of Model Test and Numerical Simulation

5.5.1 Soil Penetration Resistance during Pile Penetration

The measured soil penetration resistance during the movement of the penetrating pile was plotted against the soil depth in Figure 5.11a, while the penetration rate is shown in Figure 5.11b. The measured soil penetration resistance was approximately 120 N. Further increase in the soil penetration resistance as the pile approached the base of the soil tank as shown in Figure 5.11a can be attributed to the effect of base boundary. The undrained shear strength s_{u} of the soft soil estimated from the empirical correlation with the measured cone penetration resistance using the cone factor N_{kt} between 11 and 19 (ASTM 2012; Lunne, Powell & Robertson 1997) varied from 1.8 kPa to 3 kPa. The undrained shear strength s_{u} of the soft soil measured by the shear vane and those inferred from the unconfined compressive strength tests for soil specimens sampled after the model test varied from 2.2 kPa to 3.5 kPa.

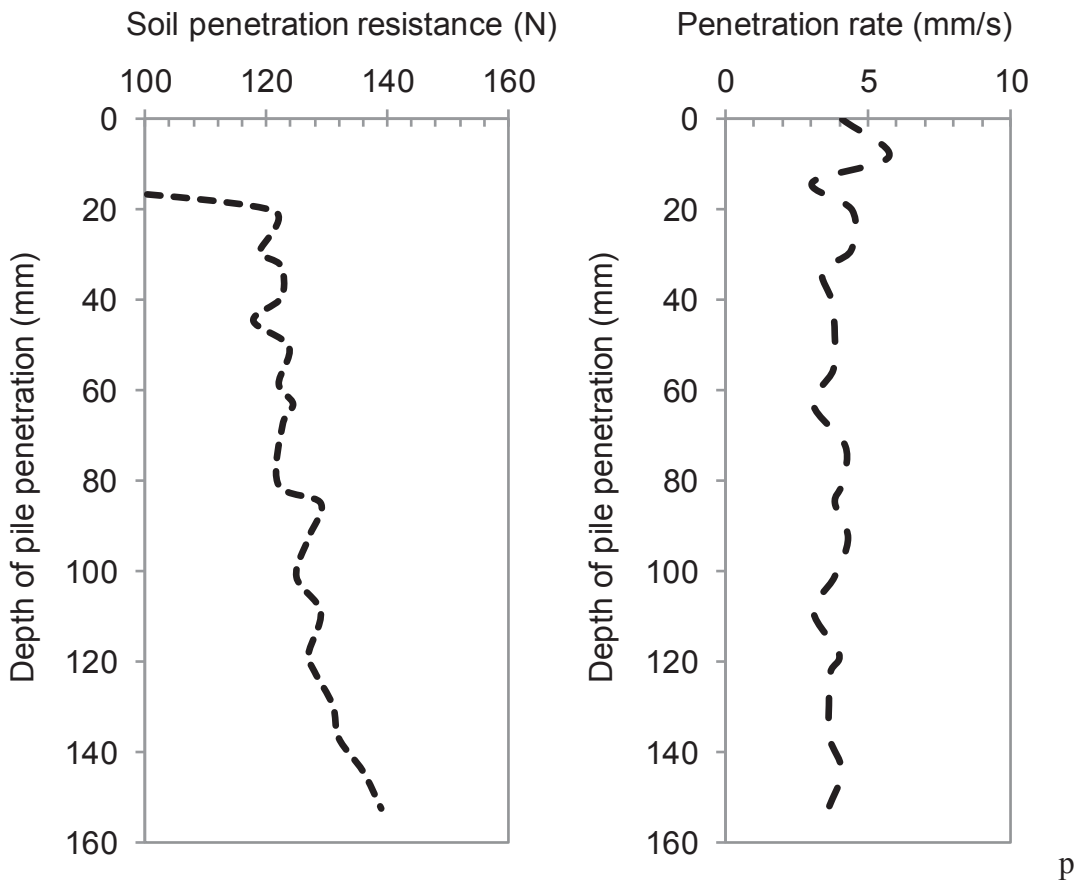

Figure 5.11 a) Soil penetration resistance with depth and (b) the pile penetration rate

5.5.2 Predicted versus Measured Excess Pore Water Pressures

Figure 5.12 shows the short-term evolution in the excess pore water pressures during and after the pile penetration. The excess pore water pressure increased due to pile jacking; however, the arrival of the maximum excess pore water pressures for each observation point had noticeable delayed effects. Since the pores in the saturated soft soil were filled with water, the excess pore water pressure induced by the jacked in pile penetration may have continuously transmitted through the soil medium.

The observed steady decrease in magnitudes of the excess pore water pressures with the elapsed time as shown in Figure 5.12 was different to the total radial stress responses due to jacked pile installation reported in the literature, where a sharp fall was observed.

Approximately five hours after the penetration of the jacked-in pile was completed, the peak excess pore water pressures reached 6.6 kPa to 9.2 kPa. The measured maximum pore water pressures were approximately 3× s_u to 4× s_u, which was in general agreement with the typical predicted excess pore water pressure immediately after installation using the theoretical parametric with the computer code CAMFE (Carter 1978). Considering the limited thickness of the soil, it was not surprising that no obvious difference was observed between the peak values of the excess pore water pressures measured by the transducers of different depths.

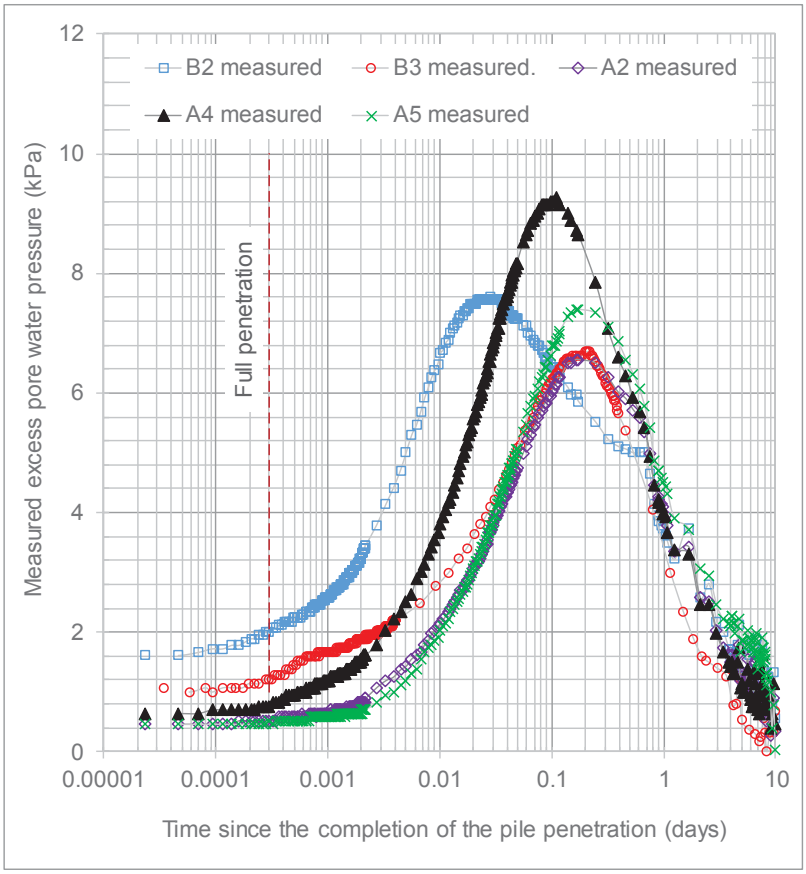

Figure 5.12 Evolution of the excess pore water pressure due to jacked in pile penetration

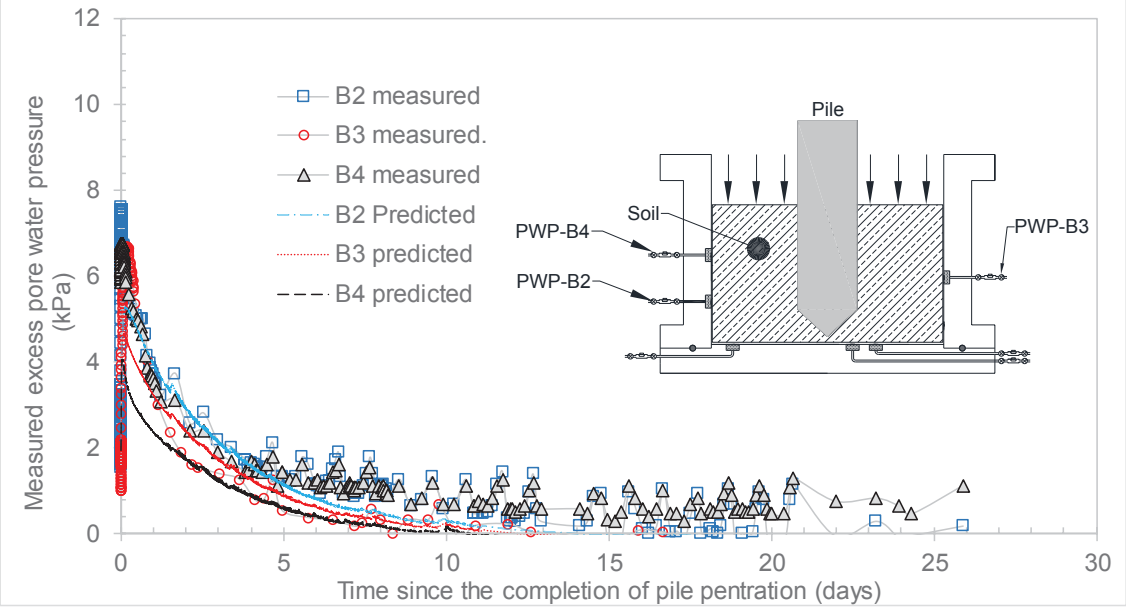

Figure 5.13 Evolution of excess pore water pressures along the wall of the soil tank at three locations: PWP-B2, PWP-B3, and PWP-B4

After reaching the peak, the excess pore water pressure gradually decreased because of the pore pressure dissipation. Figure 5.13 shows that more than 95% excess pore water pressure dissipated after two weeks after pile penetration, where the pore pressures returned to just above hydrostatic values. In Figure 5.13, the evolution of the measured excess pore water pressures induced by the jacked in pile penetration was compared with the results of the finite difference analysis at three locations PWP-B2, PWP-B3, and PWP-B4. It can be seen that while the numerical analyses are able to provide a clear difference in predicted excess pore water pressures between the predicting locations, the instrumentation for measuring pore water pressures was not sufficiently accurate to pick up such small difference.

Figure 5.14 shows the evolution of the excess pore water pressures for the observation points at the base level of the soil tank. The excess pore water pressures induced by the

pile penetration at the locations of PWP-A2, PWP-A4 and PWP-A5 were reported. The decay of excess pore water pressures at the observation points near the base was similar to the dissipation of the excess pore water pressures near the wall of the soil tank. However, there were some key differences. Firstly, it was evident that the excess pore water pressures at observation locations closer to the pile tip (PWPT-A4 and PWPT-A5) were greater than the excess pore water pressure measured further away from the centre of the tank (i.e. PWPT-A2). Secondly, both the numerical model and the model test results indicated that shortly after reaching the peaked values, the excess pore water pressures at these locations converged towards a similar value at equalisation and decayed together towards the hydrostatic pressures.

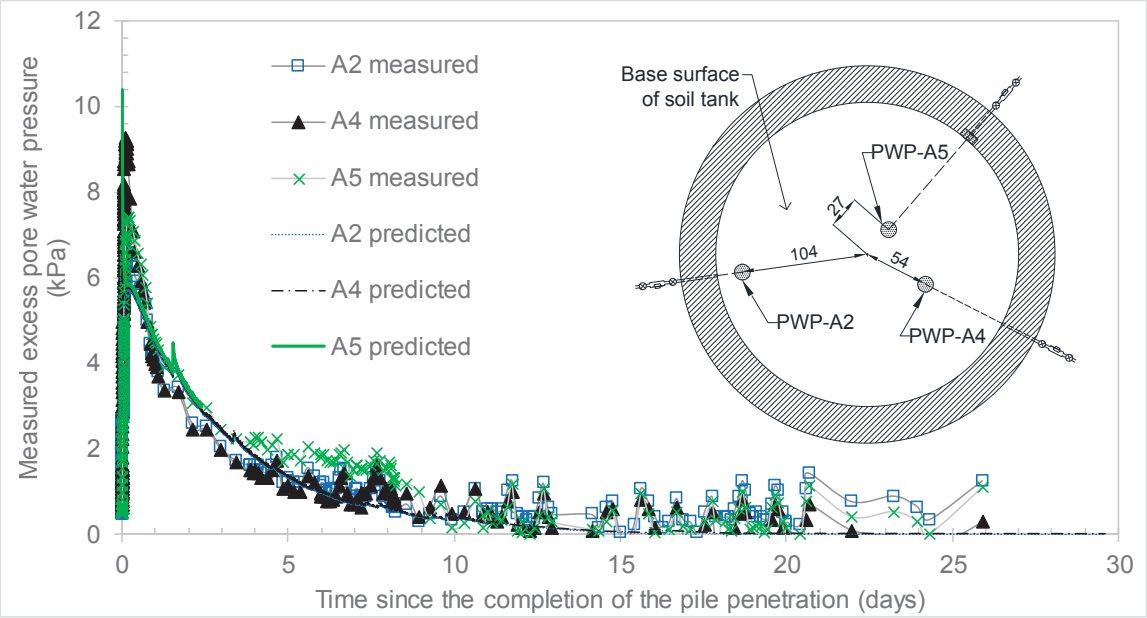

Figure 5.14 Evolution of the excess pore water pressures along the base of the soil tank

5.5.3 Predicted versus Measured Surface Soil Movement

During the downward penetration of the model pile, the soil was displaced away from the model pile. The disturbed soil was forced to move upwards, causing soil heave and

associated uplift of the overlying dead weights. The measured soil heave captured by the three LVDTs placed on the top of the surcharge weights was approximately 11.5 mm. The measured heave agrees well with the predicted soil heave assuming constant volume under undrained conditions (i.e. the volume of the soil heave would be equal to the volume of the penetrating pile). Some discrepancy would be attributed to a small squeeze of soft soil through the gap between the soil, the pile, and the surcharge.

The measured soil consolidation settlement after the pile penetration was compared with the predicted settlement using *FLAC*^{3D} as shown in Figure 5.15. Within 24 hours after pile penetration, the finite difference approach predicted a slow rate of settlement; however, the predicted consolidation process accelerated with a higher rate of consolidation at a later stage. Despite some mismatch in the rate of consolidation, the total final settlement was well predicted by the finite difference approach. It is noted that the written code for the *FLAC*^{3D} analysis offered the option to update the permeability as the void ratio decreases by, for example, using a relation expressed by Equation (4.1), which is based on Taylor's permeability index C_k. The code lines are attached in the Appendix B. With this feature, realistic predictions of the rate of excess pore pressure dissipation can be achieved because the permeability of the very soft soil will decrease upon compression. The decreases in void ratio occurred not only in the undisturbed soil, but also in the plastic zone, leading to further delay in the dissipation of excess pore pressure and a lower rate of the soil consolidation.

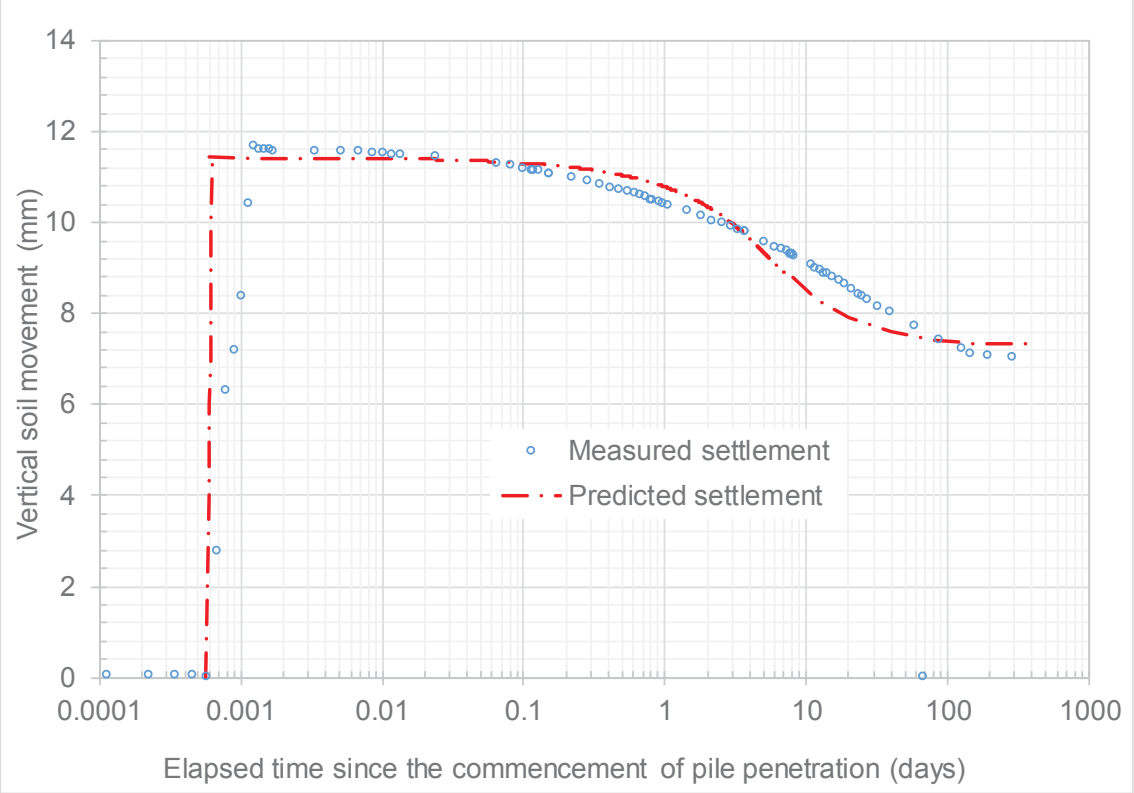

Figure 5.15 Measured and predicted soil consolidation settlement during and after pile penetration

5.6 Summary

This chapter presents the results of a laboratory model test and a back-analysis study on the soil responses to the jacked-in pile penetration in terms of excess pore water pressures and consolidation settlement. In the laboratory model test, a closed-ended circular pile was jacked into a very soft soil and the soil heave and subsequent consolidation settlement were monitored together with the evolution of the excess pore water pressure. The model test results were compared with the 3D large strain numerical approach based on the combined use of the cylindrical and spherical cavity expansions. The numerical simulations conducted using the finite difference code *FLAC*^{3D} included the undrained

analyses simulating the jacked pile penetration and the soil consolidation process. The results of the model test and the back analysis indicate the following:

- A noticeable delay in the arrival of the peak pore water pressures was observed at the monitoring points.
- The measured soil displacement and the evolution of the excess pore water pressure were represented well by the proposed numerical model.
- The results obtained provide valuable insights into the installation of jacked-in piles in soft clay, and are a valuable source of validation materials for more complex numerical simulations.

CHAPTER 6 Practical and Construction Aspects of CMC Installation Effects

6.1 Introduction

The first part of this chapter (Section 6.2) presents the results of a numerical investigation on the CMC installation effect on an existing bridge pile using the three-dimensional finite difference software package *FLAC*^{3D}. The results of this study indicate that when the CMC is long and the existing bridge pile is slender, the pile bending moment and pile lateral movement, induced by the CMC installation effect, can be significant.

The second part of this chapter (Section 6.3) presents the key sustainability aspects of using CMC technology and highlights some potential aspects for further development. Future research directions are discussed to enhance sustainable design practice. These include general discussions on the issues of economic design with trial field tests, the use of recycled industrial by-products for grout mix, improved design, maximising the resiliency of structures and the energy consumption. The CMC installation effects on the surrounding soils and environment are also discussed sensibly in this study.

6.2 Bridge Pile Response to Lateral Soil Movement Induced by Installation of Controlled Modulus Columns

6.2.1 Objectives

The controlled modulus column (CMC) ground improvement technique aims to create an improved composite ground, consisting of a grid of rigid inclusions installed in soft soil

overlaid with a granular load transfer layer (Plomteux, Porbaha & Spaulding 2004). The column installation process involves penetrating an auger into the ground under a torque and thrust provided by a drilling rig, followed by grout injection through the hollow stem while raising the tool. The auger is purposely designed to enable lateral soil compaction during augering and prevent the soils from moving upward when raising the auger. When construction sites involving CMC are located in close proximity of existing sensitive structures such as an existing bridge foundation, if proper installation sequence is not considered, the risk of damaging adjacent structures due to lateral soil movement can be high (Brown 2005; Hewitt, Summerell & Huang 2009; Plomteux, Porbaha & Spaulding 2004). Hence, it is often necessary to prepare a risk assessment and construction planning before construction starts. Although these tasks have become a routine for piling contractors, assessing installation effects, especially the lateral soil movement due to installation, remains a serious challenge. Available assessment methods for installation effects include the cavity expansion theory (Carter, Randolph & Wroth 1979), strain path method (Baligh 1985) and more rigorous analyses using numerical modelling. The cavity expansion theory, which is the most common method, studies the changes in pore water pressure and stresses due to the creation or the expansion of a cavity. Current contributions to CMC application found in the literature include a numerical study by Rivera et al. (2014) based on the cavity expansion theory using PLAXIS-2D and a field investigation of installation effects on the surrounding soils by Suleiman et al. (2016). However, assessment of the CMC installation effects on the adjacent existing structures has not been reported in the literature notably due to a number of reasons. Firstly, the modelling of pile installation process involves large mesh distortion and can be time-consuming. Secondly, the existing analytical methods are unable to capture the complex three-dimensional soil-structure interaction and construction sequence. Section 6.2

presents a 3D numerical model to investigate the response of an existing bridge pile subjected to loading due to the lateral soil movement induced by the installation of nearby CMCs.

6.2.2 Numerical modelling

To simulate the CMC installation process, three-dimensional numerical modelling using *FLAC*^{3D} v.5.01 was carried out in large strain mode. 3D grids were created to represent a soil profile consisting of a soft clay layer, overlying bedrock (Figure 6.1a). An existing bridge pile and six proposed CMC positions are located in the centre of the 3D model. The radial cylindrical mesh represents CMCs and piles, while the cubical meshes form the outer soil regions. The lateral boundaries were extended 20 times the CMC diameter, from the outmost CMC or pile to minimize the boundary effects.

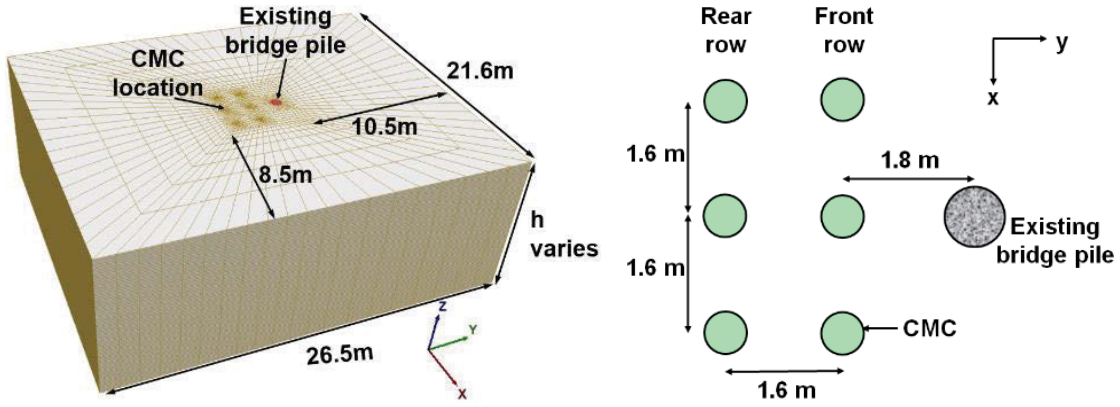

(a) (b)

Figure 6.1 (a) FLAC^{3D} *finite difference grid and (b) the layout of CMCs and the existing bridge pile*

The existing bridge pile is 0.75 m in diameter (d) and is located at 1.8 m centre-to-centre (c/c) from the nearest CMC. The pile is assumed socketed into the bedrock. The construction of two rows of CMCs next to the existing bridge pile was simulated in this

study (Figure 6.2b). Each row has three columns oriented in the x-direction. CMCs have a diameter d_{CMC} = 225 mm and spaced at 1.6 m c/c in a square pattern. All CMCs are installed to the top of bedrock or very stiff ground. The model grid is generated using *FISH* programming language to facilitate the parametric studies. The 3D grid shown in Figure 6.1a developed for a model height h = 9.6 m comprises 179,200 zones and 165,616 grid points.

6.2.3 Material Modelling

Soil properties were derived from site investigation data from a highway upgrade project in Australia. The modified Cam-Clay (MCC) material model was adopted to represent the behaviour of soft clay. The adopted parameters include the slope of normal consolidation line (NCL) λ = 0.29, and the slope of elastic swelling line κ = 0.073. The NCL line is defined by a reference pressure p'_{ref} = 74 kPa and a specific volume υ_{ref} = 2.55. Based on the oedometer results, an overconsolidation ratio OCR of 1.6 was adopted for the entire depth. Therefore, the pre-consolidation pressure varies linearly with depth. The adopted effective friction angle ϕ' is 28° and the frictional constant of the critical state line is M = 1.11. The lateral stress coefficient K_0 for lightly overconsolidated clay can be related to that of the normally consolidated clay via OCR and was estimated to be 0.75 (i.e. simulating anisotropic stress conditions). Other typical properties for soft clay including a dry density of 1300 kg/m^3, a porosity of 0.5 and an effective Poisson's ratio ν' = 0.3 were also adopted. It is noted that for a structured clayey soil, due to increase in the mean effective stress as well as deviatoric stress, cementation degradation may occur influencing the deformation of the ground immediately after the installation (Nguyen, Fatahi & Khabbaz 2014).

Pile and CMCs were considered impermeable and were modelled using solid elements. The pile is characterized by an isotropic linear elastic model, described by a Young's modulus of 20 GPa, a Poisson's ratio of 0.2 and a density of 2400 kg/m^3. The Mohr-Coulomb (MC) material model was used to represent CMC behaviour. In this study, it was assumed that the CMC grout set quickly after injection. Hence, a grout density of 2400 kg/m^3, bulk modulus K = 3.23 GPa, shear modulus G = 2.42 GPa, the cohesion c' = 300 kPa, the friction angle ϕ'= 5°, and a tensile strength σ^t = 520 kPa were adopted for CMC simulation. The stiffness and the tensile strength of CMCs were estimated according to Eurocode 2 (BSI 2004) using a characteristic compressive strength of sand concrete f_{ck} = 10 MPa.

6.2.4 Interfaces, Boundary and Initial Conditions

To allow gapping or sliding between the soft clay and CMC/pile, interface elements with insignificant tensile strength were employed. The interface behaviour is determined by the friction angle and cohesion, which were set equal to those of the soft clay. The interface normal stiffness k_n and shear stiffness k_s are estimated using Equation (3.8) as recommended by Itasca (2012).

The soil at the side boundaries in Figure 6.1a was fixed against the displacement normal to the boundary planes. The top boundary is free and was considered permeable (free draining). The bottom boundary is restrained vertically, for the purpose of the radial cavity expansion. The initial conditions include the initial hydrostatic pore water pressure assuming groundwater table at the ground surface; and initial effective stresses due to soil self-weight, assuming a gravitational acceleration of 9.81 m/s^2. However, near-surface soils in reality may be partially saturated and a more realistic coupled flow-deformation behaviour of unsaturated soils should be considered (Ho, Fatahi & Khabbaz 2014; Khalili

& Khabbaz 1998; Khoshghalb & Khalili 2013). Once the in-situ stresses are established, the bridge pile was installed by simply changing material properties in the pile zones, from those of soil to concrete and the system was stepped to equilibrium.

6.2.5 Modelling CMC Installation

The simulation of the CMC installation process is executed in two stages: (*i*) creating a cylindrical borehole and (*ii*) backfilling the borehole with CMC grout.

Cavity creation is most easily modelled numerically by expanding a pre-existing cavity of initial radius r_i to a new cavity of radius r_f, as recommended by Carter, Randolph & Wroth (1979). Assuming undrained expansion, the condition of constant volume can be considered and hence, the radius r_f at end of the expansion can readily be estimated using a simple relationship: $r_f = ({r_i}^2 + {r_{CMC}}^2)^{0.5}$ where r_{CMC} = 225 mm. An optimal initial radius r_i was determined, being sufficiently small to maintain reasonable numerical accuracy. At the same time, this radius should not be too small, to avoid excessive mesh distortion. Parametric studies indicate that r_i = 65 mm (i.e. approximately $\frac{1}{4}$ of r_{CMC}) is adequate for the adopted geometry and mesh. The first step of creating a cavity was to turn the soil within the initial cavity of r_i = 65 mm into "null" material (i.e. material removed). In the next step, outward normal velocities were applied to the cavity wall so that, upon mechanical stepping in a large strain mode, the wall displaced in the radial direction until achieving the final cavity radius of 234 mm. It is noted that, during expansion, the tangential velocity at the wall was fixed to zero. The deformed mesh as a result of cavity creation at the first CMC is shown in Figure 6.2.

Before filling the borehole with the CMC grout, the applied velocities at the cavity wall were removed and the model is stepped to equilibrium. Following grouting, the base of

the newly formed CMC was restrained vertically. The soil/CMC interface elements were inserted and the system was then stepped to equilibrium to complete the CMC installation. The subsequent CMC installations were simulated in a similar manner, according to a sequence shown in Figure 6.3, i.e. starting with the rear row (CMCs 1 to 3) and then progressing to the front row (CMCs 4 to 6).

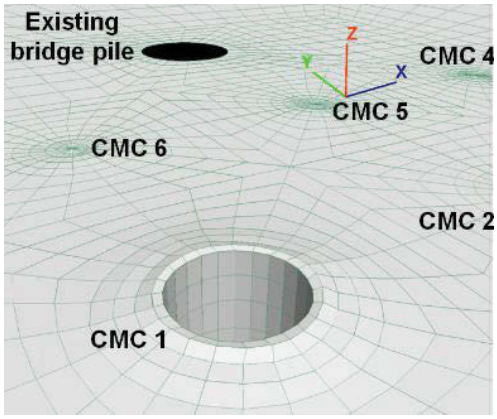

Figure 6.2 Deformed mesh after undrained cavity creation at the first CMC

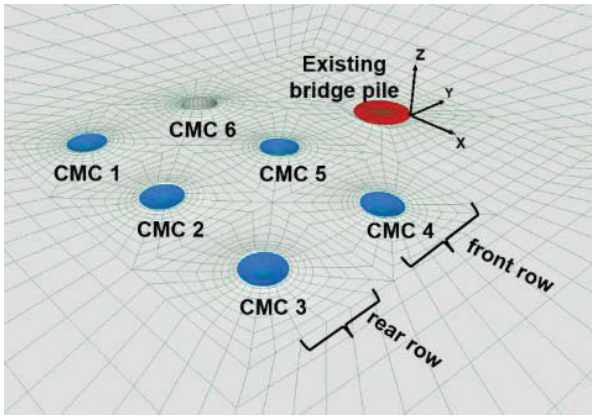

Figure 6.3 The order of CMC installation

6.2.6 Results and Discussion

Soil movement due to CMC installation is verified against a number of assessment methods published in the literature, firstly, under plane strain condition: (i) analytical closed-form undrained cavity creation solution (i.e. expansion from $r_i = 0$), suggested by Carter, Randolph & Wroth (1980) for pile driving (ii) recommended numerical procedure by Carter, Randolph & Wroth (1979) and (iii) *FLAC*^{3D} with varying initial cavity radii (*Figure 6.4*). It is found that numerical analyses with the currently adopted r_i = 65 mm or so yield soil movement somewhere between the closed-form solution ($r_i = 0$) and the numerical results suggested by Carter, Randolph & Wroth (1979) (r_i = 130 mm). Hence,

the soil movement is much dependent on the chosen r_i. In addition, the soil movement at various depths of the 3D model is compared with the plane strain solution (Figure 6.5). At the ground surface, with much heave occurring, the estimated radial soil movement is the least. The radial soil movement at larger depths is greater, but less than the soil movement numerically analysed under plane strain condition.

Figures 6.6 to 6.9 present the results of the numerical simulation of CMC installations in a soft clay layer extending to a depth of 9.6 m below the ground surface, with pile length L = 9.6 m. In particular, Figure 6.6 shows that during installation the pile head moves away from the CMCs as expected. However, the pile head also moves slightly sideways, i.e. in the negative x direction. It is noted that the direction of pile head movement can be different if the installation sequence differs from that described in Figure 6.3. The side-way movement of pile head in the x direction is the consequence of the change in the direction of the lateral soil movement induced by the installation of different CMCs.

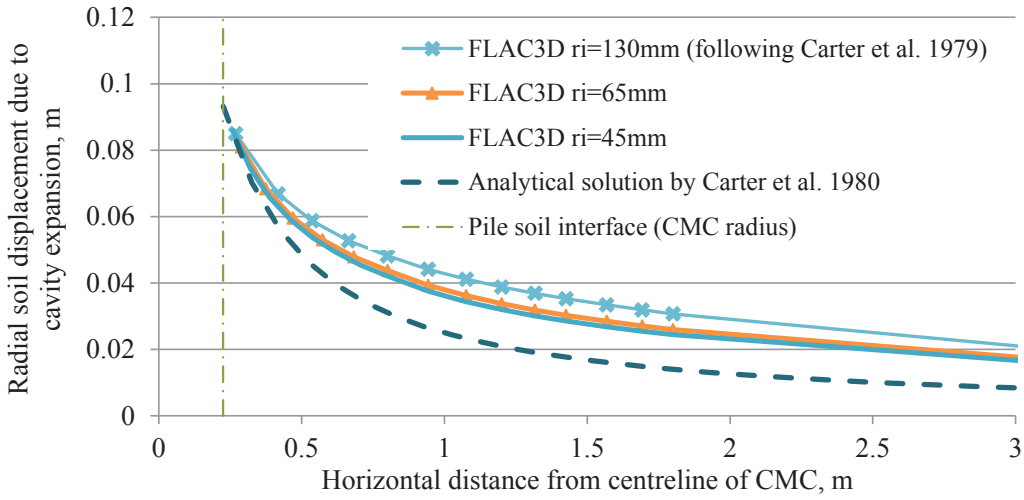

Figure 6.4 *Radial soil movement due cavity expansion versus horizontal distance from CMC axis*

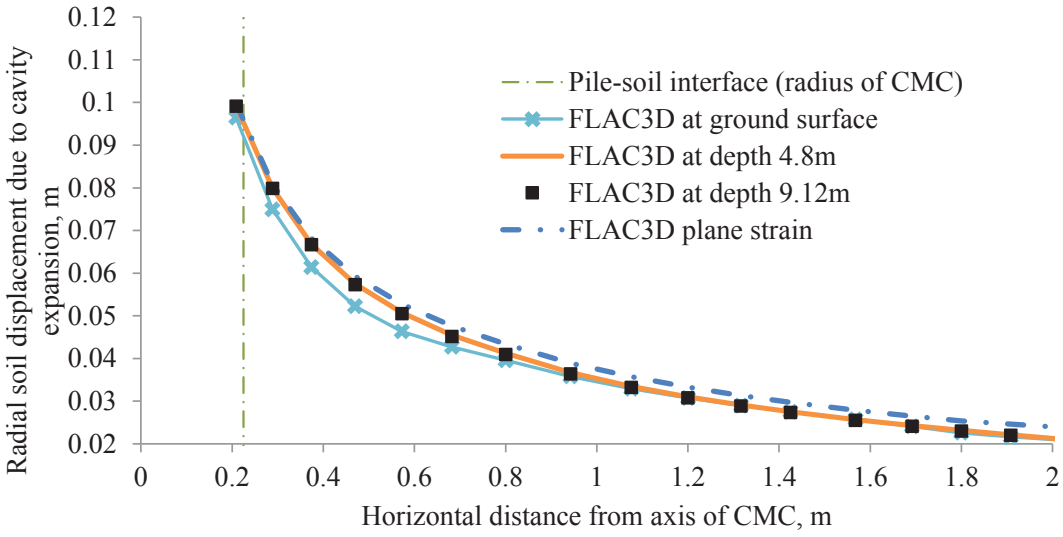

Figure 6.5 Radial soil displacement versus horizontal distance from CMC axis by depths

Figure 6.7 presents a cross section through the pile centre together with the contour of the excess pore water pressure at the completion of all CMC installations. It is clearly observed that the pore water pressures increase significantly in front of the pile along line A-B, while the pore water pressures behind the pile are less than the initial hydrostatic

pore pressures, due to the decompression of the soil. Figure 6.8a illustrates the excess pore water pressure in front of the pile (i.e. along line A-B shown in Figure 6.7), due to the undrained cavity expansion. The excess pore water pressure due to the installation of the rear row is relatively small; however, a substantial increase in excess pore water pressure occurs when the front row CMCs are installed. The installation of CMC 5, which is the closest CMC to the bridge pile, causes the most significant increase in the generated excess pore water pressure. The excess pore pressure is expected to decay inducing elastic viscoplastic deformation (Le, Fatahi & Khabbaz 2015). The normal stresses acting on the pile shaft presented in Figure 6.8b indicate a similar pattern to the pore water pressure reported in Figure 6.8a.

The response of the existing bridge pile foundation to the lateral soil movement induced by the CMC installation process was recorded in terms of lateral deflection in the y direction (Figure 6.9a) and the induced bending moment (Figure 6.9b). As expected, the lateral deflection increases as more CMCs are installed, with much greater effect due to the front row than the rear row. A maximum pile lateral deflection of approximately 49 mm occurs at the top of the bridge pile. According to Stewart, Jewell & Randolph (1994), the horizontal displacement of less than 25 mm is often considered to be acceptable and movements greater than 50 mm are generally unacceptable. When the pile is longer and hence more slender, the pile movement may be more significant. The calculated maximum bending moment in the pile is approximately 1,140 kN.m, which occurs at the bottom of the bridge pile. In this study, the soil is homogenous with the soil undrained shear strength increasing linearly with depth, resulting in a straightforward prediction of the maximum bending moment location. It should be noted that for a stratified soil profile, the location of the maximum bending moment may be positioned elsewhere. In addition, it is noted that the head restraint is not provided to the existing pile. According to Poulos

(1994), the existence of restraint at the pile head may lead to bending moments that are two or more times the value for an unrestrained pile head.

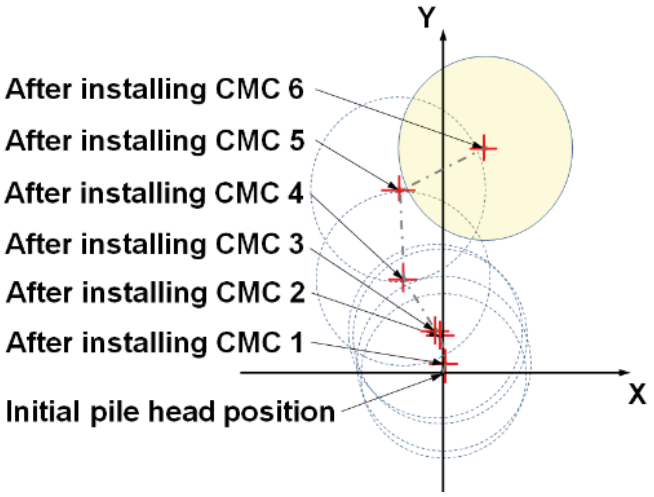

Figure 6.6 Pile head movement during CMC installation process (L_{pile} = 9.6m)

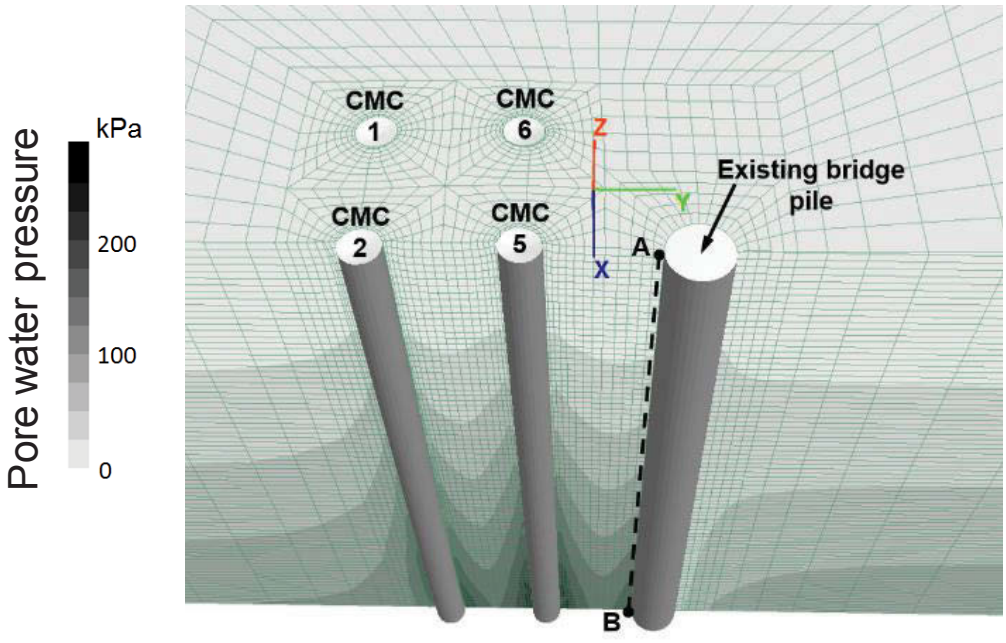

Figure 6.7 Pore water pressure upon complete installation of the final CMC

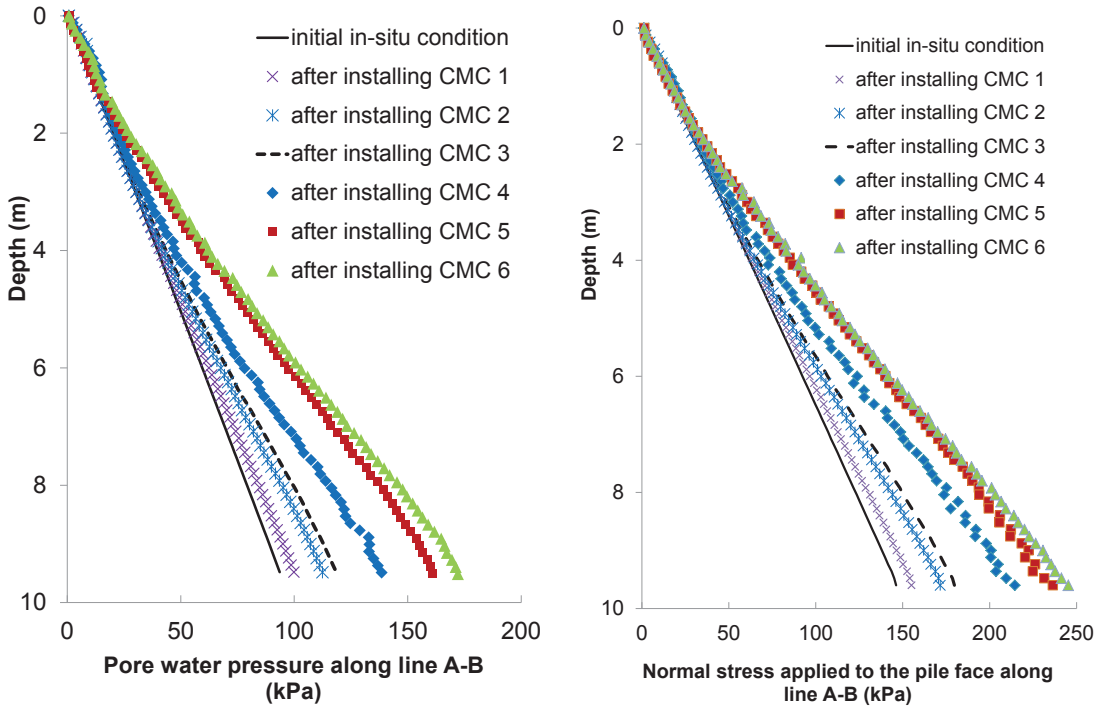

(a) (b)

Figure 6.8 (a) Pore pressure near pile face (b) Normal stress acting on pile face after CMC installation

A parametric study was carried out to quantify the effect of varying the soft soil thickness, hence the lengths of the CMCs and bridge pile, on the CMC installation effect on the behaviour of the bridge pile. Therefore, two more sets of analyses were carried out, with the adopted soil thicknesses of 4.8 m and 7.2 m, in addition to the previous set of analysis corresponding to the soil thickness of 9.6 m. A single bridge pile diameter was adopted for all analyses; hence, the pile slenderness increases with the increase in the pile length (or the soil thicknesses). The results, shown in Figures 6.10a and 6.10b, indicate that for pile lengths of 4.8 m, 7.2 m and 9.6 m, the pile head lateral movements are 4 mm, 23 mm and 49 mm; and the corresponding pile bending moments are 275 kNm, 740 kNm and 1,140 kNm, respectively.

The results indicate that the soft soil thicknesses and the CMCs' length have significant effects on the bridge pile response to the lateral soil movement induced by the CMC installation. Thus, any realistic assessment of CMC installation effects on the existing surrounding structures, particularly piles, should include detailed considerations of CMCs, piles and soft soil properties.

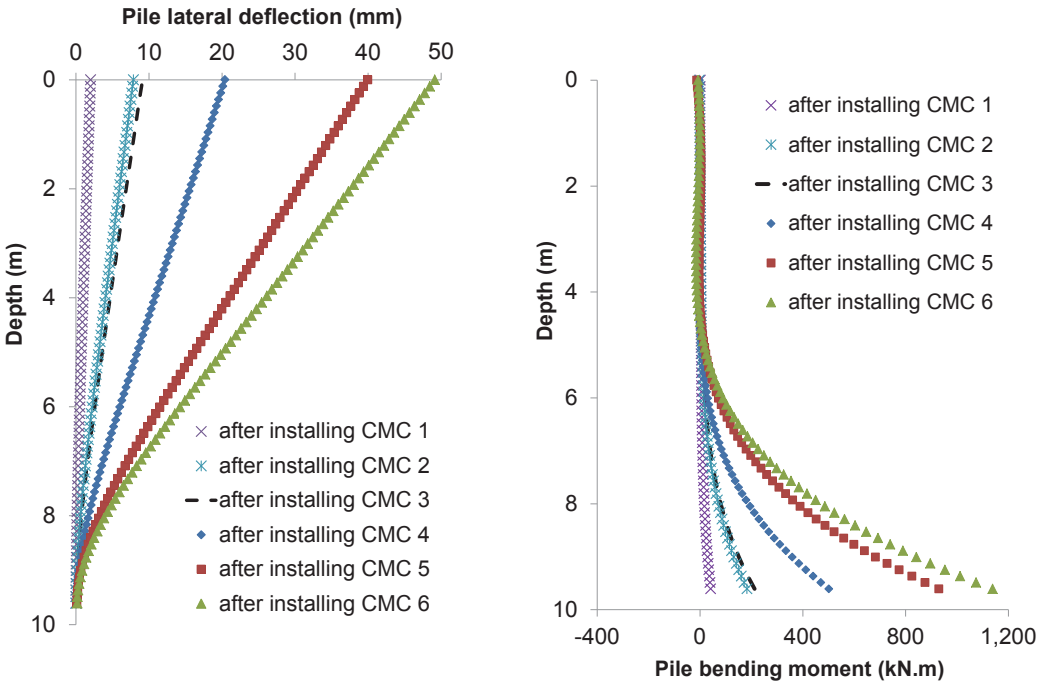

(a) (b)

Figure 6.9 Bridge pile response: (a) lateral deflection and (b) bending moment

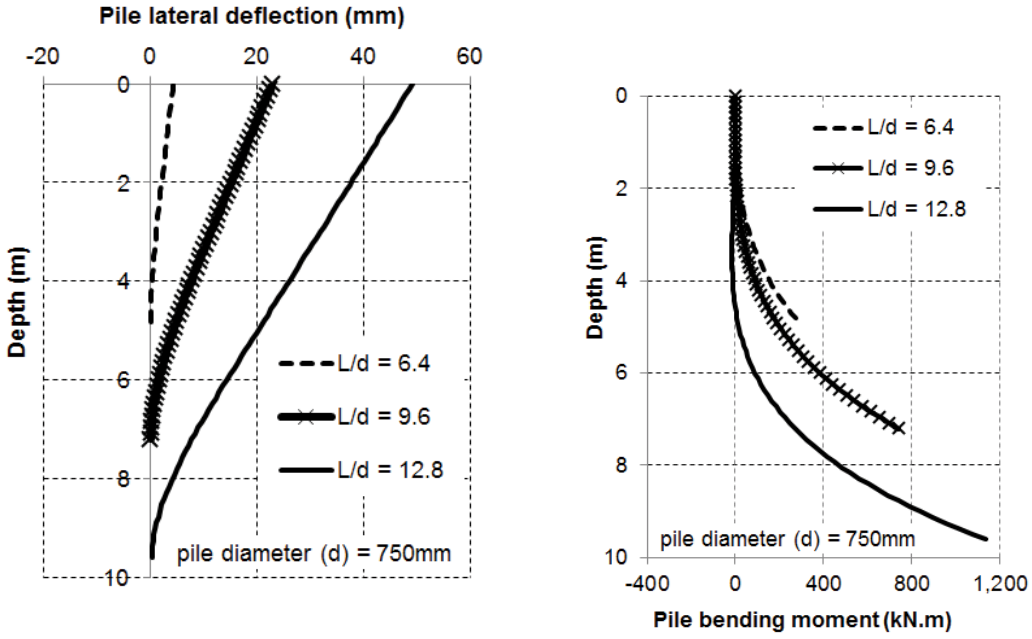

(a) lateral deflection (b) bending moment

Figure 6.10 Bridge pile response upon complete installation of the final CMC for three model depths

6.2.7 Summary

The installation process of controlled modulus columns (CMC) in soft soil has been simulated using *FLAC*^{3D} to investigate the short-term effect on an existing bridge pile. The results indicate the feasibility of simulating the installation process numerically. The numerical results show that undrained excess pore water pressure in front of the bridge pile and the normal stress applied on the bridge pile increase as more CMCs are installed. As the CMCs are longer and the bridge pile is more slender, the lateral pile deflection increases. The results indicated that the lateral pile deflection due to the horizontal soil movement induced by the CMC installation can be significant; hence, it highlights the

importance of accurate assessment of CMC installation effect on the surrounding structures prior to construction, in addition to traditional observation methods commonly adopted during construction.

6.3 Sustainability Considerations for Ground Improvement Technique Using Controlled Modulus Columns

6.3.1 Objectives

The sustainability concept has been increasingly accepted to be a key aspect of modern engineering design and construction, most noticeably in government-supported projects. Since geotechnical engineering is one of the key parts of construction, geotechnical engineers have opportunities with the power to deliver project outcomes that are not only economical, safe but also sustainable. Ground improvement techniques aim to increase ground-bearing capacity, improve stability, and reduce short and long-term ground settlements. These techniques have an impact on the environment, local ecological systems and ground conditions. Appropriate techniques are increasingly demanded due to decreasing available and favourable land for construction and redevelopment of urban areas. Today a large number of ground improvement methods exist in the industry, with each serving a limited number of purposes. Selection of one or a combination of two or more methods requires a deep understanding of various ground treatment methods. Decision making should rely on trials, design requirement, project budget and time restraint, ground and site conditions. Alongside with control of quality, durability, cost and safety, authorities also require design and construction of infrastructure to consider environmental outcomes, forming important aspects of sustainable development.

Although sustainability in geotechnical engineering has been addressed by a number of authors (Abreu et al. 2008; Holt et al. 2010; Jefferson et al. 2007), little attention on sustainable development has been placed during the process of geotechnical design and implementation. The geotechnical community should set out specific sustainability outcomes with tangible results to be achieved within a set time frame. At this stage, it will be very likely that any sustainability policies/requirements attached to the contract works may receive mixed responses from businesses.

To target sustainability outcomes in geotechnical engineering and ground improvement works, three major "triple bottom line" Economic, Environment and Social impact proposed by Elkington (1997) should be followed in combination with "financial, social, human, natural and produced" factors. Economic benefits and social reactions should not be considered as barriers to the sustainable development. In fact, adoption of sustainable solutions should be considered to enhance the competitiveness in bidding and winning projects. Today sustainability in geotechnical engineering targets (i) reduction in energy consumption, (ii) lower carbon emission during implementation and (iii) decrease in material usage. This should be accompanied with the increased use of reused, recycled or green materials and locally available materials instead of importing (Mitchell & Kelly 2013). Geotechnical engineers should be aware of and equipped with methods of sustainability assessment (e.g., how the carbon footprint is estimated).

One way to achieve those outcomes would be through technological innovations. One of the relatively new innovative ground improvement methods is the controlled modulus column (CMC) ground improvement technique. This technology was first developed in France. Today CMC has become a method of choice for many projects having tight construction schedule or with concerns related to soft soils and contaminated ground.

CMC possesses several features that are distinct from those of more traditional methods such as prefabricated vertical drains, stone columns, deep soil mixing or piled embankment foundation. CMC has been used considerably in Europe with increasing popularity in the US. The technique has recently been used in a number of projects in Australia, mainly involving the construction of bridge approach embankments, port development and warehouse foundation with the aim to reduce both total and differential settlements and to accelerate construction sequence (Fok et al. 2012; Wong & Muttuvel 2012b). The Gerringong Upgrade project is one of the recent projects where CMC have been successfully utilised for bridge and road construction (Fulton Hogan 2013).

Section 6.3 summarises the key sustainability aspects of using CMC technology and highlights some aspects that are potential for development. Future research directions are discussed to enhance sustainable design practices. These include fuel consumption during operations, economic design with trial field tests, the use of recycled industrial by-products for grout mix, improved design, maximising the resiliency of structures and the energy consumption.

6.3.2 Sustainability Aspect of CMCs

The key contribution of CMC technology to the sustainable development is the production of very limited soil cuttings to the ground surface, thanks to the auger that is specially designed to displace soils laterally. This feature is particularly useful for construction projects involving contaminated or landfill sites, making CMC a cost-effective ground improvement technique associated with the reduction of cost for spoil disposal and handling compared to the contiguous flight auger (CFA) piling or bored piles (Masse et al. 2011; Walker, Masse & Swift 2011). Besides performing well in soft or loose soils, CMC is also suitable for soils with significant organic content or acid sulphate

soils. Integrity pile testing by Kirstein & Wittorf (2013) indicated that CMC can also be performed well in very soft soils although additional vertical drains had to be installed in the soft soil surrounding the columns. Environmental benefits can also be achieved through a vibration free and quasi-static installation process, as opposed to dynamic vibratory methods e.g. stone columns or driven piles. This allows CMC to be installed near sensitive structures.

The second advantage of CMC over other traditional methods is associated with a high production rate, which means overhead cost saving and suitable for projects with tight construction schedules. Hole drilling and concrete injection are carried out in one go without risk of hole collapses. Experience shows that many bored piling projects suffered extended delay due to the unforeseen ground conditions. CMC column strength develops quickly, does not rely on the surrounding soil strength, and is effective in settlement control. Hence, CMC is often selected to support bridge approach embankment, to fast track the bridge construction (Plomteux & Lacazedieu 2007; Plomteux, Porbaha & Spaulding 2004).

Thirdly, with CMC, saving can be achieved by various ways. Using displacement auger, the risk of necking is minimised leading to saving in the volume of injected grout. The load transfer layer functions in place for a more costly structural pile caps and concrete slabs. Fok et al. (2012) indicated that a 10 to 15% cost saving was achieved by using CMC compared to the deep soil mixing technique. Sometimes up to 30% in saving could be achieved (Angelo 2007). When making a judgement in terms of time, cost and long term performance (Higgins 2014), it is considered that CMC may be positioned between deep soil mixing and piling with quick results and lower post-construction settlement.

When scoring sustainability for a ground improvement method, the estimated carbon footprint can often be an important indicator. Carbon footprint is the sum of all emissions of CO_2 in a year, induced by ground improvement activities and by the production of materials used in construction. The estimated carbon footprint from CMC operation and associated materials was 25% lower than those calculated for traditional piling methods (Masse et al. 2011; Spaulding, Masse & LaBrozzi 2008; Walker, Masse & Swift 2011). Those emissions were calculated assuming no steel is used for CMC and that production of steel generally emits more carbon dioxide than cement related products.

Today, access to new tools to assess several environmental indicators for various competing solutions allows for the rapid comparison of ground improvement techniques and assists both contractors and clients in retaining the "best for project" schemes. Figure 6.11 illustrates such a comparison being performed on a range of solutions in accordance with the European Norm 15804.

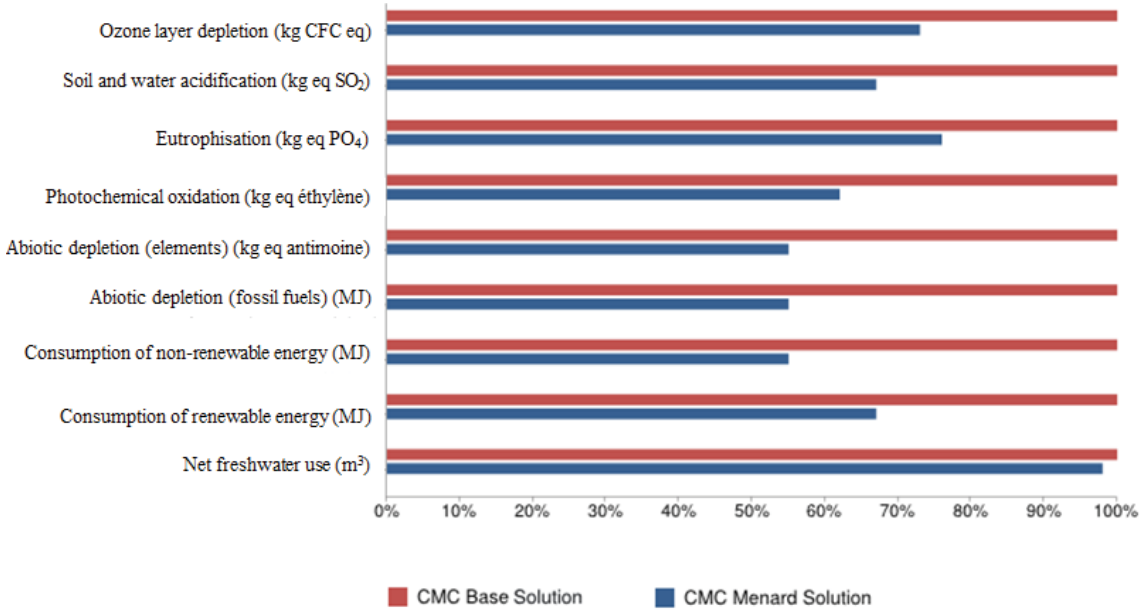

Figure 6.11 NF EN 15804 Indicators – Comparison of various CMC schemes (Prism solution – courtesy of Menard Bachy)

Sustainable development also means design for durability and robustness to maximise the future resilience of a structure. The quality of CMC columns is subject to a real-time monitoring system where installation parameters are recorded, allowing the operator to adjust the drill rate and installation depths, in combination with prior column design and drawings. This is particularly important for a site having a varying ground profile with depth and/or with heterogeneous soils. The durability of the grout columns within a specific design life also relates to the properties of the mix i.e. the ability of the columns to resist chemic attack and weathering. Although the grout column will somewhat deteriorate with time, the addition of fly ash can improve column durability. In fact, grout incorporating high volume fly ash was found to create grout columns with very low permeability and a high resistance to the passage of chloride ions (Bilodeau et al. 1994).

Every ground improvement method serves just a limited number of purposes. Decision making in the selection of ground improvement methods will have to rely on the project requirement, local sustainability policies, ground, site conditions and others. Specifically,

within its functions, there are still areas for future development of CMC, which will be discussed in the next section.

6.3.3 Potential Development in Terms of Sustainability for CMC

Many potential development approaches can be underlined when dealing with sustainability for controlled modulus columns (CMC). They are summarised in this section.

6.3.3.1 Economic Design

Economic design, an important aspect of sustainable development, can be achieved by various ways. In a CMC system, the load transfer layer provides arching effects, allowing structural or embankment loads to be transferred to the columns and to the founding stratum. Wong & Muttuvel (2012b) carried out a limited study, indicating that it may be possible to reduce the thickness of the load transfer layer and the use of geotextiles for embankments that are sufficiently high. Similarly, for warehouse building constructions, due to the presence of the concrete floor slabs, geogrid reinforcement was rarely placed within the load transfer layer (Masse et al. 2011). Such economic designs are currently carried out on a case-by-case basis and no standardised method has been proposed. In fact, if the load transfer layer is not provided, the soil arching developed in the embankment fill alone may break due to traffic dynamic loads, seismic effects and flooding. Further rigorous numerical and experimental investigations are required.

In medium to large projects, the economic design proposal can be confirmed by construction of CMC test pads. The purposes of the test pads are not only to optimise the final design but also for the design optimisation in future projects. According to Farouz

(2014), with every $1 spent for the rigid inclusion test pads, $4 of savings could be achieved in the long run.

6.3.3.2 Grout Mix Design

Grout mix design may be modified with further considerations of using industrial by-products such as ground blast-furnace slag, coal ash and fly ash with various contents, depending on the design strength requirements. The most appropriate grout mix for good pumpability is a specially designed lean sand-mix mortar or pea-gravel concrete, often with fly ash to increase workability. Concrete has been considered less costly than grout and has been increasingly used in the US and Europe for CFA and displacement columns (Brown, Thompson & Lazarte 2007). Whether concrete or grout, the mix producers should make more use of local materials rather than importing in order to reduce the transport cost and fuel consumption. To increase tensile strength for columns, some recycled fibres such as polypropylene and recycled carpet may be added to the grout mix. The addition of fibres was found to reduce the cement content for stabilising poor clayey soils, particularly for applications associated deformations under seismic loading (Fatahi et al. 2013). Sustainability relates to savings in design and building resilient structures; however, such designs should have sufficient testing and verification to meet strength and durability requirements.

6.3.3.3 Installation Effects

The installation effects are rarely considered to estimate columns' skin friction capacity. Designers seem to have little confidence in the use of increased soil parameters in the actual design and no systematic approach has been established. In fact, most CMC or rigid inclusions in general, are installed through soft or loose soils and founded on stiffer founding stratum. The installation of displacement columns, despite causing compaction

effects, usually creates a thin smeared or disturbed zone around the columns, depending on the type of auger and soil types. For column installation in loose sands, soils are densified everywhere immediately after installation. For clayey soils, strength gain and column set-up can be achieved at later stages depending on the amount of generated excess pore water pressure (Carter, Randolph & Wroth 1980). A recent numerical study was carried out by Rivera et al. (2014) to study the increase in the radial effective stress σ_r' and the earth pressure coefficients K in clayey soils due to CMC installation. Figure 6.12 shows some increase in K value at the end of construction within a zone of up to 10 times column radius r_0. Although the results of this study are very useful, field test and performance verification have not been carried out. Further studies should be accompanied by thorough site investigation before CMC design and employing recent technology advancement e.g. the French ASIRI National Project (2012).

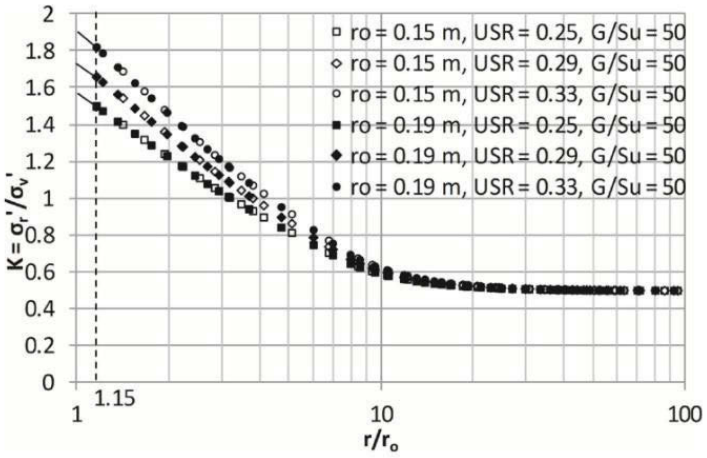

Figure 6.12 Distribution of radial effective stress in terms of K at the end of construction with varying CMC radius r_0, varying undrained strength ratio (USR = s_u/σ'_v) and a constant soil rigidity index G/s_u of 50 (Rivera et al. 2014)

6.3.3.4 CMC for Expansion Soils

The performance of CMC installed in expansive soils is unknown. Although deep columns can be designed to bypass such soil horizons, CMC should also be able to resist

potential tension and uplift effects. While CMC is non-reinforced and relatively weak in tension, the shaft may fail under excessive tension and the column may move upwards when the clay expands (Manjriker 2006). In such cases, one of the possible solutions would be to add fibre reinforcement to the grout mix to provide additional tensile strength for the columns. In fact, it was found that the tensile strength of the cement-treated clay increased with the addition of carpet fibres (Fatahi, Khabbaz & Fatahi 2012; Nguyen, Fatahi & Khabbaz 2014). Figure 6.13 presents a sample of cement-treated clay with added geofibres.

Figure 6.13 A typical fibre reinforced cement-treated clay sample (photo courtesy of Dr Lam Nguyen)

6.3.3.5 CMC subject to Slope Instability and Seismic Loadings

Sustainable development also means design to maximise the future resilience of a structure against slope instability and seismic loadings. CMC is typically non-reinforced and often designed to mainly support uniform vertical loading. If CMC columns are

located at the batter of the embankment, or subject to seismic events, the column capacity to resist negative bending moment may be of particular concern. Under such non-vertical or dissymmetric loading, the excessive shear forces and bending moments may be induced.

To support reinforced soil wall (RSW) blocks at a site near Newcastle, one of the seismically active zones in Australia, the outer rows of CMC were reinforced with steel bars (Wong & Muttuvel 2011). High strength grout may be required if additional strength is required to resist cracks developed in negative bending resisting elements. In addition to the capacity of CMC columns, quality and thickness of the Load Transfer Platform strongly affect the intensity of shear forces and bending moments in the columns, and therefore the behaviour of the foundation, under seismic effects (Simon 2012). Similar to design approach using micropiles presented in the French national project on micropiles (Juran & Weinstein 2008), some CMC columns may be installed symmetrically inclined in small angles to make use of the axial capacity. If implemented, this solution may potentially replace other costly solutions such as using larger and/or reinforced columns. The use of CMC or other rigid inclusions in seismic related projects is still a general concern to the designers, demanding a set of general design guidelines.

6.3.3.6 Carbon Footprint

The amount of carbon footprint from a CMC system is generally less than other traditional piling methods. CMC columns normally have smaller diameters compared to typical bored piles. In addition, CMC columns are not normally designed to socket into hard stratum. Considering only the diesel consumption of the machinery during installation, however, displacement methods may require larger torque and vertical force than using continuous flight auger methods for an equivalent column diameter. Research by

NeSmith & Fox (2009) indicated that the installation effort required to drill a new hole adjacent to the previously drilled hole was higher due to densified soils caused by the installation effects. While CMC auger has been optimised to significantly reduce the soil resistance, future research on auger geometry would further reduce soil resistance and hence the energy consumption.

The environmental impacts of a pile foundation and the CMC soil treatment solution were compared by Masse, Parinella & Wyman (2011), which shows that a 25% reduction in the carbon footprint of the foundations can be achieved by adopting CMCs instead of deep pile foundations. The comparison in the carbon footprint as shown in Figure 6.14 was based on the difference in quantity and carbon footprint values for the concrete, timber, steel, and grout for use in constructing the piles and the CMCs only. CMC ground treatment solution resulted in a substantial reduction in equivalent carbon emission as compared to the original pile foundations. The authors noted that this carbon footprint assessment does not include any benefits of the accelerated schedule associated with adoption of CMC, nor with the additional carbon footprint required to dispose and decontaminate of potentially contaminated soils associated with the deep foundation scheme. In general, the authors suggested that an approximate total reduction in carbon footprint ranging from 35% to 50% may be achieved with the CMC alternate design.

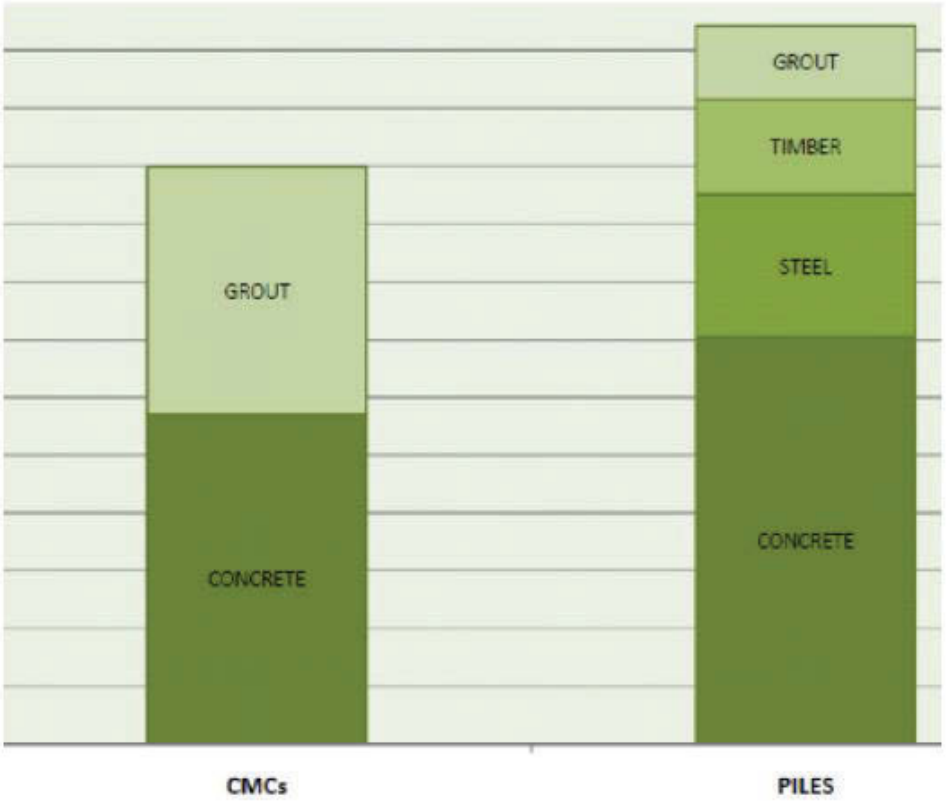

Figure 6.14 Equivalent carbon comparison between CMCs and Piles (after Masse et al. (2011))

Spaulding, Masse & LaBrozzi (2008) analysed the carbon footprint for a luxury townhouse project (68 units) in Weehawken, New Jersey USA. The site was underlain by a stiff upper layer of urban fill underlain by up to 23 m of highly compressible organic silts and clays. The deep driven piles to be founded at 33 m depth was originally required. The alternative solution using CMC would mean that the column can be socketed at much shallow depths (23 m in this project). Carbon emissions of using driven H-piles with a structural slab in comparison with that of the solution consisting of CMCs supporting a slab-on-grade were estimated. CMC solution produced a total emission of 1857 t eq. C, half of that of the driven pile foundations. Interestingly, this reduction in emission could offset the environmental impact of the residents who would live in the newly built town houses for two and a half years.

According to Inclusol (2010), a substantial reduction of carbon consumption of up to 30% by can be achieved by adopting rigid inclusions (a general foundation term for CMCs) instead of traditional pile foundations. This assessment was made for a water sport centre close to River Loire in the West of France. The distributed load on slab varied between 5 and 20 kPa. Originally, the piles were required due to the thickness of very compressible colluviums and thick low to medium dense sands and clayey sands. The original solution required 1784 linear metre of piles, beams, formwork, and suspended floors while the new rigid inclusion solution (i.e. rigid inclusions) involved 4466 linear metre of inclusions, load transfer mattress, slabs on grade and strip/base footings. The total iron used for rigid inclusion solution only accounted for about 10% of the total iron used for pile solutions. The calculated total impact on global warming expressed in terms of Carbon Dioxide (CO_2) Equivalent was 196 for piles and 137 for rigid inclusions (t eq. $C0_2$), which corresponded to a 30% reduction for using rigid inclusions.

6.3.3.7 Large Soil Displacement due to CMC Installation

Although CMC is a vibration free method, large displacement caused by the installation process could cause damage to the surrounding built environment (Brown 2005) if proper installation sequence is not considered during implementation. If the soil deformation is excessive, the shape of the adjacent CMC may not be maintained, leading the reduction in the bending stiffness. This concern, relevant to sustainable development, will be presented in the following section. Recommendations for the required improvement in predicting lateral displacement and simulation of the CMC installation are provided.

6.3.4 Summary

The evaluation of controlled modulus column (CMC) technology with respect to the sustainability has been taken into consideration. Evidently, CMC provides a sustainable

solution to the ground engineering including eliminating cost for spoil disposal, a high production rate, project saving with displacement methods and load transfer layers, controlled quality and durability, and lower carbon emission in comparison to piling. Research directions to improve CMC for sustainable development have also been discussed including economic design with trial field tests, the use of recycled industrial by-products for grout mix, rigorous design, maximising the resiliency of structures and the energy consumption during operations.

CHAPTER 7 Conclusions and Recommendations for Future Research

This final chapter consisted of three parts. Section 7.1 provides a summary of the contents of this thesis, Section 7.2 summarises the main conclusions of this research work, and Section 7.3 proposes a number of potential studies for future research.

7.1 Summary

The review of literature indicated that the installation of soil-displacement columns, such as controlled modulus columns (CMC) as a ground improvement technique, displaced the soils surrounding the columns and affected the previously installed columns. The review suggested that installation sequences be optimised to curtail the impact of ground improvement on the performance of previously installed columns. Therefore, the first part of this research study was carried out to investigate how groups of CMCs installed in different sequences could affect previously installed columns. Two different column installation sequences were adopted. Appropriate material models were adopted for CMC and soft soil. Coupled consolidation analyses in large strain mode, incorporating soil-CMC interaction were carried out using finite difference code *FLAC*^{3D}. The creation of CMCs was based on the idea of combined cylindrical and spherical cavity expansions. The numerical approach adopted was validated using the results of the laboratory model test and a number of existing analytical methods. The effects of using different column installation sequences on the lateral soil movement, soil heave and maximum excess pore

water pressures near existing CMCs and on the predicted bending moments generated in the existing columns induced by installing new columns were investigated. In addition, the study highlights the effects of curing periods on the performance of already installed concrete columns under the impact of installing new nearby columns.

The second major component of this research focused on the experimental aspects of soil-displacement columns, with particular interest on the installation effect on the early age concrete inclusions. A large-scale laboratory model test was carried out to study the soil behaviour and the response of a newly formed concrete column subjected to ground movement induced by installing surrounding columns. A pile penetration system and a soil tank instrumented with state-of-the-art soil instrumentation have been designed and constructed for installing seven reduced scale concrete column, which were cast in-situ in soft soil from low strength concrete using a displacement piling method. A network of strain gauges were embedded inside the concrete inclusion to measure the column bending moment, which was made possible by coining an innovative electrical circuit to reduce the volume of lead wires of the strain gauges. Accumulated soil heave measured by 3D scanning, the stress change and the excess pore water pressure in the soil, together with the uplift and the bending moment of the affected column were reported.

7.2 Conclusions

7.2.1 Effects of Installation Sequences on Previously Installed Concrete Columns

The outcome of the study presented in Chapter 3 revealed several aspects of column installation effects and sequences of installation that are difficult to observe by regular field and laboratory means:

- The lateral displacement of soil induced by installing a single CMC extends beyond the two CMCs previously installed in a row nearby. Thus, if two adjacent columns are constructed in quick succession, the induced lateral displacement could accumulate and extend to the next three adjacent columns.
- For the installation Sequence No. 1 and No. 2 depicted in Figure 3.2, the lateral movement of in-situ soil and soil heave near the existing CMCs due to installation Sequence No. 2 were greater than Sequence No. 1 by approximately 15% and 25%, respectively.
- During the installation of adjacent CMCs, most of the soil heave near the existing CMCs occurred in the upper half of the soft soil layer, and continued for weeks after installation. In fact, four weeks after installation, post-installation surface heave accounted for 10% of ground heave generated during installation.
- The maximum induced excess pore water pressure generated in the front face of existing CMCs due to installation Sequence No. 2 was almost twice as much that caused by installation Sequence No. 1. The influence zone of excess pore water pressure induced by CMC installation was narrower than the lateral displacement and soil heave.

- Consolidation analysis should be included when assessing the effect of installation and the build-up of excess pore water pressure as construction proceeds to account for the lag between the installations of two successive CMCs.
- During installation, the soil surface heave was approximately three times more than the column head uplifts. The ground movement induced by the installation of new CMCs can cause an uplift of existing CMCs by approximately 2% of their diameter (D) at the column head and approximately 0.01D at the tip. CMCs continued to heave for a couple of days after installation and then settled as the soil consolidated. The ensuing uplift may require a short-term surcharge to allow the column to settle back to depth specified in the design.
- The predicted bending moments generated in existing CMCs due to installation Sequence No. 2 were almost 22% more than the corresponding values from Sequence No. 1. The bending moment induced in existing CMC due to nearby installation decreased by almost 8% after three weeks of stress equilibrium and soil consolidation.
- Subject to loadings from nearby installations, the maximum bending moment induced in a one day old CMC occurred at the interface of soft and stiff clay; however when cured for 28 days the maximum bending moment of CMCs shifted up towards the soft clay layer.
- The existing CMC E2 at its 28-day strength experienced approximately 50% more maximum bending moments due to Sequence No. 2 than the corresponding value predicted due to Sequence No. 1 (i.e. when installing away from the existing CMCs).

7.2.2 Responses of Early Age Concrete Inclusions Subject to Nearby Installations

Based on the results of the laboratory model test presented in this Chapter 4, the following conclusions can be drawn:

- The uplift of the existing concrete column after one-day curing induced by the surrounding installations halved the amount of soil heave induced midway between the columns. However, the magnitude of uplift experienced by the existing concrete column at its very early age (i.e. less than 3 hour curing period) induced by the surrounding installations was similar to the surface heave of the surrounding soil.
- The amount of uplift experienced by the central column induced by each subsequent installation was similar.
- The uplift of a column base was associated with a large amount of suction at the base of the column. However, as the installation progressed, the suction reduced.
- Excess pore water pressure increased as more columns were installed, but reduced during the time lag between two columns.
- Lateral loadings generated by the installation of the surrounding columns could affect the integrity of the existing column, especially at early age.
- The results of the model test can be used as suitable data for future computer modelling in the authors' follow up paper.

Although the model test was performed at $1g$ and at corresponding low stress level, it is believed that the observation of mechanisms of the response of the rigid inclusions and soils, which was the prime emphasis of this study, will still be relevant.

7.2.3 Effects of Pile Penetration in Comparison with Cavity Expansion Numerical Modelling

In Chapter 5, the validation of the numerical approach adopted in Chapter 3 was conducted using a laboratory model test. The soil responses due to the penetration of a closed-ended circular pile in terms of the soil heave and subsequent consolidation settlement were compared with the 3D large strain numerical approach based on the combined use of the cylindrical and spherical cavity expansions. The numerical simulations conducted using the finite difference code *FLAC*^{3D} included the undrained analyses simulating the jacked pile penetration and the soil consolidation process. The test results indicates that a noticeable delay in the arrival of the maximum pore water pressures was observed at the monitoring points. The measured soil displacement and the evolution of the excess pore water pressure were represented well by the proposed numerical model. The results provide valuable insights into the installation of jacked-in piles in soft clays, and are valuable source of validation materials for more complex numerical simulations.

7.2.4 Practical and Construction Aspects of CMC Installation Effects

The results of a numerical study was presented to investigate the responses of the existing bridge pile subject to the installation of nearby CMCs for ground improvement, considering two options of installation sequences. The numerical results shows that undrained excess pore water pressures in front of the bridge pile and the normal stress applied on the bridge pile increase as more CMCs are installed. As the CMCs are longer and the bridge pile is more slender, the lateral pile deflection increases. The results indicated that the lateral pile deflection due to the horizontal soil movement induced by the CMC installation could be significant. Hence, the study highlights the importance of

accurate assessment of CMC installation effect on the surrounding structures prior to construction, in addition to traditional observation methods commonly adopted during construction.

The evaluation of controlled modulus column (CMC) technology with respect to the sustainability has also been made in Chapter 6. Evidently, CMC provides a sustainable solution to the ground engineering including eliminating cost for spoil disposal and treatment, a high production rate, project saving (with displacement piling methods and load transfer layers), good quality control, and lower carbon emission in comparison to conventional piling. Research directions to improve CMC for sustainable development have also been discussed including economic design with trial field tests, the use of recycled industrial by-products for grout mix, the resiliency of structures and the energy consumption during operations.

7.3 Recommendations for Future Research

This area of research can be further expanded by conducting the following studies:

- This research focused on the soil displacement effects due to idealised cavity expansion (e.g. jacking closed-end circular piles). Future research may employ the reduced-scale hollow stem displacement augers, while concrete pumping can be simulated with an appropriate pressure-controlled pumping system. Aggregate for the grout materials should be sized relative to the inner diameter of the hollow stem auger for pump-ability.
- While it was necessary to balance the numerical accuracy and computational time, fine mesh may lead to heavily distorted mesh. A finite element program incorporating nonlinear analysis and adaptive meshing techniques including Arbitrary Lagrangian

and Eulerian (ALE) or Coupled Eulerian-Lagrangian (CEL) can be used in future research to simulate the pile installation process. In saturated clay, such programs should be able to perform coupled hydraulic mechanical and stress analyses. The alternative solution would be using a three-dimensional discrete element code such as PFC^{3D} with Computational Fluid Dynamics (CFD) solvers, because installation process may be simulated realistically with piles penetrating gradually into the ground surface without any mesh distortion that is often encountered in continuum analyses. It is worth mentioning that the number of particles in PFC^{3D} can be reduced by using smaller particles nearer the auger tips than those further away.

- In the present study, concrete for CMC was modelled by Hoek-Brown plasticity model with tension yield criterion. This model did not include the stiffness degradation and cracking. Future research should attempt to model the columns by concrete damage plasticity model.
- The present numerical simulations for the soil displacement due to installation and subsequent consolidation settlements considered a post-installation period of only 28 days; however, in practice, the surcharge period may be longer. For natural soft soils, creep effects may account for a major component of the long-term settlements, which should be incorporated in future research. The soil modified by column installation process is expected to change the column load capacity with time, which will be largely affected by the long-term creep.
- Time-dependent behaviour of concrete material used in the ground improvement works should be further investigated. Currently such strength development may be modelled using Plaxis 2D and Plaxis 3D version 2018 using the Concrete Model.
- It is recommended that future CMC projects should invest an adequate amount of field instrumentation works before and during column installations and retain a proper

record of column installations as a basis to improve the assessment methods. Future research may test the proposed numerical model against data from real field problems, such as trial embankments, to confirm the validity of the results.

- A number of known assessment methods are currently available to predict soil movements caused by installing soil-displacement columns (CMCs or DDCs). However, universities and engineering consultants should continue to advance the prediction methods, develop practical guidelines for practicing engineers to assess risks during construction stage and incorporate the installation effects on the long term structural and geotechnical designs. It is highly recommend that column installation effects to be included in future design methods of CMC soil treatment.

References

Abreu, D., Jefferson, I., Braithwaite, P. & Chapman, D. 2008, 'Why is sustainability important in geotechnical engineering?', *GeoCongress 2008: Geosustainability and Geohazard Mitigation*, pp. 821-8.

Abu-Farsakh, M., Tumay, M. & Voyiadjis, G. 2003, 'Numerical Parametric Study of Piezocone Penetration Test in Clays', *International Journal of Geomechanics*, vol. 3, no. 2, pp. 170-81.

ACI Committee 318 2014, *Building Code Requirements for Structural Concrete (ACI 318M-14) and Commentary (ACI 318RM-14)*, 0870312642, American Concrete Institute.

Almeida, M.S., Danziger, F.A. & Lunne, T. 1996, 'Use of the piezocone test to predict the axial capacity of driven and jacked piles in clay', *Canadian Geotechnical Journal*, vol. 33, no. 1, pp. 23-41.

Alpan, I. 1967, 'The empirical evaluation of the coefficient K_0 and K_{0r}', *Soils and Foundations*, vol. 7, no. 1, pp. 31-40.

Ambily, A. & Gandhi, S.R. 2007, 'Behavior of stone columns based on experimental and FEM analysis', *Journal of geotechnical and geoenvironmental engineering*, vol. 133, no. 4, pp. 405-15.

Angelo, W.F. 2007, 'Lateral soil displacement gains ground on U.S. projects', *Engineering News-Record*, vol. 258, no. 11, 19 March 2007, p. 16.

Asaoka, A. 1978, 'Observational Procedure of Settlement Prediction', *Soils and Foundations*, vol. 18, no. 4, pp. 87-101.

ASIRI National Project 2012, *Recommendations for the design, construction and control of rigid inclusion ground improvements - Amélioration des sols par inclusions rigides*, Presses des Ponts et Chaussées, Paris.

ASTM 2012, *Standard Test Method for Electronic Friction Cone and Piezocone Penetration Testing of Soils*, ASTM D5778 − 12, ASTM International, West Conshohocken, PA.

ASTM 2016a, *Standard Test Method for Low Strain Impact Integrity Testing of Deep Foundations, D5882 - 16*, ASTM International, West Conshohocken, PA 19428-2959. United States.

ASTM 2016b, *Standard Test Methods for Laboratory Miniature Vane Shear Test for SaturatedFine-Grained Clayey Soil*, ASTM D4648/D4648M-16, ASTM International, West Conshohocken, PA.

Baligh, M.M. 1985, 'Strain path method', *Journal of Geotechnical and Geoenvironmental Engineering*, vol. 111, no. 9, pp. 1108-36.

Bao, X., Morikawa, Y., Kondo, Y., Nakamura, K. & Zhang, F. 2012, 'Shaking table test on reinforcement effect of partial ground improvement for group-pile foundation and its numericalsimulation', *Soils and Foundations*, vol. 52, no. 6, pp. 1043-61.

Basu, P. & Prezzi, M. 2009, *Design and applications of drilled displacement (screw) piles*, 2326-6325, Publication FHWA/IN/JTRP-2009/28. Joint Transportation Research Program, Indiana Department of Transportation and Purdue University, West Lafayette, Indiana.

Basu, P., Prezzi, M. & Salgado, R. 2013, 'Modeling of Installation and Quantification of Shaft Resistance of Drilled-Displacement Piles in Sand', *International Journal of Geomechanics*, vol. 14, no. 2, pp. 214-29.

Bazzar, K., Bouatiaoui, M. & Alaoui, A.H. 2013, 'Performance approach the durability of high volume fly ash concrete', *International Journal of Engineering Science and Innovative Technology*, vol. 2, no. 2, pp. 1-11.

Bergado, D. 1990, 'Settlements of Bangna-Bangpakong Highway on Soft Bangkok Clay', *Journal of Geotechnical Engineering*, vol. 116, no. 1, pp. 136-55.

Bétons de sable 1994, *Caractéristiques et pratiques d'utilisation*, Presses des Ponts, Réalisé sous l'égide du projet national Sablocrete.

Bilodeau, A., Sivasundaram, V., Painter, K. & Malhotra, V. 1994, 'Durability of concrete incorporating high volumes of fly ash from sources in the USA', *ACI Materials Journal*, vol. 91, no. 1, pp. 3-12.

Bishop, R., Hill, R. & Mott, N. 1945, 'The theory of indentation and hardness tests', *Proceedings of the Physical Society*, vol. 57, no. 3, p. 147.

Black, J., Sivakumar, V., Madhav, M. & Hamill, G. 2007, 'Reinforced stone columns in weak deposits: laboratory model study', *Journal of Geotechnical and Geoenvironmental Engineering*, vol. 133, no. 9, pp. 1154-61.

Bolton, M. & Powrie, W. 1987, 'The collapse of diaphragm walls retaining clay', *Géotechnique*, vol. 37, no. 3, pp. 335-53.

Bond, A. & Jardine, R. 1991, 'Effects of installing displacement piles in a high OCR clay', *Géotechnique*, vol. 41, no. 3, pp. 341-63.

Bowles, J.E. 1997, *Foundation analysis and design*, McGraw-Hill, New York.

Brandenberg, S.J., Boulanger, R.W., Kutter, B.L. & Chang, D. 2005, 'Behavior of pile foundations in laterally spreading ground during centrifuge tests', *Journal of Geotechnical and Geoenvironmental Engineering*, vol. 131, no. 11, pp. 1378-91.

Brinkgreve, R., Kumarswamy, S. & Swolfs, W. 2016, 'PLAXIS 3D 2016 Manual', *PLAXIS bv, Delft*.

Brinkgreve, R., Swolfs, W. & Engin, E. 2011, 'PLAXIS 2D Reference manual', *Delft University of Technology and PLAXIS bv The Netherlands*.

Brinkgreve, R. & Vermeer, P. 1999, *Plaxis: finite element code for soil and rock analyses: version 7:[user's guide]*, Balkema.

Brown, D., Thompson, W.R. & Lazarte, C.A. 2007, *Design and construction of continuous flight auger piles*, Federal Highway Administration, United States.

Brown, D.A. 2005, 'Practical considerations in the selection and use of continuous flight auger and drilled displacement piles', *ASCE - Geotechnical Special Publication No 132*, Texas, US, pp. 251-61.

BS EN 1992-1-1 2015, *Eurocode 2: Design of Concrete Structures: Part 1-1: General Rules and Rules for Buildings*, 0580451917, British Standards Institution, UK.

Bustamante, M. & Gianeselli, L. 1998, 'Installation parameters and capacity of screwed piles', *Proceedings of International Geotechnical Seminar on Deep Foundations on Bored and Auger Piles, BAP III. Balkema, Rotterdam*, pp. 95-108.

Cao, L., Teh, C. & Chang, M. 2001, 'Undrained cavity expansion in modified Cam clay I: Theoretical analysis', *Géotechnique*, vol. 51, no. 4, pp. 323-34.

Cao, L.F., Chang, M.-F., Teh, C.I. & Na, Y.M. 2001, 'Back-calculation of consolidation parameters from field measurements at a reclamation site', *Canadian Geotechnical Journal*, vol. 38, no. 4, pp. 755-69.

Carter, J. 1978, *CAMFE, a computer program for the analysis of a cylindrical cavity expansion in soil*, University of Cambridge, Department of Engineering.

Carter, J., Booker, J. & Yeung, S. 1986, 'Cavity expansion in cohesive frictional soils', *Géotechnique*, vol. 36, no. 3, pp. 349-58.

Carter, J.P., Randolph, M.F. & Wroth, C.P. 1979, 'Stress and pore pressure changes in clay during and after the expansion of a cylindrical cavity', *International Journal*

for Numerical and Analytical Methods in Geomechanics, vol. 3, no. 4, pp. 305-22.

Carter, J.P., Randolph, M.F. & Wroth, C.P. 1980, 'Some aspects of the performance of open- and closedended piles', *Numerical methods in offshore piling*, Thomas Telford Publishing, The Institution of Civil Engineers, London, pp. 165-70.

Castro, J. & Karstunen, M. 2010, 'Numerical simulations of stone column installation', *Canadian Geotechnical Journal*, vol. 47, no. 10, pp. 1127-38.

Ceccato, F., Beuth, L. & Simonini, P. 2016, 'Analysis of Piezocone Penetration under Different Drainage Conditions with the Two-Phase Material Point Method', *Journal of Geotechnical and Geoenvironmental Engineering*, vol. 142, no. 12, pp. 04016066 1-15.

Chadwick, P. 1959, 'The quasi-static expansion of a spherical cavity in metals and ideal soils', *The Quarterly Journal of Mechanics and Applied Mathematics*, vol. 12, no. 1, pp. 52-71.

Chai, J.-C., Julfikar Hossain, M., Carter, J. & Shen, S.-L. 2014, 'Cone penetration-induced pore pressure distribution and dissipation', *Computers and Geotechnics*, vol. 57, pp. 105-13.

Chai, J.-C., Miura, N. & Koga, H. 2007, 'Closure to "Lateral Displacement of Ground Caused by Soil–Cement Column Installation" by Jin-Chun Chai, Norihiko Miura, and Hirofumi Koga', *Journal of Geotechnical and Geoenvironmental Engineering*, vol. 133, no. 1, pp. 124-6.

Chai, J. & Carter, J.P. 2012, 'Lateral displacements due to installation of soil-cement columns', *ISSMGE Technical Committee TC 211 International Symposium on Ground Improvement (IS-GI BRUSSELS 2012): Recent Research, Advances & Execution Aspects of Ground Improvement Works: Proceedings of a Meeting held 31 May-1 June 2012, Brussels, Belgium*.

Chai, J., Carter, J.P., Miura, N. & Zhu, H. 2009, 'Improved prediction of lateral deformations due to installation of soil-cement columns', *Journal of geotechnical and geoenvironmental engineering*, vol. 135, no. 12, pp. 1836-45.

Chai, J., Miura, N. & Koga, H. 2005, 'Lateral Displacement of Ground Caused by Soil–Cement Column Installation', *Journal of Geotechnical and Geoenvironmental Engineering*, vol. 131, no. 5, pp. 623-32.

Chai, J.C., Hossain, M.J., Yuan, D., Shen, S. & Carter, J. 2015, 'Pore pressures induced by piezocone penetration', *Canadian Geotechnical Journal*, vol. 53, no. 3, pp. 540-50.

Chaiyaput, S., Bergado, D.T. & Artidteang, S. 2014, 'Measured and simulated results of a Kenaf Limited Life Geosynthetics (LLGs) reinforced test embankment on soft clay', *Geotextiles and Geomembranes*, vol. 42, no. 1, pp. 39-47.

Chatte, R. & Lauzon, M. 2011, 'Embankment Construction Using Controlled Modulus Columns for Nouvelle Autoroute 30 Project in Beauharnois (Qc)', *Proceedings of the Pan-American Canadian Geotechnical Society-Geotechnical Conference*, Toronto, Ontario, Canada, pp. 2-6.

Chen, J.-F., Han, J., Oztoprak, S. & Yang, X.-M. 2009, 'Behavior of single rammed aggregate piers considering installation effects', *Computers and Geotechnics*, vol. 36, no. 7, pp. 1191-9.

Chen, S. & Abousleiman, Y. 2012, 'Exact undrained elasto-plastic solution for cylindrical cavity expansion in modified Cam Clay soil', *Géotechnique*, vol. 62, no. 5, pp. 447-56.

Chen, S. & Abousleiman, Y. 2016, 'Drained and undrained analyses of cylindrical cavity contractions by Bounding Surface plasticity', *Canadian Geotechnical Journal*, vol. 53, no. 9, pp. 1398-411.

Chen, S.L. & Liu, K. 2018, 'Undrained cylindrical cavity expansion in anisotropic critical state soils', Géotechnique.

Chou, W.-I. & Bobet, A. 2002, 'Predictions of ground deformations in shallow tunnels in clay', *Tunnelling and Underground Space Technology*, vol. 17, no. 1, pp. 3-19.

Chow, Y. & Teh, C. 1990, 'A theoretical study of pile heave', *Géotechnique*, vol. 40, no. 1, pp. 1-14.

Cirión, A., Paulín, J., Racinais, J. & Glandy, M. 2013, 'Displacement rigid inclusions', *The 18th International Conference on Soil Mechanics and Geotechnical Engineering: Challenges and Innovations in Geotechnics*, vol. 1, ISSMGE, Paris, pp. 2453-5.

Clough, G.W., Rad, N.S., Bachus, R.C. & Sitar, N. 1981, 'Cemented sands under static loading', *Journal of the Geotechnical Engineering Division*, vol. 107, no. 6, pp. 799-817.

Cognon, J.M. 2004, *Concrete pile made of such a concrete and method for drilling a hole adapted for receiving the improved concrete pile in a weak ground*, U.S. Patent US 6,672,015.

Collins, I.F. & Yu, H.S. 1996, 'Undrained cavity expansions in critical state soils', *International Journal for Numerical and Analytical Methods in Geomechanics*, vol. 20, no. 7, pp. 489-516.

Comodromos, E.M., Papadopoulou, M.C. & Rentzeperis, I.K. 2009, 'Effect of Cracking on the Response of Pile Test under Horizontal Loading', *Journal of Geotechnical and Geoenvironmental Engineering*, vol. 135, no. 9, pp. 1275-84.

Cooke, R., Price, G. & Tarr, K. 1979, 'Jacked piles in London Clay: a study of load transfer and settlement under working conditions', *Géotechnique*, vol. 29, no. 2, pp. 113-47.

Cortellazzo, G. & Simonini, P. 2001, 'Permeability evaluation and its implications for consolidation analysis of an Italian soft clay deposit', *Canadian geotechnical journal*, vol. 38, no. 6, pp. 1166-76.

Craig, W. 1985, 'Modeling pile installation in centrifuge experiments', *11th International Conference on Soil Mechanics and Foundation Engineering*, vol. Golden jubilee, CRC Press San Francisco, US, pp. 1101-4.

Dassault Systemes 2017, *Abaqus/CAE Online Documentation*, <http://help.3ds.com/2017/English/DSSIMULIA_Established/SIMULIA_Established_FrontmatterMap/DSDocAbaqus.htm?ContextScope=all&id=06bd125b77f8472aa38e1f33fd8ecf1a#Pg0&ProductType=DS&ProductName=DSSIMULIA_Established>.

Dijkstra, J., Broere, W. & Heeres, O.M. 2011, 'Numerical simulation of pile installation', *Computers and Geotechnics*, vol. 38, no. 5, pp. 612-22.

Doherty, P., Igoe, D., Murphy, G., Gavin, K., Preston, J., McAvoy, C., Byrne, B.W., McAdam, R., Burd, H.J., Houlsby, G.T., Martin, C.M., Zdravković, L., Taborda, D.M.G., Potts, D.M., Jardine, R.J., Sideri, M., Schroeder, F.C., Muir Wood, A., Kallehave, D. & Skov Gretlund, J. 2015, 'Field validation of fibre Bragg grating sensors for measuring strain on driven steel piles', *Géotechnique Letters*, vol. 5, no. 2, pp. 74-9.

Dyson, G.J. & Randolph, M. 2001, 'Monotonic Lateral Loading of Piles in Calcareous Sand', *Journal of Geotechnical and Geoenvironmental Engineering*, vol. 127, no. 4, pp. 346-52.

Elkadi, A.S.K., van Lottum, H. & Luger, H.J. 2014, 'A 3D coupled Eulerian-Lagrangian analysis of the dynamic interaction of jack-up legs with the seabed', *Numerical Methods in Geotechnical Engineering*, CRC Press, pp. 1255-9.

Elkington, J. 1997, 'Cannibals with forks', *The triple bottom line of 21st century*.

Engin, H.K., Brinkgreve, R.B.J. & van Tol, A.F. 2015, 'Simplified numerical modelling of pile penetration – the press-replace technique', *International Journal for Numerical and Analytical Methods in Geomechanics*, vol. 39, no. 15, pp. 1713-34.

Fang, Z. & Yin, J. 2007, 'Responses of Excess Pore Water Pressure in Soft Marine Clay around a Soil–Cement Column', *International Journal of Geomechanics*, vol. 7, no. 3, pp. 167-75.

Farouz, E. 2014, 'CBIS Project- Ground Improvement Approach CH2MHill', paper presented to the *GEO-Omaha 2014*, Scott Conference Center, Omaha, Nebraska.

Fatahi, B., Fatahi, B., Le, T. & Khabbaz, H. 2013, 'Small-strain properties of soft clay treated with fibre and cement', *Geosynthetics International*, vol. 20, no. 4, pp. 286-300.

Fatahi, B., Khabbaz, H. & Fatahi, B. 2012, 'Mechanical characteristics of soft clay treated with fibre and cement', *Geosynthetics International*, vol. 19, no. 3, pp. 252-62.

Finnie, I. & Randolph, M. 1994, 'Punch-through and liquefaction induced failure of shallow foundations on calcareous sediments', *International Conference on Behaviour of Offshore Structures, Boston, MA*, pp. 217-30.

Fok, N., Qiu, T., Vincent, P. & Kreminsky, M. 2012, 'A case study of ground improvement using semi-rigid inclusions for breakwater road bridge', *International Conference on Ground Improvement and Ground Control*, ed. C.R.a.J.S.V. Buddhima Indraratna, Research Publishing Services, Wollongong, pp. 629-43.

Fulton Hogan 2013, *Gerringong Upgrade Project - Mt Pleasant to Toolijooa Road*, <http://www.fultonhogan.com/Global/EPL%20Reports/EPL%20Monthly%20Report%20Aug%202013.pdf>.

Ghosh, B., Fatahi, B. & Khabbaz, H. 2016, 'Analytical Solution to Analyze LTP on Column-Improved Soft Soil Considering Soil Nonlinearity', *International Journal of Geomechanics*, vol. 17, no. 3, p. 04016082.

Golden Software, L. 2017, 'Surfer version 15.1 - Contouring, Gridding, and 3D Surface Mapping Software. ', Golden, Colorado 80401-1866.

Guetif, Z., Bouassida, M. & Debats, J.M. 2007, 'Improved soft clay characteristics due to stone column installation', *Computers and Geotechnics*, vol. 34, no. 2, pp. 104-11.

Guo, F. & Lehane, B. 2016, 'Lateral response of piles in weak calcareous sandstone', *Canadian Geotechnical Journal*, vol. 53, no. 9, pp. 1424-34.

Hagerty, D.J. & Peck, R.B. 1971, 'Heave and lateral movements due to pile driving', *Journal of the Soil Mechanics and Foundations Division*, vol. 97, no. 11, pp. 1513-32.

Hamann, T., Qiu, G. & Grabe, J. 2015, 'Application of a Coupled Eulerian–Lagrangian approach on pile installation problems under partially drained conditions', *Computers and Geotechnics*, vol. 63, pp. 279-90.

Hamidi, B., Masse, F., Racinais, J. & Varaksin, S. 2016, 'The boundary between deep foundations and ground improvement', *Proceedings of the Institution of Civil Engineers-Geotechnical Engineering*, vol. 169, no. 2, pp. 201-13.

Han, J. & Gabr, M.A. 2002, 'Numerical Analysis of Geosynthetic-Reinforced and Pile-Supported Earth Platforms over Soft Soil', *Journal of Geotechnical and Geoenvironmental Engineering*, vol. 128, no. 1, pp. 44-53.

Han, W., Liu, S., Zhang, D. & Zhou, H. 2011, 'Characteristics Analysis of Cavity Expansion with Anisotropic Initial Stress in a Two-Dimensional Numerical Model', *Geo-Frontiers 2011: Advances in Geotechnical Engineering*, ASCE, pp. 4186-94.

He, B., Wang, L. & Hong, Y. 2016, 'Capacity and failure mechanism of laterally loaded jet-grouting reinforced piles: Field and numerical investigation', *Science China Technological Sciences*, vol. 59, no. 5, pp. 763-76.

Hewitt, P., Summerell, S.J. & Huang, Y. 2009, 'Bridge Approach Treatment Works on the Coopernook to Herons Creek Section of the Pacific Highway Upgrade', *Sydney Chapter annual symposium, Geosynthetics-New materials for modern infrastructure*, Australian Geomechanics Society, Sydney, pp. 51-60.

Hewlett, W.J. & Randolph, M.F. 1988, 'Analysis of piled embankments', *Ground engineering*, vol. 21, no. 3, pp. 12-8.

Higgins, R.B. 2014, 'Pacific Highway - Create public value for money', Presentation for Roads Australia.

Hill, R. 1950, *The mathematical theory of plasticity*, vol. 11, Oxford university press.

Hird, C., Ni, Q. & Guymer, I. 2011, 'Physical modelling of deformations around piling augers in clay', *Géotechnique*, vol. 61, no. 11, pp. 993-9.

Ho, L., Fatahi, B. & Khabbaz, H. 2014, 'Analytical solution for one-dimensional consolidation of unsaturated soils using eigenfunction expansion method', *International Journal for Numerical and Analytical Methods in Geomechanics*, vol. 38, no. 10, pp. 1058-77.

Hoek, E. & Brown, E.T. 1980, 'Empirical strength criterion for rock masses', *Journal of Geotechnical and Geoenvironmental Engineering*, vol. 106, no. GT9 - ASCE 15715, pp. 1013-35.

Hoek, E. & Brown, E.T. 1997, 'Practical estimates of rock mass strength', *International Journal of Rock Mechanics and Mining Sciences*, vol. 34, no. 8, pp. 1165-86.

Holmberg, S. 1979, 'Bridge approaches on soft clay supported by embankment piles', *Geotechnical Engineering*, vol. 10, no. 1, pp. 77-89.

Holt, D.G.A., Chapman, D.N., Jefferson, I. & Braithwaite, P.A. 2010, 'Sustainable Geotechnical Design', *GeoFlorida 2010: Advances in Analysis, Modeling & Design*, pp. 2925-32.

Hsi, J. 2008, 'Bridge Approach Embankments Supported on Concrete Injected Columns', *GeoCongress 2008: Geosustainability and Geohazard Mitigation*, New Orleans, Louisiana, United States, pp. 612-9.

Huang, C.-H., Lin, S.-K., Chang, C.-S. & Chen, H.-J. 2013, 'Mix proportions and mechanical properties of concrete containing very high-volume of Class F fly ash', *Construction and Building Materials*, vol. 46, pp. 71-8.

Huang, J. & Han, J. 2009, '3D coupled mechanical and hydraulic modeling of a geosynthetic-reinforced deep mixed column-supported embankment', *Geotextiles and Geomembranes*, vol. 27, no. 4, pp. 272-80.

Huang, W., Sheng, D., Sloan, S.W. & Yu, H.S. 2004, 'Finite element analysis of cone penetration in cohesionless soil', *Computers and Geotechnics*, vol. 31, no. 7, pp. 517-28.

Ilyas, T., Leung, C.F., Chow, Y.K. & Budi, S.S. 2004, 'Centrifuge Model Study of Laterally Loaded Pile Groups in Clay', *Journal of Geotechnical and Geoenvironmental Engineering*, vol. 130, no. 3, pp. 274-83.

Inclusol, D.f.i. 2010, 'The ecoconomic and sustainability benefits of rigid inclusions'.

Indraratna, B., Balasubramaniam, A. & Sivaneswaran, N. 1997, 'Analysis of settlement and lateral deformation of soft clay foundation beneath two full-scale embankments', *International Journal for Numerical and Analytical Methods in Geomechanics*, vol. 21, no. 9, pp. 599-618.

Itasca 2012, *FLAC3D - Fast Lagrangian Analysis of Continua in 3 Dimensions, Version 5.01, User's Guide manual*, Itasca Consulting Group, Incorporated., Minneapolis.

Jaeger, R., DeJong, J. & Boulanger, R. 2011, 'Cylindrical Cavity Expansion Analysis of Variable Penetration Rate Cone Penetration Testing Using an Anisotropic Soil Model', *Geo-Frontiers 2011*, American Society of Civil Engineers, pp. 2288-97.

Jefferson, I., Hunt, D.V., Birchall, C.A. & Rogers, C.D. 2007, 'Sustainability indicators for environmental geotechnics', *PROCEEDINGS-INSTITUTION OF CIVIL ENGINEERS ENGINEERING SUSTAINABILITY*, vol. 160, INSTITUTION OF CIVIL ENGINEERS, p. 57.

Jenck, O., Dias, D. & Kastner, R. 2009, 'Three-Dimensional Numerical Modeling of a Piled Embankment', *International Journal of Geomechanics*, vol. 9, no. 3, pp. 102-12.

Juran, I. & Weinstein, G. 2008, *Forever-Synthesis of the Results and Recommendations of the French National Project on Micropiles.*, Schnabel Engineering: Dallas TX.

Karam, G. & Tabbara, M. 2009, 'Hoek–Brown strength criterion for actively confined concrete', *Journal of Materials in Civil Engineering*, vol. 21, no. 3, pp. 110-8.

Kelesoglu, M.K. & Springman, S.M. 2011, 'Analytical and 3D numerical modelling of full-height bridge abutments constructed on pile foundations through soft soils', *Computers and Geotechnics*, vol. 38, no. 8, pp. 934-48.

Kelly, R., Muttuvel, T. & Chan, K. 2011, 'Lateral Displacements in Soft Soil Due to Installation of Vibro-Stone Columns Using the Dry Method', *Geo-Frontiers Congress 2011*, ASCE, Dallas, Texas, United States, pp. 549-56.

Kelly, R.B., Pineda, J.A., Bates, L., Suwal, L.P. & Fitzallen, A. 2017, 'Site characterisation for the Ballina field testing facility', *Géotechnique*, vol. 67, no. 4, pp. 279-300.

Khalili, N. & Khabbaz, M. 1998, 'A unique relationship of chi for the determination of the shear strength of unsaturated soils', *Geotechnique*, vol. 48, no. 5.

Khoshghalb, A. & Khalili, N. 2013, 'A meshfree method for fully coupled analysis of flow and deformation in unsaturated porous media', *International Journal for Numerical and Analytical Methods in Geomechanics*, vol. 37, no. 7, pp. 716-43.

Kim, B.T., Kim, N.-K., Lee, W.J. & Kim, Y.S. 2004, 'Experimental load transfer curves of laterally loaded piles in Nak Dong River sand', *Journal of Geotechnical and Geoenvironmental Engineering*, vol. 130, no. 4, pp. 416-25.

Kim, K., Prezzi, M., Salgado, R. & Lee, W. 2008, 'Effect of Penetration Rate on Cone Penetration Resistance in Saturated Clayey Soils', *Journal of Geotechnical and Geoenvironmental Engineering*, vol. 134, no. 8, pp. 1142-53.

Kim, S., Burd, H.J. & Milligan, G. 1998, 'Model testing of closely spaced tunnels in clay', *Géotechnique*, vol. 48, no. 3, pp. 375–88.

King, D.J., Bouazza, A., Gniel, J.R., Rowe, R.K. & Bui, H.H. 2017, 'Geosynthetic reinforced column supported embankments and the role of ground improvement installation effects', *Canadian Geotechnical Journal*, pp. 1-18.

Kirstein, J.F. & Wittorf, N. 2013, 'Improvement of soft fat clay using rigid inclusions and vertical drains', *Proceedings of the 18th International Conference on Soil Mechanics and Geotechnical Engineering, Paris 2013*, International Society for Soil Mechanics and Geotechnical Engineering, Paris, pp. 2513-6.

Ko, J., Jeong, S. & Lee, J.K. 2016, 'Large deformation FE analysis of driven steel pipe piles with soil plugging', *Computers and Geotechnics*, vol. 71, pp. 82-97.

Kovari, K. & Amstad, C. 1982, 'A new method of measuring deformations in diaphragm walls and piles', *Géotechnique*, vol. 32, no. 4, pp. 402-6.

Kurian, N.P. & Shah, S.J. 2009, 'Studies on the behaviour of screw piles by the finite element method', *Canadian Geotechnical Journal*, vol. 46, no. 6, pp. 627-38.

Ladanyi, B. 1964, 'Expansion of a cavity in a saturated clay medium', *Journal of Terramechanics*, vol. 1, no. 2, p. 96.

Lam, L., Wong, Y. & Poon, C. 2000, 'Degree of hydration and gel/space ratio of high-volume fly ash/cement systems', *Cement and Concrete Research*, vol. 30, no. 5, pp. 747-56.

Larisch, M. 2014, 'Behaviour of Stiff, fine grained soil during the installation of screw auger displacement piles', PhD thesis, University of Queenland, Queensland.

Larisch, M.D., Kelly, R. & Muttuvel, T. 2015, 'Improvement of soft soil formations by Drilled Displacement Columns', in B. Indraratna, J. Chu & C. Rujikiatkamjorn (eds), *Ground Improvement Case Histories: Embankments with Special Reference to Consolidation and Other Physical Methods*, Elsevier Science, Oxford.

Le, T.M., Fatahi, B. & Khabbaz, H. 2015, 'Numerical optimisation to obtain elastic viscoplastic model parameters for soft clay', *International Journal of Plasticity*, vol. 65, pp. 1-21.

Lee, C.J. 2013, 'Numerical analysis of pile response to open face tunnelling in stiff clay', *Computers and Geotechnics*, vol. 51, pp. 116-27.

Lehane, B. & Jardine, R. 1993, 'The behaviour of a displacement pile in Bothkennar clay', *Predictive soil mechanics - Proceedings of The Wroth Memorial Symposium 1992*, Thomas Telford, London, St Catherine's College, Oxford, pp. 421-35.

Li, L., Li, J. & Sun, D.a. 2016, 'Anisotropically elasto-plastic solution to undrained cylindrical cavity expansion in K0-consolidated clay', *Computers and Geotechnics*, vol. 73, pp. 83-90.

Li, L., Li, J., Sun, D.a. & Gong, W. 2017, 'Analysis of Time-Dependent Bearing Capacity of a Driven Pile in Clayey Soils by Total Stress Method', *International Journal of Geomechanics*, vol. 17, no. 7, p. 04016156.

Liu, H., Zhou, H., Kong, G., Qin, H. & Zha, Y. 2017, 'High pressure jet-grouting column installation effect in soft soil: Theoretical model and field application', *Computers and Geotechnics*, vol. 88, pp. 74-94.

Liu, H.L., Ng, C. & Fei, K. 2007, 'Performance of a Geogrid-Reinforced and Pile-Supported Highway Embankment over Soft Clay: Case Study', *Journal of Geotechnical and Geoenvironmental Engineering*, vol. 133, no. 12, pp. 1483-93.

Liyanapathirana, D.S. 2009, 'Arbitrary Lagrangian Eulerian based finite element analysis of cone penetration in soft clay', *Computers and Geotechnics*, vol. 36, no. 5, pp. 851-60.

Lo, S.R., Mak, J., Gnanendran, C.T., Zhang, R. & Manivannan, G. 2008, 'Long-term performance of a wide embankment on soft clay improved with prefabricated vertical drains', *Canadian Geotechnical Journal*, vol. 45, no. 8, pp. 1073-91.

Lunne, T., Powell, J. & Robertson, P.K. 1997, *Cone Penetration Testing in Geotechnical Practice*, CRC Press, Taylor & Francis Group, London.

Manjriker, G. 2006, 'Design of Driven Piles and Pile Groups', *The Foundation Engineering Handbook*, CRC Press.

Masse, F., Brockbank, B. & Pearlman, S.L. 2004, 'CMC (Controlled Modulus Columns): Potential Application to Canadian Soils with a New Trend in Ground Improvement', *Geo-Quebec 2004: the 57th Canadian Geotechnical Conference and 5th Joint CGS/IAH-CNC Conference*, Canada, pp. 32-9.

Masse, F., Parinella, C. & Wyman, R. 2011, 'Redevelopment of Brownfield sites using Controlled Modulus Columns as an alternate to Deep Foundations', *Pan-Am CGS Conference on Soil Mechanics and Geotechnical Engineering*, Canada.

Masse, F., Pearlman, S., Walker, M. & Swift, S. 2011, 'Sustainable Use of Controlled Modulus Columns in Brownfield Redevelopment Projects', *"Case studies and recent advances in ground improvement"- A Specialty Seminar presented by ASCE Metropolitan Geotechnical Group*, New York, NY.

Masse, F., Quandelle, B.R., Brandon, M., Buschmeier, B. & Shatzer, K. 2017, *Ground Reinforcing Device*, US Patent 2017 /0342674 Al.

Mayne, P.W. & Kulhawy, F.H. 1982, 'Ko - OCR Relationships in Soil', *Journal of the Geotechnical Engineering Division*, vol. 108, no. 6, pp. 851-72.

McCarthy, M.J. & Dhir, R.K. 2005, 'Development of high volume fly ash cements for use in concrete construction', *Fuel*, vol. 84, no. 11, pp. 1423-32.

McVay, M.C., Wasman, S.J., Consolazio, G.R., Bullock, P.J., Cowan, D.G. & Bollmann, H.T. 2009, 'Dynamic soil–structure interaction of bridge substructure subject to vessel impact', *Journal of Bridge Engineering*, vol. 14, no. 1, pp. 7-16.

Mehta, P.K. 2004, 'High-performance, high-volume fly ash concrete for sustainable development', *Proceedings of the international workshop on sustainable*

development and concrete technology, Iowa State University Ames, IA, USA, pp. 3-14.

Menard Bachy 2012, 'Ensuring Ground Strength - Vic Project Feature Breakwater Road Alignment', *Australian National Construction Review*, p. 125.

Mesri, G. & Choi, Y. 1985, 'Settlement analysis of embankments on soft clays', *Journal of Geotechnical Engineering*, vol. 111, no. 4, pp. 441-64.

Michalowski, R.L., Wojtasik, A., Duda, A., Florkiewicz, A. & Park, D. 2018, 'Failure and Remedy of Column-Supported Embankment: Case Study', *Journal of Geotechnical and Geoenvironmental Engineering*, vol. 144, no. 3, p. 05017008.

Mitchell, J.K. & Kelly, R. 2013, 'Addressing some current challenges in ground improvement', *Proceedings of the ICE - Ground Improvement*, vol. 166, no. 3, pp. 127-37.

Mohamad, H., Soga, K., Pellew, A. & Bennett, P.J. 2011, 'Performance Monitoring of a Secant-Piled Wall Using Distributed Fiber Optic Strain Sensing', *Journal of Geotechnical and Geoenvironmental Engineering*, vol. 137, no. 12, pp. 1236-43.

Muir Wood, D. 1990, *Soil Behaviour and Critical State Soil Mechanics*, Cambridge University Press.

Muir Wood, D. 2004, *Geotechnical Modelling*, vol. 1, CRC Press.

Naik, T.R., Ramme, B.W., Kraus, R.N. & Siddique, R. 2003, 'Long-Term Performance of High-Volume Fly Ash. Title No. 100-M18', *ACI Materials Journal*, pp. 150-5.

Nash, D., Powell, J. & Lloyd, I. 1992, 'Initial investigations of the soft clay test site at Bothkennar', *Géotechnique*, vol. 42, no. 2, pp. 163-81.

Nazem, M., Carter, J. & Airey, D. 2009, 'Arbitrary Lagrangian–Eulerian method for dynamic analysis of geotechnical problems', *Computers and Geotechnics*, vol. 36, no. 4, pp. 549-57.

Nazem, M., Sheng, D., Carter, J.P. & Sloan, S.W. 2008, 'Arbitrary Lagrangian–Eulerian method for large-strain consolidation problems', *International Journal for Numerical and Analytical Methods in Geomechanics*, vol. 32, no. 9, pp. 1023-50.

NeSmith, W. & Fox, J. 2009, 'Practical Considerations for Design and Installation of Drilled Displacement Piles', *Contemporary Topics in Deep Foundations*, American Society of Civil Engineers, pp. 438-46.

Nguyen, H.H., Khabbaz, H., Fatahi, B., Vincent, P. & Marix-Evans, M. 2014, 'Sustainability considerations for ground improvement technique using controlled modulus columns', *AGS mini-syposium "Resilient Geotechnics"*, eds H. Khabbaz & C. Rujikiatkamjorn, Australian Geomechanics Society, Sydney Australia, pp. 170 - 84.

Nguyen, L.D., Fatahi, B. & Khabbaz, H. 2014, 'A constitutive model for cemented clays capturing cementation degradation', *International Journal of Plasticity*, vol. 56, pp. 1-18.

Ni, Q., Hird, C. & Guymer, I. 2009, 'Physical modelling of pile penetration in clay using transparent soil and particle image velocimetry', *Géotechnique*, vol. 60, no. 2, pp. 121-32.

Noor Muneerah PG Haji Jeludin, D., Sivakumar, V., O'Kelly, B. & Mackinnon, P. 2015, 'Experimental Observations of Settlement of Footings Supported on Soft Clay Reinforced with Granular Columns: Laboratory Model Study', *Journal of Geotechnical and Geoenvironmental Engineering*, vol. 142, no. 1, p. 04015063.

Ong, D., Leung, C. & Chow, Y. 2006, 'Pile behavior due to excavation-induced soil movement in clay. I: Stable wall', *Journal of Geotechnical and Geoenvironmental Engineering*, vol. 132, no. 1, pp. 36-44.

Ooi, P.S.K. & Ramsey, T.L. 2003, 'Curvature and Bending Moments from Inclinometer Data', *International Journal of Geomechanics*, vol. 3, no. 1, pp. 64-74.

Osthoff, D. & Grabe, J. 2018, 'Deformational behaviour of steel sheet piles during jacking', *Computers and Geotechnics*, vol. 101, pp. 1-10.

Palmer, A.C. 1972, 'Undrained plane-strain expansion of a cylindrical cavity in clay: a simple interpretation of the pressuremeter test', *Géotechnique*, vol. 22, no. 3, pp. 451-7.

Pan, J., Goh, A.T., Wong, K. & Teh, C. 2000, 'Model tests on single piles in soft clay', *Canadian Geotechnical Journal*, vol. 37, no. 4, pp. 890-7.

Pearlman, S. 2012, 'Controlled Modulus Columns: Innovation in Ground Improvement', *Deep foundations*, pp. 73-5.

Pearlman, S.L. & Porbaha, A. 2006, 'Design and monitoring of an embankment on controlled modulus columns', *Transportation Research Board*, pp. 96-103.

Pestana, J., Hunt, C. & Bray, J. 2002, 'Soil Deformation and Excess Pore Pressure Field around a Closed-Ended Pile', *Journal of Geotechnical and Geoenvironmental Engineering*, vol. 128, no. 1, pp. 1-12.

Phuong, N.T.V., van Tol, A.F., Elkadi, A.S.K. & Rohe, A. 2016, 'Numerical investigation of pile installation effects in sand using material point method', *Computers and Geotechnics*, vol. 73, pp. 58-71.

Phutthananon, C., Jongpradist, P., Yensri, P. & Jamsawang, P. 2018, 'Dependence of ultimate bearing capacity and failure behavior of T-shaped deep cement mixing piles on enlarged cap shape and pile strength', *Computers and Geotechnics*, vol. 97, pp. 27-41.

Plomteux, C. & Lacazedieu, M. 2007, 'Embankment Construction on Extremely Soft Soils Using Controlled Modulus Columns for Highway 2000 Project in Jamaica', *Proceedings of the 16th Southeast Asian Geotechnical Conference, Kuala Lumpur, Malaysia 8 - 11 May 2007*.

Plomteux, C., Porbaha, A. & Spaulding, C. 2004, 'CMC Foundation System for Embankment Support—A Case History', *GeoSupport 2004 : Drilled Shafts, Micropiling, Deep Mixing, Remedial Methods, and Specialty Foundation Systems*, eds J.P. Turner & P.W. Mayne, vol. GSP 124, ASCE, Florida, pp. 980-92.

Poorooshasb, H. & Meyerhof, G. 1997, 'Analysis of behavior of stone columns and lime columns', *Computers and Geotechnics*, vol. 20, no. 1, pp. 47-70.

Porbaha, A. 1998, 'State of the art in deep mixing technology: part I. Basic concepts and overview', *Proceedings of the Institution of Civil Engineers - Ground Improvement*, vol. 2, no. 2, pp. 81-92.

Potyondy, J.G. 1961, 'Skin friction between various soils and construction materials', *Géotechnique*, vol. 11, no. 4, pp. 339-53.

Poulos, H. 1994, 'Effect of pile driving on adjacent piles in clay', *Canadian Geotechnical Journal*, vol. 31, no. 6, pp. 856-67.

Pournaghiazar, M., Khalili, N. & Russell, A.R. 2012, 'Linking cone penetration resistances measured in calibration chambers and the field', *Géotechnique Letters*, vol. 2, no. April-June, pp. 29-35.

Priebe, H. 1995, 'The Design of vibro replacement', *Ground engineering*, vol. 28, no. 10.

Pucker, T. & Grabe, J. 2012, 'Numerical simulation of the installation process of full displacement piles', *Computers and Geotechnics*, vol. 45, pp. 93-106.

Qi, W.G., Gao, F.P., Randolph, M.F. & Lehane, B.M. 2016, 'Scour effects on p–y curves for shallowly embedded piles in sand', *Géotechnique*, vol. 66, no. 8, pp. 648-60.

Randolph, M. 2003, 'Science and empiricism in pile foundation design', *Géotechnique*, vol. 53, no. 10, pp. 847-75.

Randolph, M. & Hope, S. 2004, 'Effect of cone velocity on cone resistance and excess pore pressures', *The international symposium on engineering practice and performance of soft deposits*, Osaka, pp. 147–52.

Randolph, M.F., Carter, J.P. & Wroth, C.P. 1979, 'Driven piles in clay - the effects of installation and subsequent consolidation', *Géotechnique*, vol. 29, no. 4, pp. 361-93.

Randolph, M.F. & Wroth, C.P. 1979, 'An analytical solution for the consolidation around a driven pile', *International Journal for Numerical and Analytical Methods in Geomechanics*, vol. 3, no. 3, pp. 217-29.

Reul, O. & Randolph, M. 2003, 'Piled rafts in overconsolidated clay: comparison of in situ measurements and numerical analyses', *Géotechnique*, vol. 53, no. 3, pp. 301-15.

Rivera, A.J., Olgun, C.G., Brandon, T.L. & Masse, F. 2014, 'Numerical modeling of controlled modulus column installation in soft soils using a linear elastic perfectly plastic soil model', *8th European Conference on Numerical Methods in Geotechnical Engineering*, CRC Press, The Netherlands, pp. 571-6.

Roads and Maritime Services NSW 2017, *RMS Specification D&C R225 - Concrete Injected Columns*, <http://www.rms.nsw.gov.au/business-industry/partners-suppliers/documents/specifications/dc_r225.pdf>.

Rollins, K.M., Gerber, T.M., Lane, J.D. & Ashford, S.A. 2005, 'Lateral Resistance of a Full-Scale Pile Group in Liquefied Sand', *Journal of Geotechnical and Geoenvironmental Engineering*, vol. 131, no. 1, pp. 115-25.

Rollins, K.M., Peterson, K.T. & Weaver, T.J. 1998, 'Lateral load behavior of full-scale pile group in clay', *Journal of geotechnical and geoenvironmental engineering*, vol. 124, no. 6, pp. 468-78.

Roscoe, K.H. & Burland, J. 1968, *On the generalized stress-strain behaviour of 'wet' clay*, Cambridge University Press, Cambridge.

Roy, M., Blanchet, R., Tavenas, F. & Rochelle, P.L. 1981, 'Behaviour of a sensitive clay during pile driving', *Canadian Geotechnical Journal*, vol. 18, no. 1, pp. 67-85.

Sabetamal, H., Nazem, M., Carter, J.P. & Sloan, S.W. 2014, 'Large deformation dynamic analysis of saturated porous media with applications to penetration problems', *Computers and Geotechnics*, vol. 55, pp. 117-31.

Sagaseta, C. 1987, 'Analysis of undraind soil deformation due to ground loss', *Géotechnique*, vol. 37, no. 3, pp. 301-20.

Sagaseta, C. & Whittle, A. 2001, 'Prediction of Ground Movements due to Pile Driving in Clay', *Journal of Geotechnical and Geoenvironmental Engineering*, vol. 127, no. 1, pp. 55-66.

Sagaseta, C., Whittle, A.J. & Santagata, M. 1997, 'Deformation analysis of shallow penetration in clay', *International Journal for Numerical and Analytical Methods in Geomechanics*, vol. 21, no. 10, pp. 687-719.

Sawwaf, M.E. 2006, 'Lateral Resistance of Single Pile Located Near Geosynthetic Reinforced Slope', *Journal of Geotechnical and Geoenvironmental Engineering*, vol. 132, no. 10, pp. 1336-45.

Shen, S.-L., Han, J. & Du, Y.-J. 2008, 'Deep mixing induced property changes in surrounding sensitive marine clays', *Journal of Geotechnical and Geoenvironmental Engineering*, vol. 134, no. 6, pp. 845-54.

Shen, S.-L., Miura, N. & Koga, H. 2003, 'Interaction mechanism between deep mixing column and surrounding clay during installation', *Canadian Geotechnical Journal*, vol. 40, no. 2, pp. 293-307.

Shen, S.-L., Wang, Z.-F., Yang, J. & Ho, C.-E. 2013, 'Generalized approach for prediction of jet grout column diameter', *Journal of Geotechnical and Geoenvironmental Engineering*, vol. 139, no. 12, pp. 2060-9.

Shen, S. & Miura, N. 1999, 'Soil fracturing of the surrounding clay during deep mixing column installation', *Soils and Foundations*, vol. 39, no. 5, pp. 13-22.

Shen, S.L., Wang, Z.F. & Cheng, W.C. 2017, 'Estimation of lateral displacement induced by jet grouting in clayey soils', *Géotechnique*, vol. 67, no. 7, pp. 621-30.

Siddique, R. 2004, 'Performance characteristics of high-volume Class F fly ash concrete', *Cement and Concrete Research*, vol. 34, no. 3, pp. 487-93.

Sideris, K., Manita, P. & Sideris, K. 2004, 'Estimation of ultimate modulus of elasticity and Poisson ratio of normal concrete', *Cement and Concrete Composites*, vol. 26, no. 6, pp. 623-31.

Simon, B. 2012, 'General Report - session 5 - Rigid Inclusions and Stone Columns', paper presented to the *ISSMGE - TC 211 International Symposium on Ground Improvement IS-GI*, Brussels, 31 May and 1 June 2012

Skinner, H., Powell, J.J.M., Morris, J. & England, M. 2003, 'Results from a piling trial on bored, CFA and rotary displacement piles in stiff clay', *BGA International Conference on Foundations: Innovations, observations, design and practice*, pp. 825-34.

Slatter, J.W. 2000, 'The fundamental behaviour of displacement screw piling augers', PhD thesis, Monash University.

Smethurst, J. & Powrie, W. 2007, 'Monitoring and analysis of the bending behaviour of discrete piles used to stabilise a railway embankment', *Géotechnique*, vol. 57, no. 8, pp. 663-77.

Smith, D.M. 1991, *Mechanical Properties of Mass Concrete at Early Ages*, Department of The Army Us Army Corps Of Engineers, Washington DC, SL-91-14.

Spaulding, C., Masse, F. & LaBrozzi, J. 2008, 'Ground improvement technologies for a sustainable world', *Civil engineering of American Society of Civil Engineers*, vol. 78, no. 4, pp. 891-8.

Standards Australia 2009, *Piling—Design and installation, AS 2159 - 2009*, Standards Australia, Sydney, Australia.

Standards Australia 2014a, *Compressive strength tests - Concrete, mortar and grout specimens*, AS 1012.9:2014, Standards Australia, Sydney, Australia.

Standards Australia 2014b, *Determination of indirect tensile strength of concrete cylinders ('Brazil' or splitting test)*, AS 1012.10—2000 Reconfirmed 2014, Standards Australia, Sydney, Australia.

Standards Australia 2014c, *Methods of testing concrete - Determination of the static chord modulus of elasticity and Poisson's ratio of concrete specimens*, AS 1012.17-1997 (R2014), Standards Australia, Sydney Australia.

Standards Australia 2017, *Geotechnical Site Investigations*, AS 1726:2017, Standards Australia, Sydney, Australia.

Steenfelt, J., Randolph, M. & Wroth, C. 1981, 'Instrumented model piles jacked into clay', *Proceedings of the 10th International Conference on Soil Mechanics and Foundation Engineering, Stockholm, Edited by N. Flodin. AA Balkema, Rotterdam*, vol. 2, pp. 857-64.

Stewart, D.P., Jewell, R.J. & Randolph, M. 1994, 'Design of piled bridge abutments on soft clay for loading from lateral soil movements', *Géotechnique*, vol. 44, no. 2, pp. 277-96.

Suleiman, M., Ni, L., Davis, C., Lin, H. & Xiao, S. 2016, 'Installation Effects of Controlled Modulus Column Ground Improvement Piles on Surrounding Soil', *Journal of Geotechnical and Geoenvironmental Engineering*, vol. 142, no. 1, p. 04015059.

Taghavi, A., Muraleetharan, K.K., Miller, G.A. & Cerato, A.B. 2015, 'Centrifuge Modeling of Laterally Loaded Pile Groups in Improved Soft Clay', *Journal of Geotechnical and Geoenvironmental Engineering*, vol. 142, no. 4, p. 04015099.

Tan, S.-A. & Chew, S.-H. 1996, 'Comparison of the hyperbolic and Asaoka observational method of monitoring consolidation with vertical drains', *Soils and Foundations*, vol. 36, no. 3, pp. 31-42.

Tan, S., Tjahyono, S. & Oo, K. 2008, 'Simplified Plane-Strain Modeling of Stone-Column Reinforced Ground', *Journal of Geotechnical and Geoenvironmental Engineering*, vol. 134, no. 2, pp. 185-94.

Tan, T.S., Inoue, T. & Lee, S.L. 1991, 'Hyperbolic Method for Consolidation Analysis', *Journal of Geotechnical Engineering*, vol. 117, no. 11, pp. 1723-37.

Taylor, D.W. 1948, *Fundamentals of soil mechanics*, vol. 66, Chapman And Hall, Limited.; New York.

Teh, C.-I. 1987, 'An analytical study of the cone penetration test', PhD thesis, University of Oxford.

Tehrani, F.S., Nguyen, P., Brinkgreve, R.B.J. & van Tol, A.F. 2016, 'Comparison of Press-Replace Method and Material Point Method for analysis of jacked piles', *Computers and Geotechnics*, vol. 78, pp. 38-53.

Tho, K.K., Chen, Z., Leung, C.F. & Chow, Y.K. 2014, 'Enhanced analysis of pile flexural behavior due to installation of adjacent pile', *Canadian Geotechnical Journal*, vol. 51, no. 6, pp. 705-11.

Tolooiyan, A. & Gavin, K. 2011, 'Modelling the Cone Penetration Test in sand using Cavity Expansion and Arbitrary Lagrangian Eulerian Finite Element Methods', *Computers and Geotechnics*, vol. 38, no. 4, pp. 482-90.

Truong, P. & Lehane, B. 2017, 'Effects of pile shape and pile end condition on the lateral response of displacement piles in soft clay', *Géotechnique*, pp. 1-11.

Turatsinze, A. & Garros, M. 2008, 'On the modulus of elasticity and strain capacity of self-compacting concrete incorporating rubber aggregates', *Resources, conservation and recycling*, vol. 52, no. 10, pp. 1209-15.

Van Eekelen, S.J.M., Bezuijen, A. & van Tol, A.F. 2013, 'An analytical model for arching in piled embankments', *Geotextiles and Geomembranes*, vol. 39, pp. 78-102.

Van Impe, W. 1988, 'Considerations in the auger pile design', *Proc. of the 1st Int. Geotechnical Seminar on Deep Foundations on Bored and Auger Piles, BAP I, Balkema, Rotterdam*, pp. 193-217.

Vermeer, P.A. & De Borst, R. 1984, 'Non-associated plasticity for soils, concrete and rock', *Heron*, vol. 29, no. 3, pp. 1-64.

Vesic, A.S. 1972, 'Expansion of cavities in infinite soil mass', *Journal of Soil Mechanics & Foundations Div*, vol. 98, no. sm3.

Voottipruex, P., Suksawat, T., Bergado, D.T. & Jamsawang, P. 2011, 'Numerical simulations and parametric study of SDCM and DCM piles under full scale axial and lateral loads', *Computers and Geotechnics*, vol. 38, no. 3, pp. 318-29.

Walker, M., Masse, F. & Swift, S. 2011, 'CMC an attractive alternative structural magazine', *Structure Magazine*, pp. 13-5.

Wang, Z.-F., Shen, S.-L., Ho, C.-E. & Kim, Y.-H. 2013, 'Investigation of field-installation effects of horizontal twin-jet grouting in Shanghai soft soil deposits', *Canadian Geotechnical Journal*, vol. 50, no. 3, pp. 288-97.

Weaver, T.J., Ashford, S.A. & Rollins, K.M. 2005, 'Response of 0.6 m Cast-in-Steel-Shell Pile in Liquefied Soil under Lateral Loading', *Journal of Geotechnical and Geoenvironmental Engineering*, vol. 131, no. 1, pp. 94-102.

White, D. & Bolton, M. 2004, 'Displacement and strain paths during plane-strain model pile installation in sand', *Géotechnique*, vol. 54, no. 6, pp. 375-97.

Wilson-Fahmy, R., Ro, K.S. & Leiendecker, K. 2011, 'Evaluation of Four Ground Improvement Techniques for Embankment Support Over Soft Ground', paper presented to the *A Specialty Seminar presented by ASCE Metropolitan Geotechnical Group*, New York.

Wong, I.H. & Poh, T.Y. 2000, 'Effects of jet grouting on adjacent ground and structures', *Journal of Geotechnical and Geoenvironmental Engineering*, vol. 126, no. 3, pp. 247-56.

Wong, P. & Muttuvel, T. 2012a, 'Design of embankments supported on controlled modulus columns', *International Journal of Geotechnical Engineering*, vol. 6, no. 2, pp. 207-13.

Wong, P. & Muttuvel, T. 2012b, 'Economic Design of Controlled Modulus Columns for Ground Improvement ', *11th Australia New Zealand Conference on Geomechanics (ANZ 2012)*, Melbourne, Australia, pp. 680-5.

Wong, P.K. & Muttuvel, T. 2011, 'Support of Road Embankments on Soft Ground using Controlled Modulus Columns', *Proceedings of the International Conference on Advanced Geotechnical Engineering, Perth, Western Australia*, Perth, Australia, pp. 621-6.

Wu, Y.-F. & Zhou, Y.-W. 2010, 'Unified strength model based on Hoek-Brown failure criterion for circular and square concrete columns confined by FRP', *Journal of Composites for Construction*, vol. 14, no. 2, pp. 175-84.

Yang, K. & Liang, R. 2006, 'Methods for deriving py curves from instrumented lateral load tests', *Geotechnical testing journal*, vol. 30, no. 1, pp. 31-8.

Yoshitake, B.I., Wong, H., Ishida, T. & Nassif, A.Y. 2014, 'Thermal stress of high volume fly-ash (HVFA) concrete made with limestone aggregate', *Construction and Building Materials*, vol. 71, pp. 216-25.

Yu, H.-S. 2000, *Cavity expansion methods in geomechanics*, Kluwer Academic Publishers, The Netherlands.

Yu, H.-S. & Houlsby, G. 1991, 'Finite cavity expansion in dilatant soils: loading analysis', *Géotechnique*, vol. 41, no. 2, pp. 173-83.

Zhang, H. & Choi, B. 2015, 'Controlled modulus column design and construction on a highway project on east coast of Australia', *International Conference on Soft*

Ground Engineering 2015 in Singapore - Advances in Soft Ground Engineering, eds C. F. Leung, T.K. and & S.C. Chian, Research Publishing, Singapore, pp. 165-76.

Zhou, H., Liu, H., Kong, G. & Huang, X. 2014, 'Analytical solution of undrained cylindrical cavity expansion in saturated soil under anisotropic initial stress', *Computers and Geotechnics*, vol. 55, pp. 232-9.

Zhou, H., Liu, H. & Yuan, J. 2018, 'A novel analytical approach for predicting the noncylindrical pile penetration-induced soil displacement in undrained soil by combining use of cavity expansion and strain path methods', *International Journal for Numerical and Analytical Methods in Geomechanics*.

Zhou, H., Liu, H., Zha, Y. & Yin, F. 2017, 'A general semi-analytical solution for consolidation around an expanded cylindrical and spherical cavity in modified Cam Clay', *Computers and Geotechnics*, vol. 91, pp. 71-81.

Zytynski, M., Randolph, M.F., Nova, R. & Wroth, C.P. 1978, 'On modelling the unloading-reloading behaviour of soils', *International Journal for Numerical and Analytical Methods in Geomechanics*, vol. 2, no. 1, pp. 87-93.

Appendix A

A1. Asaoka's method

The Asaoka (1978) observational method is the most commonly adopted method in the geotechnical engineering field for predicting final settlement of soil foundations or a soil sample under loading, e.g. Bergado (1990), Cao et al. (2001), Cortellazzo & Simonini (2001), and Mesri & Choi (1985). In this study, the final settlement of the soil sample was estimated using this method based on the monitoring data from the laboratory test results. Settlement data from the field or in the laboratory is often in form of a series of settlements ρ measured at some time intervals.

Step 1: If ρ_k is the settlement measured at time $t + \Delta t$, and ρ_{k-1} is the settlement measured Δt days earlier (i.e. at time t), then the following equation can be used to predict the final settlement (Asaoka 1978).

$$\rho_k = \beta_o + \beta_1 \rho_{k-1}$$

where β_o and β_1 are the intercept and slope, respectively. It is noted that the above equation was derived from the consolidation theory by Mikasa (1963), which was originally the relationship of the coefficient of consolidation c_v and soil strain ϵ. It is also noted that for convenience, settlement measurements are often interpolated from the raw field data so that the settlement values are achieved at equal time interval Δt. Note that some literature indicates that the accuracy of the graphical method depends mainly on a time interval Δ_t.

Step 2: Once the coefficients β_o and β_1 are determined, the final consolidation settlement ρ_f can be calculated based on the following equation:

$$\rho_f = \beta_o/(1-\beta_1)$$

Step 3: The degree of consolidation at time t can then be calculated as a ratio of ρ_t over ρ_f.

Accurate prediction of settlement requires data beyond 60% consolidation (Tan & Chew 1996). They concluded that using early settlement data in the Asaoka plot from 0% to 30% would give very low estimate of ρ_f. The use of 30% to 60% consolidation underestimates ρ_f by 10%.

The Asaoka plot constructed using the settlement monitoring results obtained during the sample preparation (i.e. preconsolidation) is shown below:

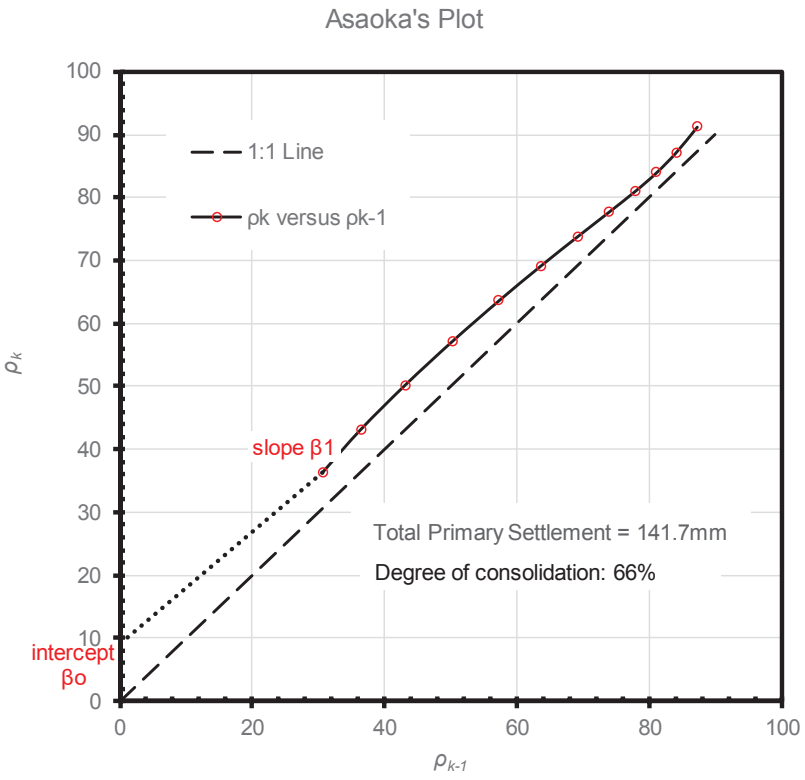

Figure A1.1 Asaoka method for predicting final settlement of the clay sample based on the current settlement data

A2. The Hyperbolic method

The Hyperbolic method for settlement prediction was proposed by Tan, Inoue & Lee (1991). The theoretical basis of this method is as follows: When the settlement T_v is plotted as T_v/U_v versus T_v, the plot consists of an initial concave segment up to U_{60} and a linear segment between U_{60} and U_{90}. The linear portion of the plot has the following form:

$$\frac{T_v}{U} = \alpha T_v + \beta$$

where α and β are the slope and intercept of the hyperbolic plot. Note that the two dotted lines drawn from the origin have slopes of 1/0.6 and 1/0.9 while the slope of the linear segment of the hyperbolic plot is a unique number α_i=.821, which is applicable only to Terzaghi theory.

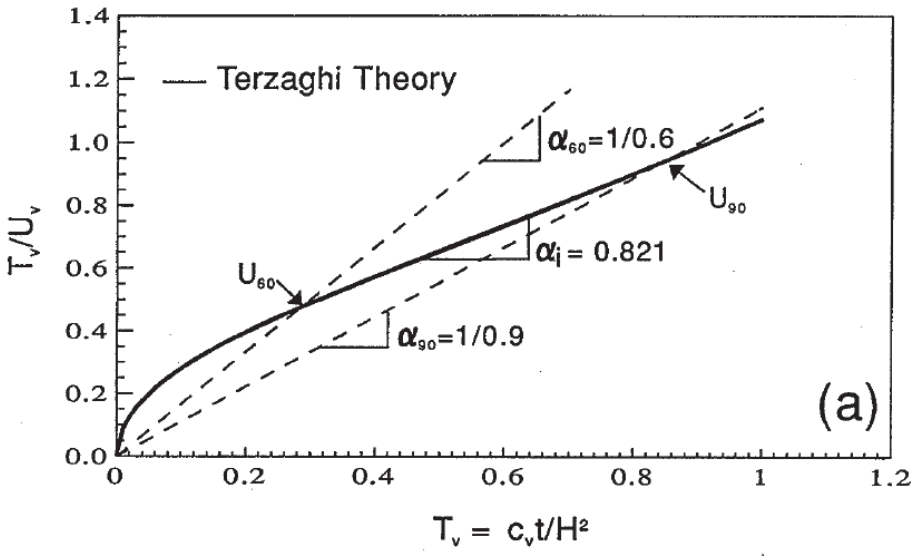

Figure A2.1 Hyperbolic plot of Terzaghi theory (after Tan and Chew, 1996)

If settlement data (i.e. settlement δ versus time t) are plotted in the form of *t/δ* vs *t*, as shown Figure A2.2, the same features as the theoretical plot shown in Figure A2.1 are obtained. The slopes of dotted lines are as followed:

$$S_{60} = \left(\frac{1}{0.6}\right) * S_i/\alpha_i$$

and

$$S_{90} = \left(\frac{1}{0.9}\right) * S_i/\alpha_i$$

where S_i is the slope of the linear segment of the t/δ versus t plot. The ultimate primary settlement can be estimated as $\delta_{60}/0.6$ or $\delta_{90}/0.9$.

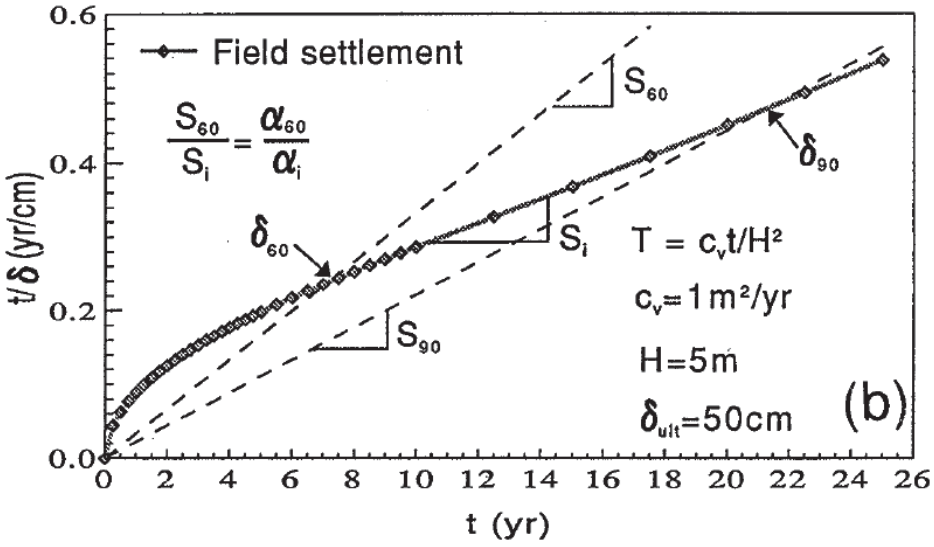

Figure A2.2 The hyperbolic method for final settlement prediction (after Tan and Chew, 1996)

Figure A2.3 shows the resulted hyperbolic plot for predicting final settlement prediction based on the laboratory data obtained during the soil preparation and preloading.

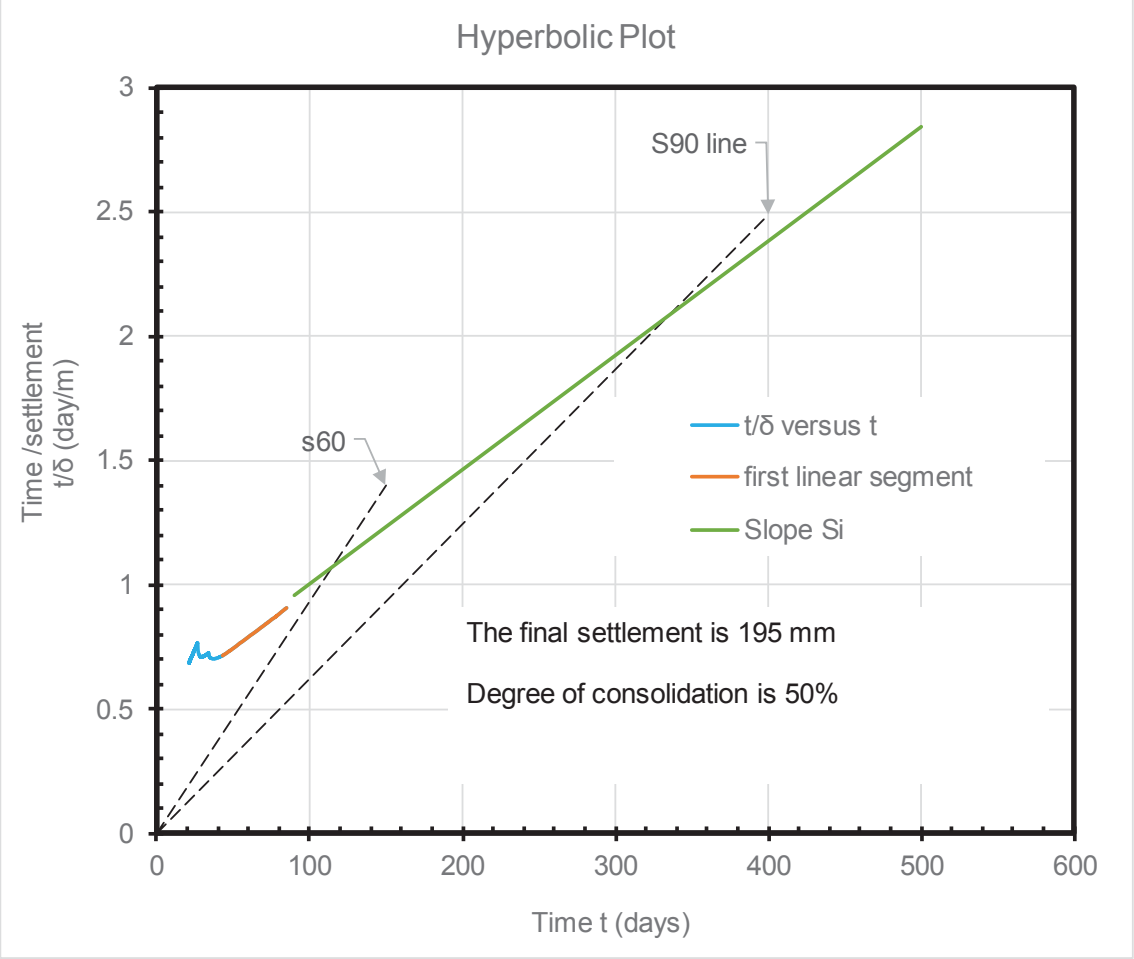

Figure A2.3 The hyperbolic plot for the prediction of final settlement based on the laboratory monitoring data obtained in this study

Appendix B

The following *FLAC*^{3D} code contains functions written in *FISH* language to allow permeability variation with void ratio during the consolidation process. Firstly, a *FISH* function called "storeini_perm" was written to store the initial permeability.

```
def storeini_perm
    local p_z = zone_head
    loop while p_z # null
```

```
        z_extra(p_z,1) = z_prop(p_z,'permeability')

        p_z = z_next(p_z)

    endloop

end

@storeini_perm
```

The second *FISH* function called "set_perm" was written to update permeability in accordance with the current void ratio. This function comes with a c_k of 1.5.

```
; ------------------------------------------------------------------------------------------

def set_perm

    local p_z = zone_head

    local c_k = 1.5

    loop while p_z # null

        local vsinc = (1)* z_prop(p_z,'cam_ev') ; <= accumulated total
        ;volumetric strain.

        local czv = (1)* z_prop(p_z,'cv')

        local new_perm = z_extra(p_z,1) * 10^(vsinc * czv / c_k)

        z_prop(p_z,'permeability') = new_perm

        p_z = z_next(p_z)

    endloop

end

@set_perm

set fishcall 13 set_perm

; ------------------------------------------------------------------------------------------

;------------------------------------------------------------------------------------------
```